The Manufacture and Compressive Ductility of Ultra-High Performance Fiber Reinforced Concrete Utilising Conventional Materials

Prepared by

Md. Habibur Rahman Sobuz

B.Sc (Civil Engineering) and M.Sc (Structural Engineering)

A dissertation submitted for the degree of
Doctor of Philosophy (Structural Engineering)
The School of Civil, Environment and Mining Engineering
The University of Adelaide
Australia

-February 2016-

ABSTRACT

Concrete is a revolutionary material and has been used in civil engineering applications since the ancient Romans period. In the past century concrete has undergone significant change with the development of high strength concretes, and more recently self-compacting and fibre reinforced concretes. In the past decades, significant effort has been devoted to the development of ultra-high performance concrete and one of the latest developments is the ultra-high performance fiber reinforced concrete (UHPFRC). UHPFRC is characterised by high strength and ductility. This advanced concrete is currently used in some structural elements; however the high cost of manufacture, required production control sand lack of industry training has precluded its potential structural applications. Based on the above explanations, the first main goal of this thesis is to develop a wide range of UHPFRC utilising conventional materials and production methods. An experimental investigation is then conducted in order to quantify the size dependent stress-strain compressive behaviour and ductility of UHPFRC. It is then shown how this can be incorporated into a numerical segmental moment-rotation (M/θ) approach to allow for the simulation of flexural ductility of reinforced UHPFRC beams. It is expected that this advancement will aid in the design of UHPFRC structures.

A large-volume of experimental work has been conducted in this thesis to achieve the aforementioned goals. The first part of the experimental investigation involved developing a significant number of UHPRFC mixes to confirm the potential to manufacture using conventional materials and production methods, that is, the use of conventional aggregates, mixers and curing techniques. The main focus of the first part of research was to quantify the variation in rheological and strength properties of UHPFRC with changes the fineness modulus by using conventional aggregates. Additionally to further reduced the financial and environmental cost of production the use of granulated slag and coarse aggregate as a full or partial replacement for conventional fine aggregate was investigated in this research. The results of this study were then compared to the results of mixes designed with expensive silica sand and which were subjected to heat curing technique as this is the current convention for the manufacture of UHPFRC in the construction industry.

The second part of the experimental study investigated the size dependent stress-strain behaviour of UHPFRC under concentric loading including different types of fibers (3D, 4D and 5D) and different volume-fractions (0-3%). This was done as quantifying the stress-strain behaviour and therefore ductility is essential for the design of structural elements. In the last portion of the thesis it is then shown how the flexural ductility of reinforced UHPFRC beams can be simulated with segmental moment-rotation (M/θ) approach by utilising the size dependent stress-strain relationships.

STATEMENT OF ORIGINALITY

I am Md. Habibur Rahman Sobuz, certify that this work contains no material which has been accepted for the award of any other degree or diploma in any university or other tertiary institution and, to the best of my knowledge and belief, contains no material previously published or written by another person, except where due reference has been made in the text.

I give consequent to this copy of my thesis, when deposited in the University Library, being available for loan and photocopying, subject to the provisions of the Copyright Act 1968.

I also give permission for the digital version of my thesis to be made available on the web, via the University's digital research repository, the Library catalogue and also web search engines, unless permission has been granted by the University to restrict access for a period of time.

Md. Habibur Rahman Sobuz	Date

ACKNOWLEDGEMENT

I would like to express my sincere gratitude and appreciation to Emeritus Professor Deric Oehlers, who supervise me wonderfully in my PhD research. I would also grateful to Dr. Phillip Visintin for his supervision through the PhD research work life time and the completion of PhD thesis. Their invaluable advice, continuing supervision and support, encouragement, patience and weekly regular consultation were generous help throughout of PhD reached me the final level.

I would also like to thank Associate Professor Abdul Hamid Sheikh for his valuable guidance and support throughout my studies, and Dr. Mohammad Ali for his precious suggestion and ideas in the research. Special thanks are giving to my graduate friend Mr. Manpreet Singh for his assistance in laboratory work, discussion and encouragement during the study period.

I am extremely thankful to laboratory staffs Mr. Jon Ayoub, Mr. Brenton Howie, Mr. Garry, Mr. Ian Cates, Mr. Simon, Mr. Dale, Mr. Steven Huskinson, Mr. Andrew Heathershaw for their great assistance, help and suggestion to perform the experimental work. I want to give special thanks to Mr. Jon Ayoub for his most great and valuable support and good cooperation in the mixing of concrete and instrumentation.

The financial support from the International Post Graduate Research Scholarship (IPRS) Australian Post Graduate (APA) and the University of Adelaide are highly appreciated.

Finally, I am very much grateful to my parents, wife and children and family members for their love, continuing support, motivation, understanding and encouragement during my PhD start to final day. I dedicate this PhD thesis to my beloved country Bangladesh.

TABLE OF CONTENTS

LIST OF FIGURES

LIST OF TABLES

LIST OF PUBLICATIONS

Based on the research work, one journal paper has been submitted for publication from the first part of research and another one is preparing from the second part of research.

Sobuz, H.R., Visintin, P., Mohamed Ali, M.S., Singh, M., Griffith, M.C., Sheikh, A.H. (2016) Manufacturing Ultra-High Performance Concrete Utilising Conventional Materials and Production Methods, *Construction and Building Material, Vol. 111, pp. 251–261.*

Sobuz, H.R., Visintin, P. and Oehlers, D. J. (2016) "Hinge Rotation Capacity of Reinforced Concrete Beams with Ultra-high Performance Fiber Reinforced (UHPFRC)" (Under Preparation).

CHAPTER 1

INTRODUCTION

1.1 Introduction

In recent decades the concrete industry has rapidly expanded with the development new cement and concrete composites, this has been driven by the need for higher strength concretes with more ductility and the desire for more durable and environmentally friendly civil structural engineering applications in the worldwide. Technological advancements including new generation water reducing admixture and retarders as well as the development of new types of fibres with increased anchorage have enabled the development of fiber reinforced cementitious matrix concrete. These concretes have been shown to have favourable mechanical properties and durability characteristics such that the design life of structures can be greatly increased and maintenance costs reduced thereby saving on overall costs of structures (Naaman & Wille, 2012).

Cementitious matrix concretes are typically characterised by being self-consolidating concrete (SCC) and when of high strength can be classified as High Performance Concrete (HPC) or Ultra High Performance Concrete (UHPC). The high strength grades of HPC and UHPC make them brittle in nature and hence fibres, typically manufactured from high strength steel, are included in the cement matrix to produce High Performance Fibre Reinforced Concrete (HPFRC) and Ultra-High Performance Fibre Reinforced Concrete (UHPFRC) which have improved toughness and ductility. It is strongly believe that HPFRC and UHPFRC are currently emerging all other types of concrete and it will be well suited for the future concrete in the construction industries (Naaman & Wille, 2012).

UHPFRC is a new type of advanced cementitious matrix implying the concrete's function or capability that has been developed in recent decades in concrete development that exhibits superior qualities to those of conventional concrete. There has been a growing use of UHPFRC around the world (Acker & Behloul, 2004; Cavill & Chirgwin, 2004; Rebentrost, 2005). Due to its high strength, ductility, toughness and durability HPFRC and UHPFRC have been recognised as an important new construction material well suited to situations where: (i) high performance such as seismic or blast resistance is required; (ii) where high durability is desirable such as for expensive civil infrastructure including as bridges and; (iii) to buildings of architectural importance where UHPFRC allows for the construction of long and slender members.

The favourable material characteristics of UHPFRC are achieved by developing a material with a very dense matrix in fresh state, with water-cement ratios typically less than 0.2. Owing to the low water to cement ratio, the addition of high-range water reducing admixtures and the presence of fibres achieving adequate rheological properties such that UHPFRC can be used in practices has posed significant problems. These problems have been addressed by applying principals of particle packing with specially graded silica sands and through the use of new high performance high-range water reducing admixtures. The particle packing of the sands strongly affects the rheological and hardened properties of concrete. The design of UHPFRC is based upon the optimization of the density of the cementitious matrix. An optimum particle packing of the granular ingredients of concrete is the key function to produce good and durable concrete (Brouwers & Radix, 2005; Hüsken, 2010; Neville, 1995; Obla et al., 2003). It is demonstrated that a significant correlation between the quantity of high-range water reducer and the packing density

of sands which require to obtain a flow mixture (Stark & Mueller, 2008). Optimization of the packing density has resulted in decreased the total porosity of the mixing material which in turn shows high strength and excellent durability (Kwan & Mora, 2002). Particle packing of fine aggregates and uniformly distributed short steel fibers used in the mix, which prevents the formation of early-age micro-cracking and crack propagation (Lange et al., 1997).

In today's growing construction industry, UHPFRC is considered one of the leading materials; and its application is limited by the lack of design codes in the worldwide. An adequate design criterion is essential to increase the application for such materials in structural engineering. Therefore, the required applications of a particular reinforced concrete structure govern its concrete mix design philosophy. From the early developments, the construction industry embraced the ideology for significant innovation in the mix design of concrete and its flexibility in developing high performance concretes in an ever progressive construction industry. There have been started using concrete admixtures such as pozzolanic materials, high range water reducer admixture (HRWRA) and other performance based materials to produce high performance concrete in the past few decades. The mix constituents of UHPFRC is proposed which substantially differ from the conventional fiber concrete or high performance concrete (HPC) and is consisted of large amount of cement, silica fume and small content of steel fiber (De Larrard 1994, Richard and Cheyrezy 1995, Rossi et al. 2005, Habel et al. 2006).

There are still some complexities for the increase of UHPFRC uses in a wide range of practical applications. UHPFRC mix design guideline is not yet fully understood in the research community. Rheological and hardened properties of UHPFRC strongly depend on dosages of admixtures and water uses in the mix, amount of fine

and coarse aggregate, casting and mixing process. Although several mix design of UHPFRC guidelines are available in the literature; however this limited number of information may scare the potential users in practical applications. So, the UHPFRC mixture with the above influencing variability and limited guideline are still a major challenge for large-scale structural applications. Also, it should make simpler mix design and producing method that could be allowed in construction industry depending on the structural requirements.

The above mentioned gap of the research requires still deep research in the advancement of ultra-high performance fiber concrete for practical applications. Having now addressed several major issues with mix design of UHPFRC (Graybeal, 2007; Habel et al., 2008; Kim et al., 2011; Wille et al., 2011; Yoo et al., 2015; Yu et al., 2014). Characterization of the material behaviors of UHPFRC has improved to such a level that the large-scale structural application of this concrete is on the horizon. To date, number of experimental investigation has been conducted on the mechanical properties of UHPFRC in the material level (De Larrard 1994, Richard and Cheyrezy 1995, Rossi et al. 2005, Habel et al. 2006). Structural application of UHPFRC is now becoming an increasing concern of UHPFRC research community, several practical applications in Australia, New Zealand and worldwide in the last decades (Cavill & Chirgwin, 2004; Perry & Zakariasen, 2004; Rebentrost, 2005; Vicenzino et al., 2005) and a wide variety of other projects (Acker & Behloul, 2004; Buitelaar, 2004; Semioli, 2001) have identified future possibilities.

Researches to date indicate that UHPFRC has the great potential to increase the use of concrete into new forms for different practical application as mentioned above. This is evident in the new development of ultra-high performance concrete in the last decades. Currently, the preparation of UHPFRC requires special consideration of raw

materials, specialized mixing and curing regimes such as steam or pressure curing (Wang et al., 2012). There is a lack of research in the research community to obtain rheological and hardened properties of UHPFRC with common technology such as without intensive mixers, without steam curing and with simple dosage criteria. As an example, particle packing theory may be applied to optimised the density of the mix by using specially graded silica sands and enhance the followability of mix (de Larrard & Sedran, 1994), while high intensity mixers can help distribute fine mineral admixtures such as silica fume and multi-stage curing including steam or pressure or heat curing can increase the strength (Dils et al., 2012a). The effect of the mixer size and mixing parameters can strongly affect to the rheological and hardened properties (Dils et al., 2012a; Dils et al., 2012b). The requirement for a high proportion of cement and expensive silica sand for UHPFRC production along with the need for specialist curing currently represents a barrier to the more widespread up take of UHPFRC. Therefore, a simplification of the UHPFRC manufacture and processes is required for large-scale structural application for construction industry. For this reason in this thesis a primary aim is to develop UHPFRC mixes using conventional available materials, manufacturing regimes (mixers) with simpler mixing processes, simple admixture and water dosages criteria and curing techniques used in the manufacture of normal strength concrete, this is done with the aim of simplifying the design of UHPFRC mixes and reducing the overall cost of manufacture.

The number of researches (Ambily et al., 2015; Van Tuan et al., 2011) in recent years, who have investigated utilising waste materials (Yang et al., 2012a; YANG et al., 2012b; Yang et al., 2009) such as ground granulated blast furnace slag or rice husk ash in this study the potential to use granulated lead smelter slag as a fine aggregate is investigated with the aim of reducing the environmental impact of UHPFRC and its production cost. Similarly, the use of coarse aggregates in the

mixes is beneficial due to their low specific surface, which leads in a decrease of paste volume fraction required for the mix. This indicates a decrease in the cement amount, reducing the production costs and autogenous shrinkage. A small number of experimental researches have been carried out by using coarse aggregate (CA) to produce ultra-high performance fiber reinforced concrete (Ma et al., 2004; Wang et al., 2012; YANG et al., 2012b). There is still requires much research to obtain the optimum coarse aggregate to fine aggregate (CA: FA) ratio in UHPFRC mixes to achieve the effect over the desired properties. In this thesis, mix designs are also investigated with the addition of coarse aggregate to quantify the optimal ratio of CA: FA in order to achieve good flowable mix and high compressive strength.

The uniaxial compressive strength and ductility of concrete are considered crucial material properties in the design of concrete structures. The development of considerable ductility in the ultimate limit stage is a key function for the design of reinforced concrete structures. Ductility is a very important characteristic, because it is directly associated to structural safety and the capacity to redistribute internal forces of the structures. Ultra-high performance concrete can attain compressive strength exceeding of 150MPa and up to 800MPa with special curing conditions such as steam or pressure, thermal or heat curing with expensive silica sands (Graybeal & Davis, 2008; Graybeal, 2007; Richard & Cheyrezy, 1995; Wille et al., 2011). The research has been carried out to understand the factors that influence the compressive behaviour of UHPFRC, when steam or pressure treatment is absence in the curing technique (Askar et al., 2012; Bumanis et al., 2015; Heinz et al., 2012; Safi et al., 2014). The compressive strength and post-peak response is enhanced through the incorporation of steel fibers. However, only limited research has attempted to quantify strength and ductility behaviours of UHPFRC with common manufacturing

technology such as curing conditions without steam or pressure, thermal or heat curing and without specialised materials, mixture and mixing process.

Ultra-high Performance Fiber Reinforced Concrete exhibits significant ductility behaviour under the compression through the use of short discontinuous fibers, which is an essential characteristic to achieve ductility response. A limited amount of research has been conducted to quantify the full compressive stress strain and ductility behaviour of UHPFRC under concentric loading (Wille et al., 2014; Wille et al., 2011) with expensive fine silica sands with single fiber type. Although few researches (Allena & Newtson, 2011; Yang et al., 2009) have investigated mechanical and ductility responses of UHPFRC in a small-scale by using natural fine aggregate with single fiber type and amount; however there are to date no depth research in the literature quantifying the effect of fiber type and volume fraction with conventional sand. The material ductility of UHPFRC is not only dependent on the constituents of UHPFRC such as the volume fraction of fibres and the type of fibers incorporated into the mix (Kazemi & Lubell, 2012), it is also influenced by the size and shape of the specimen as considered. A number of experimental investigation on concrete specimens subjected to uniaxial compression (Del Viso et al., 2008; Kampmann, 2012; Kazemi & Lubell, 2012; Kim & Yi, 2002) concluded that the size effects are due to the strain localization after the peak load. Size effect is of importance characteristic in civil engineering structures. Concrete structures are designed according to the strength of a standard specimen size however it is known that the structural response and failure are expected to be size dependent, for example the rotation capacity of a plastic hinge is size dependent due to concrete softening (Bigaj & Walraven, 2002). Several experimental investigations has been carried out on the plastic rotation capacity of RC beams in bending including size-scale effect (Hemmati et al., 2013; Kheyroddin & Naderpour, 2007; Lopes &

Bernardo, 2003; Oehlers et al., 2008). Carpinteri et al. (2009) proposed a numerical model to describe the plastic rotation capacity of RC beams with nonlinear fracture mechanics models. Although extensive researches have been conducted on the mechanical strength of UHPFRC; however considering fiber type and fiber volume fraction, size dependent compressive stress strain and cracking behaviours of UHPFRC has not yet been clearly understood and requires further investigation. It is therefore the secondary aim of this thesis to quantify the size dependent stress strain behaviour of UHPFRC as well as to show how this size dependent stress strain behaviour can be used to quantify the plastic hinge behaviour of UHPFRC beams.

1.2 Objectives and Tasks

To fulfil objectives of this research this thesis reports on research in the following areas:

- The development of ultra-high performance fiber reinforced concrete with conventional materials and methods. Rheological and hardened properties are investigated with different dosages of superplasticizer and water content and the axial and lateral stress-strain behaviours of each individual mix quantified to understand the behaviour of UHPFRC.

- The size effect and compressive ductility behaviour of UHPFRC under concentric loading with different types and varies content of fiber is quantified. Failure modes and crack pattern is assessed to understand the nature of the concrete failure on the material level.

- Incorporating the size dependent compressive material properties of UHPFRC, a numerical segmental moment-rotation approach is developed to simulate the behaviours of reinforced concrete members.

1.3 Structure of Dissertation

This dissertation is composed of seven chapters to achieve the above mentioned objectives as follows and outlined in Figure 1.1.

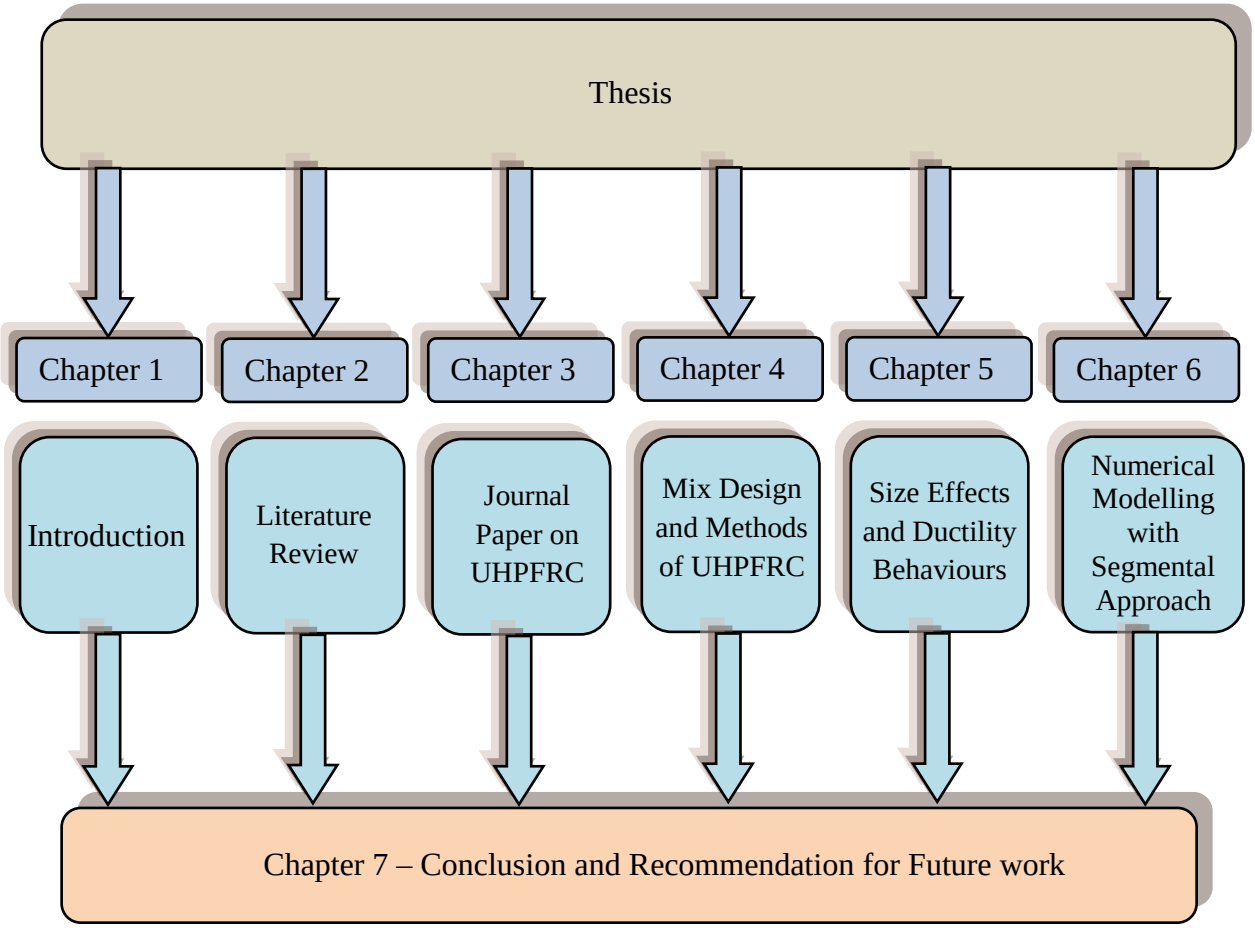

Fig.1.1 Layout of the thesis

Chapter 1 provides brief introductory background, research significance and objectives of the dissertation.

Chapter 2 covers the literature review on mix design and methods of UHPFRC, methods and instrumentation of testing, axial and lateral behaviour of UHPFRC, softening and size effect responses and ductility behaviours of UHPFRC in compression.

Chapter 3 the journal paper 'Manufacturing Ultra-High Performance Concrete Utilising Conventional Materials and Production Methods' is presented in which the investigating the potential to manufacture UHPFRC from conventional sands and coarse aggregates is investigated.

Chapter 4 further information on the development of UHPFRC with conventional sands and coarse aggregates which could not be included in the journal paper is presented as well as an investigation into the development of UHPFRC using expensive higher performance silica sands. Rheological and hardened properties of UHPFRC, axial and lateral stress-strain behaviours and their comparison are also discussed in this chapter.

Chapter 5 deals with the experimental investigation on size effect and compressive ductility behaviour of UHPFRC with different types and content of fibre.This chapter also discusses the variation in failure modes and crack pattern of UHPFRC for each type and content of fiber specimens. The failure mode and stress-strain behaviour obtained from specimens of different sizes and shapes are compared.

Chapter 6 presents the analysis of the compressive axial and lateral size effect test results of UHPFRC from Chapter 5 and empirical expression are developed in term of stress and deformation of the concrete softening wedge. A numerical segmental moment-rotation analysis of reinforced concrete members is developed incorporating the compressive material properties including the size effect responses of UHPFRC.

Chapter 7 summarises the major findings of the current research and outlines recommendation for future research.

CHAPTER 2

LITERATURE REVIEW

This chapter provides a state of the art of ultra-high performance fiber reinforced concrete (UHPFRC) manufacturing, testing techniques for UHPFPC material properties and a description of material behaviours. A review of the pertinent literature is first carried out in this chapter which represents the material constituents, mix designs, curing regimes, fiber effects and fresh properties in the production of UHPFRC. Secondly, UHPFRC compressive strength, axial and lateral contraction, and failure characteristics are reviewed from the previous experimental works and summarized. Special attention is paid in different testing technique and method of measurement of contraction to capture the descending branch after the peak load. The size-effect and ductility responses of different types of UHPFRC due to fiber volume and fibre type are considered from previous studies and included herein. Finally, this chapter reviews the most significant literature on numerical modelling using the segmental approach to analyse reinforced concrete beams. This is done as it will be the modelling technique extended for UHPFRC within this thesis.

2.1 An Historical Perspective of Ultra-high Performance Concrete

Since the 1970s significant research has been conducted with the aim of developing high strength cementitious composites for civil and structural applications. Early research in this area utilised novel vacuum mixing processes in order to produce high strength cement pastes with low water to cement ratios porosities such that compressive strengths in the order of 230MPa were achieved (Yudenfreund et al., 1972a; Yudenfreund et al., 1972b). In the early 1980s, polymer-modified cementitious materials that consisted of macro-defect-free (MDF) cements, densified

small particle concrete and silica fume were first introduced by the Imperial Chemical Industries (Alford & Birchall, 1985; Bache, 1987; Birchall et al., 1981). In this research it was found that compressive strengths exceeding 200MPa was possible with the inclusion of these novel materials and this work can be considered the precursor to modern UHPFRC. Following the work by the Imperial Chemical Industries, Hjorth et al. (1983) patented and commercialised densified small particle concrete with micro silica and superplasticizer (SP) content. With the inclusion of both mineral and chemical admixtures Hjorth et al. (1983) was able to obtain compressive strengths between 120 MPa and 250MPa.

In the early and mid of 1990s, reactive powder concrete (RPC), were introduced and commercialised in the concrete industry (de Larrard & Sedran, 1994; Li & Leung, 1992; Richard & Cheyrezy, 1995). The first attempt taken towards the development of UHPC by de Larrard and Sedran (1994) and the subsequent developments and commercialization of RPC in the form of UHPC was made by Richard and Cheyrezy (1995). According to Richard and Cheyrezy (1995), the highest compressive strength ultra-high performance ductile concrete is achieved through the use of special curing conditions including thermal and pressure treatment. In this work it was shown that compressive strengths of 650MPa were possible by curing at a temperature 400^0C, and a pressure of 50MPa. The introduction of 10% volume of steel fibers and steel aggregate further increased the compressive strength to 800MPa.

More recently research in UHPFPC has focused on the development more practical concretes and currently the general definition of a UHPFRC is an advanced cementitious concrete which shows compressive strengths exceeding 150MPa and with superior durability properties and well dispersed and optimum volume fraction

of steel fibers provide to sufficient ductility behaviours under compression and tension (AFGC/SETRA, 2002). Improvements characteristics of UHPFRC compared to conventional and high performance concrete are achieved through the reduction of water-cement ratios to less than 0.2, special aggregate selection criteria based on optimizing particle packing density, the use of high performance aggregates such as silica powder and silica quartz sand. Furthermore specialized curing conditions such as high temperature, high pressure or steam curing are also common. The use of these high performance materials and production techniques has led to the development of UHPFRC with pre-cracked direct tensile strengths of to 13.3MPa through the use of twisted fiber at 3% fiber volume fraction and post-cracking tensile strength obtained 19.6MPa (Wille et al., 2014a). In addition, the ultra-high performance fiber reinforced concrete shows long strain hardening behaviour under tension (Graybeal & Baby, 2013; Habel, 2004; Wille et al., 2014a).

More recently increased research focus has been devoted to simplifying the manufacture of UHPFRC in order to reduce both the financial and environmental cost of production research whilst achieving similar material properties. This research has focused on the use of conventional fine aggregate, coarse aggregate, and the inclusion of waste materials in the form of ground granulated blast furnace (Ambily et al., 2015; Ma et al., 2004; Yu et al., 2014).

2.2 Advantages and Applications of UHPFRC

The development of UHPFPC in the last two decades has motivated new developments in structural engineering. This main advantage of this concrete over the ordinary concrete is the superior compressive strength, good tensile strength with strain hardening, better workability, durability, and ductility behaviours. It is worth mentioning that although UHPFRC is more expensive than the normal strength

concrete when comparing the UHPFRC with ordinary concrete, the design life of structures, strength and durability should be taken into account. That is the higher strength means that less material is required to meet strength requirements and hence lighter weight structures are possible. Moreover, handling, transportation and installation of UHPFPC members are easier due to the ultra-light weight property of UHPFPC, compared to conventional RC or prestressed concrete members. This can provide the cost of savings and increase factor of safety in the construction industry (Voo & Foster, 2010). Ultra-high performance concrete has also been shown to be highly durable to chemical attacks in severe atmospheric environments (AFGC/SETRA, 2002) such that it can be expected that service lives can be increased and maintenance costs reduced compared to normal concrete structures (Piotrowski & Schmidt, 2012).

The major applications of UHPFRC are in the structural engineering such as bridge girders, decks, structural art such as balconies, pipelines, in rehabilitation and repair applications and in industrial construction (Lei et al., 2012). The world's first road bridge was constructed with UHPFPC at Shepherds Gully Creek, NSW Australia in 2004 (Cavill & Chirgwin, 2004). This was followed by the construction of several pedestrian footbridges constructed around the railway area in Auckland, New Zealand including Papatoetoe and Penrose Station in 2006 and 2007 (Rebentrost, 2005; Wight et al., 2007). The first application of ultra-high performance fiber reinforced concrete truss elements in Sherbrooke footbridge was successfully completed in 1997 at Canada. Sermaises footbridge in France in 2002 and Sakata Mirai footbridges in 2002 and Akakura footbridges in 2004 in Japan are the three applications of UHPFPC. The Seonyu Pedestrian Bridge in South Korea is the showcase structures of UHPFPC applications in 2002. Perry and Zakariasen (2004)

used the UHPFRC for an innovative Train station canopy at Calgary, Canada in 2004. After that, another applications of UHPFRC as a thin precast concrete roof shell done by Vicenzino et al. (2005) in Canadian LRT station. Then, the UHPFRC have been used to construct the structures in many countries like Franch, Germany, USA, Malaysia, Australia and South Korea. Nowadays, construction industries are thinking about increasing application of UHPFRC in large projects including the prestressed and precast members, for architectural purposes as well as for the repair and strengthening of structures, construction in aggressive environments, composite structure and structures in high seismic zones.

2.3 Mix Design and Production Methods of UHPFRC

UHPFRC concept is derived from the ordinary concrete and it creates new possibility in the worldwide concrete manufacturer. However, the current conception of UHPFRC has to evolve to obtain best material properties by the appropriate selection of mix constituents. In this section, a major review of related research pertaining to each aspect of material composition with previous mix design approach, mixing and preparation technique, dedicated curing regimes and associate testing and instrumentation is presented in the subsequent section. Special attention is paid in the different dosages and processes used to cast UHPFRC, resuming their influence to the rheological and hardened properties.

2.3.1 Mixture composition

The performance of UHPFRC is dependent on the careful selection of raw materials in combination with adequate proportioning and quality control throughout the production process. This product has a number of different material compositions depending on their particular application. The constituent material compositions

were determined based on optimization of the granular mixture and produced highly homogeneous concrete matrix. The basic composition of conventional UHPFRC is a dosage of high volumes of cement and silica fume, silica powder and silica quartz sand, high-range water reducing admixture (HRWRA) or SP and water. Steel fibres can be added to UHPC to make UHPFRC; typically steel fibers are added at a dosage of approximately 2% by volume fraction as this has been found to be optimal in terms of maintaining workability. A basic composition of UHPFRC is presented graphically in Figure 2.1 and an example of an existing mix design taken from the literature is shown in Table 2.1 (Graybeal, 2007).

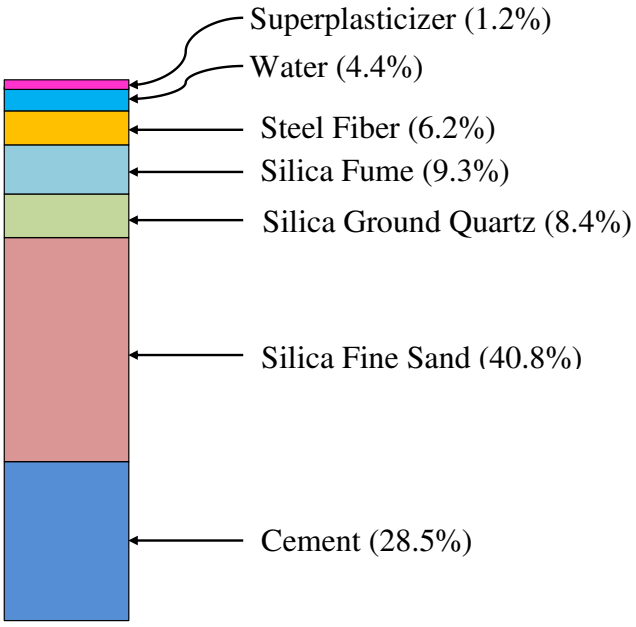

Fig.2.1 Graphical representation of UHPFRC composition

Table 2.1 Typical composition of UHPFRC (Graybeal, 2007)

Material	Amount (kg/m3)	Percentage by Weight
Portland cement	712	28.5
Silica Fine Sand	1020	40.8
Silica Ground Quartz	211	8.4
Silica Fume	231	9.3
Steel Fibres	156	6.2
Water	110	4.4
Superplasticizer	31	1.2

2.3.1.1 Cement

The first fine particle cement with an average diameter of approximately 15μm is used to produce UHPFRC concrete. Compared to conventional concrete UHPFRC is manufactured using a large proportion of Portland cement, typically in the range of 700 to 1100kg/m^3 (Wille et al., 2011). For example Graybeal (2007) manufactured of UHPFRC with 710kg/m^3 cement, while Habel et al. (2008) and Rossi (2013) required cement at 1087kg/m^3 and 1050kg/m^3 respectively in order to obtain acceptable material properties. Due to the higher cement content of UHPFRC mixes significant heat is generated during hydration and thus, sulphate resisting cement, which has low amounts of C_3A accelerates which causes a better time distribution of the exothermic reaction and leads in smaller autogenous shrinkage and better accelerates the hydration process. Due to the hydration process, the demand for water in the paste to surround the cement particles leads to a higher mix viscosity. Sakai et al. (2008) studied the influence of C_3A on rheological property and found C_3A contents of than 8% will provide a low influence of viscosity observed it was further observed that observed cement with low C_3A and soluble alkali greatly influence of the performance of SP, which is significant as UHPFRC mixes aim to minimise water to cement ratios in order to increase strength. Although it has been shown that type II/V cement can lead to the best strength and workability of UHPFRC its availability is limited around the world. Hence further research has been conducted using Type I Portland cement with a low C_3A content and moderate fineness of 4000 cm^2/g by ((Stiel et al., 2004; Wille et al., 2011; Yazici, 2007)). In this research the reduced fineness of the cement reduces the specific surface area of the particles thus leading to a reduced water demand, thus reduced water-binder ratios may deliver similar workability and higher compressive strength of UHPFRC mixes (Heinz & Ludwig, 2004; Terzijski, 2004).

2.3.1.2 Aggregate

The aggregates most of which retained by 4.75mm sieve referred as coarse aggregates, whereas the aggregate passes through 4.75mm sieve is considered as fine aggregate or sand. To produce UHPFRC, silica powder and silica quartz sand are combined to obtain the adequate granulometry and used as fine aggregate. Sand particle sizes typically range between 600μm maximum to below 150μm. The use of these silica powders and silica quartz sands represent a barrier to the more widespread application of UHPFRC as they are typically specifically graded and hence not widely available and if availed are very expensive. In UHPFRC dosages, the water demand of granular mixes strongly depends on the specific surface and the packing density of aggregates (Lohaus & Ramge, 2008). Due to the large specific surface silica powder and quartz sands strongly influence the water to cement ratio required for achieving workability and hence mix designs utilising these materials are not widely transferable to regions where identical materials are not available. The packing density of the sands strongly affects the rheological and hardened characteristics of concrete. It is important to notice that there is a significant correlation between the packing density of the sands and the quantity of SP necessitated obtaining a flowable mix (Stark & Mueller, 2008).

Numerous researches have been conducted on UHPFRC by using expensive silica sand (Graybeal, 2007; Habel et al., 2008; Wille et al., 2011; Yu et al., 2014) however, due to the availability and cost issues associated with obtaining these materials some research effort has been directed towards investigating the possibility of adding coarse aggregate employed different coarse aggregate to UHPFRC (Wang et al., 2012; YANG et al., 2012). The advantage of using coarse aggregates in the UHPFRC mixes is their low specific surface, which provides in a reduction of the

paste volume fraction required. It reveals a reduction in the cement amount which reduces the cost of production. Consequently, the rheological and hardened properties will be affected due to coarse aggregate addition in the mixture. A number of researchers have carried out on UHPFRC production using coarse aggregates addition with diameters 8mm (Scheydt et al., 2008) and maximum diameters 11 mm (Skazlić et al., 2008). However, there are no useful information on the aggregate ratio selection to enhance the flowability and strength. Researchers have also studied the possibility of using waste materials such as granulated blast furnace slag or rich husk as partial replacement of cement or sand to produce UHPFRC (Ambily et al., 2015; Van Tuan et al., 2011; Van, 2013; Yazıcı et al., 2008). Yang et al. (2009) carried out the effect of recycled glass cullet and two types of local natural sand as a replacement of expensive silica sand and cement replaced by silica fume and GGBS to produce UHPFRC at lower cost. Although little number of researches has been conducted to prepare UHPFRC using waste materials, however its addition has to be concentrated properly for producing good characteristics concrete.

2.3.1.3 Silica fume

Silica fume is the industrial by-product of silicon alloys and consists of amorphous SiO_2. Silica fume particle sizes are much smaller than cement at approximately 50-100 times finer. In UHPFRC silica fume acts not only as a micro-filler, increasing the density and workability but also as a supplementary cementations material reacting with calcium hydroxide thereby enhancing the final strength as well as bond between particles due to its pozzolanic properties (Shihada & Arafa, 2010; Yan et al., 1999). The interfacial transition zone between paste and aggregates is also enhanced because of it pozzolanic activity (Rossignolo, 2007). The effectiveness of silica fume has been shown to depends on the dispersion of the agglomerated silica fume

particles; with the better advantages only arising if adequate mixing is possible (Terzijski, 2004). There are some methods to achieve a useful distribution before the mixing, which is the silica fume sonication (Rodríguez et al., 2012). The optimum content of silica fume in UHPFRC preparation has been shown to be between 20% and 30% of cement content (Rougeau & Borys, 2004; Talebinejad et al., 2004; Wille et al., 2011). Within this range the ultrafine silica powder results in improved material properties by Tafraoui et al. (2009) however, if added in excess in the UHPFRC mixes it may decreased both workability and compressive strength (Rougeau & Borys, 2004; Shihada & Arafa, 2010).

2.3.1.4 Steel fibers

The steel fiber is an important constituent in UHPFRC. A great deal of research and development has been carried out with the fibers on the effects in the types, volume fraction, and orientations. The inclusion of steel fiber has a significant effect on the softening region of UHPFRC. Steel fibers act as discrete distributed reinforcement within UHPFRC, crossing micro and macro cracks which form due to shrinkage or under load and hence they provide ductility to an otherwise brittle failures material, improve the load carrying capacity and allow significant capacity during concrete softening (Habel et al., 2008; Kim et al., 2011; Yoo & Yoon, 2015; Yoo et al., 2015).

Researches into UHPFRC typically focuses on materials with steel fiber contents, that is volume fractions of total material or weight percentage of cement and the contents of between of between 1.0 and 2.5% (Graybeal, 2007; Wille et al., 2011); however some of the experiment has been conducted with 3% or more steel fiber content (Kazemi & Lubell, 2012; Lubell & A.S., 2011). Typical properties of different types of steel fibers are shown in Table 2.2 and 2.3.

Table 2.2 Properties of different types of steel fibers (Kim et al., 2011)

Fiber Type	Name of fiber	Diameter (mm)	Length (mm)	Density (g/cc)	Tensile Strength (MPa)	Elastic Modulus (GPa)
Macro	Smooth (SL-)	0.30	30	7.9	2580	200
	Hooked A (HA-)	0.375	30	7.9	2311	200
	Hooked B (HB-)	0.775	62	7.9	1891	200
	Twisted (T-)	0.30	30	7.9	2428	200
Micro	Smooth (SS-)	0.20	13	7.9	2788	200

Table 2.3 Properties of different types of steel fibers (Yoo& Yoon 2015)

Fiber Type	Diameter -d_f (mm)	Length- L_f (mm)	Aspect ratio (L_f/d_f)	Densi -ty (g/cc)	Tensile Strength (MPa)	Elastic Modulus (GPa)
Smooth steel fiber	0.2	13.0	65.0	7.9	2788	200
	0.2	19.5	97.5	7.9	2500	200
	0.3	30.0	100.0	7.9	2580	200
Twistedsteel fiber	0.3	30.0	100.0	7.9	2428	200

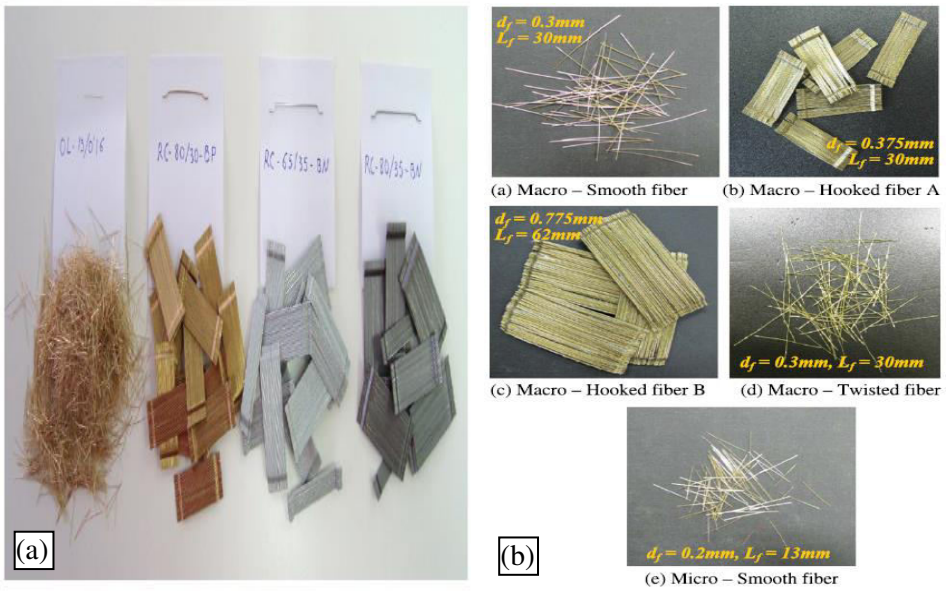

Fig.2.2 (a) Effect of different types of fiberon UHPFRC production (Camacho Torregrosa, 2014) (b) Effect of fiber types and amount on UHPFRC preparation (Kim et al., 2011)

Several researches have been investigated on the UHPFRC preparation with different aspect ratio of fibers, different types of fibers and amount and the orientation of fibers as shown in Figs.2.2(a) and 2.2(b) (Camacho Torregrosa, 2014; Kim et al., 2011; Sbia et al., 2014; Wille et al., 2014a; Wille et al., 2014b). The influence of

UHPFRC incorporating both steel fibers with coarse aggregate has been studied by (YANG et al., 2012; Yang et al., 2009) where it has been shown that the interaction between fibres and aggregate can significantly influence workability. Hence, it is still a great challenge to achieve better workability and strength of UHPFRC with optimum amount of steel fiber and type in the research community.

2.3.1.5 Superplasticizer

SP used in the manufacture of UHPFRC is typically third generation high-range water reducing admixtures, which act to disperse the water in the mix and capable to reduce the water amount up to a 40%. The influence of SP content on the rheological and hardened properties evaluation of UHPFRC have been reported by ((Collepardi et al. (1999); (Hirschi & Wombacher, 2008)) to be a reduction in interfacial tension between particles, a release of water trapped amongst the cement particles, retarding effect of cement hydration and change in morphology of hydrant cement. The aim of using SP in the concrete mixes is to increase workability, reduce the mixing water and reduce both water-cement ratio at given workability and high early strength, in order to save cement and reduce creep, shrinkage and thermal strains cause by the heat of hydration (Collepardi et al., 1999). Wille et al. (2011) studied the influence of high range water reducer on UHPFRC over a range 1 to 8% weight of cement. They observed that the optimum range of high range water reducer between 1.4 to 2.4% in the mix design. It is also important to notice that the critical dosages of SP is the dominating factor in the UHPFRC mixes and it reveals that there is no significant increase of fluidity, and exact time between the end mixing and the hardening of the concrete (Scheydt et al., 2008; Terzijski, 2004). A limited research has been done on critical dosages of SP in UHPFRC mixes, however further investigation need to be carried out in this regards when considered for structural application.

2.3.1.6 Water

To obtain high compressive strength of concrete, the water to cement ratio of the concrete should be optimised such that the minimum quantity required to achieve adequate workability is used. Reducing the water to cement ratio leads to a reduction in capillary porosity action and hence increase the strength and durability (Yaman et al., 2002) furthermore, reducing the water content ensures entrapped air cannot disperse and influence the concrete mix design. In a study by Schmidt and Fehling (2005) optimum water-binder ratio between was shown to be between 0.18 and 0.25 depending on the admixture, mixture type and process and particle size distribution.

2.3.2 Mixing procedure

To produce UHPFRC intensive mixing is typically required to ensure adequate mixing of the constituents due to the difficulty in dispersing condensed silica fume agglomerates and fibres within the mix (Kazemi & Lubell, 2012). The influence of mixing procedure and mixture type affects the rheological and mechanical behaviour of UHPFRC (Dils et al., 2012; Mazanec & Schiessl, 2008; Schachinger et al., 2004). A higher mixing speed can reduce the mixing time of UHPFRC; however over speeding can lead to change the behaviour of UHPFRC (Dils et al., 2012). The parameter related to the mixing determines the overall efficiency of the mixer. According to the (EN-206-1, 2002), variability of different influencing factor divides the efficiency of the mixers as ordinary mixers, high performance or intensive mixers. Intensive mixer is a widely accepted mixing in the field of the UHPFRC which consist of a rotating pan transporting the material to be mixed and an eccentrically mounted tool performs the mixing function to mix the concrete. Dils et al. (2012) investigated that an intensive mixer with rotating pan has the negligible variation of error than the type mixers so it reveals intensive mixers.

The mixing process of UHPFRC can be done according to the following procedure. Initially, all of the dry components cement, silica fume and fine aggregate and coarse aggregate are mixed together and then the water and admixture added with well combined dry components. The mix is continued until it appears flowable and then the fiber is added and rotates the machine for 5 minutes for uniform mix. The mixing procedure of UHPFRC is shown step wise from beginning to end in Fig.2.3.

Fig.2.3 Mixing procedure of UHPC (Graybeal, 2005)

Mixing time required for UHPFRC preparation with different type of mixtures is not the same. The total mixing time of UHPFRC depend on the mixture type, volume of the mix and rotating speed. Rotating speed usually taken between 7 and 25minutes (Wille et al., 2011; Yu et al., 2014) depending on the fines content and mixer power (Schachinger et al., 2004) for uniform flowable UHPFRC mixes. Friction of the particle increased when the coarse aggregate is added in the mix leading to higher energy consumption, hence the time required to fluidize the concrete is lower (Ma et al., 2004). However, the finest constituents require the longer time of mixing which leads to less friction between particles with the fluid. Hence, it is obvious that with an increasing the aggregate diameter decreases the time of mixing. The method of admixture addition also influence the workability of UHPFRC (Schachinger et al., 2004; Schießl et al., 2010) with research suggesting that the admixture can be divided into two amounts and first part is added after the water added in the mix. After that, the second part is added after agglomerates are formed in the mix (Kazemi & Lubell, 2012) and it provides higher workability (Stähli, 2008).

2.3.3 Casting and curing regimes

The casting process is important to obtain the good mechanical behaviour of UHPFRC. It is chosen based on the concrete element employed for the test and fiber orientation is of great importance for UHPFRC casting element. This process is very effective when linear elements pouring and enhances the casting speed present of fibers in the mixes. After mixing, casting should be done quickly to avoid the setting of concrete. The total casting time depends on the number of specimens and specimen volume. The fresh UHPFRC poured into three layers and each layer vibrates on a shake table for homogeneous mix in the mould. After the mixing it can be helpful wait few minutes prior to the pouring for the entrapped air arise in the

mixes. Before vibration of mould, it is suggested that air should be removed from the concrete to increase homogeneity of mix which can lead to improved rheological and mechanical behaviours (Schachinger et al., 2004).

Curing is the traditional way to enhance hydration of cement and pozzolanic reaction of silica fume and consists of a control of temperature and moisture movement from the concrete (Habel et al., 2006; Prem et al., 2013; Wille et al., 2012). Curing leads to better strength development due to more water allows for the hydration of the cement paste. It is also improve the compressive strength, get better resistance to abrasion and reduces surface dusting of specimens (Austin et al., 1992). Curing can be done in several ways for UHPFRC with conventional, steam, pressure, autoclave, thermal and heat curing all having been investigated. The conventional and steam cured is shown in Fig.2.4. Conventional curing is the most popular technique for UHPFRC; however nowadays heat or steam curing also achieves much more acceptance from the research community (Askar et al., 2012; Graybeal & Davis, 2008; Graybeal, 2007; Justs et al., 2010; Yang et al., 2009). The advantage of heat or steam curing is to achieve early age strength, eliminate shrinkage, decrease creep coefficient and save time for testing (Fehling et al., 2007). The best performance of UHPFRC at early age strength is achieved with heat curing at higher temperature (Hong et al., 2010). The pozzolanic reaction is stronger at high temperature when silica fumes and Portland cement present in the mixes. At early age best strength of UHPFRC can achieved with heat curing at high temperature level; however heat curing can be avoided due to the energy consumption (Hong et al., 2010). Consequently, some of the studies investigated that the UHPFRC shows higher strength values using conventional aggregate except at an early age where heat curing accelerates strength gain (Kazemi & Lubell, 2012; Wang et al., 2012; Wille et al., 2011; Yu et al., 2014).

A little number of researchers has been carried out on UHPFRC preparation with water curing conditions. Research investigated by Camacho and Serna (2010) observed that the UHPFRC specimens compressive strength did not increase cured around 80^0C in water for 24 time period hours comparing with 28 days strength in 20^0C conventional curing. When the cement reaches a peak rate of hydration that is the appropriate time to apply the heat curing. Hence, the reactions induced by the temperature are higher that time. Consequently, researchers (Askar et al., 2012; Toropovs et al., 2013) concluded that the heat or water boiling curing methods enhanced the early age compressive strength of UHPFRC which is contradictory with Camacho and Serna (2010). Therefore, it is required further investigation on strength characteristics of UHPFRC specimens with heat or water curing, especially at early age strength.

Fig.2.4 Curing process (a) Specimen stored at 20^0C (b) The specimens cured with steam (Camacho Torregrosa, 2014).

2.4 Rheological Properties of UHPFRC

Rheological properties refer to measures of the workability of UHPFRC. Ensuring adequate workability of the concrete is important as only with correct placement will the full strength and durability potential of the concrete be achieved. Concrete can be

considered workable when it shows no segregation or bleeding. Rheological properties of UHPFRC is depends on the cement, silica fume, fine or coarse aggregate, SP, water and type and amount of steel fiber addition in the mix. The main variable factors are the cement, SP and water content in the UHPFRC mix. Rheological property is depends on the fluidity of cement paste. The other factors such as temperature, humidity, method of compaction, methods of placement also affects the rheological properties of UHPFRC.

2.4.1 Effect of superplasticizer content

The purpose of using SP in the UHPFRC mixes is to increase workability, reduce the mixing water, reduce creep and shrinkage cause by the heat of hydration (Collepardi et al., 1999). Rheological properties of concrete are greatly influence by the type of high range water reducer and its chemical reaction with cement paste. The most common type of SP used for UHPFRC manufacture are based on polycarboxylate group (Schröfl et al., 2008). Some of the researchers investigated the effect of SP on the rheological behaviour of UHPFRC (Schießl et al., 2010; Wille et al., 2011). The addition time of SP during the mix has great influence the rheological properties of UHPFRC. It is observed that mixing sequence of SP or addition method has greatly influence the rheological properties of UHPFRC (Schachinger et al., 2004; Shihada & Arafa, 2010). Few investigation suggested that stepwise addition of SP increase the workability of the mix that leads to the less air void and the higher cement activity and more effective the formation of first germs of primary ettringite throughout the mixing (Tue et al., 2008). Dils et al. (2012) found that a delayed addition of SP can improve workability, especially when low water-cement ratio is used. Similar finding also observed by Hemalatha et al. (2015) that acceptable flow is noticed when SP addition time delayed but there are no influences on the hardened property. Wille et

al. (2011) studied the influence of high range water reducer on UHPFRC over a range 1 to 8% weight of cement. They observed that the optimum range of high range water reducer between 1.4 to 2.4% of cement weight increased both the flow ability and compressive strength. The compressive strength of concrete using SP shows higher strength and reduces the water content up to 32-33% (Basile et al., 1989). No segregation and bleeding of concrete occur and high amount of workability can achieved due to the addition of SP in the UHPFRC mix (Aignesberger & Kern, 1981).

2.4.2 Effect of fiber type and content

Rheological properties of UHPFRC are considerably affected by the fiber type and content, aspect ratio, orientation and distribution (Camacho Torregrosa, 2014; Kazemi & Lubell, 2012). Several researches have investigated UHPFRC with different aspect ratio of fibers, different types of fibers and amount and the orientation of fibers to achieve good mechanical strength as shown in Figs. 2.2(a) and 2.2(b) (Camacho Torregrosa, 2014; Kim et al., 2011; Sbia et al., 2014; Wille et al., 2014a; Wille et al., 2014b). However, the studied by Rossi (1992) concluded that volume fraction and aspect ratio of the fibers produce a decrease of the workability. Table 2.4 represents the properties of different types of steel fibers by Camacho Torregrosa (2014). It is also shown in Table 2.4 that number of fiber per kilogram needed based on the fiber weight and length. Kazemi and Lubell (2012) carried out an experimental investigation on UHPFRC using locally available materials and a volume fraction of short smooth steel fibers between 0 to 5%. They concluded that the maximum of fiber volume fraction of between 3 or 4% provides reasonable workability in terms of casting and finishing. Yoo et al. (2014) investigated the effect of fiber length and placement method on the compressive, flexural and softening behaviours of UHPFRC. They also demonstrated the fiber orientation characteristics

of this concrete. Fiber orientation is a great influencing factor to produce good characteristics of UHPFRC and it is controlled the flow behaviour and it governs by the direction of flow, gravity and wall effect (AFGC/SETRA, 2002). Numerous researchers concluded that rheological and mechanical properties have significant effect with different amount and type of fiber content in the mix (Ahmad et al., 2014; Al Madhoun; Ponikiewski & Gołaszewski, 2013).The coarse aggregate addition in the UHPFRC with steel fibers is affected the workability compare with without coarse aggregate in the mix (YANG et al., 2012; Yang et al., 2009).

Table 2.4 Properties of different types of steel fibers (Camacho Torregrosa 2014)

Fiber Type	Diameter-d_f (mm)	Length-L_f (mm)	Aspect ratio (L_f/d_f)	Tensile Strength (MPa)	No. of Fiber per kg
Smooth steel fiber	0.160	13.0	81.0	2000	490.0
Macro hooked fiber-A	0.375	30.0	80.0	2300	38.60
Macro hooked fiber-B	0.540	35.0	64.8	1200	16.10
Macro hooked fiber-C	0.440	35.0	79.6	1200	24.30

2.5 Hardened Properties of UHPFRC

The most basic and arguably most significant property of concrete is its compressive strength and corresponding stress-strain characteristics. Compression strength of UHPFRC is generally depends on the shape and size of the specimen, rate of load application, curing regime conditions, manufacturing technique, method of capping, fiber orientation, and type and amount of steel fiber addition in the mix.

2.5.1 Axial behaviour in compression

The uniaxial stress-strain response is the measure of specimen behaviours under compression loading. This is the direct relationship between compressive strength of concrete and stress-strain based properties. Compressive stress-strain responses of different concrete have shown significant variation because of heterogeneous nature

of concrete. Compressive strength of concrete is the basic and most important material parameter for design concrete structures. That's why it can be a useful and easy way parameter to develop a dosage optimization. One of the very potential concrete parameter relationships correlates the stress-strain response of the concrete material, compressive strength and secant stiffness. In the recent years, ultra-high performance concrete has shown excellent compressive strength behaviours under concentric axial loading. Researchers are giving effort to find out the full behaviours of new class of UHPFRC. Due to its high compressive behaviour, the parameters related to the behaviours including method of measurement, testing technique and set up and capture the descending or softening branch are different than the normal concrete.

2.5.1.1 Method of measurement

Generally, the hardened concrete properties are determined by following the standard compressive strength tests method. Many recognised standards (ASTM-C469-94, 1994; BS-1881-121:1983, 1983) have given detailed guidelines for the measurement of the strain corresponding to stress in compression for conventional concrete using cylinder and cube specimens. Ultra-high performance concrete compressive testing method does not follow the same trend as conventional strength concrete due to its ductile characteristic after the post-peak or softening region. The main major challenge of UHPFRC testing is to obtain the full stress strain response on softening branch. This concrete shows very high compressive strengths exceeds more than 150MPa at failure stage. So, it is required advanced test set up to get the softening branch of UHPFRC. The suitable loading rate and type should be determined before the testing of UHPFRC. Some of the researcher did not measure the deformation platen to platen of UHPFRC and hence have only quantified the ascending branch of

the stress strain relationship (Graybeal, 2007). New test methods has been invented to capture the softening branch of UHPFRC with platen to platen deformation measurement by Hassan et al. (2012) and Prabha et al. (2010). Hassan et al. (2012) developed a simple test method to capture full stress strain behaviour of UHPFRC by measuring platen to platen deformation of specimens. They achieved very good ductility response with their new test methods. The research also recommended that the test method described in both (BS-1881-121:1983, 1983) and (ASTM-C469-94, 1994) standards were unsuitable for UHPFRC, especially in the measurements of post-cracking behaviour for UHPFRC specimens. Kazemi and Lubell (2012) used the deflection control test method and suitable loading rate to obtain the full stress strain response of UHPFRC with variation of fiber volume fraction. They were determined very good ductility response by using their test methods. Prabha et al. (2010) designed a test methods under deflection control loading recommended by Rilem (2000) to capture the post-peak response of UHPFRC. They found that the designed test method is suitable to obtain good stress-strain response of UHPFRC. From the above circumstances, it can be seen that very few test methods has been developed to determine the post-peak response of UHPFRC until final failure; however there are still need to be quantified ductility response with a suitable design methods of measurement platen to platen to obtain full behaviours of UHPFRC.

2.5.1.2 Ascending branch or peak behaviour

Ascending branch of stress-strain behaviours of concrete material is important criteria and a basic concrete parameter. In the stress-strain curve of UHPFRC, the linear elastic materialistic behaviour is more obvious than the conventional concretes, particularly the specimen behaviours at long term (Lappa, 2007). It is investigated that with an increasing the compressive strength decreased the pre-peak

nonlinearity. Additionally, the basic shape of the ascending branch of the compressive stress-strain responses of UHPC remains unchanged when applied the steam treatment applied on cylinders (Graybeal, 2007). Concrete modulus of elasticity is derived from the ascending part of the stress-strain curve and that can be used in numerical simulation to obtain member serviceability behaviours. There are no permanent deformation occur at the initial stage of elastic region of curve. The maximum compressive strength attained in the end part of elastic region is the peak strength of the concrete where fibre does not affect significantly relatively small effect on the pre-cracking compressive strength and elastic modulus. The modulus of elasticity of UHPFRC is higher than the conventional concretes. Moreover, the modulus of elasticity of UHPFRC with the presence of steel fiber increased by 6-10% than the ultra-high performance concrete (Hassan et al., 2012). Ascending curve of UHPFRC depends on the curing process, type of aggregate used in the mixes, and the paste volume fraction. Modulus of elasticity is higher when coarse aggregate added in the mixes with steam cured specimens (Yang et al., 2009). The dispersion of the data is high since the modulus of elasticity greatly depends on coarse aggregate used in the mixes.

Several researchers have determined fundamental empirical based numerical approximations to get the ascending branch of concrete using basic material properties (Carreira & Chu, 1985; Hognestad, 1951; Neville, 1995; Popovics, 1998). All of these efforts were done for normal strength concrete. However, there are very limited numbers of work carried out on the uniaxial stress-strain response of UHPFRC, especially ascending branch behaviours (Del Viso et al., 2008; Graybeal, 2007; Lubell & A.S., 2011). Graybeal (2007) predicted the ascending branch equation which relates the strength gain over time and modulus of elasticity as a function of compressive strength. He also conducted an experimental investigation

on UHPFRC and compare with predicted equations. He found that modulus of elasticity of UHPFRC can be predictable within the compressive strength range 25 to 193 MPa. The predictable equation gives good representation in the ascending branch. Also, the compressive stress-strain behaviour of UHPFRC is within 5% of linear elastic at 80% compressive strength. Del Viso et al. (2008) also agree that there is a loss of linearity before reaching the peak strength amongst the similar types of specimens. However, Lubell and A.S. (2011) observed that stress-strain response of UHPFRC is linear until the peak compressive strength with respect to specimen size and fiber content.

2.5.1.3 Post-peak or softening branch

The softening or descending branch of stress-strain behaviours of concrete material plays an important role to quantify the overall performance of concrete structure at failure and having concrete material ductility is important in ensuring structures behave in a ductile manner, since it is essential to avoid a brittle failure of the structure by ensuring enough deformation at the ultimate limit stage. Ductility is rooted in a material ability to dissipate energy, especially after energy dissipation has initiated. Moreover, the descending branch of UHPFRC is mainly depends on the loading control, fiber volume fraction and fiber type. Due to the brittle behaviour of the resulting matrix, UHPFRC mix consists of the steel fiber reinforcement. Softening behaviour is enhanced through the inclusion of steel fiber at optimum content. In addition, fiber influence on the post-cracking behaviour and failure mechanism is more obvious for UHPFRC specimen. UHPFRC specimen exhibits elastic nature up to approximately 90–95% of their peak strength, followed by compressive strain hardening response (Hassan et al., 2012). Strain softening governs due to the presence of fibres after the peak strength that leads to the interaction

between the fibres and the matrix contributes to ductile compressive failure. It is concluded that the nature of softening response for the UHPFRC specimens under compression is difficult to determine until failure. This can be attributed to the truth that fibres volume fraction, fiber type, orientation and distribution of fiber has effect on the ductility nature of UHPFRC. Further investigation on the ductility response of UHPFRC is needed to achieve consistent material properties.

Numerous works have proposed models for the softening branch for normal strength concrete using basic material properties (Carreira & Chu, 1985; Desayi & Krishnan, 1964; Popovics, 1973; Saenz, 1964; Tsai, 1988; Yip, 1998). Some of the research proposed the softening branch equation for high strength concrete with or without confinement (Attard & Setunge, 1996; Hsu & Hsu, 1994; Mander et al., 1988; Wee et al., 1996). There are still scarce in the literature to predict the softening response of UHPFRC under compression with suitable test method. A small number of works have been investigated to capture the softening branch of UHPFRC (Habel et al., 2008; Hassan et al., 2012; Kazemi & Lubell, 2012; Lubell & A.S., 2011; Sbia et al., 2014). Hassan et al. (2012) conducted the experimental investigation on the development of appropriate test methods to determine the mechanical properties including ductility response of UHPFRC both compressive and tensile stress-strain behaviour reinforced with steel fibers. They developed a simple test method to capture the softening behaviours of UHPFRC and improved ductility response substantially in compression. Moreover, it was found that the developed simple method is very suitable to determine the softening response of UHPFRC until failure stage. An experimental investigation carried out and softening branch was captured by using of displacement control test method by (Kazemi & Lubell, 2012; Lubell & A.S., 2011). They observed that higher fiber volume fraction shows a short region of hardening response followed by a good descending branch.

2.5.1.4 Size effect responses

It is commonly known that the material properties and behaviour of concrete is directly related to the size and geometrical effects of the specimen. It has been widely observed that the size of the concrete specimen subjected to concentrate loading controls its behavior. This observable fact is known as a ‘‘size effect’’. Size effect is known as a relative change of the structural properties including the peak resistance, strain at peak stress and the slope of the softening branch (ductility). A small number of researches have been conducted on the influence of specimen size with different fiber content and compressive behavior of ultra-high performance fiber reinforced concrete (Graybeal & Davis, 2008; Kazemi & Lubell, 2012). The length of the damage zone has been estimated to be about 2-3 times the width of the specimen (Van Mier et al., 1997). It is constructive to observe the modeling of tension localization of concrete to compare with localization under compression. The damage part of concrete specimen grows in length, and the density increases during the post-peak part of the test. Some of the studies have been concentrated on cracking of specimen during post-peak response (Kotsovos 1983; Shah and Sankar 1987; Torrenti et al. 1993; van Mier 1984; and Vonk 1992). The failure in uniaxial compression is due to a localization of the damage in a certain zone as it was shown by Van Mier (1984). In addition, RILEMTC 148 “Strain Softening of Concrete” focused on localization in compression. Van Vliet and Van Mier (1996) extended the round robin test program developed by RILEM TC 148 to prisms whose slenderness ratio was between 0.25 and 2.0, and Jansen et al. (1995, 1997) varied the slenderness between 2.0 and 5.5.

The compressive and post-peak response of ultra-high performance fiber concrete is improved through the inclusion of steel fibers (Hassan et al., 2012; Kazemi & Lubell, 2012). Several research has conducted the relationship between various cylinder and

cube sizes on the compressive strength and stress-strain response of concrete (Del Viso et al., 2008; Graybeal, 2007). Graybeal and Davis (2008) found that cube specimens gave higher compressive strength than the cylinders and the strength increased about 14%. On the other hand, the smaller sizes of specimens tend to show higher compressive strengths and decreased the strength up to 15% when the specimen sizes make it doubled (Lubell & A.S., 2011). Another experimental investigation carried out by Kazemi and Lubell (2012) and compared the influence of specimen size and shape on the compressive strength of UHPFRC with V_f= 0-5% of short smooth steel fibers. Fig.2.5 shows the clear picture of size effect of UHPFRC for cylinders and cubes specimens.

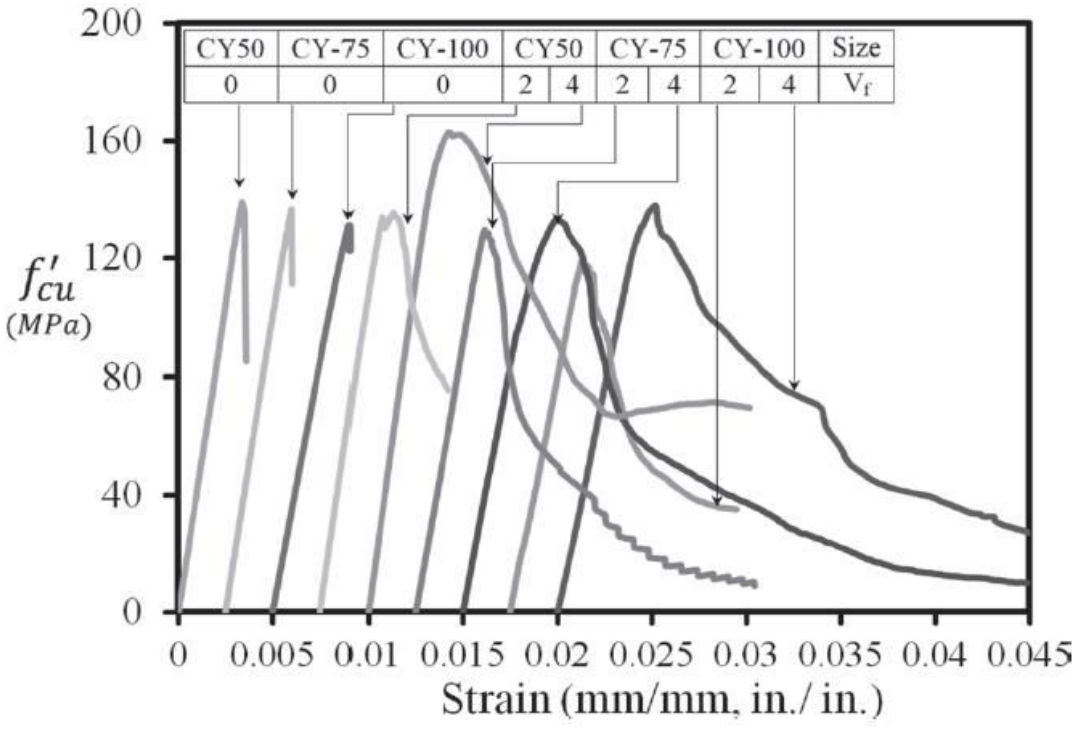

Fig.2.5 Typical stress-strain curves from compressive tests of different cylinder sizes (Kazemi & Lubell, 2012)

The curves are offset horizontally to avoid overlap because the initial slopes of each curve are similar. Mixtures with steel fibers exhibited ductile post-peak responses because the steel fibers partially restrained the lateral expansion and enabled larger axial deformations. They observed that smaller specimen sizes showed higher

compressive strengths than larger specimens but no clear relationships were established between the peak compressive strength of cylinder and cube samples of different sizes as the fiber volume fraction changed.

One of the recent works has been done on size dependent stress-strain model for unconfined concrete by Chen et al. (2013). They proposed that concrete deformation due to compression is both a material property and a shear-friction mechanism and it can be obtained stress-strain relationship by considering the deformations that is size dependent. They also proposed a relationship of the stress-strain curve from cylinder tests of one specific length can be modified to determine that for any size of cylinder. Depending on the method of measuring the strain, it is know that the global stress-strain relationships depends on both the shape which will be defined as standard compression cylinder tests in which the slenderness factor μ equals 2.

$$\mu = \frac{L_{pr}}{d_{pr}} \qquad \text{Equation (2.1)}$$

and the size of the specimen which will be defined as

$$\eta = \frac{L_{pr-1}}{L_{pr-2}} \qquad \text{Equation (2.2)}$$

Where, (L_{pr-1}) = a specific size of specimen

(L_{pr-2}) = specimens of any size

It is observed that that when μ exceeds 2, the strength f'_c hardly varies, and also the length is increased, that is the strength is independent of the size factor η.

Fig.2.6 shows the size dependent stress-strain behavior of different length of concrete specimens. The global strain of 200mm specimen can be expressed by the equation.

$$(\varepsilon_{axgl-200})_n = \left[\left(\varepsilon_{axgl-test}\right)_n - \left(\varepsilon_{mat}\right)_n\right]\frac{L_{pr-test}}{L_{pr-200}} + \left(\varepsilon_{mat}\right)_n \qquad \text{Equation (2.3)}$$

Where

$(\varepsilon_{mat})_n$ = material strain

$(\varepsilon_{axgl\text{-}test})_n$ = test value of global strain

$L_{pr\text{-}test}$= test value of specimen length

However, for the specific strain ε_{co} at the peak stress f_c, the above equation can be written as

$$\varepsilon_{co-200} = (\varepsilon_{co-test} - \frac{f_c'}{E_c})\frac{L_{pr-test}}{200} + \frac{f'_c}{E_c} \qquad \text{Equation (2.4)}$$

Where $\varepsilon_{co\text{-}200}$ is the global strain at the peak stress f_c

$\varepsilon_{co\text{-}test}$ is the measured global strain at the peak stress in the test.

E_c is the tangent modulus of concrete

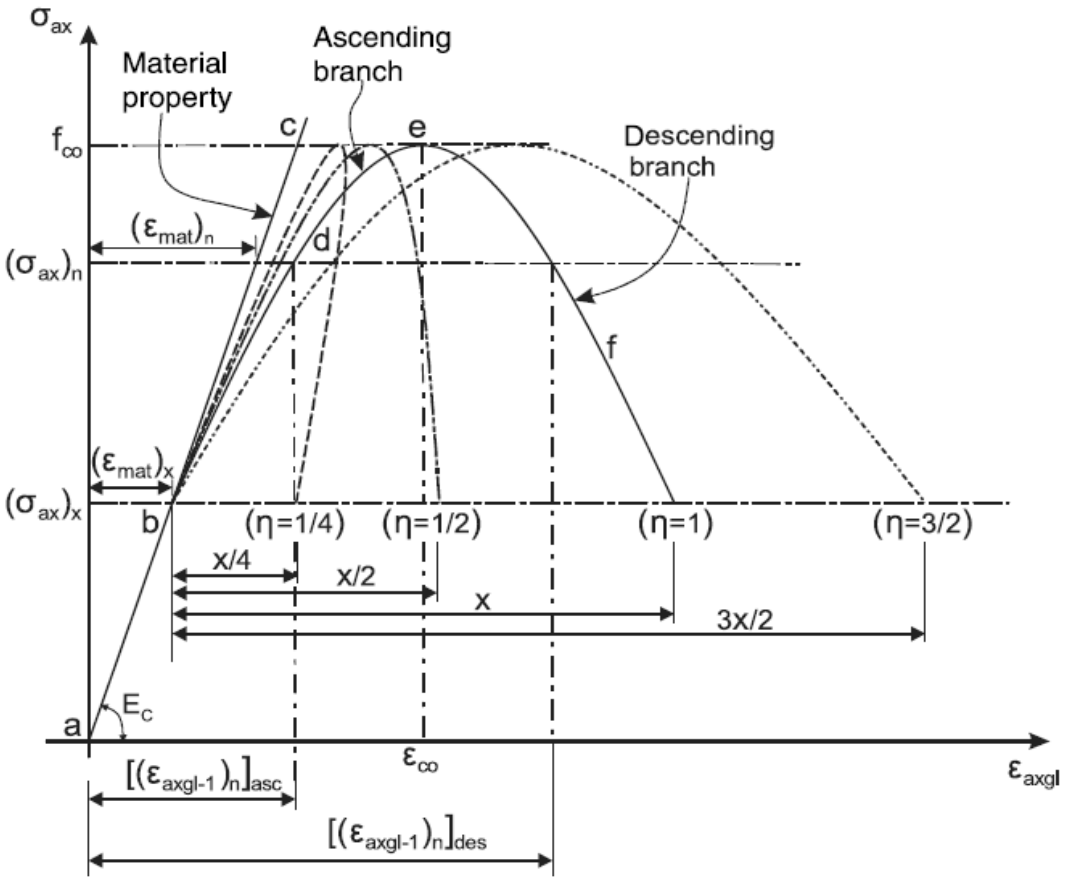

Fig.2.6 Size dependent stress-strain behaviour of concrete by Chen et al. (2013)

To determine the best relationship between ε_{co200} and f_c, linear regression is given

$$\varepsilon_{co-200} = 4.76\times10^{-6} f'_c + 2.13\times10^{-3} \qquad \text{Equation (2.5)}$$

They used the Popovics (1973) equation to determine the stress-strain response which can be written in the form:

$$\sigma_{ax} = f_c' \frac{\left[\frac{(\varepsilon_{ax})_{pop}}{\varepsilon_{co-200}}\right] r}{r - 1 + \left[\frac{(\varepsilon_{ax})_{pop}}{\varepsilon_{co-200}}\right]^r} \qquad \text{Equation (2.6)}$$

Where

$(\varepsilon_{ax})_{pop}$ is the strain in Popovics expression

$r = E_c/[E_c - (f'_c/\varepsilon_{co-200})]$ Equation (2.7)

ε_{co-200} is the strain for cylinders of length 200 mm.

To derive the stress-strain relationship for any size of specimen finally the above mentioned equation can be written in the following form.

$$\varepsilon_{axgl} = \left[(\varepsilon_{ax})_{pop} - \varepsilon_{mat}\right]\frac{200}{L_{pr}} + \varepsilon_{mat} \qquad \text{Equation (2.8)}$$

Chen et al. (2013) computed the response for different length of specimen which satisfied the slenderness requirement $\mu \geq 2$. The peak strength averaged values were 48 MPa, 90MPa and 41 MPa these are plotted in Fig.2.7(a), (b) and (c) respectively. The slenderness μ ranged from 2 to 4 and the prism lengths L_{pr} ranged from 200 mm to 800 mm. It is observed that the increasing of the length of the specimen shows steeper response. Moreover, it can be seen in both of the figures that the analysis can also simulate the snap-back and it more pronounced with highest length of specimen.

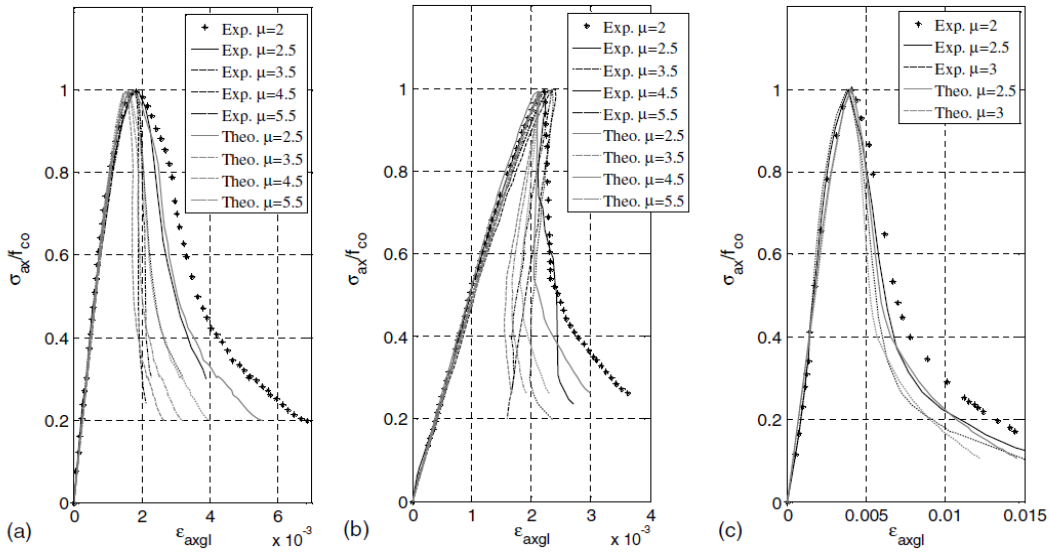

Fig.2.7 Stress-strain response of cylinders with variation of sizes (Chen et al., 2013)

The comparison of the stress-strain curves for selected height-to-diameter ratios determined by Jansen and Shah (1997). It is observed in Fig.2.8 that the pre-peak portion of the curves shows no significant effect due to length changes; however the post-peak curves are highly dependent on the specimen length and shows significant changes. They also observed the localization of the specimen. The length of the failure zone of the longer specimens is near about 300mm or 3 times the specimen diameter. Similar finding is also observed by others for long slender specimens.

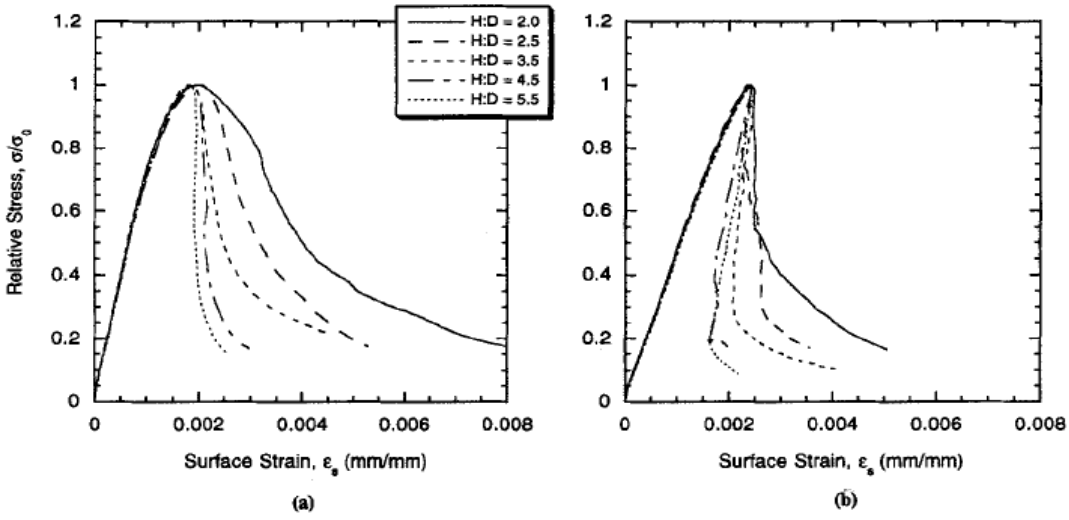

Fig.2.8 Typical stress-strain behaviour for range of height-to-diameter ratio (a) Normal strength (b) High strength concrete (Jansen & Shah, 1997)

Fig.2.9 shows comparison of stress-strain curves for cylinders specimens of each size and shape. It is seen that a sudden drop in the load takes place after the peak load and there are no significant changes in the softening branch between the scaled tested cylinders. Stress-strain curve under compression of different slenderness ratio is illustrated in Fig.2.10. Compression failure a description of the stress-strain diagram before the peak, and after the peak, may be expected to be a more realistic material model than just a simple stress-strain curve. It is observed that snap back of the curve is more pronounced with increasing the length of the specimen by means of steeper curve. Complete stress-strain curve of different slenderness ratio is presented in Fig. 2.11. It can be seen that an increase in stiffness was observed with increasing slenderness ratio of the specimen; however the ultimate strain gives almost similar value.

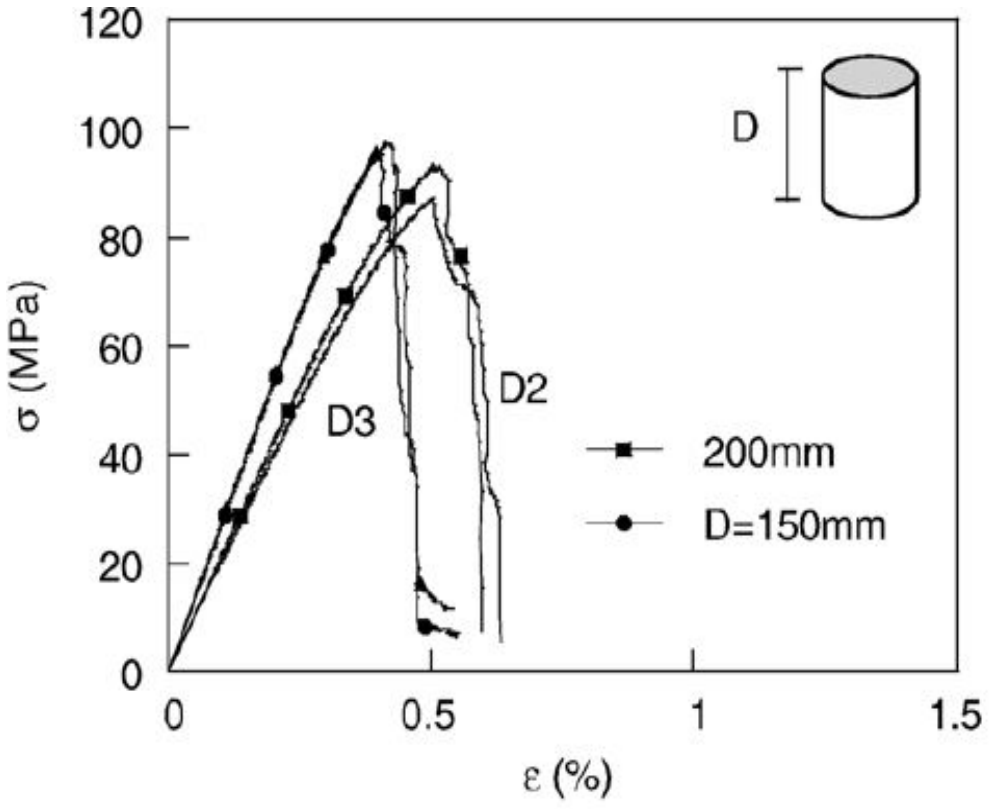

Fig.2.9 Typical stress-strain behaviour for range of height-to-diameter ratio with size effect on peak strength (Del Viso et al., 2008)

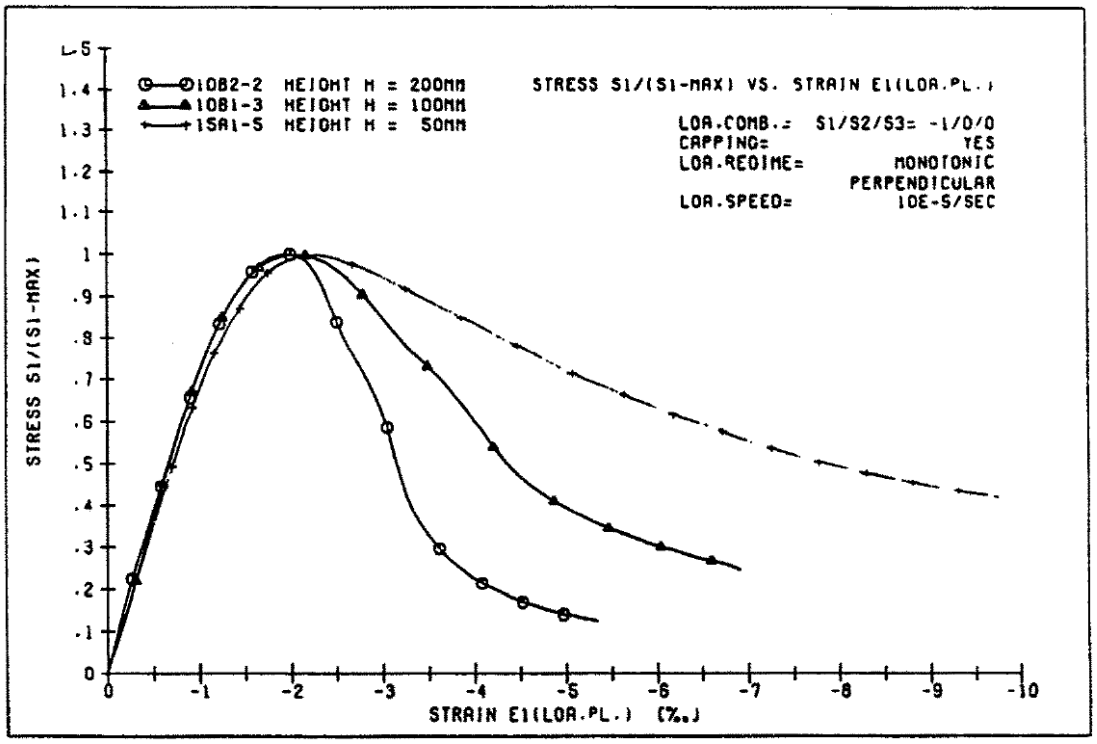

Fig.2.10 Stress-strain curve under compression for different length of specimen (Hillerborg, 1990)

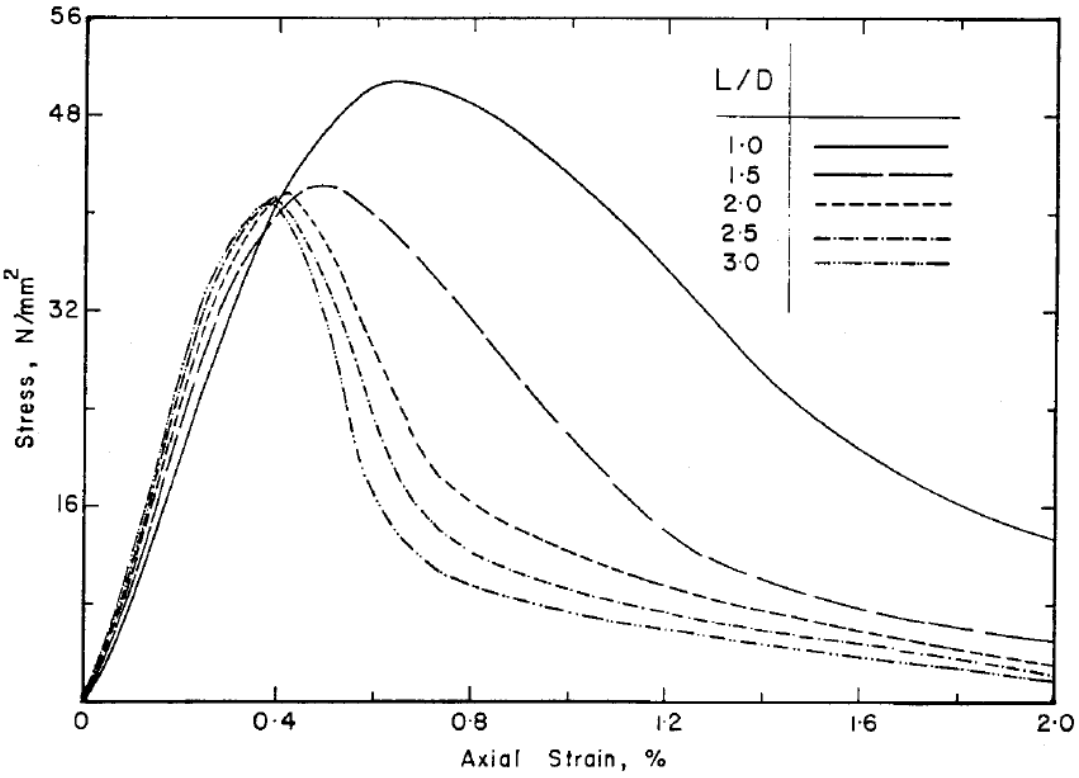

Fig.2.11 Complete stress-strain curve of different slenderness ratio (Sangha &Dhir, 1972)

2.5.1.5 Influence of steel fiber type and amount

The influence of the addition of short discontinuous steel fibres reinforcement increased both compressive strength and ductility characteristics. Steel fibers improved the brittle nature of the resulting matrix of UHPFRC when includes fiber reinforcement. The volume fraction of about 2% added to the UHPFRC mix to obtain the good strength and post-peak response (Hassan et al., 2012). However, Kazemi and Lubell (2012) was investigated the ductility response of UHPFRC formulated up to 4% volume fraction of short steel fibers and achieved good ductile post-peak response until failure. A small amount of research has been conducted in recent years on UHPFRC to determine the ductility behaviour with different methods of testing and instrumentation (Wille et al., 2014a; Wille et al., 2012).Structural performance of UHPFRC with different fiber length has been conducted by Yoo et al. (2015). They concluded that an increase in fiber length and twisted steel fibers resultant to the improvement of post-peak and ductility behaviours. A similar finding was also observed using twisted steel fiber by Wille et al. (2014a) to obtain the strain hardening response of UHPFRC for direct tensile loading. The effect of different macro steel fibers with volume content 0-1.5% on the flexural response of hybrid UHPFRC was carried out by Kim et al. (2011). They observed that longer hooked end and twisted steel fibers with 1.5% fiber content exhibit better flexural, deflection capacity and energy absorption capacity than other fibers. Sbia et al. (2014) investigated that the optimum reinforcement system, which comprised Polyvinyl alcohol (PVA) and Carbon nanofiber (CNF) of 0.37 and 0.047 volume percentage of UHPFRC improved the flexural strength, deflection capacity and compressive strength. Al-Jubory (2013) carried out an experiment on reactive powder concrete with different types and volume fractions of 1-2% steel fibers. He found that fibers have shown good performance in terms of both the higher strength properties and the

ultimate failure stage due to the higher volume fraction of fiber. It can be seen that the compressive strength and post-peak ductility responses are enhanced through the incorporation of short steel fibers in the UHPFRC mixes. Consequently, to date very small number of research has carried out to quantify the ductility post-peak behaviours compare to the fiber volume fraction and different fiber type.

2.5.2 Dilation behaviour in compression

Dilation of specimens is the measurement of expansion amount under compression loading. It has a strong correlation with compressive strength of concrete and stress-strain behaviours at elastic and softening region. Also, it correlates the stress-strain response of the concrete material, modulus of concrete, peak strength, and post-peak response. Although research has been quantified on the dilation behaviour of high strength concrete theoretically and experimentally, however very much limited information found in the literature on dilation behaviour of UHPFRC.

2.5.2.1 Method of measurement

Ultra-high performance concrete shows very high compressive strengths than the conventional concrete. Due to its higher strength capacity, the failure mode exhibits explosive type. Therefore, new and advanced test set up method is required to achieve the softening post-peak branch when incorporating fiber. The fiber volume fraction has a significant effect on the post-peak softening response of UHPFRC (Kazemi & Lubell, 2012). Generally; dilation strain of the UHPFRC specimen's measured by strain gauge (Graybeal, 2007; Hassan et al., 2012; Kim et al., 2011). However, strain gauge can measure up to the peak strain after that it cannot capture the softening part. Dilation should be measured by the LVDT in the lateral direction of the specimens. There are very scarce the literature to capture the dilation deformation of UHPFRC into the softening region.

2.5.3 Test rig and instrumentation

The design of the test rig is based on the specimen geometry and the required information. For specimens under compression is required steel platen at top and bottom to apply the concentric load uniformly. Strain gauges attached on the specimen surface with glue are used to measure the strain for both axial and lateral direction and these provide information only until the onset of cracks associated with concrete softening. LVDT's are used to measure the axial and lateral contraction of the specimens and provide information on the total contraction of the concrete including sliding along softening wedges and hence provide an indication of the full stress strain behaviour (Chen et al., 2013).

2.6 Summary

Based on the literature review presented in this chapter, the following points are observed:

Most of the experimental investigation was conducted on mix design and manufacturing of UHPFRC utilising expensive silica sand which exhibit higher compressive strength. Researchers have also reported the UHPFRC manufacturing with granulated blast furnace slag and coarse aggregate addition as a replacement of fine or coarse aggregate. It is important to understand under what circumstances the properties of UHPFRC changes. To contribute to this understanding, mixing methods, casting of specimen and curing regimes are the fundamental factors that influence the properties of UHPFRC. Numerous experimental investigations carried out to find out the reason of changing the behaviour. Few researchers examined the cost efficiency study of UHPFRC. Limited number of work have been investigated on the UHPFRC properties utilising local materials or addition of coarse aggregate to

achieve the similar compressive strength as like silica sand mixes and leads to reduce the cost. It can be observed from literature review, although very little work has been conducted on UHPFRC to obtain the suitable mix design, effect of fineness modulus of sand and the cost associated with conventional material use instead of expensive silica sand is very limited in the literature.

It can be seen from the literature review that a small number of researches has been carried out on the influence of specimen size and ductility behaviour with the variation of fiber content and type. Size effect and ductility behaviour depends on the testing technique and measurement method of deformation, especially after the post-peak load. Several researchers conducted their experiment on UHPFRC with the new test method and measurement technique. Most of the experimental researches conducted on the size effect behavior of normal and high strength concrete. A number of researches predicted the size effect responses with the variation of slenderness. Although very little work has been carried out on the size effect and ductility responses on UHPFRC, however there are still need to do much effort on the size effect and ductility behaviour of UHPFRC variation of fiber content and type with suitable method of testing and measurement technique. Finally, these size dependent ductility responses of specimens can be incorporated to determine the rotation capacity of plastic hinges in UHPFRC members. It was observed that dilation strain of UHPFRC measured by the strain gauge; however strain gauge can cannot capture the softening post-peak part. There are still need to be investigated the dilation deformation of UHPFRC to capture the softening branch by LVDT.

CHAPTER 3

MANUFACTURING ULTRA-HIGH PERFORMANCE CONCRETE UTILISING CONVENTIONAL MATERIALS AND PRODUCTION METHODS

Ultra-High Performance Fiber Reinforced Concrete (UHPFRC) is a recent advancement in concrete technology and is characterised by very high concrete compressive strengths (greater than 150MPa) and high material ductility. The development of strength and ductility of UHPFRC depends on its preparation, curing technique and mixture proportions. The mixing of UHPFRC has been shown to be significantly different to that of normal strength concrete and substantial research effort has been devoted to developing UHPFRC mix designs utilising highly specialised materials (Perry & Zakariasen, 2004).

Currently to achieve these material properties, careful consideration of raw materials and specialised mixing and curing techniques are typically required (Wang et al. 2012). For example in terms of materials:

a) Coarse aggregate is removed to enhance homogeneity;
b) High quantities of superplasticiser or water reducing agents are used to achieve low water : cement (w:c) ratios and hence improve strength;
c) Specially graded sands, silica fume and glass powders are used to reduce porosity, improve particle packing density and improve strength.

Moreover, the concepts of particle packing can be applied in order to optimise the density and flowability of a mix through the introduction of specifically graded materials (de Larrard and Sedran 1994). De Larraed and Sedran (1994) also proposed different approaches to design the concrete with optimised particle packing which is

an extension of the concepts of Fuller and Thomson (1907) who first showed over a century ago that the packing density of concrete aggregate has a major influence on the material properties of the resulting concrete. More recently based on the ideas of De Larraed and Sedran (1994), Fennis et al. (2009) have developed an ecological concrete mix design based on optimising particle packing.

In addition to utilising specialist materials, improved material properties can be obtained through specialised mixing and curing techniques, for example:

a) The use of a high intensity mixer can improve the dispersion of fine particles and blending of the cement and mineral admixtures (Dils et al. 2012);
b) Multi-stage curing processes, including steam curing may increase strength and the rate of strength gain;
c) The application of pressure during setting may reduce porosity and increase strength (Dugat et al. 1996; Teichman and Schmidt 2004).

While it is possible through the use of relatively complex materials, mixing and curing techniques to develop UHPFRC with strengths regularly exceeding 200MPa (Bonneau et al. 1997; Ipek et al. 2011) and in excess of 500MPa (Dugat et al. 1996; Teichman and Schmidt 2004), the increased complexity and hence cost of producing UHPFRC imposes limits on its widespread application. Initial uptake of UHPFRC has been primarily focused on high cost and long life infrastructure such as bridges (Greybeal and Hartmann 2005; Steinberg 2009) and to military applications where high strength and/or ductility is required such as for resistance to blast and impact loading (Wu et al. 2009; Yi et al. 2012). In order to broaden and increase the application of UHPFRC it is required that cost effective manufacturing techniques for using commonly available materials and methods of production be found (Trafraoui et al. 2009; Wang et al. 2012).

In Chapters 3 and 4 a series of optimised mixes are developed in order to provide mix design guidelines for the most appropriate water cement (*w:c*) and superplasticiser cement (*sp:c*) ratio required to achieve a target strength and workability for a particular aggregate grading.

In Chapter 3 the journal paper 'Manufacturing Ultra-High Performance Concrete Utilising Conventional Materials and Production Methods' is presented in which the investigating the potential to manufacture UHPFRC from conventional sands and coarse aggregates is investigated.

In Chapter 4 further information on the development of UHPFRC with conventional sands and coarse aggregates which could not be included in the journal paper are presented as well as an investigation into the development of UHPFRC using expensive higher performance silica sands.

Manufacturing Ultra-High Performance Concrete Utilising Conventional Materials and Production Methods

Sobuz, H.R., Visintin, P., Mohamed Ali, M.S., Singh, M., Griffith, M.C., Sheikh, A.H.

Sobuz, H.R., Visintin, P., Mohamed Ali, M.S., Singh, M., Griffith, M.C., Sheikh, A.H. (2016) Manufacturing Ultra-High Performance Concrete Utilising Conventional Materials and Production Methods.
Construction and Building Material, Vol. 111, pp. 251–261.

Manufacturing Ultra-High Performance Concrete Utilising Conventional Materials and Production Methods
Construction and Building Material, Vol. 111, pp. 251–261.

Sobuz, H. R. (Candidate)

Performed all of the experimental work, analysis of data and wrote manuscript

I hereby certify that the statement of contribution is accurate and give permission for the inclusion of the paper as thesis chapter

Signed.....Date.....

Visintin, P.

Supervised and contributed to the research

I hereby certify that the statement of contribution is accurate and give permission for the inclusion of the paper as thesis chapter

Signed.....Date.....

Mohamed Ali, M. S.

Help as a group member and manuscript evaluation

I hereby certify that the statement of contribution is accurate and give permission for the inclusion of the paper as thesis chapter

Signed.....Date.....

Singh, M.

Helped in experimental work and manuscript evaluation

I hereby certify that the statement of contribution is accurate and give permission for the inclusion of the paper as thesis chapter

Signed.....Date.....

Griffith, M. C.

Help to evaluate and edit the manuscript

I hereby certify that the statement of contribution is accurate and give permission for the inclusion of the paper as thesis chapter

Signed.....Date.....

Sheikh, A. H.

Assisted in manuscript evaluation

I hereby certify that the statement of contribution is accurate and give permission for the inclusion of the paper as thesis chapter

Signed.....Date.....

Manufacturing Ultra-High Performance Concrete Utilising Conventional Materials and Production Methods

Sobuz, H.R., Visintin, P., Mohamed Ali, M.S., Singh, M., Griffith, M.C. Sheikh, A.H..

Abstract

Ultra-High Performance Fiber Reinforced Concrete (UHPFRC) which is characterised by high strength and, when reinforced with steel fibres, high ductility, has the potential to revolutionise the construction industry. The application of UHPFRC is currently mainly limited to landmark projects due to the high cost of manufacture, which often involve specialist materials such as specially graded sands and the need for complex mixing and curing regimes. Moreover, mix designs are commonly proprietary information or incompletely reported. As a result of the complexity of material requirements and the restricted nature of complete mix design details it can be difficult to reproduce reported results. This paper aims to address these issues by investigating the potential for producing UHPFRC using widely available fine and coarse aggregates. It is shown that UHPFRC of compressive strengths in the range of 130-160MPa can be produced using commonly graded aggregates without the requirement for complex mixing or curing regimes. It has been shown that the fineness modulus of aggregates as well as the superplasticiser content strongly influences the compressive strength. An investigation of the axial and lateral stress- strain relationship of the mixes investigated show they possess a substantial residual stress plateau post softening.

Keywords: ultra-high performance concrete; workability; strength; axial stress strain; lateral stress strain

3.1 Introduction

A demand for high strength concrete in the construction industry has led to the development of Ultra-High Performance Fiber Reinforced Concrete (UHPFRC), also known as reactive powder concrete (Graybeal & Davis, 2008; Graybeal, 2007; Habel et al., 2008; Habel et al., 2006; Richard & Cheyrezy, 1995; Wille et al., 2011; Yu et al., 2014). UHPFRC is characterised primarily by its high strength and when reinforced with steel fibres, high material ductility.

Currently to achieve these material properties, careful consideration of raw materials and specialised mixing and curing techniques are typically required (Wang et al., 2012).

For example in terms of materials:

d) Coarse aggregate is removed to enhance homogeneity;
e) High quantities of superplasticiser or water reducing agents are used to achieve low water: cement (w:c) ratios and hence improve strength;
f) Specially graded sands, silica fume and glass powders are used to reduce porosity, improve particle packing density and improve strength.

Moreover, the concepts of particle packing can be applied in order to optimise the density and flowability of a mix through the introduction of specifically graded materials (de Larrard & Sedran, 1994). Additionally, improved material properties can be obtained through specialised mixing and curing techniques, for example:

d) The use of a high intensity mixer can improve the dispersion of fine particles and blending of the cement and mineral admixtures (Dils et al., 2012);
e) Multi-stage curing processes, including steam curing may increase strength and the rate of strength gain;

f) The application of pressure during setting may reduce porosity and increase strength (Dugat et al., 1996; Teichmann & Schmidt, 2004).

While it is possible through the use of relatively complex materials, mixing and curing techniques to develop UHPFRC with strengths regularly exceeding 200MPa (Bonneau et al., 1997; Ipek et al., 2011) and in excess of 500MPa (Dugat et al., 1996; Teichmann & Schmidt, 2004), the increased complexity and hence cost of producing UHPFRC imposes limits on its widespread application. Initial uptake of UHPFRC has been primarily focused on high cost and long life infrastructure such as bridges (Graybeal & Hartmann, 2005; Steinberg, 2009) and to military applications where high strength and/or ductility is required such as for resistance to blast and impact loading (Wu et al., 2009; Yi et al., 2012). In order to broaden and increase the application of UHPFRC it is required that cost effective manufacturing techniques for using commonly available materials and methods of production be found (Tafraoui et al., 2009; Wang et al., 2012).

In this investigation UHPFRC with sufficient workability for placement around reinforcement and with a target compressive strength of 150MPa is sought. This mix design is to be achieved without specialised curing and using materials frequently used in the manufacture of normal and high strength concrete. Additionally the potential to use high volumes of granulated lead-smelter slag which would otherwise go to landfill is investigated; this is done with the view to offsetting the environmental impact of the production of UHPFRC which is significant due to the high cement content (Ambily et al., 2015).

In this study particular attention is paid to the influence of aggregate grading because although the strength of fully compacted concrete with a given w:c ratio is largely independent of the grading of the aggregate, without sufficient workability, the

concrete cannot be compacted sufficiently to achieve its maximum strength (Neville, 1981). Hence grading of fine aggregate (FA) plays a significant albeit indirect role in achieving workable mix designs with low w:c ratios. Furthermore the influence of the addition of coarse aggregate (CA) is considered as is has the potential to further decrease the cost of UHPFRC manufacture. Considering the influence of coarse aggregate is an important consideration in this study as with high strength mortars the granular skeleton formed by the aggregate can become the weakest phase and hence the strength is no longer a function of the total w:c but also of the aggregate type and quantity.

The primary output of this research is a series of optimised mixes providing mix design guidelines for the most appropriate w:c and superplasticiser : cement (sp:c) ratio required to achieve a target strength and workability for a particular aggregate grading. For each mix design investigated the mechanical properties including the full axial and lateral stress strain relationships are provided. This guidance should decrease the amount of future effort to achieve UHPFRC mixes without the need for highly specialised materials, mixing procedures or curing conditions.

While it is recognised that the differing mineral composition, source and solidness of the different aggregates considered may also have an influence on the strength and workability of the mix designs here the behaviour is only quantified in terms of FM as this information is widely available to the practicing concrete technologist.

3.2 Experimental Program

A total of 40 mix designs were trialled, 24 without the addition of coarse aggregate and 16 with. It should be noted that mixes with only fine aggregate have been given the designation FA and mixes with both fine and coarse aggregate the designation CA.

The primary objective of these mixes was to identify the influence of fine aggregate grading on the properties of fresh and hardened UHPFRC and hence provide guidance on the optimal w:c and sp:c ratios for each aggregate grading. The secondary objective was to identify the influence of the addition of coarse aggregate in various quantities such that economy can be improved. For both mixes with and without coarse aggregate the scope of this work is limited to the use of materials commonly used in the manufacture of concrete.

3.2.1 Material specifications

All test specimens were manufactured at the University of Adelaide where the concrete was batched in an 80 litre pan mixer. The basic proportions of the concrete mix is comprised of a 1:1:0.266:0.233 ratio by weight of sulphate resisting cement, aggregate (total of fine and coarse aggregates), silica fume and steel fibres.

In all mixes sulphate resisting cement with a fineness index of 365m^2/kg, a 28 day compressive strength as determined in accordance with AS/NZS-2350.11:06 (2006)of 60MPa and a 28 day mortar shrinkage strain determined in accordance with AS/NZS-2350.13:06 (2006) of 650 micro-strain was used. In all mixes the undensified silica fume used had a chemical composition of major compounds as shown in Table 3.1 and a bulk density of 625kg/m^3. The steel fibres were cold drawn hooked end wire fibres with a total length of 35 mm, an aspect ratio of 64 and a minimum yield strength of 1100MPa. A third generation high range water reducer with an added retarder was used to improve the workability and will hereafter be referred to as the superplasticiser.

Table 3.1 Chemical composition of undensified silica fume

SiO_2	SO_3	Na_2O	K_2O	Cl	LOI

89.6%	0.83%	0.11%	0.23%	0.16%	3.8%

In order to determine the influence of a wide range of fine aggregate sources and grading, four fine aggregates were investigated: a washed river sand, a mined sand, a manufactured sand and a granulated lead smelter slag. The grading curve and fineness modulus (FM) of each sand are shown in Figure 3.1 and corresponding mix designs to investigate the influence of fine aggregate type are given in Table 3.2.

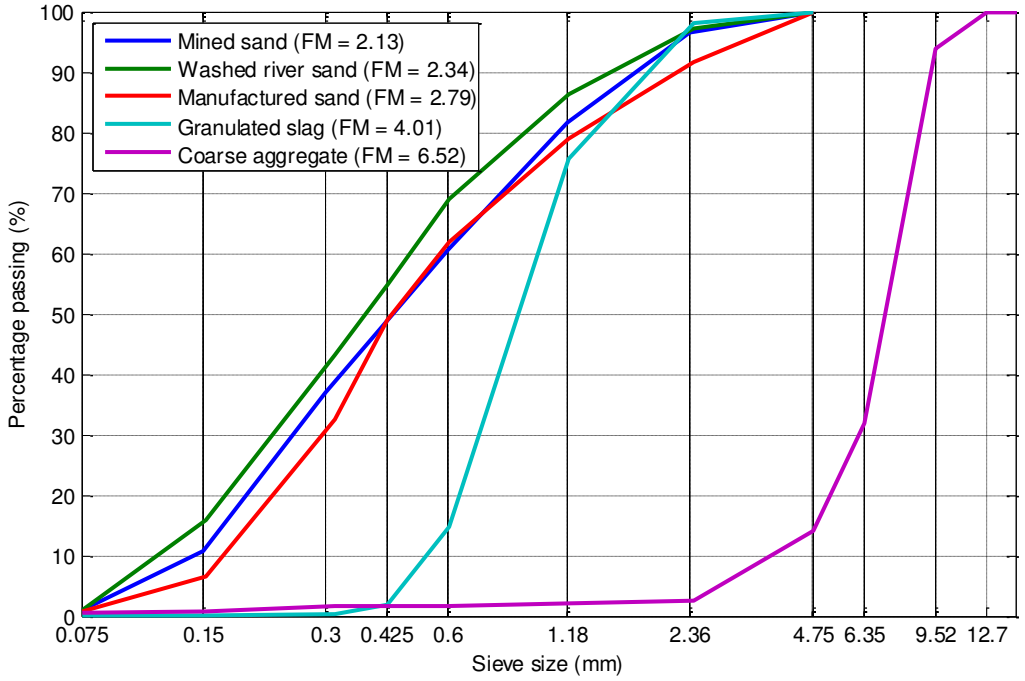

Fig.3.1 Grading of sands

Table 3.2 Mix designs to investigate grading of fine aggregate

Mix number	FM	W:C	SP:C	Total W:C
1-FA	2.13	0.1775	0.045	0.20675
2-FA	2.13	0.17	0.0565	0.20675
3-FA	2.13	0.165	0.0642	0.20675
4-FA	2.13	0.1775	0.0192	0.190

5-FA	2.13	0.17	0.0307	0.190
6-FA	2.13	0.165	0.0384	0.190
7-FA	2.34	0.1775	0.045	0.20675
8-FA	2.34	0.17	0.0565	0.20675
9-FA	2.34	0.165	0.0642	0.20675
10-FA	2.34	0.1775	0.0192	0.19
11-FA	2.34	0.17	0.0307	0.19
12-FA	2.34	0.165	0.0384	0.19
13-FA	2.79	0.1775	0.045	0.20675
14-FA	2.79	0.17	0.0565	0.20675
15-FA	2.79	0.165	0.0642	0.20675
16-FA	2.79	0.1775	0.0192	0.190
17-FA	2.79	0.17	0.0307	0.190
18-FA	2.79	0.165	0.0384	0.190
19-FA	4.01	0.1775	0.045	0.20675
20-FA	4.01	0.17	0.0565	0.20675
21-FA	4.01	0.165	0.0642	0.20675
22-FA	4.01	0.1775	0.0192	0.190
23-FA	4.01	0.17	0.0307	0.190
24-FA	4.01	0.165	0.0384	0.190

Note: Mix design consists of a 1:1:0.266:0.233 ratios by weight of sulphate resisting cement, aggregate (total of fine and coarse aggregates), silica fume and steel fibres.

It should be noted that in Table 3.2 the total w:c ratio refers to the sum of added water and the free water within the superplasticiser. Mix designs to determine the influence of coarse aggregate addition are shown in Table 3.3. In this investigation

the coarse aggregate was a crushed bluestone with a grading as shown in Figure 3.1, a FM of 6.52 and a maximum size of 10 mm. In all mixes utilising coarse aggregate washed river sand with a FM of 2.34 was used as the fine aggregate.

Table 3.3 Mix designs to investigate the influence of coarse aggregate

Mix number	CA:FA	w:c	SP:c	Total w:c
25-CA	0.33	0.165	0.0642	0.20675
26-CA	0.43	0.165	0.0642	0.20675
27-CA	0.54	0.165	0.0642	0.20675
28-CA	0.67	0.165	0.0642	0.20675
29-CA	0.82	0.165	0.0642	0.20675
30-CA	1.00	0.165	0.0642	0.20675
31-CA	1.22	0.165	0.0642	0.20675
32-CA	1.50	0.165	0.0642	0.20675
33-CA	1.86	0.165	0.0642	0.20675
34-CA	3.00	0.165	0.0642	0.20675
35-CA	1.00	0.17	0.0565	0.20675
36-CA	0.33	0.17	0.0565	0.20675
37-CA	1.50	0.17	0.0565	0.20675
38-CA	1.86	0.17	0.0565	0.20675
39-CA	1.00	0.1775	0.045	0.20675
40-CA	1.00	0.165	0.0384	0.190

Note: Mix design consists of a 1:1:0.266:0.233 ratio by weight of sulphate resisting cement, aggregate (total of fine and coarse aggregates), silica fume and steel fibres.

3.2.2 Mixing procedure, sample preparation and testing

For all mix designs the mixing procedure consisted of first mixing all the dry components, that is the cement, silica fume and aggregates for 1 minute in the pan mixer until well combined. The water and superplasticiser were then added and the concrete mixed until visibly flowable; this took between 7 and 35 minutes depending on the total water content. After the concrete started to flow, the fibres were added and mixed for a further 5 minutes.

Following mixing the slump and flowability of the concrete was tested by conducting a slump flow test and flow test through a J-ring according to (ASTM-C1611/C1611M-09b, 2009; ASTM-C1621/C1621M-09a, 2009). Following this the concrete was cast in 100x200 mm cylinder moulds and cured in a fog room until the time of testing. Compression testing was undertaken at 7, 28, 56 and 90 days in order to quantify the compressive strength gain over time. At day 90, specimens were instrumented with 4 Lateral Variable Displacement Transducers (LVDTs) to measure the total platen to platen axial deformation and 3 LVDTs equally spaced at mid-height to measure the total lateral dilation.

3.3 Results

To assess the flowability of the UHPFRC both with and without coarse aggregate and with and without fibres standard flow testing according to (ASTM-C1611/C1611M-09b, 2009; ASTM-C1621/C1621M-09a, 2009) including the use of a J-ring to assess passing ability around reinforcement was undertaken. The results of this testing is summarized in Table 3.4.

Table 3.4 Workability of UHPFRC with and without coarse aggregate

mix	slump flow (mm)		Slump flow with J-ring (mm)	
	before fibre addition	after fibre addition	before fibre addition	after fibre addition
1-FA	552.5	725	635	600
2-FA	622.5	753	657.5	612.5
3-FA	672.5	773	672.5	627.5
4-FA	490	568	465	437.5
5-FA	437.5	485	432.5	377.5
6-FA	371	285	310	280
7-FA	710	660	732.5	535
8-FA	610	645	712.5	535
9-FA	680	718	742.5	577.5
10-FA	500	528	500	410
11-FA	407.5	448	412.5	337.5
12-FA	257.5	333	295	257.5
13-FA	577.5	620	600	462.5
14-FA	627.5	665	677.5	495
15-FA	707.5	668	692.5	547.5
16-FA	470	493	455	380
17-FA	460	428	442.5	345
18-FA	192.5	305	227.5	235
19-FA	707.5	720	597.5	540
20-FA	577.5	680	605	522.5
21-FA	782.5	720	770	575
22-FA	550	588.5	607.5	485

23-FA	565	557.5	502.5	395
24-FA	285	305	262.5	227.5
25-CA	-	675	-	-
26-CA	-	652	-	-
27-CA	-	628	-	-
28-CA	-	538	-	-
29-CA	-	570	-	-
30-CA	-	558	-	-
21-CA	-	538	-	-
32-CA	-	517	-	-
33-CA	-	495	-	-
34-CA	-	475	-	-
35-CA	-	530	-	-
36-CA	-	610	-	-
37-CA	-	468	-	-
38-CA	-	295	-	-
39-CA	-	425	-	-
40-CA	-	233	-	-

3.3.1 Behaviour of fresh concrete without coarse aggregate

The slump flow of the mixes without coarse aggregate are shown graphically in Figure 3.2 where it can be seen that the slump flow of the concrete is strongly influenced by both the total w:c ratio and the sp:c ratio, and that the slump flow increases approximately linearly with the sp:c ratio over the range of w:c ratios investigated. It is also worth noting that in some instances, for example total w:c =0.207, FM = 2.13, in Figure 3.2 the slump flow increased after fibre addition,

indicating that the additional mixing time after fibre addition improved the action of the superplasticiser.

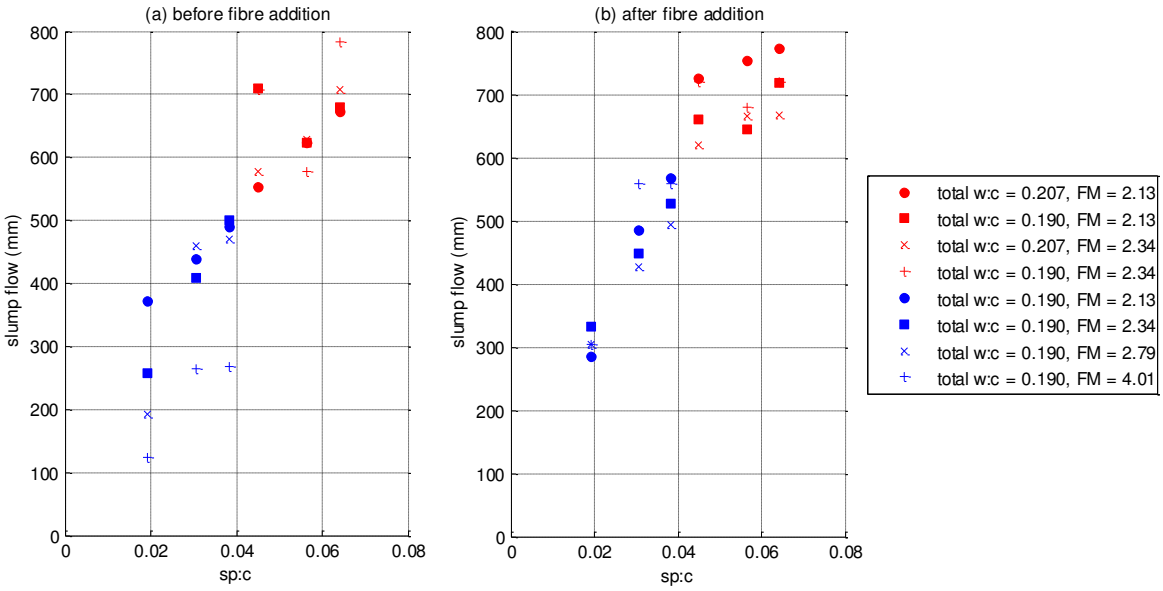

Fig.3.2 Slump flow (without J-ring) of mixes before and after fibre addition

Further examining Figure 3.2(a), it can be seen that there is a small dependency of slump flow on the FM, that is in general mixes with a higher FM have a smaller slump flow, particularly at the lower total w:c ratios where the difference in slump flow due to FM can be in the range of 300 mm. While a dependency of slump flow on FM is expected due to particle pacing and the lubricating action of small particle sizes (Stark & Mueller, 2008)the influence of FM appears to be less significant in Figure 3.2(b), that is after fibre addition. This result suggests that the mechanical interlocking of fibres is a more significant mechanism in controlling the flowability of the concrete in the presence of fibres.

As it has been identified that FM is significant in quantifying the slump flow prior to the addition of fibres, particularly at low total w:c ratios and low sp:c ratios, all the slump flow test results are replotted in Figure 3.3 as a function of the sp:c ratio normalised by the FM.

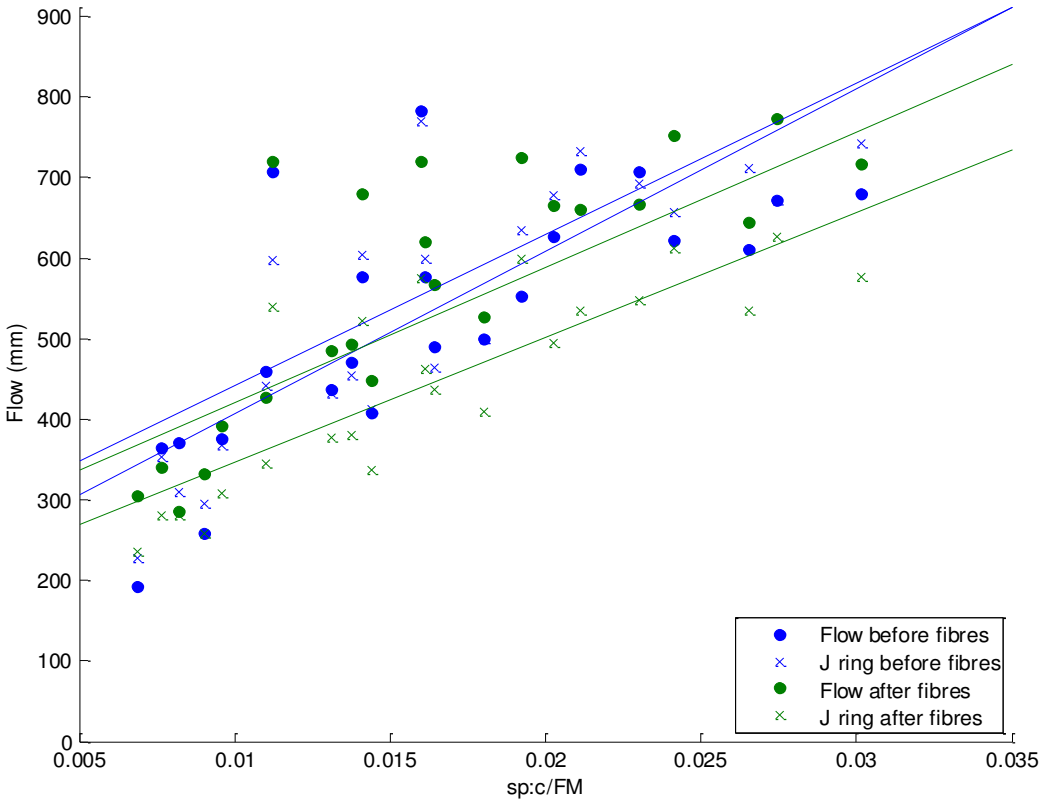

Fig.3.3 Slump flow of mixes with and without fibres

In Figure 3.3 comparting the lines of best fit of the slump flow before and after fibre addition it can be seen that the influence of fibres is relatively independent of the sp:c and FM and that they result in a reduction of flow of between 150 and 200 mm depending on the presence of the J-ring. Further the similarity of the slopes through the lines of best fit as well as the significant overlap of test data between tests with and without the J-ring suggests that the mixes developed could be utilised as high strength self-compacting concrete.

3.3.2 Behaviour of fresh concrete with coarse aggregate

To show the influence of the addition of coarse aggregate, the relative change in slump flow after the addition of fibers for mixes with coarse aggregate is shown in

Figure 3.4, that is the slump flow of the mix with coarse aggregate normalised by the identical mix without coarse aggregate.

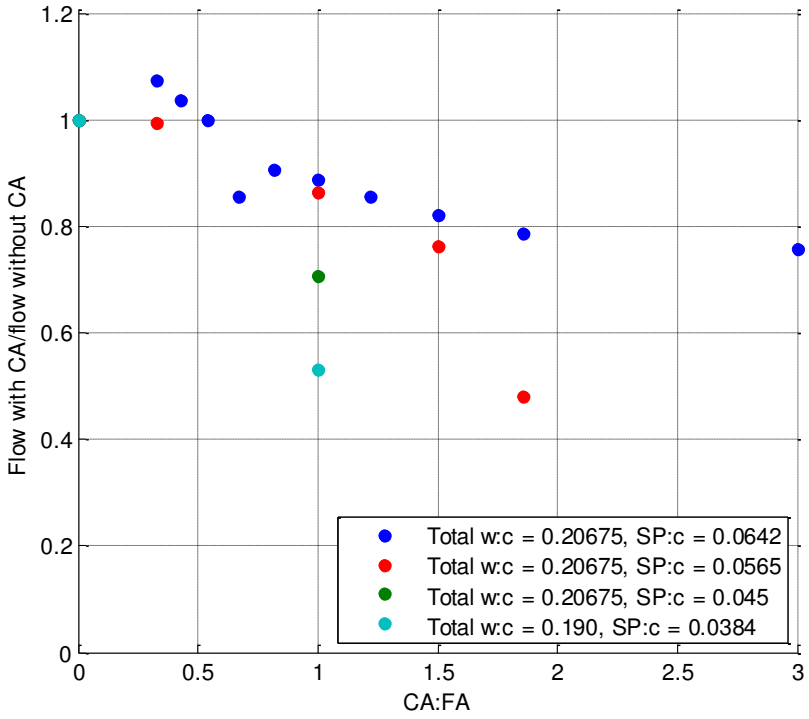

Fig.3.4 Change in concrete flowability with CA addition

In Figure 3.4 it can be seen that for mixes with high w:c ratios the addition of CA has a positive or negligible effect for CA:FA ratios less than 0.5 due to the well graded nature of the combined coarse and fine aggregate. For CA:FA ratios greater than 0.5 substantial reductions in slump flow occur, particularly for low w:c ratios where interlocking of the angular coarse aggregate particles results in higher internal friction (EFNARC, 2002). Additionally it can be expected that as the proportion of CA increases, additional interlocking of fibres with the CA will occur and may result in fibre balling, further reducing slump flow. It should be noted that because only slump flow readings with fibres were taken for mixes with CA the relative influence of the aggregate interlocking and fibre interlocking mechanisms cannot be quantified.

3.3.3 Hardened material properties

The compressive strength of mixes to investigate sand FM are presented in Table 3.5 where it can be seen that in general the goal of achieving 150MPa concrete with standard materials and curing techniques was achieved.

Table 3.5 Compressive strength of UHPFRC without coarse aggregate

Mix designation	7 days (MPa)	28 days (MPa)	56 days (MPa)	90 days (MPa)
1-FA	117	139	149	141
2-FA	117	145	152	147
3-FA	112	147	143	146
4-FA	123	150	153	150
5-FA	120	149	148	146
6-FA	128	153	153	155
7-FA	107	136	138	144
8-FA	102	141	150	138
9-FA	107	141	153	141
10-FA	131	146	148	139
11-FA	130	143	157	150
12-FA	123	137	162	158
13-FA	112	138	149	153
14-FA	110	141	151	154
15-FA	110	138	153	143
16-FA	121	150	134	154
17-FA	119	148	151	151
18-FA	124	148	155	151
19-FA	91	128	139	131

20-FA	83	121	134	131
21-FA	97	126	132	129
22-FA	118	131	136	131
23-FA	105	128	134	130
24-FA	103	129	136	131

3.3.4 Discussion of compressive strength results

The progression of compressive strength gain of each mix without coarse aggregate is shown in Figure 3.5 where, because the total water to cement ratio can be expected to most strongly influence strength, the results are divided into two plots in which the w:c ratio is constant. Furthermore, within each plot tics with the same colour represent mixes with the same FM and tics with the same shape represent mixes with the same sp:c ratio.

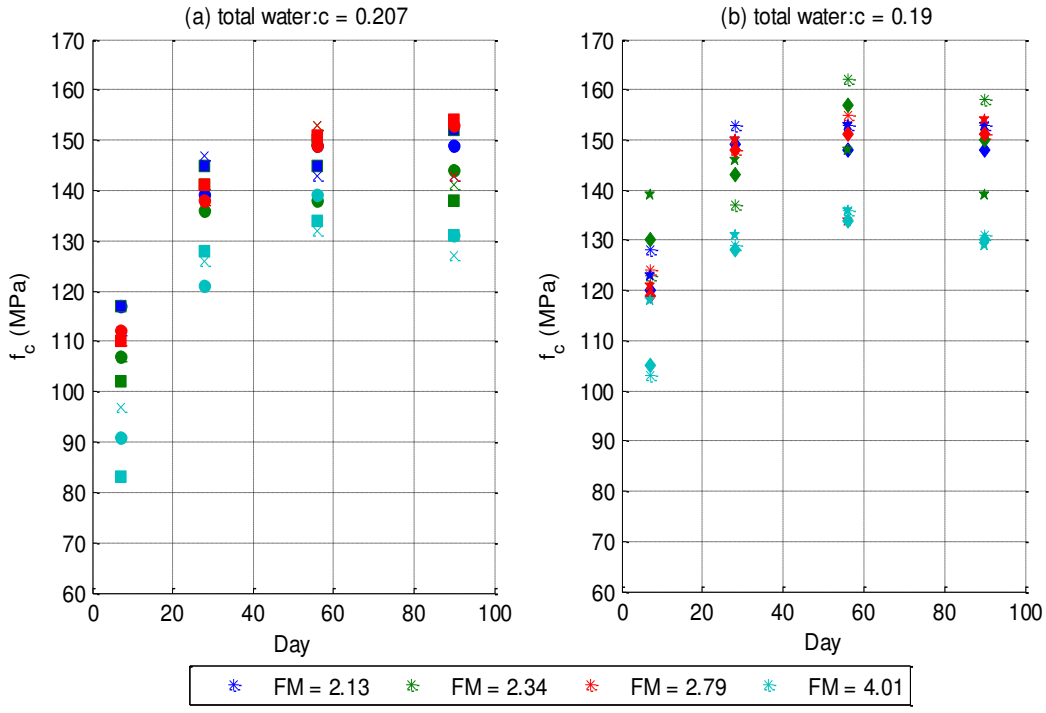

Fig.3.5 Compressive strength gain over time for mixes without CA

In Figure 3.5 it can be seen that in general mixes achieved approximately 80% of their final 90 day compressive strength (f_c) after 7 days and only marginal gains in strength were achieved after 28 days. It can also be noted that in some cases a reduction in strength between day 56 and 90 occurs and is most significant in those mixes with the lowest total free w:c ratio and with a higher fineness modulus. This loss of strength can be attributed to the formation of internal micro cracks due to shrinkage, which is restrained primarily by the fibres, but also by the aggregate as suggested by the correlation between the loss of strength and FM. The tendency for a minor reduction in strength over time due to shrinkage suggests further research to quantify the final strength of UHPFRC may be required, particularly given studies tracking strength gain over time are currently very limited.

Examining the results in Figure 3.5 in more detail, the influence of the sp:c ratio when the total w:c ratio is fixed can be seen in Figure 3.6, where again the mixes have been separated according to the total w:c ratio. For clarity only day 7 and day 90 compressive strengths are plotted and which are represented by the circular and cross shaped tics respectively.

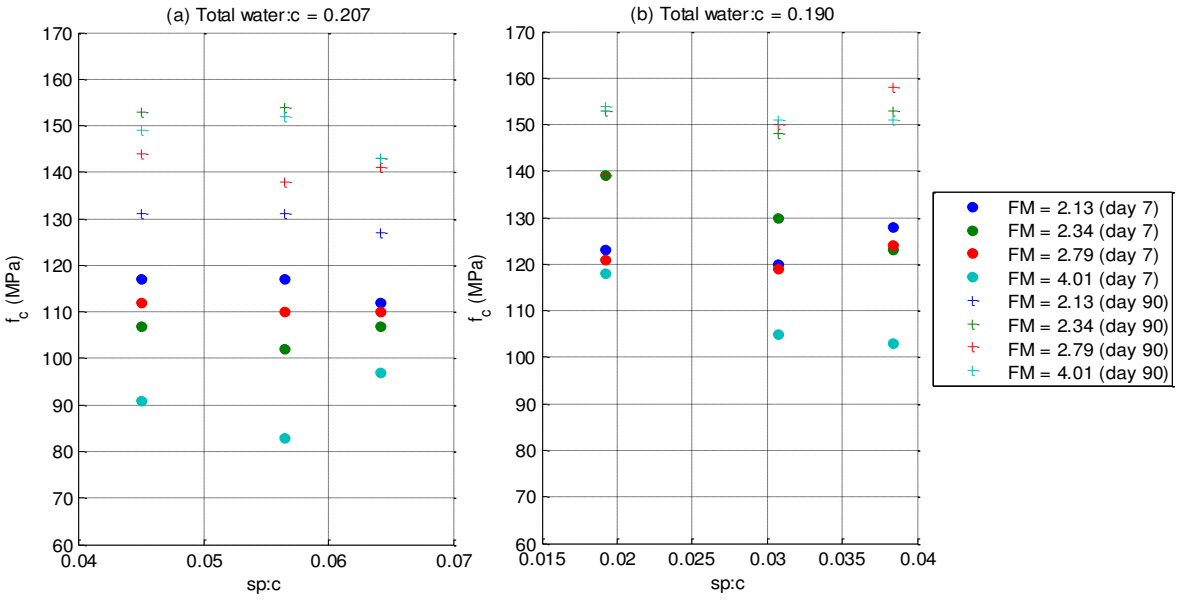

Fig.3.6 Influence of sp:c ratio of compressive strength

Firstly considering the results in Figure 3.6(a) it can be seen that there appears to be a reduction in compressive strength with increasing sp:c ratios. This is however not observed in Figure 3.6(b) where total w:c ratios are lower, except for in the case of the highest FM which corresponds to the use of slag as a FA. In this case it can be expected that the reactivity of the slag is increasing chemical shrinkage thus leading to increased micro-cracking and strength reductions (Lee et al., 2006). The reduction in strength with increasing sp:c ratios can be attributed to the reduction in initial surface hydration of C_3S (Gagn et al., 1996; Odler & Becker, 1980) which is primarily responsible for reducing early age compressive strengths and hence the rate of strength gain.

Further examining the summary of results in Figure 3.5, as indicated by the vertical scatter of results, the FM is strongly correlated with the compressive strength, particularly at early ages. Hence the compressive strength is plotted as a function of the FM in Figure 3.7, in which each series consists of 4 mixes with identical total w:c and sp:c ratios. It should be noted that to improve clarity only 7 and 90 day strengths have been plotted and in Figure 3.7 blue tics represent 7 day test results and the red tics 90 day results and mixes with the same tics have the same total w:c and sp:c ratio.

It can be seen in Figure 3.7 by from the lines of best fit that there is a consistent and significant reduction in strength with increasing FM which appears to be independent of the mix design apart from in the case of very low w:c and sp:c ratios where a slight increase in strength occurs with FM. This suggests that there may be insufficient water for rapid hydration of the cement in these cases. As the rate of reduction in compressive strength is independent of the mix design, that is the total w:c and sp:c ratio, the reduction in strength with FM can be attributed to the packing

density of the sand rather than the water requirement for hydration of the cement, that is the FM acts as a limit to strength rather than the w:c ratio.

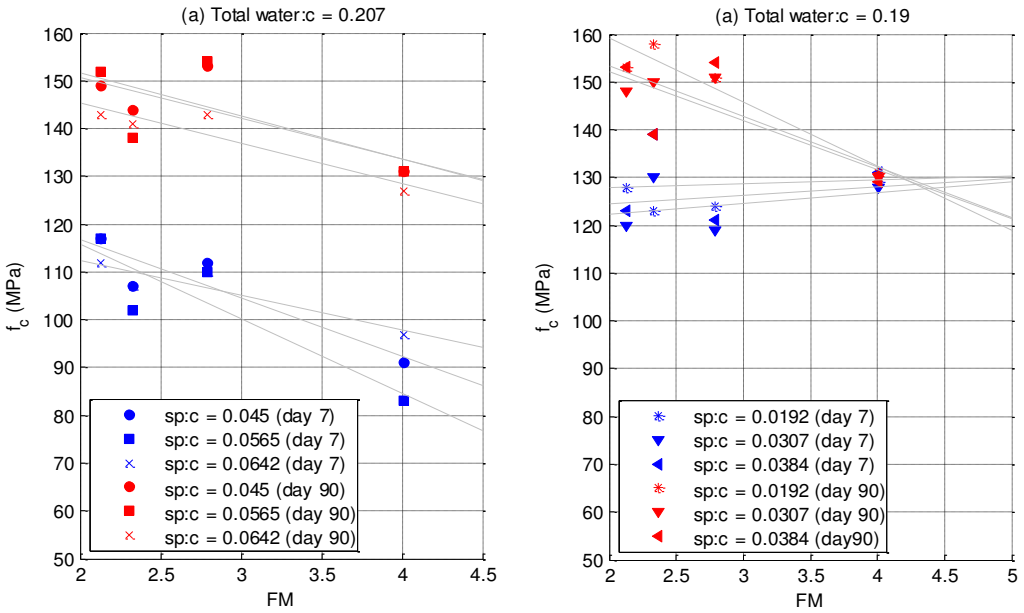

Fig.3.7 Influence of FM on compressive strength

Having identified trends in compressive strength with both sp:c ratio and FM, Figure 3.8 shows the variation in f_c with the sp:c ratio normalised by FM as this is expected to more clearly show the influence of sp:c.

It can now be seen in Figure 3.8 that the compressive strength is strongly correlated to the sp:c/FM ratio and from the trend lines that this correlation is not sensitive to either the total w:c ratio or time. This increase in strength can be attributed to the reduction in entrained air as the sp:c increases. In other words, the increase in superplasticiser results in increased instability of air voids and therefore an overall reduction in the entrained air, which can be expected to result in an increase in compressive strength of between 3 and 5% per percentage loss of entrained air (Neville, 1981; Safiuddin et al., 2008). This finding is similar to that shown by Wille et al. (2011) where the compressive strength of UHPFRC was defined directly as a

function of entrained air, however in this case the definition has been extended to being in terms of FM which is significant as the FM is potentially more easily determined and hence should be available to all concrete technologist when undertaking mix design.

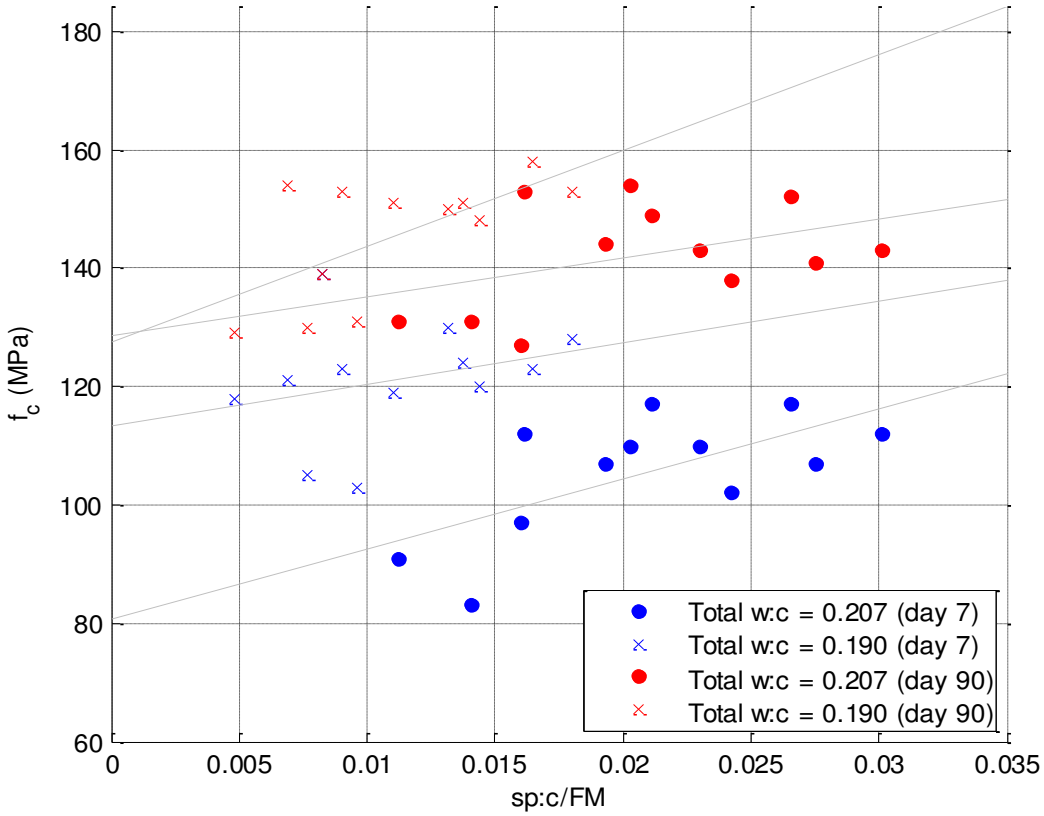

Fig.3.8 Influence of FM on fc

3.3.5 Influence of coarse aggregate

In order to quantify the influence of coarse aggregate on the compressive behaviour of UHPFRC a series of 16 trial mixes as listed in Table 3.6 were conducted to identify the optimal CA:FA ratio. It should be noted that these trials were carried out with the same total w:c and sp:c ratios as the mixes without coarse aggregate for comparison purposes and in all trial mixes only 7 day strengths were measured. A summary of the strength results is presented in Table 3.6

Table 3.6 Compressive strength of UHPFRC with coarse aggregate

Mix designation	7 days (MPa)	28 days (MPa)	56 days (MPa)	90 days (MPa)
25-CA	120	-	-	-
26-CA	119	-	-	-
27-CA	114	-	-	-
28-CA	110	-	-	-
29-CA	117	147	144	135
30-CA	116	-	-	-
31-CA	111	-	-	-
32-CA	113	-	-	-
33-CA	115	-	-	-
34-CA	115	-	-	-
35-CA	113	144	148	138
36-CA	116	-	-	-
37-CA	115	-	-	-
38-CA	114	-	-	-
39-CA	121	145	147	139
40-CA	129	-	-	-

To show the influence of coarse aggregate addition on compressive strength, Figure 3.9 shows a comparison of the 7 day compressive strengths with aggregate normalised against the strength of identical mixes without coarse aggregate. It can be observed that in all cases the addition of coarse aggregated led to an increase in 7 day strength, in some cases of up to 14%. Further looking at Figure 3.9 it can be noted that the greatest and most consistent improvement in strength occurs when the CA:FA ratio is less than 0.5 which suggests within this range the greatest compaction

of the coarse aggregate skeleton with the mortar phase is possible, it should however be noted that this conclusion is based on a limited data set and further investigations are required to identify the optimal CA:FA ratio.

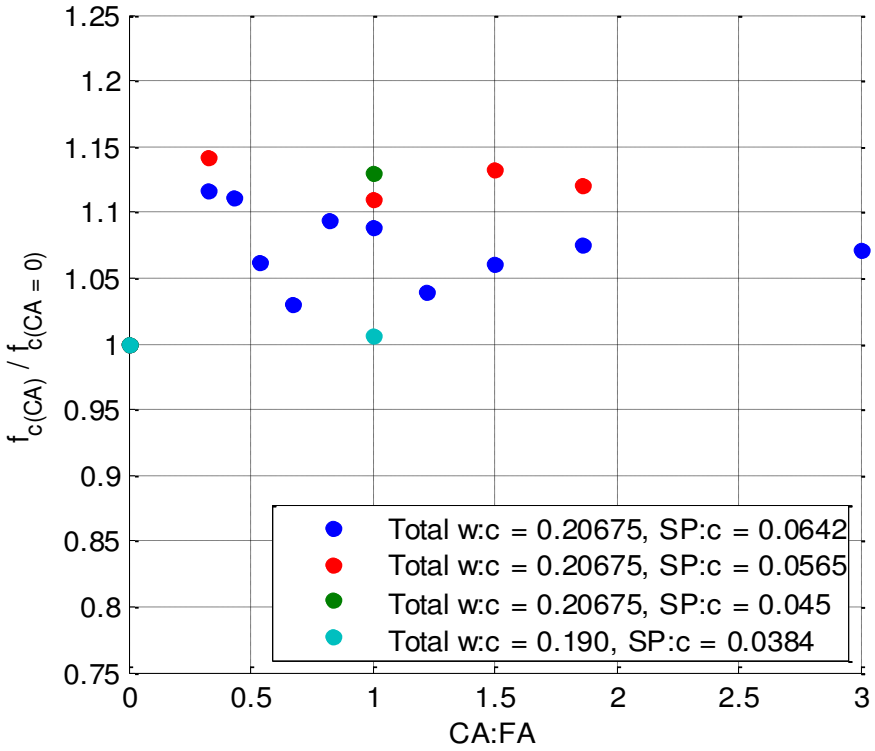

Fig.3.9 Increase in 7 day compressive strength due to CA addition

Although the inclusion of coarse aggregate led to an increase in early age strength of up to 14% in Figure 3.9, at later ages the strength of mixes with coarse aggregate had dropped to as low as 93% of the strength of the mix without CA. The reduction in strength can be attributed to increased restraint of the mortar phase by the coarse aggregate during drying shrinkage which results in increased micro-cracking (Hobbs, 1974).

Based on the results of the trial mixes with coarse aggregate, mixes 25-CA, 35-CA and 39-CA were considered for further study and including tracking the gain in compressive strength over time; the results of which are shown in Figure 3.10.

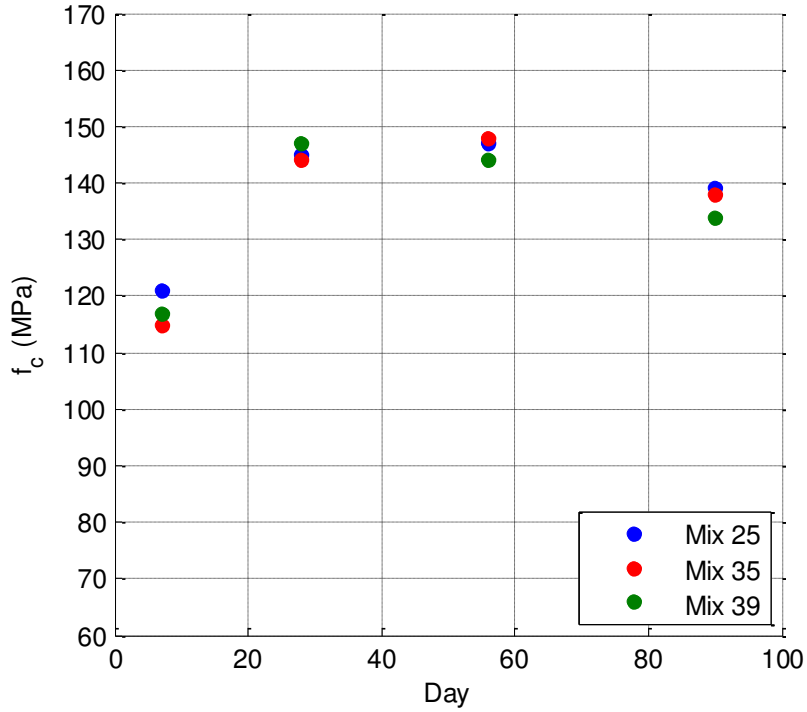

Fig.3.10 Compressive strength gain over time for mixes with CA

In general, from Figure 3.6 and Figure 3.10 it can be seen that there is potential to incorporate coarse aggregate into UHPFRC mixes, albeit with a reduction in compressive strength in this case in the range of 0 to 7%. It has also been shown that the inclusion of coarse aggregate requires consideration of not only the w:c but also the CA:FA ratio when designing a mix as the presence of CA leads to a substantial increase in micro cracking due to shrinkage which suggests that that further research is required to reduce the shrinkage of the cement paste when coarse aggregate is involved.

3.3.6 Stress-strain relationship

Figure 3.11 shows the 90 day axial and lateral stress strain relationships for each mix design in Table 3.2 and 3.3.

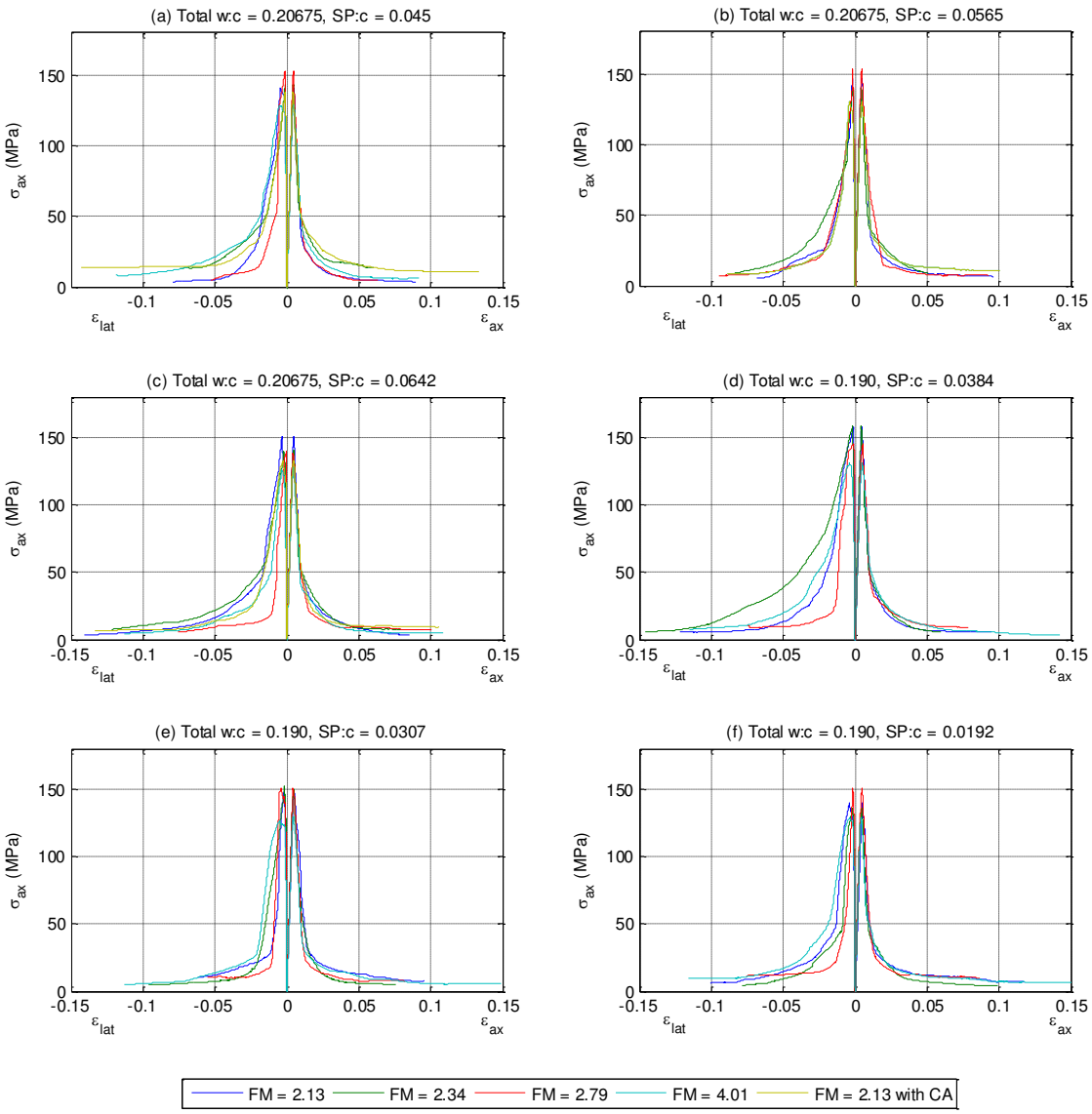

Fig.3.11 90 day axial and lateral stress strain relationships

From Figure 3.11 it can be seen that the material behaved in a linear fashion until the peak stress was achieved. This is followed by a relatively rapid reduction in strength until a stable stress plateau which gives the material substantial ductility. It can also be noted that the material undergoes significant stable dilation during softening indicating it may be efficiently confined.

As the stress strain relationship for each mix is similar in shape, the axial and lateral stress strain relationship for each mix is shown normalised by the peak stress and

strain at peak stress ε_0 in Figure 3.12. Through this normalisation it can be seen that there is relatively little scatter in the axial stress strain relationship but significant scatter in the lateral stress strain relationship on the falling branch which is due to the difficulty in capturing the total dilation due to wedge sliding (Chen et al., 2013).

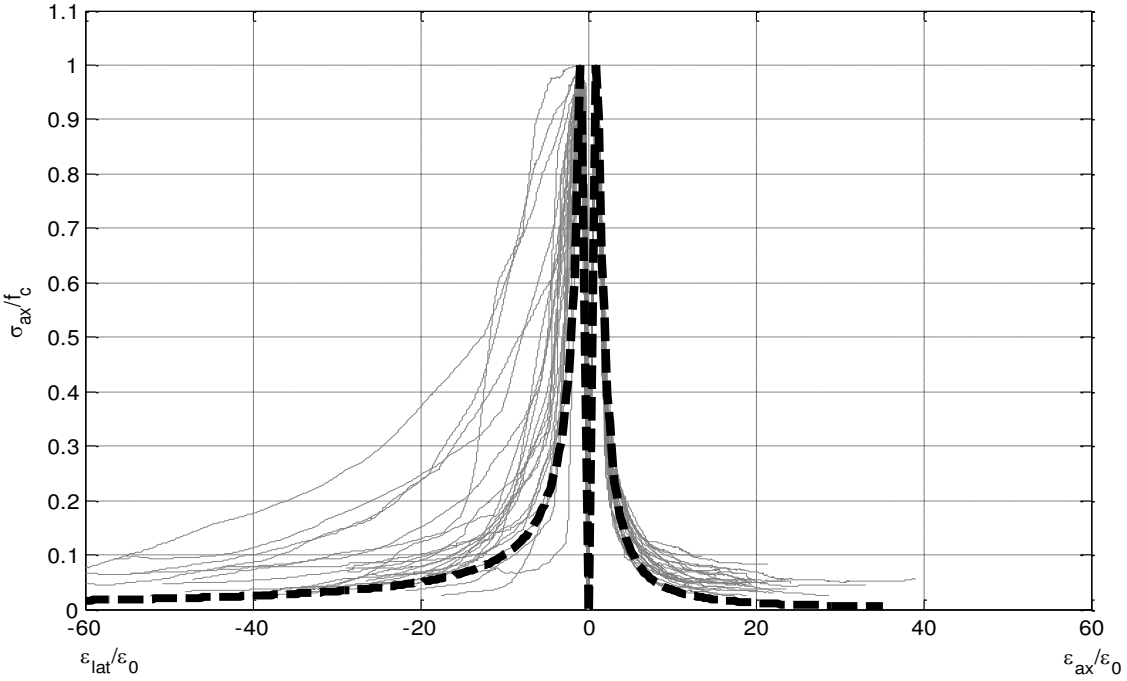

Fig.3.12 Normalised axial and lateral stress strain relationships

Based on the normalised stress strain relationships, for use in analysis a lower bound description of axial stress strain relationship can be described by:

$$\sigma_{ax} = E_c \varepsilon_{ax}; \varepsilon_{ax} \le \varepsilon_0 \qquad \text{Equation (3.1)}$$

$$\sigma_{ax} = \frac{f_c}{1+\left(\frac{\varepsilon_{ax}}{\varepsilon_0}\right)^{1.5}}; \varepsilon_{ax} > \varepsilon_0 \qquad \text{Equation (3.2)}$$

$$\sigma_{ax} = \frac{E_c}{\gamma} \varepsilon_{lat}; \varepsilon_{ax} \le \varepsilon_0 \qquad \text{Equation (3.3)}$$

$$\sigma_{ax} = \frac{f_c}{1 + \gamma\left(\frac{\varepsilon_{lat}}{\varepsilon_0}\right)}; \varepsilon_{ax} > \varepsilon_0 \qquad \text{Equation (3.4)}$$

which is shown as the heavy dashed line in Figure 3.12 and in which the elastic modulus E_c, strain at peak stress ε_0 and Poisson's ratio γ for each mix is presented in Table 3.7.

Table 3.7 Mechanical properties of mix designs

Mix number	f_c (MPa)	E_c(MPa)	ε_0	γ
1-FA	141	36100	0.00472	0.300
2-FA	147	35800	0.00910	0.355
3-FA	150	35000	0.00485	0.358
4-FA	140	30100	0.00484	0.220
5-FA	148	35000	0.00508	0.206
6-FA	158	37300	0.00468	0.191
7-FA	143	38400	0.00439	0.264
8-FA	140	36900	0.00434	0.238
9-FA	140	36200	0.00478	0.370
10-FA	136	35600	0.00428	0.240
11-FA	150	36700	0.00476	0.232
12-FA	158	40900	0.00448	0.462
13-FA	153	37300	0.00452	0.270
14-FA	153	38000	0.00445	0.447
15-FA	138	37600	0.00427	0.131
16-FA	151	10200	0.00484	0.222
17-FA	151	37800	0.00427	0.189
18-FA	145	37900	0.00514	0.120

19-FA	129	36300	0.00474	0.305
20-FA	130	35500	0.00470	0.284
21-FA	128	33900	0.00460	0.348
22-FA	129	35500	0.00426	0.228
23-FA	130	33600	0.00449	0.277
24-FA	131	35200	0.00496	0.272
25-CA	133	37100	0.00432	0.168
35-CA	138	36000	0.00444	0.170
39-CA	138	38200	0.00450	0.190

3.3.7 Influence of slag as a sand replacement

Based on the results in Figures 3.2, 3.5 and 3.8 it can be seen that the use of granulated slag as a replacement for conventional geological sands does not alter the behaviour of the resultant concrete outside that which would be expected by increasing the coarseness of the filler. That is, the increased coarseness leads to a reduction in the packing density and hence reduced compressive strength for a given w:c ratio. This result suggests that there is potential to utilise granulated slags as a filler material in high performance concrete where ultra-high strengths are not required.

3.4 Conclusion

Due to its superior strength and ductility UHPFRC has the potential to revolutionise the construction industry. Currently UHPFRC is typically produced using specially graded fine aggregates in conjunction with complex mixing and curing regimes. This complexity limits the widespread repeatability of mix designs and increases the cost of UHPFRC production.

Through a systematic trial of 40 mix designs utilising coarse and fine aggregates commonly used in the manufacture of normal strength concrete the influence of total free water to cement ratio, superplasticiser to cement ratio and fineness was studied. Major outcomes of this study are:

1. Using conventional natural and manufactured fine aggregates, including granulated slag, it is possible to produce concrete with good workability and compressive strengths in the range of 130-160MPa without specialist mixing or curing regimes.

2. Based on the empirical results it has been shown that there exists a strong inverse correlation between the fineness modulus of the fine aggregate and the compressive strength and this relationship is independent of the total water to cement ratio and the superplasticiser ratio.

3. It has been shown that the compressive strength can be related to the sp:c/FM which is not sensitive to the w:c ratio. This behaviour is attributed to the reduction in entrained air as the sp:c increases which in turn leads to a reduction of air voids and therefore an increase in concrete density.

4. A decrement in strength due to the formation of micro cracks due to shrinkage between day 56 and 90 has been observed for mixes both with and without coarse aggregate. Further study is required to quantify the extent of this strength decrement and it is suggested that for concretes with a high cement ratio such as UHPC that the 28 day strength may not be an adequate representation of strength for use in structural design.

5. The addition of a small quantity of coarse aggregate where the ratio of CA:FA is less than 0.5 does not lead to a reduction in workability or strength

suggesting that the economy of the mix can be improved through coarse aggregate addition.

6. The addition of coarse aggregate at ratios of CA:FA in the ratios of between 0.33 and 1.00 as tested leads to a reduction in 90 day strength of between 0 and 7% and a reduction in slump flow of up to 55%. Both the reduction in strength and the reduction in workability have been quantified over a wide range of CA:FA ratio, that is from 0 to 3.

7. Further study is required to quantify the extent of this strength decrement and it is suggested that for concretes with a high cement ratio such as UHPC that the 28 day strength may not be an adequate representation of strength for use in structural design.

8. The axial and lateral stress-strain relationship for 27 mixes both with and without coarse aggregate are reported and from these a generic axial and lateral stress-strain relationship is proposed.

Acknowledgements

The authors wish to acknowledge the financial support of the Australian Government Department of Defence's "Defence Science and Technology Organisation". The second author also acknowledges the support of the Australian Research Council ARC Discovery ProjectDP140103525 'A new generic approach for assessing blast effects on reinforced concrete members'.

References

Ambily, P., Umarani, C., Ravisankar, K., Prem, P.R., Bharatkumar, B., & Iyer, N.R. (2015). Studies on ultra high performance concrete incorporating copper slag as fine aggregate. *Construction and Building Materials 77*, 233-240.

AS/NZS-2350.11:06. (2006). Methods for testing Portland, blended and masonry cements-compressive strength. In. Sydney Standards Australia.

AS/NZS-2350.13:06. (2006). Methods for testing Portland, blended and masonry cements – determination of drying shrinkage of cement mortars. In. Sydney Standards Australia.

ASTM-C1611/C1611M-09b. (2009). Standard Test Method for Slump Flow of Self-Consolidating Concrete. In. West Conshohocken, PA: ASTM International.

ASTM-C1621/C1621M-09a. (2009). Standard Test Method for Passing Ability of Self-Consolidating Concrete by J-Ring. In. West Conshohocken, PA: ASTM International.

Bonneau, O., Lachemi, M., Dallaire, É., Dugat, J., & Aitcin, P.-C. (1997). Mechanical properties and durability of two industrial reactive powder concretes. *ACI Materials Journal 94(4)*.

Chen, Y., Visintin, P., Oehlers, D., & Alengaram, U. (2013). Size-Dependent Stress-Strain Model for Unconfined Concrete. *Journal of Structural Engineering 140(4)*, 04013088.

de Larrard, F., & Sedran, T. (1994). Optimization of ultra-high-performance concrete by the use of a packing model. *Cement and Concrete Research 24(6)*, 997-1009.

Dils, J., De Schutter, G., & Boel, V. (2012). Influence of mixing procedure and mixer type on fresh and hardened properties of concrete: a review. *Materials and Structures 45(11)*, 1673-1683.

Dugat, J., Roux, N., & Bernier, G. (1996). Mechanical properties of reactive powder concretes. *Materials and Structures 29(4)*, 233-240.

EFNARC, S. (2002). Guidelines for self-compacting concrete. *London, UK: Association House*, 32-34.

Gagn, R., Boisvert, A., & Pigeon, M. (1996). Effect of superplasticizer dosage on mechanical properties, permeability, and freeze-thaw durability of high-strength concretes with and without silica fume. *ACI Materials Journal 93(2)*.

Graybeal, B., & Davis, M. (2008). Cylinder or cube: strength testing of 80 to 200 MPa (11.6 to 29 ksi) ultra-high-performance fiber-reinforced concrete. *ACI Materials Journal 105(6)*, 603-609.

Graybeal, B., & Hartmann, J. (2005). Construction of an Optimized UHPC Vechicle Bridge. *ACI Special Publication 228*.

Graybeal, B.A. (2007). Compressive behavior of ultra-high-performance fiber-reinforced concrete. *ACI Materials Journal 104(2)*, 146.

Habel, K., Charron, J.-P., Braike, S., Hooton, R.D., Gauvreau, P., & Massicotte, B. (2008). Ultra-high performance fibre reinforced concrete mix design in central Canada. *Canadian Journal of Civil Engineering 35(2)*, 217-224.

Habel, K., Viviani, M., Denarié, E., & Brühwiler, E. (2006). Development of the mechanical properties of an Ultra-High Performance Fiber Reinforced Concrete (UHPFRC). *Cement and Concrete Research 36(7)*, 1362-1370.

Hobbs, D. (1974). Influence of aggregate restraint on the shrinkage of concrete. *ACI Journal Proceedings*, Vol. 71. ACI.

Ipek, M., Yilmaz, K., Sümer, M., & Saribiyik, M. (2011). Effect of pre-setting pressure applied to mechanical behaviours of reactive powder concrete during setting phase. *Construction and Building Materials 25(1)*, 61-68.

Lee, K., Lee, H., Lee, S., & Kim, G. (2006). Autogenous shrinkage of concrete containing granulated blast-furnace slag. *Cement and Concrete Research 36(7)*, 1279-1285.

Neville, A. (1981). Properties of concrete Pitman. In.: London.

Odler, I., & Becker, T. (1980). Effect of some liquefying agents on properties and hydration of Portland cement and tricalcium silicate pastes. *Cement and Concrete Research 10(3)*, 321-331.

Perry, V., & Zakariasen, D. (2004). First use of ultra-high performance concrete for an innovative train station canopy. *Concrete Technology Today 25(2)*, 1-2.

Richard, P., & Cheyrezy, M. (1995). Composition of reactive powder concretes. *Cement and Concrete Research 25(7)*, 1501-1511.

Safiuddin, M., West, J., & Soudki, K. (2008). Durability performance of self-consolidating concrete. *Journal of Applied Sciences Research 4(12)*, 1834-1840.

Stark, U., & Mueller, A. (2008). Optimization of packing density of aggregates. *Second International Symposium on Ultra High Performance Concrete. Kassel*, pp. 121-127.

Steinberg, E. (2009). Structural reliability of prestressed UHPC flexure models for bridge girders. *Journal of Bridge Engineering 15(1)*, 65-72.

Tafraoui, A., Escadeillas, G., Lebaili, S., & Vidal, T. (2009). Metakaolin in the formulation of UHPC. *Construction and Building Materials 23(2)*, 669-674.

Teichmann, T., & Schmidt, M. (2004). Influence of the packing density of fine particles on structure, strength and durability of UHPC. *Proceedings of the 1st International Symposium on Ultra High Performance Concrete, Kassel, Germany*, pp. 313-323.

Wang, C., Yang, C., Liu, F., Wan, C., & Pu, X. (2012). Preparation of Ultra-High Performance Concrete with common technology and materials. *Cement and Concrete Composites 34(4)*, 538-544.

Wille, K., Naaman, A.E., & Parra-Montesinos, G.J. (2011). Ultra-high performance concrete with compressive strength exceeding 150 MPa (22 ksi): A simpler way. *ACI Materials Journal 108(1)*.

Wu, C., Oehlers, D., Rebentrost, M., Leach, J., & Whittaker, A. (2009). Blast testing of ultra-high performance fibre and FRP-retrofitted concrete slabs. *Engineering Structures 31(9)*, 2060-2069.

Yi, N.-H., Kim, J.-H.J., Han, T.-S., Cho, Y.-G., & Lee, J.H. (2012). Blast-resistant characteristics of ultra-high strength concrete and reactive powder concrete. *Construction and Building Materials 28(1)*, 694-707.

Yu, R., Spiesz, P., & Brouwers, H. (2014). Mix design and properties assessment of Ultra-High Performance Fibre Reinforced Concrete (UHPFRC). *Cement and Concrete Research 56*, 29-39.

CHAPTER 4

MIX DESIGN AND METHODS OF ULTRA-HIGH PERFORMANCE FIBER REINFORCED CONCRETE

4.1 Introduction

This chapter follows from Chapter 3 in which the mix design of ultra-high performance fiber reinforced concrete (UHPFRC) utilising conventional materials was presented in journal paper format. In this chapter the work on mix design utilising conventional materials and production methods is further expanded including full descriptions of test methodologies or results which could not be included in the journal paper. Following this mix designs for UHPFRC with expensive silica sands and unconventional manufacturing techniques, including hot water curing are discussed. This is done with the aim showing UHPFRC manufactured using conventional material and production methods has similar behaviour in terms of strength to that of UHPFRC manufactured using high performance materials and techniques.

The presentation of this work is divided into the following five sections:

(i) Series – I: UHPFRC with conventional fine aggregate;

(ii) Series – II: UHPFRC with conventional fine aggregate partial replaced by coarse aggregate;

(iii) Series – III: UHPFRC with conventional fine aggregate fully replaced by granulated lead smelter slag;

(iv) Series – IV: UHPFRC with expensive fine aggregate;

(v) Series – V: UHPFRC with conventional and expensive fine aggregate and heat curing.

Each section will describe the materials used in the mix design, the mix design proportions, preparation technique, curing methods, experimental set-up, test results and discussion, conclusions and comparison of each set of results amongst the mixes. It should be noted that sections I to III are an expansion of the work presented in Chapter 3 given in order to provide additional details of the work.

4.2 Series – I: Conventional Sand as a Replacement of Expensive Silica Sand

The aim of this series is to develop an UHPFRC with conventional natural sand as full replacement of more expensive silica sand as fine aggregate. Typically UHPFRC is composed of: cement, silica powder, silica quartz sand, silica fume, superplasticizer (SP), steel fibers and water. Conventional concrete coarse and fine aggregates are replaced with fine silica sand particle with particle size ranges 150 and 600μm in order to improve homogeneity of and density of the concrete (Richard & Cheyrezy, 1995).

Currently it is believed that a high quantity of cement and well graded silica sand is required to produce UHPFRC with strengths in the range of 150 MPa. Although it is possible with these materials to produce high performance concrete they have a significant cost thus the use of these materials greatly increases the cost of construction and thus limits a more widespread uptake. From an economic standpoint, researchers are therefore seeking alternative way to produce UHPFRC at lower cost. In doing so the possibility of using waste materials such as granulated blast furnace slag or rich husk as partial replacement of cement or sand has been investigated (Ambily et al., 2015; Van Tuan et al., 2011; Van, 2013; Yazıcı et al., 2008) as well as the potential to reintroduce coarse aggregate (Wang et al., 2012).

Furthermore Yang et al. (2009) has investigated the effect of utilising recycled glass cullet and two types of local natural sand as a replacement of more expensive silica sand and replacing cement with silica fume and GGBS to produce UHPFRC at lower cost. In this investigation the mechanical and ductility properties at curing temperature 20^0C and 90^0C; however from this study the influence of varying aggregate grading, that is the fineness modulus (FM), was not quantified in terms of the fresh and hardened behaviour of UHPFRC. Although few researches (Allena & Newtson, 2011; Yang et al., 2009) have investigated the possibility of using natural fine aggregate as replacement of expensive silica sand to produce UHPFRC to reduce cost, there are to date no in-depth studies no research in the literature quantifying the effect of FM of conventional sand on the fresh and hardened behaviour of UHPFRC.

Hence in this chapter an experimental program was carried out to investigate the effect of FM on the fresh and hardened behaviour of UHPFRC. Specifically the study consisted of utilising four types of conventional fine aggregate from a variety of sources as a replacement of more expensive silica sand. Additionally a preliminary investigation was conducted to quantify the impact of the addition of coarse aggregate on UHPFRC material properties. The great benefit of using conventional materials in this study is to reduce material costs and simplify the manufacturing process by ensuring all required materials are widely available.

Standardized procedures including: the basic such as mix proportions, mixing methodology, and sample preparation and testing procedures used throughout the remainder to the chapter are presented in the following section.

4.2.1 Materials and mix proportions

All test specimens were manufactured at the University of Adelaide, South Australia where the concrete was batched in a pan mixer with an 80litre capacity. The basic proportions of the concrete mix a comprised of a 1:1:0.266:0.175 ratio by weight of sulphate resisting cement (Type SR), fine aggregate, silica fume and steel fibres (Dramix) for this study mixes.

To isolate the influence of the FM for any given type of aggregate the most basic mix design was retained in all mixes, that is the ratio of cement, silica fume and aggregate while the water and SP content was optimised in order to meet rheological requirements. In order to do this a large number of mix designs were trilled and the results of workability and 7 day strength tests used to isolate the suitable mix proportions. The resulting mix designs to investigate the influence of fine aggregate type are given in Table 4.1 in which three sources of sand with different fineness modulus were used: (i) a mined sand (FM=2.13); (ii) a washed river sand (FM=2.34); and (iii) a manufactured sand (FM=2.79). A total of 26 mix designs were trialled to get the fresh and hardened properties of UHPFRC for this investigation.

Table 4.1 Mix designs to investigate grading of fine aggregate

Mix Number	FM	W:C	SP:C	Total W:C
1-FA	2.13	0.1775	0.045	0.20675
2-FA	2.13	0.170	0.0565	0.20675
3-FA	2.13	0.165	0.0642	0.20675
4-FA	2.13	0.1775	0.0192	0.190
5-FA	2.13	0.170	0.0307	0.190
6-FA	2.13	0.165	0.0384	0.190
7-FA	2.34	0.1775	0.045	0.20675
8-FA	2.34	0.170	0.0565	0.20675
9-FA	2.34	0.165	0.0642	0.20675
10-FA	2.34	0.1775	0.0192	0.19
11-FA	2.34	0.170	0.0307	0.19
12-FA	2.34	0.165	0.0384	0.19
13-FA	2.79	0.1775	0.045	0.20675

14-FA	2.79	0.170	0.0565	0.20675
15-FA	2.79	0.165	0.0642	0.20675
16-FA	2.79	0.1775	0.0192	0.190
17-FA	2.79	0.170	0.0307	0.190
18-FA	2.79	0.165	0.0384	0.190
19-FA	2.34	0.190	0.035	0.21275
20-FA	2.34	0.1775	0.035	0.20025
21-FA	2.34	0.165	0.035	0.18775
22-FA	2.34	0.190	0.025	0.20625
23-FA	2.34	0.190	0.015	0.19975
24-FA	2.34	0.1775	0.025	0.19375
25-FA	2.34	0.1775	0.04	0.20350
26-FA	2.34	0.175	0.023	0.18995

4.2.1.1 Cement

In all mixes a sulphate resisting cement type SR with a fineness index of 365m^2/kg were used. Cement was collected from Adelaide Brighton Cement Ltd. that produces sulphate resisting cement type SR, conforming to Australian Standard (AS-3972, 2010). Sulphate resisting cement produced from Portland cement clinker and gypsum. The predominant factors in the choice of sulphate resisting cement are the high strength and durability requirements in the construction industry. The use of sulphate resisting cement was chosen over general purpose cement as the low C_3A content results in increased final strengths of the cement paste, faster hydration process, associated increase in the surface area of the particles, furthermore the reduced heat of hydration in sulphate resisting cement (Neville 1981) is beneficial in UHPFRC where high cement contents are used and any micro cracking as a result of thermal effects or shrinkage is detrimental to the compressive strength gain overtime.

4.2.1.2 Silica Fume

Silica fume is an essential component of UHPFRC as it acts both as a supplementary cementitious material as well as a filler material. That is because of its extreme fineness and high silica content silica fume reacts with calcium hydroxide present in

the cement paste creating a stronger calcium silica hydrate which results in improved bond and higher concrete strengths. It is worth noting that silica fume particles are approximately 20 times smaller than the cement particles and hence act as a filler of the voids between cement particles thus increasing concrete density. Silica fume (SiO_4) is obtained from the by-product of zirchonia ($ZrSiO_4$), silicon and ferrosilicon alloys, and are characterized by a surface area 22 m^2/g, a carbon content up to 8% and a content of $Na_2O + K_2O$ of up to 2% (Wille et al., 2011).

Together the cementitious and filling properties of silica fume act to fill the voids left by the cement particles in UHPFRC not only increasing density and strength but also enhancing rheological properties. Furthermore, the addition of silica fume can lead to enhanced durability, reduced chloride attack, enhance sulphate resistance and enhanced resistance to chemical attack (Jayakumar, 2004; Shihada & Arafa, 2010; Yan et al., 1999). In all mixes an undensified obtained from Echotech which was grey in colour was used. The silica fume had a bulk density of 625kg/m^3, median particle size 0.5μmand the specific surface area between 12 and 25 m^2/g.

4.2.1.3 Aggregate

In order to determine the influence of a wide range of fine aggregate sources and grading, four fine aggregates were investigated: a washed river sand, a mined sand, a manufactured sand and a granulated lead smelter slag. Those sand were collected from the different quarries in Adelaide, South Australia and cover the full range of fine aggregate types used throughout Australia. The sand particle size range is described by the required maximum and minimum particle sizes. The particle size range is between 600μm maximum to below 150μm.The expensive silica quartz and silica powder sands were used in this research. Grading curves of each type of conventional and expensive silica sand are shown in Figure 4.1. The influence of

coarse aggregate was investigated in this research and the grain size distribution is shown in Fig.4.1. The coarse aggregate was partially replaced with conventional sand in the mix to observe the behaviour of fresh and hardened properties of UHPFRC. The details information regarding coarse aggregate mixes will provide in the series 2.

Table 4.2 Grain size distribution raw data for fine and coarse aggregate

Sieve Size	% Passing – Mined sand	% Passing – Washed river sand	% Passing – Manufactured sand	% Passing – Slag	% Passing– Aggregate
19.5mm	-	-	-	-	100
12.7mm	-	-	-	-	99.81
9.52mm	-	-	-	-	93.85
6.35mm	-	-	-	-	31.94
4.75mm	100	99.79	100	99.5	14.02
2.36mm	98.52	97.26	89.64	87.87	2.64
1.18mm	90.33	85.51	76.34	60.33	2.05
600µm	76.02	67.08	56.33	5.00	1.75
300µm	49.05	41.79	32.64	1.833	1.59
150µm	15.91	6.91	6.445	0.416	0.87
75µm	0.933	0.254	0.727	0.133	0.63
*Critical Sieve	0	0	0	0	0.44

Table 4.3 Grain size distribution raw data for expensive silica sand

Sieve Size	% Passing Sand 60G	Sieve Size	% Passing –Sand 400G	Sieve Size	% Passing – Sand 30/60	% Passing – Sand 18/40
19.5mm	-	19.5mm	-	19.5mm	-	-
12.7mm	-	12.7mm	-	12.7mm	-	-
9.52mm	-	9.52mm	-	9.52mm	-	-
6.35mm	-	6.35mm	-	6.35mm	-	-
4.75mm	-	4.75mm	-	4.75mm	-	100
2.36mm	-	2.36mm	-	2.36mm	100	99.9
1.18mm	-	1.18mm	-	1.18mm	99.9	97.4
600µm	-	0.6µm	-	0.6µm	98.8	42.5
250µm	99.0	0.25µm	-	0.3µm	29.6	25.6
150µm	94.1	0.15µm	-	0.15µm	7.92	5.56
106µm	86.2	0.106µm	-	0.075µm	0.353	0.215
75µm	65.0	0.053	98.5	*Critical Sieve	0	0
45µm	60.0	0.045	96.8			
20µm	33.7	0.038	93.6			

10µm	19.1	0.020	70.5
2µm	5.9	0.01	40.7
1µm	5.1	0.005	21.1
*Critical Sieve	0	0.002	7.6
		0.001 *Critical Sieve	3.9

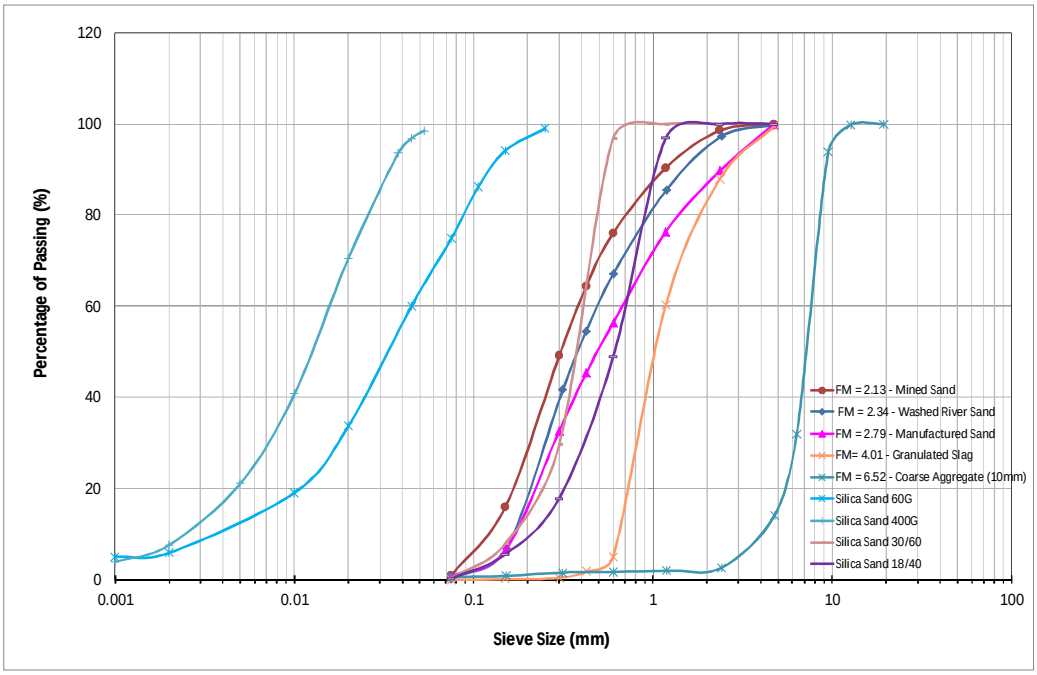

Fig.4.1 Grading of fine and coarse aggregate

4.2.1.5 Steel Fibers

Throughout this study hooked end steel fibers (*Dramix-3D-BG*) supplied by the Bekaert Ltd as shown in Figure 4.2 were used. These fibres are characterised by a high tensile strength (1345MPa) and young modulus (210MPa) according to the manufacture data sheet. The fibres have a total length of 35 mm and a diameter of 0.55mm with an aspect ratio of 65. The fibers were used at 2.25% by volume of the mixfor UHPFRC preparation.

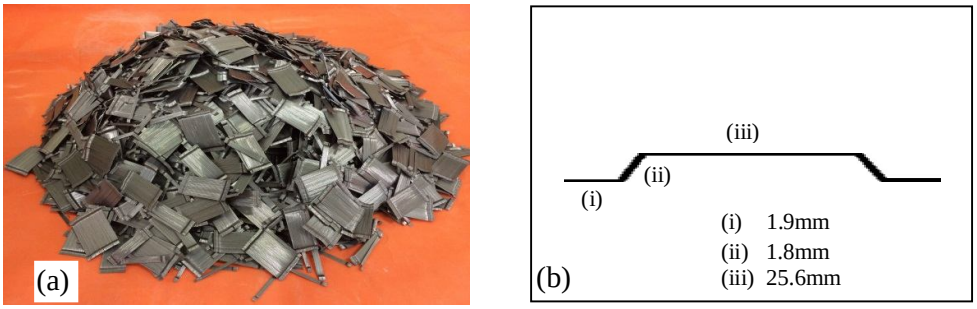

Fig.4.2 (a) Steel fiber used in UHPFRC (b) Single part of fiber with hook

4.2.1.5 Superplasticizer and Water

In all mixes a third generation polycarboxylate based high range water reducer with an added retarder (Viscocrete -10) was used to improve the workability and will hereafter be referred to as the SP. The supplier of the SP is Sika Australia Pty. Ltd. University concrete laboratory tap water was used for all of the mixes. The SP and water was the main variable factor for the all of the trial mixes. The optimum SP amount is high in UHPFRC preparation with low w:c ratios. It should be noted that in Table 4.1 the total w:c ratio refers to the sum of added water and the free water within the SP.

4.2.2 Mixing Procedure

Throughout the study all initial trial mixes were conducted in a small planetary mixer with a capacity of 20litres. These trials were conducted primarily to obtain indicative 7 day compressive strength and to observe the consistency of the mix such that the bounds of the w:c and sp:c ratios to be investigated could be identified. When using this small mixer a fiber content was limited 2.25% as further increases in fibres content caused the paddle to seize. The mixer has three rotation speeds: low, medium and high. The medium speed was applied for all of the trial mixes as this best matched the speed of the lager mixers later used in the study. Once the optimum mix design obtained from the trial mix then the large volume of mix conducted to produce ultra-high performance fiber reinforced concrete. A pan mixer consisting of

three concentric rotating steel paddles and with a capacity of 80 litres was used for all of the mixing of UHPFRC. It should be noted that in this chapter the fibre content is fixed at 2.25% in order to better isolate the influence of aggregate, in Chapter 5 the influence of varying fibre type and content will be considered.

During UHPFRC manufacture the following procedure was followed. All of the constituents were first weighed bucket and placed near the mixing machine. All the dry components which are the cement, silica fume and fine aggregates were then mixed for 3 minute until well combined. Figure 4.3(a) shows the dry mixing constituents in the pan.

Fig.4.3 (a) Mixing of constituents of UHPC (b) After mixing of UHPC

During this stage it was ensured that all dry constituents were uniformly mixed and special attention was paid to check the edges around the mixer where less efficient mixing may occur. While the dry components were mixing the water and SP were pre-mixed. The combined water and SP was then added in stages starting with 60% which was added slowly to ensure uniform mixing. Following a further 30 seconds of mixing the remainder of the water and SP was added. Mixing continued until the concrete was observed to visibly flow. An example of the UHPFRC following mixing is shown in Fig.4.3(b). A stop watch was used to calculate the total mixing

time which varied between 7 and 35 minutes depending on the total water and SP content. It was observed recently manufactured cement reacted and became flowable more quickly than cement which was several weeks old.

Prior to the addition of fibres the rheological properties were measured in each mix without fiber addition, these included: slump, slump flow and time, J-ring flow and time and blocking step parameter. The spread value was measured parallel and perpendicular of the flow. Following these measurements fibres were added and mixed for a further 5 minutes to achieve good a uniform distribution. The same fresh properties were then measured again with fiber in the mix.

4.2.3 Specimen preparation and curing regime

UHPFRC specimens were prepared using the three different types of sand (washed river sand, manufactured sand and mind sand), ground granulated lead smelter slag and coarse aggregate (10mm size) with properties as shown in Figure 4.1. In addition, the specimens were also prepared to investigate hardened properties of concrete using expensive silica sand with or without heat curing treatment. In each type of material and curing technique, a total of 14 cylinders of 100x200mm size were cast in steel moulds. The cylinders were tested for compressive strength for 7, 28, 56 and 90 days. Three of the specimens were tested for each specific water and SP content and curing age. Sometimes three specimen results are not sufficient to obtain consistence results and in this case an additional test was conducted. The preparation of concrete specimens and curing of concrete was followed standard of ASTM-C31/C31M-12 (2012).

Following the completion of the testing of the properties of the fresh concrete, the pan mixer was rotated for 1 minute to ensure consistency and flowability of the

concrete. The cylinders were then filled on a vibrating table in three layers using a scoop to move the UHPFRC from the mixing pan to the moulds as shown in Fig. 4.4(a).

Fig.4.4 (a) Cylinder being filled (b) Cylinder placed on level surface after filled (c) Specimen put on the table after demoulding (d) Marked the specimens (e) Put wet hessian and plastic sheets after demoulding (f) Curing the specimens in fog room

All of the cylinder specimens allowed for 30 seconds compaction in vibrating table for each layer. After casting the cylinders they were removed from the vibration table and placed in a level ground (Fig.4.4(b)). All of the cylinders were then allowed to cure at ambient temperature for between 24 and 48 hours until final setting was achieved. During this time, to prevent moisture loss, the specimens were covered with damp hessian and plastic as shown in Fig.4.4 (c). The moulds were kept at room temperature at around 20 ± 5^0C in summer season and 12 ± 5^0C in winter season. The specimens were then demoulded after 24 or 48 hours depending on the specimen are surface drying condition and put on the table as illustrated in Fig.4.4 (d). Each specimen was marked on the surface by white marker according to the water and SP content and date of cast refer to Fig.4.4 (e). Then, all the specimens stored in a fog room until the time of testing as shown in Fig.4.4 (f). Prior to testing, each specimens both compressive loading faces were ground carefully to obtain smooth surface.

It is worth mentioning that all preparation work including grinding of the cylinder ends has been performed 1 day prior to testing after which the cylinders were left in ambient lab conditions to dry. After grinding a check was made to ensure the ends were perpendicular and measurements of the cylinder diameter, length and weight taken. The length was measure at two opposite side and diameter measure at top, bottom and middle of the cylinder. The average value was then used to determine the volume and area of cylinders. Finally, density was measured from the geometric properties of cylinders.

4.2.4 Test set-up and instrumentation

4.2.4.1 Slump cone test (Filling ability)

Slump cone test is a measure of filling ability, or the ability of fresh concrete to flow. Slump test was done according to ASTM-C143/C143M-12 (2012) test method.

Slump test were taken without or with fibers added in the preliminary optimization stage to obtain a better understanding of effect of fibers for each mix on workability. To carry out the slump test a smooth wooden board of 900x900mm was placed on the flat surface and levelled to ensure there was no slope. The board surface was then wet to ensure it was moist throughout the test. A hollow frustum, commonly known as an Abrams cone, with the base 200mm in diameter and the top 100mm in diameter and the height 300mm were placed at the centre of the board. The mould was filled with fresh UHPFRC in three layers without applying compaction, this is different from what is expected for conventional concrete and is not required in the case of UHPFRC due to its self-compacting nature. The slump cone was then removed by raising both sides carefully in vertical direction over a duration of 2 to 5 seconds, being careful not to induce lateral or torsional motion. The slump cone was then placed to one side of the board and a length of steel reinforcement placed on top of the cone. The vertical distance between the concrete top and bottom face of the reinforcement was measured by tape refer as shown in Fig.4.5 (a) and (b) without and with fiber respectively. The test has been completed from start of the filling of concrete through removal of the cylinder mould within 2.5min.

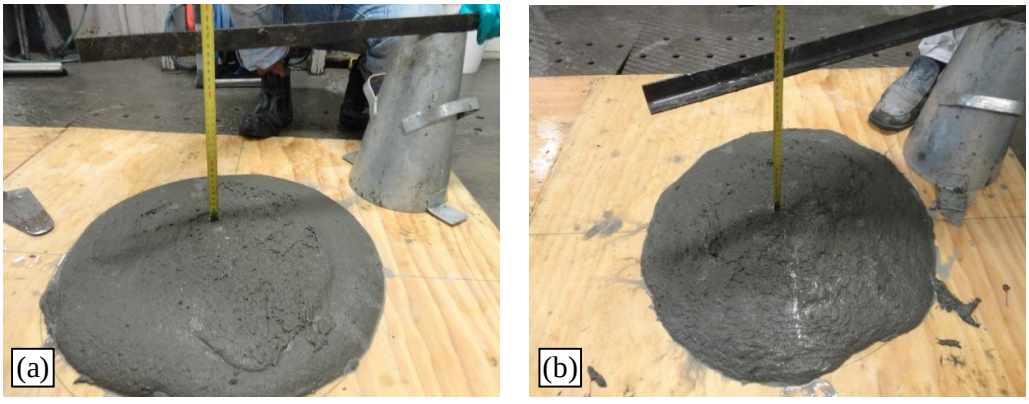

Fig.4.5 Slump measurement (a) Without fiber (b) With fiber

4.2.4.2 Slump spread measurement (Flowability)

The test aims at evaluating the workability (flowability) of fresh concrete by slump spread test. It measures two basic parameters: spread and spread time (T_{50}). The spread represents the free, unrestricted deformability and the time indicates the rate of deformation within a specified spread distance. For all of the mixes, slump spread ability of the concrete was tested by conducting a slump test according to ASTM-C1611/C1611M-09b (2009). The plane and smooth plywood base plate size of 900 x 900mm and clearly marked the circle of 200mm and 500mm diameters from center was used for all of the mixes. Abrams cone with 100mm top, 200mm bottom diameter and 300mm height was used to perform the test. The base plate was placed in the stable flat position and checked to be level. The base plate surface and inner surface of cone was kept moist with water by using moist towel until the start of the test. The cone was placed at the center of the base plate on the 200mm circle. The cone filled with the concrete without any compaction such as rodding or vibration. The surplus concrete above the top and bottom on the base plate removed. The cone was then lifted perpendicular to the base plate in such way that the concrete is allowed to move freely without any obstruction from the test cone. Figure 4.6(a) and (b) represents the slump spread without or with fiber respectively.

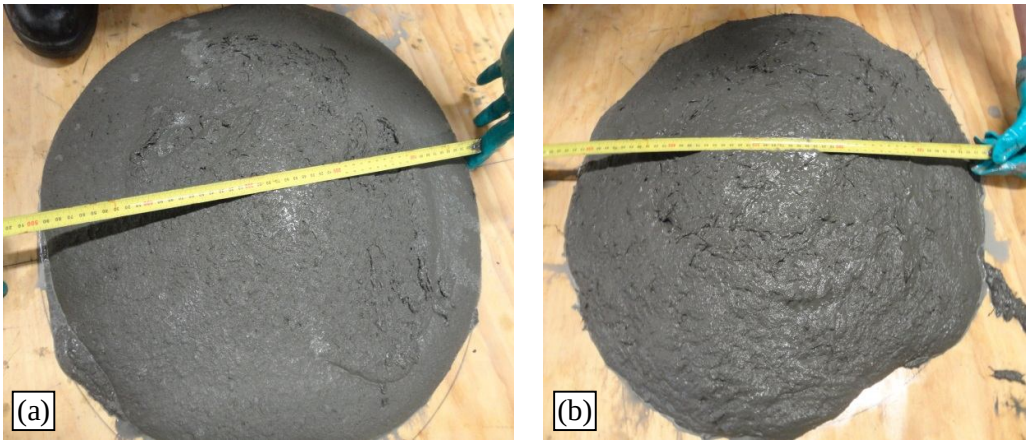

Fig.4.6 Slump spread measurement (a) Without fiber (b) With fiber

The stopwatch was started when the cone start lifting from the base plate. The time taken for the concrete flow to reach the 500mm circle was ten recorded as the T_{50} time. The largest diameter and the perpendicular diameter were measured using a steel measuring tape when the concrete spreads stopped completely. The test has been performed first without fiber in the mix and then the same test conducted with fiber. The overall test has been completed with or without fiber within the time of 2.5min.

The slump spread value (S) is the average of diameters d_{max} and d_{per}, as shown in equation (4.1).

$$S = \left(\frac{d_{\max} + d_{perp}}{2} \right) \qquad \text{Equation (4.1)}$$

Where

S represents the spread in mm to the nearest 5mm.

d_{max} is the maximum diameter of the spread

d_{perp} is the perpendicular diameter of the spread

The slump spread time T_{50} was also measured for each mix. T_{50} is expressed in second to the nearest 1/10 seconds.

4.2.4.3 J-ring test (Passing ability)

J-ring spread and blocking step of the UHPFRC concrete was measured by J-ring test according to ASTM-C1621/C1621M-09a (2009). The purpose of the test is to measure the workability (passing ability) of fresh concrete by J-ring test. It measure three basic parameters J-ring spread, spread time T_{50} and blocking step. The spread represents the restricted deformability and the time indicates the rate of deformation within a specified spread distance. The plane and smooth plywood base plate size of 900 x 900mm and clearly marked the circle of 200mm, 300mm and 500mm diameters from the center was used for all of the mixes. J-ring with 300mm outer

side diameter and 125mm height was used to perform the test. Abrams cone with 100mm top, 200mm bottom diameter and 300mm height was used to perform the test. The base plate was again placed in the stable flat levelled. Base plate surface and inner surface of cone was kept moist with water by using moist towel until testing. J-ring placed first on the base plate at 300mm circle and the cone placed at the centre of the base plate on the 200mm circle. The cone was then filled with UHPFRC without any compaction. The surplus concrete above the top and bottom on the base plate was then removed. Then, the cone was lifted perpendicular to the base plate in such way that the concrete is allowed to move freely through the J-ring reinforcement. Figs.4.7(a) and 4.8(a) and Figs. 4.7(b) and 4.8(b) represent blocking step parameters and J-ring spread measurement without and with fiber respectively.

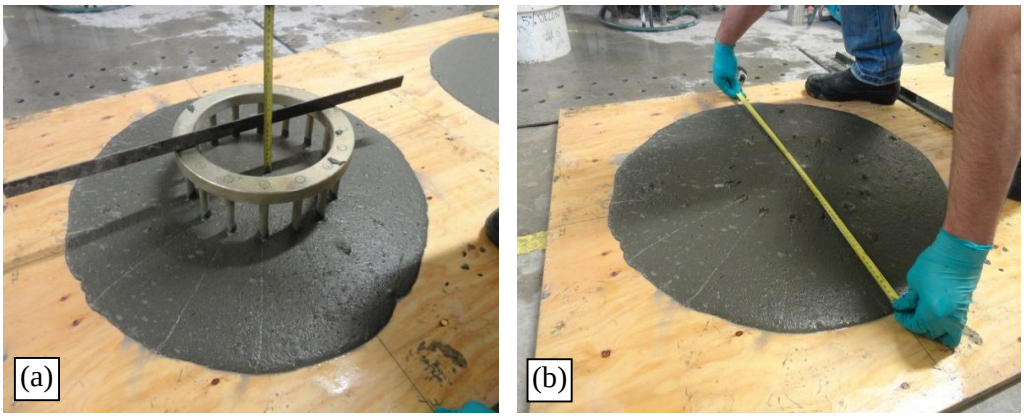

Fig.4.7 Without fiber (a) J-ring blocking Step (b) J-ring spread measurement

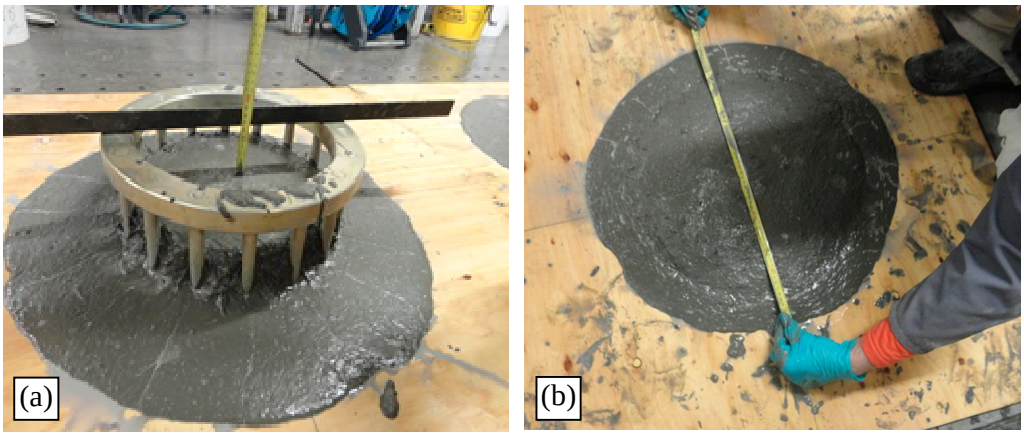

Fig.4.8 With fiber (a) J-ring blocking index (b) J-ring spread measurement

The stopwatch started when the cone start lifting from the base plate and the time taken for the front of the concrete spread to touch the 500mm circle record as the T_{50}. The J-ring was then removed from the base plate and measurements of the largest diameter and the perpendicular made by using a tape when the concrete spread stopped completely. The test was performed within a time not greater than 2.5min.

The J-ring spread value (S_J) is the average of diameters d_{max} and d_{per}, as shown in equation (4.2).

$$S_J = \left(\frac{d_{\max} + d_{perp}}{2} \right) \qquad \text{Equation (4.2)}$$

Where

S represent in mm to the nearest 5mm.

d_{max} is the maximum diameter of the spread

d_{perp} is the perpendicular diameter of other direction spread

The J-ring spread time T_{50J} was also measured for each mix. T_{50J} is expressed in second to the nearest 1/10 seconds.

The J-ring blocking step *Bj* is determine by using the equation (4.3) given below and expressed it in mm to the nearest 1mm.

$$B_J = \left(\frac{\Delta h_{x1} + \Delta h_{x2} + \Delta h_{y1} + \Delta_{y2}}{4} \right) - \Delta h_0 \qquad \text{Equation (4.3)}$$

Where

Δh_o= Mid-height of spread from concrete top to the reinforcement bottom position

Δh_{x1} = Height of the left hand side of the J-ring from concrete top to the reinforcement bottom position

Δh_{x2} = Height of the right hand side of the J-ring (parallel direction) from base to the reinforcement bottom position

Δh_{y1} = Height of the left hand side (perpendicular of other side) of the J-ring from concrete top to the reinforcement bottom position

Δh_{y2} = Height of the right hand side of the J-ring (perpendicular of other side but parallel direction for its direction) from concrete top to the reinforcement bottom position

4.2.4.4 Uniaxial compression test

All cylinder concrete specimen compression strength tests were conducted according to the standard ASTM-C39/C39M-12 (2012). The full axial and lateral stress-strain behaviour and compressive strength of UHPFRC specimens were investigated using a 5000kN 'Amsler' compression testing machine at 90 days only. Tests to obtain the compressive strength, without the stress strain relationship were also undertaken at 7, 28 and 56 days period in order to quantify the compressive strength gain over time using a 3000 kN 'Seidner' testing machine.

At day 90, in order to obtain the stress-strain response specimens were instrumented with 4 Linear Variable Displacement Transducers (LVDTs) to measure the total platen to platen axial deformation and 3 LVDTs equally spaced laterally at mid-height to measure the total lateral dilation. Two axial strain gauges were used to measure the axial strain due to concentric loads. Gauges were installed according to the specifications of the manufacturer. The basic load configuration and test set-up was constant throughout the testing for both types of machine. All of the specimens tested were 100x200mm size cylinder to determine the compressive strength and full behaviour (axial and lateral) of UHPFRC. Seidner compression testing machine with maximum capacity 3000kN was used to determine compressive strength for all types of UHPFRC mix design specimens. Testing of specimen with seidner compression testing machine is shown in Fig.4.9 (a). The load application rate was maintained

1MPa/sec for all of the specimens tested with Seidner machine. Amsler compressive testing machine with a maximum load of 5000kN was used to determine the axial and lateral stress-strain behaviour and maximum strength of all UHPFRC specimens.

Fig.4.9 (a) Testing of cylinders using Seidner compression machine (b)Test set up and instrumentation by Amsler for UHPFRC specimens

Fig.4.9 (b) shows the test set-up and instrumentation of the UHPFRC specimens. Initially, load-deformation behaviour of each specimen was measured in both the axial and lateral direction and was then converted into the corresponding stress-strain response. During the test, loading rate was increased 50kN/min in the ascending branch of concrete load-deformation curve and it maintained displacement loading rate 0.1mm/min at the end of the descending branch. Calibration of the machine and other devices were completed before start the test and all of the transducer and strain gauge readings were recorded using a high speed data acquisition system. Test results were monitored and recorded via computer and the load control system was

maintained until the peak load value of the specimen, and then it followed deflection control at the descending part. The whole system was observed in a computer screen during the testing.

4.2.5 Test results and observations

To determine the rheological properties all yellow colours in the graph indicates the mixes without fiber content and all magenta colours represent the mixes with fiber. The yellow and magenta colour of different symbol indicates different types of sand. It can be seen clearly on the rheological properties of graphs in the legend.

4.2.5.1 Influence of superplasticizer (SP), water and fineness modulus (FM) of sand on slump values of UHPFRC

The measurement of slump is an indication of the consistency and workability of a concrete mix. That is it describes the ability of fresh concrete flow. For the commercial production purposes the measurement of slump in the field is the final indication of the adequacy of concrete prior to placement. A measurement of slump can detect changes in fresh concrete that may affect it performance, that is good workability ensures it is easy to handle, compact, and also indicates the concrete will obtain adequate strength and durability. The measured slump is strongly dependent on the mix proportions particularly the proportion of water, SP and silica fume (Šerelis et al., 2015; Shihada & Arafa, 2010).

The slump test of the fresh UHPFRC both with and without fibers was measured in order to quantify the influence of SP, water and fineness modulus. The results of these tests for the mined sand, washed river sand and manufactured sand are summarised in Fig.4.10, Fig.4.11 and Fig.4.12 as follows. It should be noted that in each figure each type of symbolic tics represents one of the six mixes manufactured for each sand type, as outlined in Table 4.1.

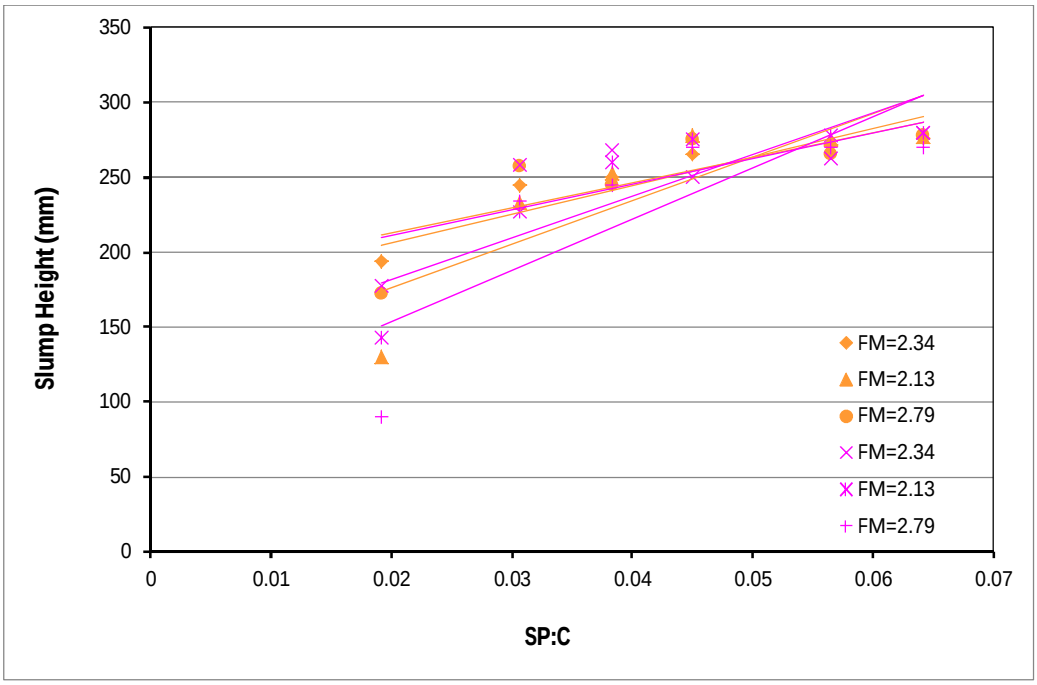

Fig.4.10 Slump versus superplasticizer (SP) content

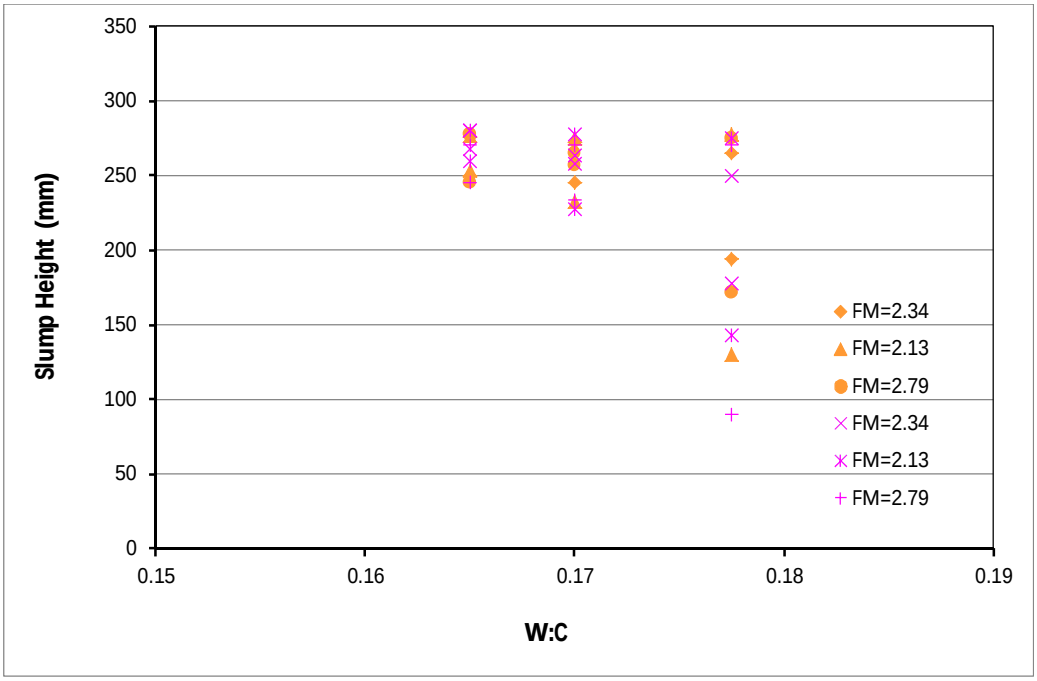

Fig.4.11 Slump versus water content

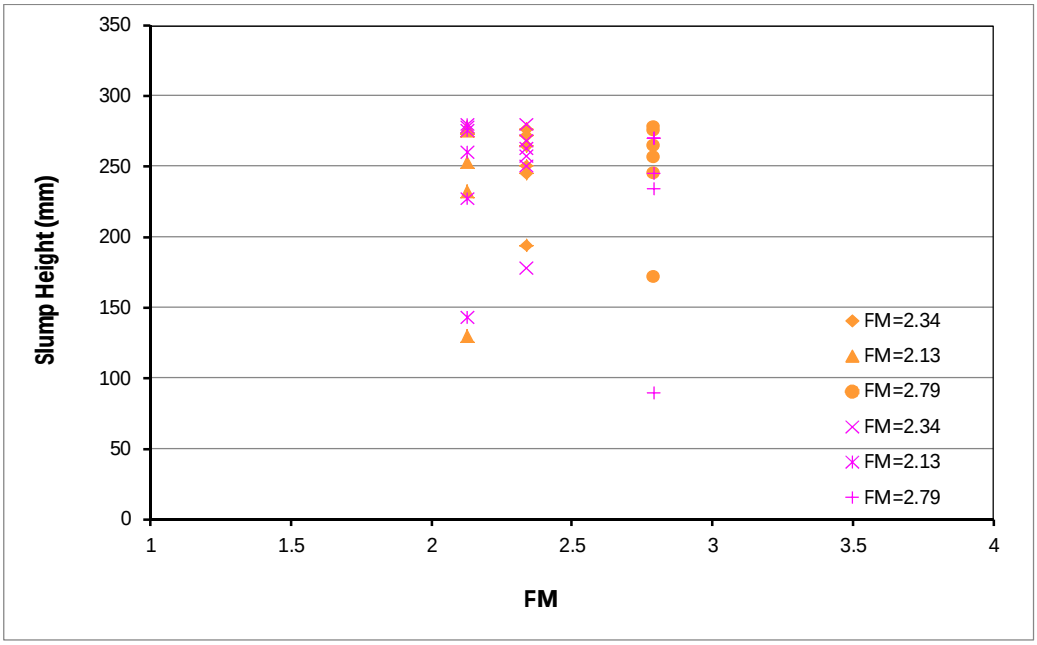

Fig.4.12 Slump versus fineness modulus (FM) of sand

It is observed from Fig. 4.10 and Fig. 4.11 that regardless of the presence of fibres, that as the SP content increases the slump increases this behaviour is consistent for all w:c ratios investigated. It is also seen from Fig.4.10 that the trend line is similar in both slope and magnitude particularly at higher SP contents which indicates that the presence of fibres has a minimal impact on the slump of the concrete. The result also shows a consistent increase in slump with SP which means indicates the results may be used as the basis for developing design rules for the quantity of SP required to meet desired water contents or to slow the setting rate.

It was also investigated during the test that the mix design nos. 3, 9 and 15 from Table 4.1 contains more SP and less water content showed higher flow able mix. This behaviour indicates the slump controlling by the SP content in the mix. It is interesting to mention from Fig. 4.11 that mix design nos. 1, 7 and 13 from Table 4.1 with total w:c = 0.20675 and mix design nos. 4, 10 and 16 from Table 4.1 with total w:c = 0.19 contains higher water shows less slump than mix design nos. 3, 9 and 15

and mix design nos. 6, 12 and 18 from Table 4.1 respectively. The increase of slump due to more SP content is attributed to the dispersion effect of cement particle which predominantly increase the fluidity of the mix resulted in decrease the viscosity of the cement paste. This behaviour is preferable to produce UHPFRC. The fluidity of the mix govern by the amount of SP adsorbed by the per unit surface area of cement.

The influence of fineness modulus (FM) of sand on the slump of UHPFRC without and with fiber mix is illustrated in Fig.4.12. Lower FM exhibits slightly higher slumps with fiber mixes; however the mix without fiber shows similar results. This behaviour is likely because mixes with finer sand release more bleed water which in turn acts to increase slump. The release of concrete bleed water is related with workability and amount of bleeding is a direct indication of the fresh properties. That is normal amounts of bleed water lead act to lubricate the concrete particles improving workability and finishing but excess bleed water is an indication of poor mix design and can lead to a reduction in strength due to segregation. The presence of excess bleed water can therefore be identified if mixes with low FM exhibit unexpectedly low strengths for a given water to cement ratio.

Throughout these tests it was observed that bleed water was increased with lower FM of fine aggregates. This finding agrees with results reported by Zhifu Yang et al. (2014). According to the mixes presented in Table 4.1, it is worth mentioning that higher SP and lowest water content mixes with FM shows the higher slump, however the same FM and water mixes with lowest SP content exhibit lower slump. This is also clear that UHPFRC with finer sand gives higher slump with desired mix design than the normal concrete aggregate mix. The high content of SP and hence retarder also acts to delay the setting time of concrete increase the workable time which is important given the high cement content of the mix.

4.2.5.2 Influence of SP, water, FM and time on slump spread of UHPFRC

The slump spread and spread time test aims at investigating flowability or filling ability and flow rate of UHPFRC in its fresh state. It is based on the slump test mentioned in ASTM 1611 (2012). This test measures two parameters; filling ability by measuring the horizontal flow spread and the spread time of concrete until 500mm circle is reached (T_{50}) is a calculates of the speed the of spread time and hence the viscosity of UHPFRC. The test has been conducted as it can be expected that the flowability of the concrete will be dependent on both the sp:c and binder ratio which acts chemically to influence the flow as well as the FM which will influence the flow based on the influence of packing density (Stark and Mueller 2008). The spread time measurement determines that how much time needed to go a certain spread distance and it is an alternate measure of the flowability of concrete. The slump spread and spread time as a function of sp:c, w:c and FM are summarised in Fig.4.13 to Fig.4.17 for all mixes.

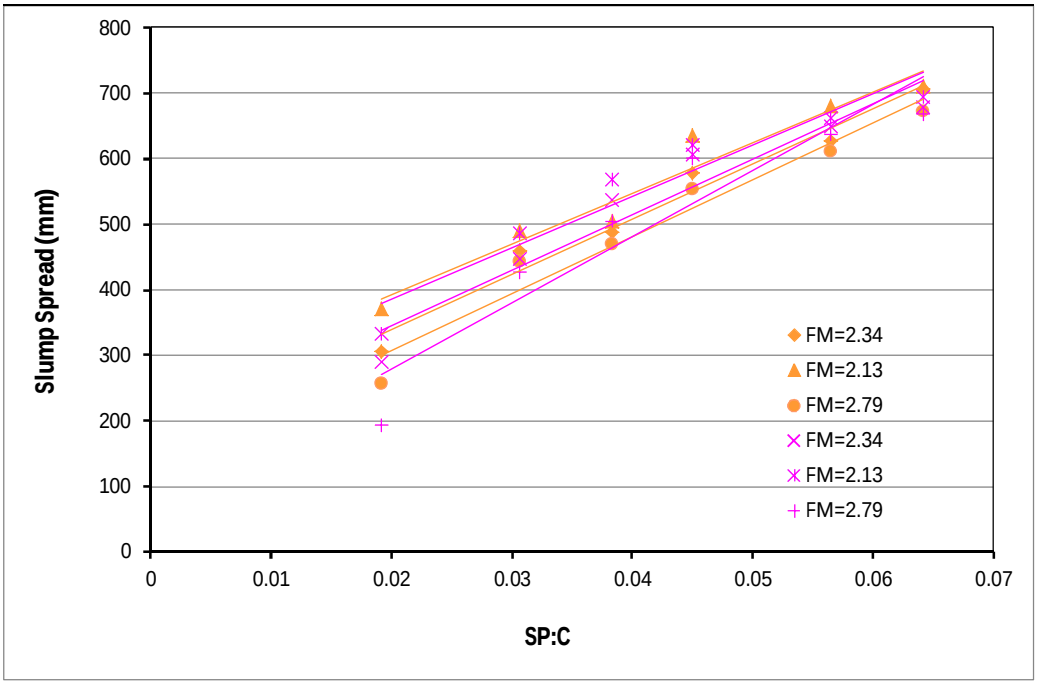

Fig.4.13 Slump spread versus superplasticizer content

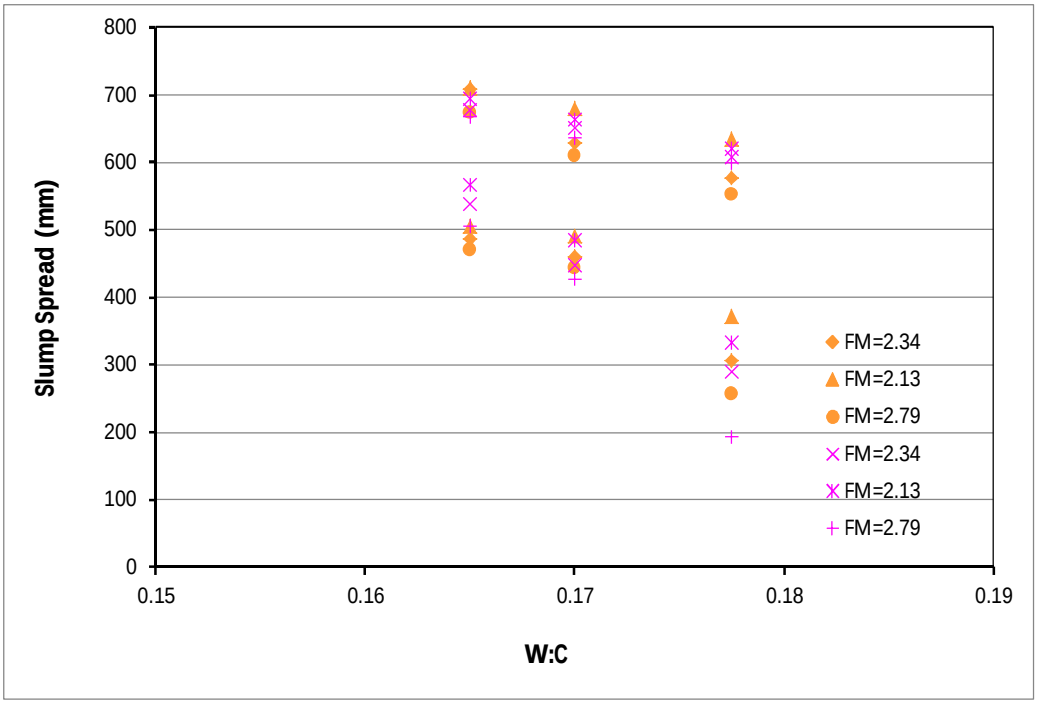

Fig.4.14 Slump spread versus water content

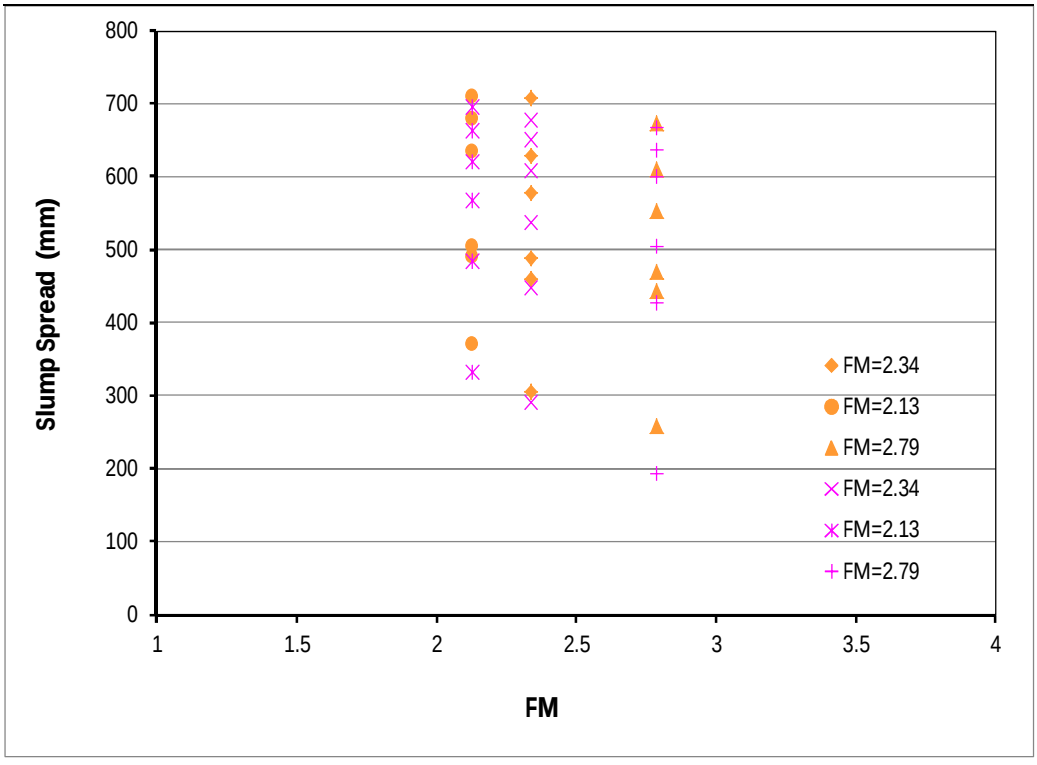

Fig.4.15 Slump versus fineness modulus (FM) of sand

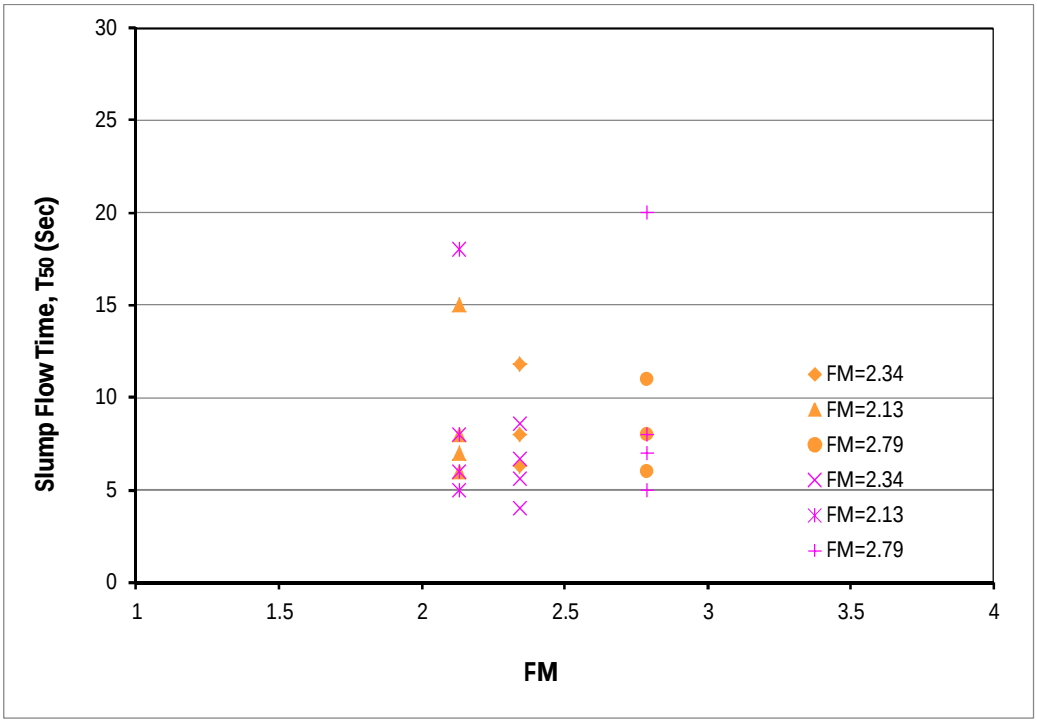

Fig.4. 16 Slump flow time (T_{50}) versus fineness modulus (FM) of sand

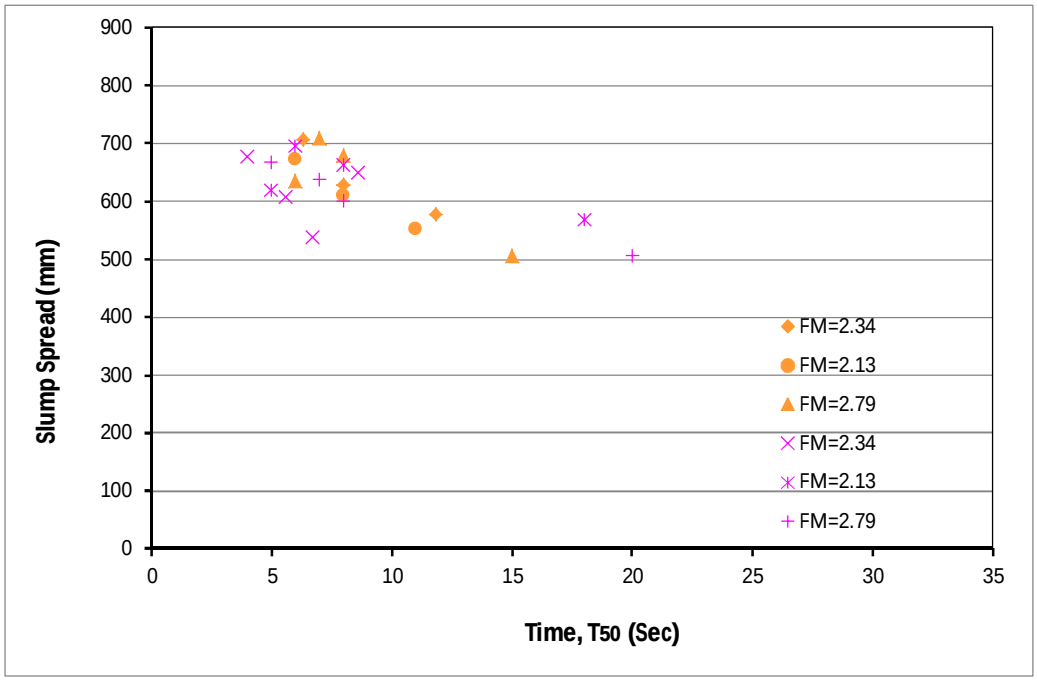

Fig.4. 17 Slump flow versus flow time (T_{50}) for UHPFRC

In Fig. 4.13 it can be observed that as the SP content increases the fresh concrete slump flowability increases regardless of the presence of fibres. From the similarity in trend lines in Figure 4.13 it can be seen that the spread of the concrete is not significantly influence by the incorporating of fibres in the mixes. It is also observed that higher content of SP shows closer spread value. The SP affect the spread of concrete mainly due to the facts that reduction in interfacial tension of constituents, retarding effect of cement hydration and release of water trapped amongst the cement particles. Increasing the amount of SP, segregation and bleeding of concrete occurs due to reduce in interfacial tension and release entrapped water of the constituents hence increased the flowability of the mixes.

Kay Wille and Gustavo (2014) observed that rheological properties of UHPFRC highly influence by the SP content. They suggested that the optimum amount of SP ranged from 1.4 to 2.4% of cement by weight provide the best spread, this results is confirmed by the test performed in this work where adequate flow was observed for SP contents ranges 2-4%. However, the lowest value of SP for UHPFRC production found to date in the technical literature that is, 1.5% (Gerlicher et al., 2008).

In Figure 4.15 it can be observed that the slump flowability of UHPFRC decreases with increased fineness modulus; also it shows a large degree of scatter results amongst the spread values of six mixes of each sand type. Fineness modulus of sand in concrete mixes is prone to bleeding and the amount of bleeding depends on sand properties and the uncompacted air void content of sand affect the amount of bleeding. Increasing the fineness modulus of sand decreased the flowability of the mixes because less bleeding occurs on the concrete surface. Consequently, it also indicates that finer sand provided in increased flowability due to more bleeding occur on the concrete surface. Similar conclusion reported by the Zhifu Yang et al. (2014)

in their research, result can be expected as from the concepts of particle packing the presence of finer particles act to lubricate coarser particles hence increasing the flowability of the mix.

In this investigation, the maximum slump spread range attained around 710mm without fiber and 700mm with fiber with FM= 2.13 for mix no. 1 and the minimum spread obtained 257.5mm without fiber and 192.5mm with fiber for FM = 2.79 for mix no. 16. However, the flow time relationship with FM is opposite; the flow time is increased with coarser sand and decreased with finer sand. This behaviour is significant when no fibers in the mix as shown in Fig.4.16. It was also observed in Fig.4.17 that the flowability is decreased with increasing the time without and with fiber UHPFRC mixes, especially for the mix with fiber. Fig.4.17 also represents that there were no time value when the flow did not exceed the 500mm flow circle. It means that the concrete was so sticky and not highly workable. In these mixes the water and SP was retained by the concrete constituents and thus the flow was slower (Yu et al., 2015). It can also be seen in Fig.4.16 and 4.17 that a longer time was taken to reach the specified distance due to the presence of fibres which indicates the interlocking of fibres in the mix has an influence of workability. It is also seen from Fig.4.14 that mix design nos. 1, 7 and 13 from Table 4.1 with total w:c = 0.20675 and mix design nos. 4, 10 and 16 with total w:c = 0.19 contains high amount of water in the mixes exhibits less slump flow than mix design nos. 3, 9 and 15 and mix design nos. 6, 12 and 18 respectively. It is concluded that lower FM and higher amount of SP increased the flow and decreased the flow when opposite trend follow without and with fiber in the mixes. It is worth mentioning that the flow time increased with coarser sand and the flow decreased resultant in longer time.

4.2.5.3 Influence of SP, water, FM and Time on J-ring spread of UHPFRC

The purpose of the J-ring spread and spread time test is to determine the passing ability and flow rate of UHPFRC through the reinforcement. The results of the J-ring test without and with the use of fiber in the mixes shown in Fig.4.18 to Fig 4.22.

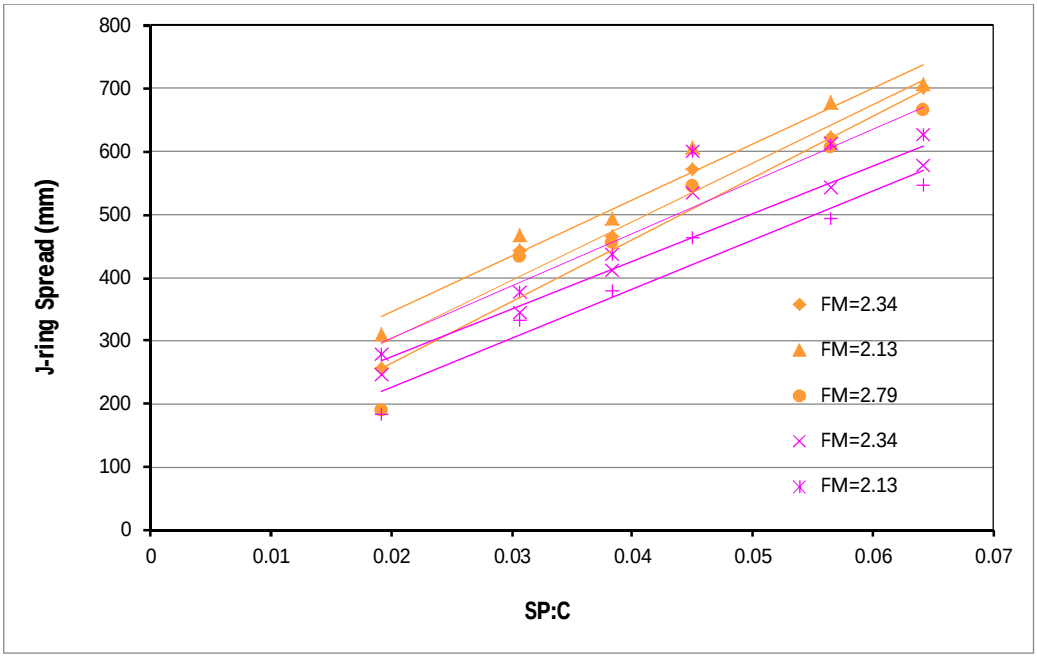

Fig.4.18 Slump versus superplasticizer of UHPFRC

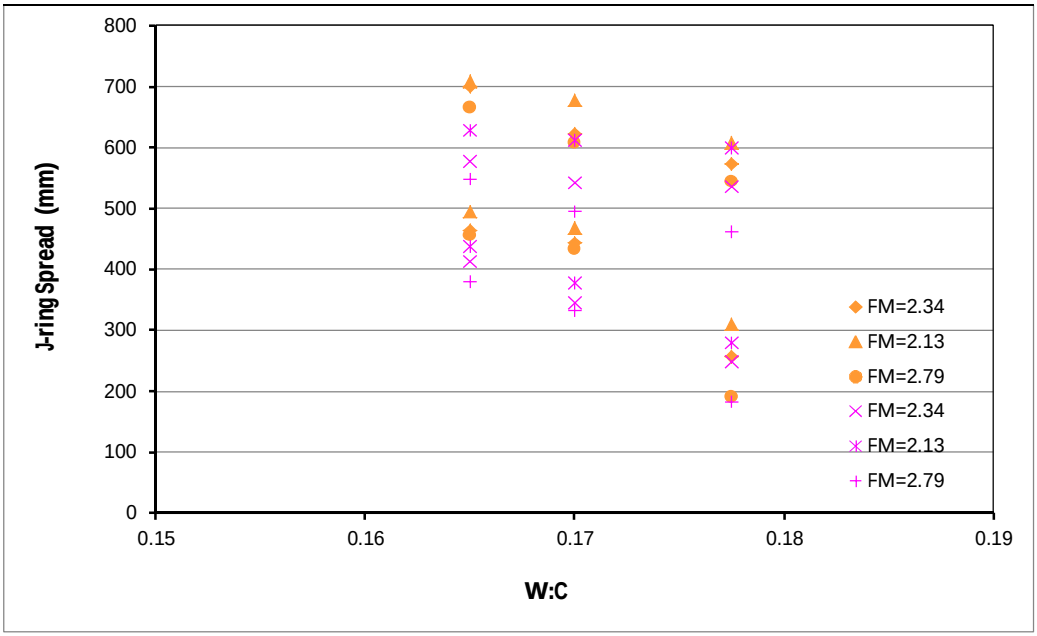

Fig.4.19 Slump versus water content

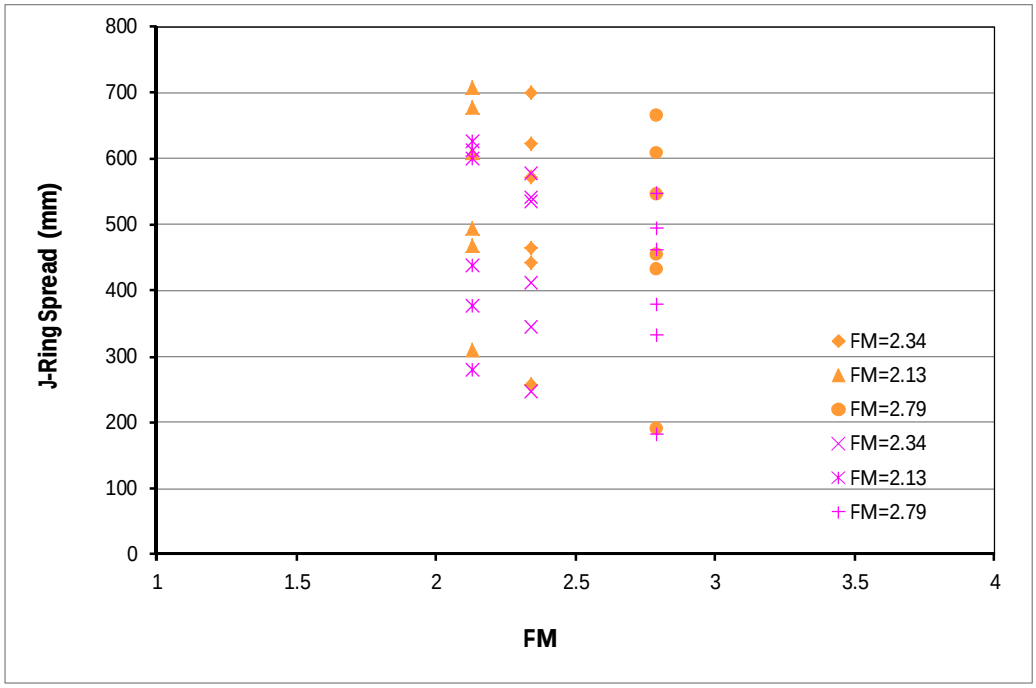

Fig.4.20 Slump versus fineness modulus (FM) of sand

This series of tests measures three parameters; passing ability by measuring the horizontal flow spread, calculating the time needed for UHPFRC to reach a defined flow distance and blocking step measures the resistance or blocking of UHPFRC. J-ring flow also measures the restricted deformability of UHPFRC due to the blocking effect of reinforcement bars and the blocking step calculates the flow passing through the narrow gaps that exist between the reinforcing bars in a real reinforced concrete structural element. It can be expected from the test results that the passing ability of the concrete will be dependent on the SP and water amount. Fineness modulus of sand also influence the flow based on the influence of packing density (Stark and Mueller 2008). The flow time measurement quantifies how much time is needed to reach a certain flow distance through the gap of steel reinforcing bars and it is depend on the passing ability of concrete. The J-ring flow diameters of all mixes were in the range 742.5-190mm and 627.5-182.5mm without and with fiber respectively. It is worth mentioning from the results that highest spread corresponded

to the mix with the lowest water and highest SP content for both mixes without and with fibers. This is the demand of UHPFRC to reduce water-cement in the mixes with increasing retarding admixture and achieved higher spread.

It is seen that fresh concrete passing ability is increasing with the increases of SP content for both without and with fiber cases, as shown in Fig.4.18 and it follows the same behaviour of slump spread of UHPFRC as previously described the reason of this behaviour in section 4.2.5.2. However, the j-ring passing ability decreases with increasing of fineness modulus (FM) of sand presented in Fig.4.20. Similar behaviour of the slump spread of UHPFRC with FM was observed in section 4.2.5.2 and the j-ring spread follows the similar reason of slump spread. It is also observed in Fig.4.18 that j-ring flow shows higher scatter of results both without and with fiber in the mixes. J-ring flow exhibits smaller value in the mix of with fiber case and this behaviour attributed to the blocking or prevent of UHPFRC flow through the J-ring steel reinforcement. It is also found from Fig.4.19 for the mix design nos. 1, 7 and 13 from Table 4.1 with total w:c = 0.20675 and for mix design nos. 4, 10 and 16 from Table 4.1 with total w:c = 0.19 contains high amount of water in the mix shows less spread than for the mix design nos. 3, 9 and 15 and mix design nos. 6, 12 and 18 from Table 4.1 respectively. The spread value decreased due to the probable increase in viscosity of the cement paste for higher water and lower SP mix; however the spread value increased resultant in decrease the viscosity of paste for lower water and higher SP content mix. It can be noticed that j-ring spread increases with lower FM and higher amount of SP and the spread decreased when opposite trend follow without and with fiber in the mixes.

The J-ring spread time (T_{50j}) test has been conducted to determine the qualitative estimation of the viscosity of the flow. This is also indicates the flow rate of

UHPFRC and how fast it reaches the specified spread distance. Plot of j-ring spread time (T_{50j}) versus fineness modulus (FM) of sand and J-ring spread versus j-ring spread time (T_{50j}) are illustrated in Figs.4.21 and 4.22. It is important to notice that j-ring spread time (T_{50j}) increased with coarser sand and decreased with finer sand before and after addition in the mixes. This behaviour is significant with fiber mixes and it indicates the fiber effect in UHPFRC as shown in Fig.4.21. The increase in spread time is attributed to the larger surface area of sand which absorbed more water and makes the flow sticky. The trend lines in Fig.4.22 indicate that the flow of the concrete with and without fibres and shows substantial scatter of results with the exception of very initial stages. It was observed that j-ring spread time increased with decreasing the flow for both without and with fiber mixes. It is specially observed with fiber mix due to the fiber effect. The spread time is increased because the fibers increase the viscosity of flow and make the flow slower.

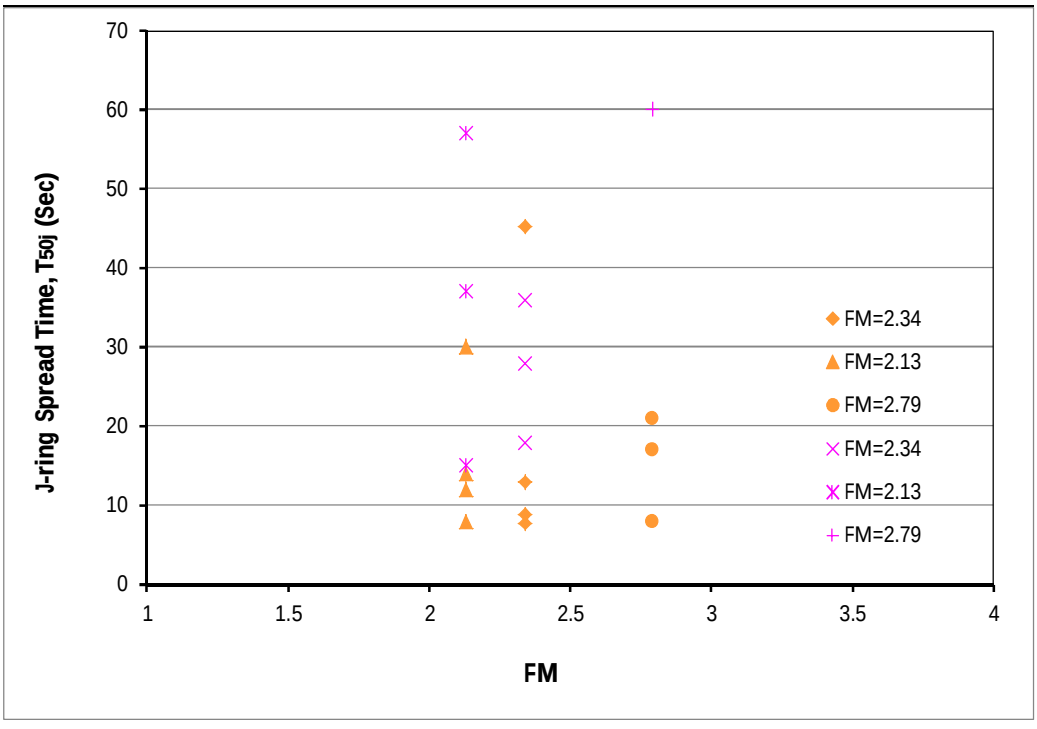

Fig.4.21 Measurement of J-ring spread with T_{50J} for UHPFRC

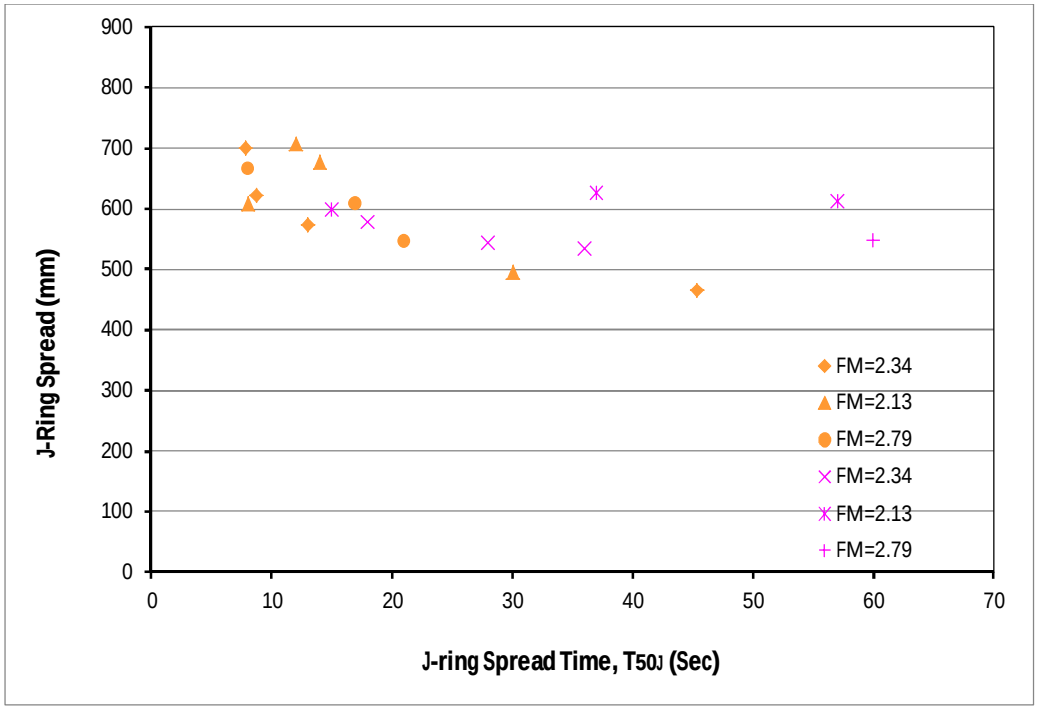

Fig.4.22 Measurement of J-ring spread with T_{50J} for UHPFRC

From the test, blocking step measures the difference in height between the center of UHPFRC and the outermost concrete of the J-ring. Blocking steps means the restriction of deformability of the flow of the mix. It also related with resistance to segregation of concrete that means the fresh concrete retain it homogeneity during the casting. It is expected from the blocking step measurement that whether the passing ability of flow through steel reinforcement is poor or high. It is seen in Fig. 4.23 that the trend lines shows scatter results without and with fiber mixes. It is observed that blocking steps are higher in mixes with fibers, that is passing ability of UHPFRC is less as the fibres act to restrict the flowability between reinforcement. It is also observed that the increasing of SP amount resultant in decreasing the blocking step of the mixes that means the passing ability of UHPFRC increased. This behaviour is attributed because of the fluidity of the mortar phase increases with increases in SP content. The similar behaviour is also observed due to the w:c content and FM of sand as shown in Fig.4.24 and Fig.4.25 respectively.

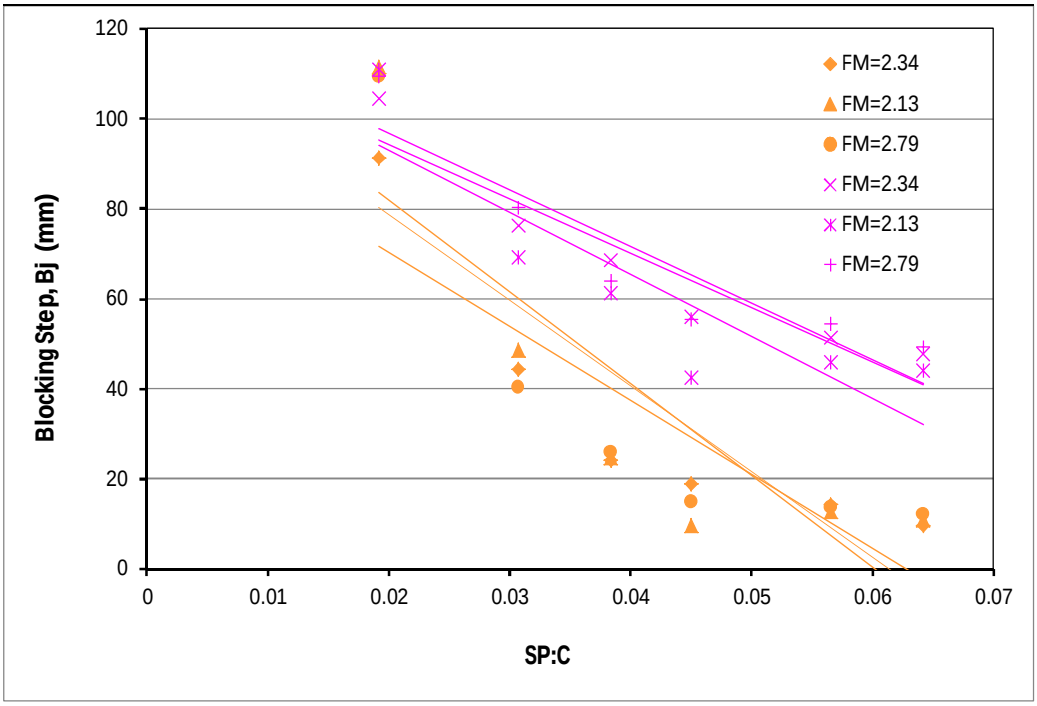

Fig.4.23 Blocking step versus superplasticizer content of UHPFRC

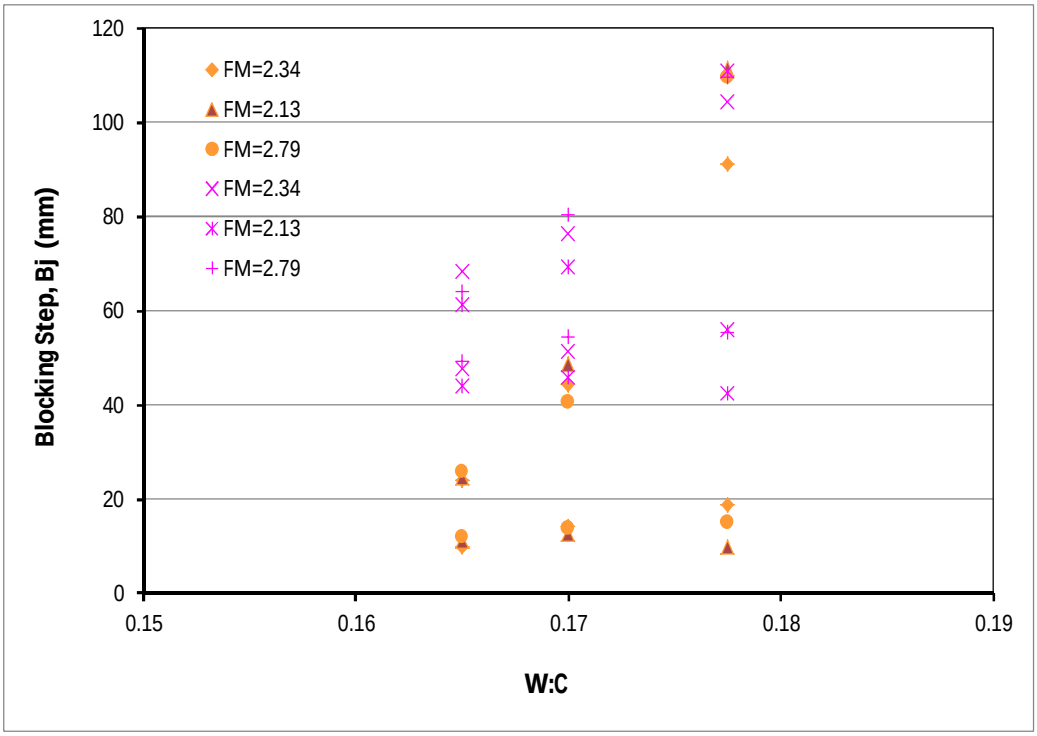

Fig.4.24 Blocking step versus water content of UHPFRC

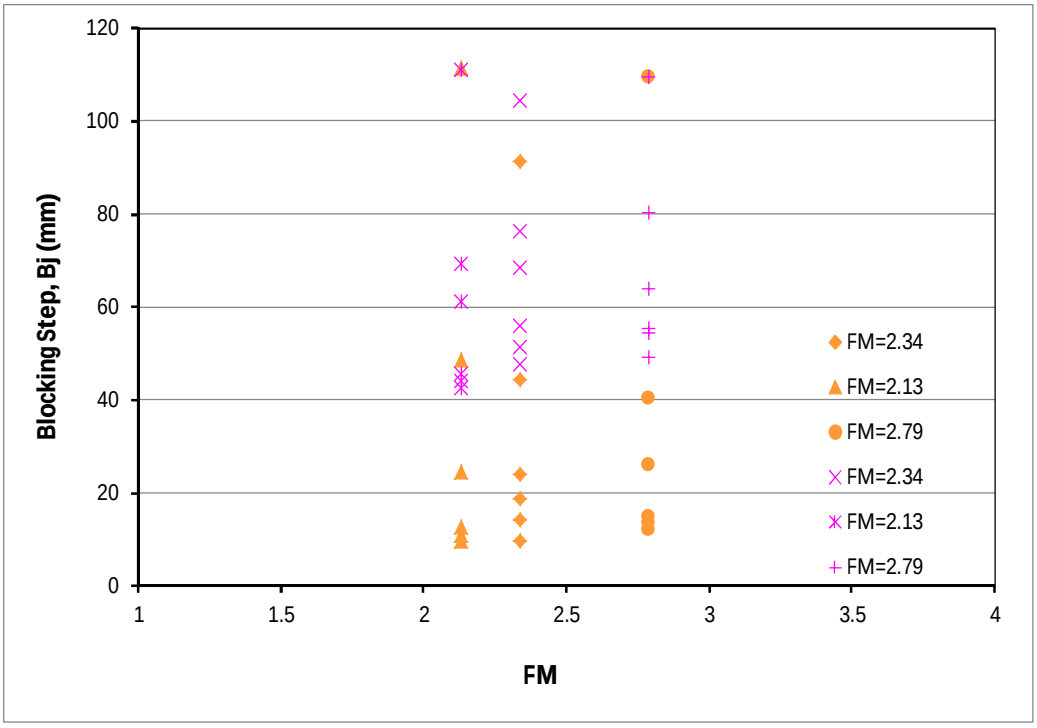

Fig.4.25 Blocking step versus fineness modulus (FM) of UHPFRC

4.2.5.4 Comparison of slump and J-ring spread test results

The slump and j-ring spread is plotted to observe the variation of flow for UHPFRC. Corresponding values of slump spread and j-ring spread shows in Fig.4.26 without and with fiber in the UHPFRC mixes and, here also, the trend is as expected, that is shown quiet similar value for without fiber mixes; however the spread with fiber exhibit scattered results. It was observed that the j-ring spread decreased about 14.76%, 9.71% and 17.9% then the slump spread for the mix 3, 9 and 12 in Table 4.1, those fiber mixes contains highest SP and lowest w:c; however the j-ring spread decreased about 1.13%, 0.422% and 1.15% then the slump spread without fiber mixes. It is clear from the results that difference of spread is more significant with fiber mixes and it indicates the great effect of fiber in the mixes. This is also happen due to the fiber increase the viscosity of flow resultant in reducing slump.

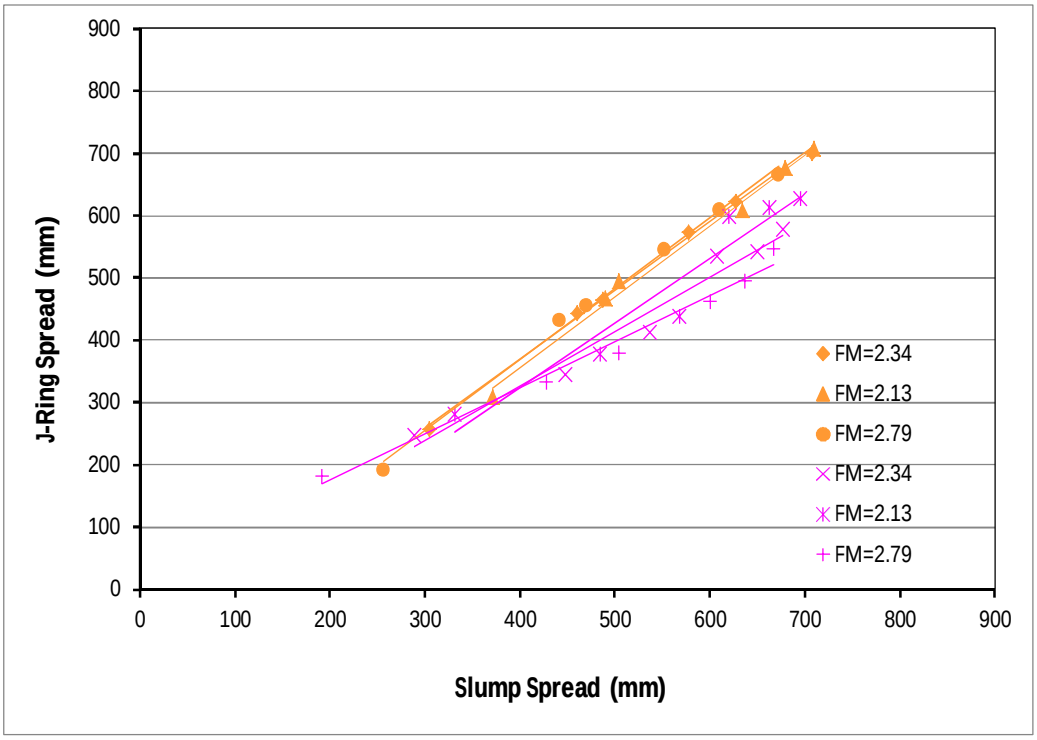

Fig.4.26 All of the measurement J-ring and slump spread values of UHPFRC

The test results of j-ring spread time (T_{50J}) and slump spread time (T_{50}) in Fig.4.27 are plotted to see the rate of deformation variation within a given flow distance for both without and with fiber mixes. As can be seen there is a considerable difference of time both with the j-ring and for the slump spread. According to the theory the j-ring spread time should be higher than slump spread due to the blocking of flow through the steel reinforcement. It is noticed that limited points are shown for both the j-ring and slump time, especially when fiber were present in mixes, which indicates for these mixes the flow did not exceed 500mm and hence no times are recorded.

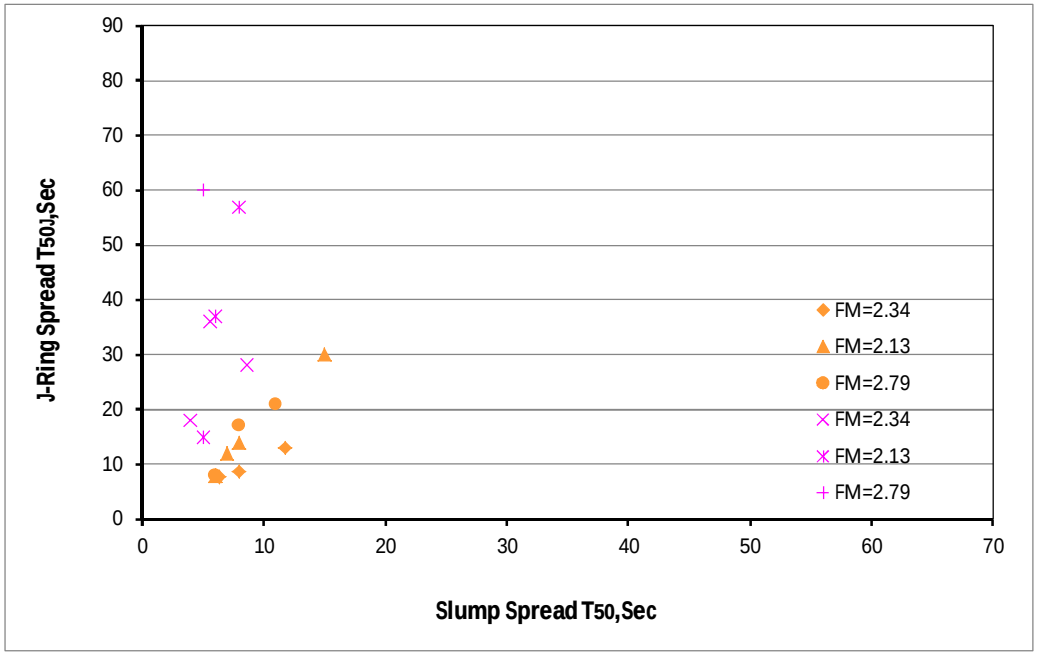

Fig.4.27 All of the measurement J-ring T_{50} and slump spread values of UHPFRC

The test result plotted in Fig.4.28 because the blocking step is a function of j-ring spread. It is observed that blocking step decreased due to the increase of j-ring spread without and with fiber mixes. This behaviour is observed substantially without fiber mixes. This seems to indicate that the less viscosity of flow increase the flow spread resultant to decrease the blocking step. The trend lines show similar behaviour at the beginning but with increasing flow scatter is increased. This indicates that j-ring spread of less than 500mm exhibit closer estimation for both without and with fiber mixes, however it shows scatter plot when the flow greater than 500mm. It is also seen that there is a good relation between blocking step and j-ring spread with fiber mixes.

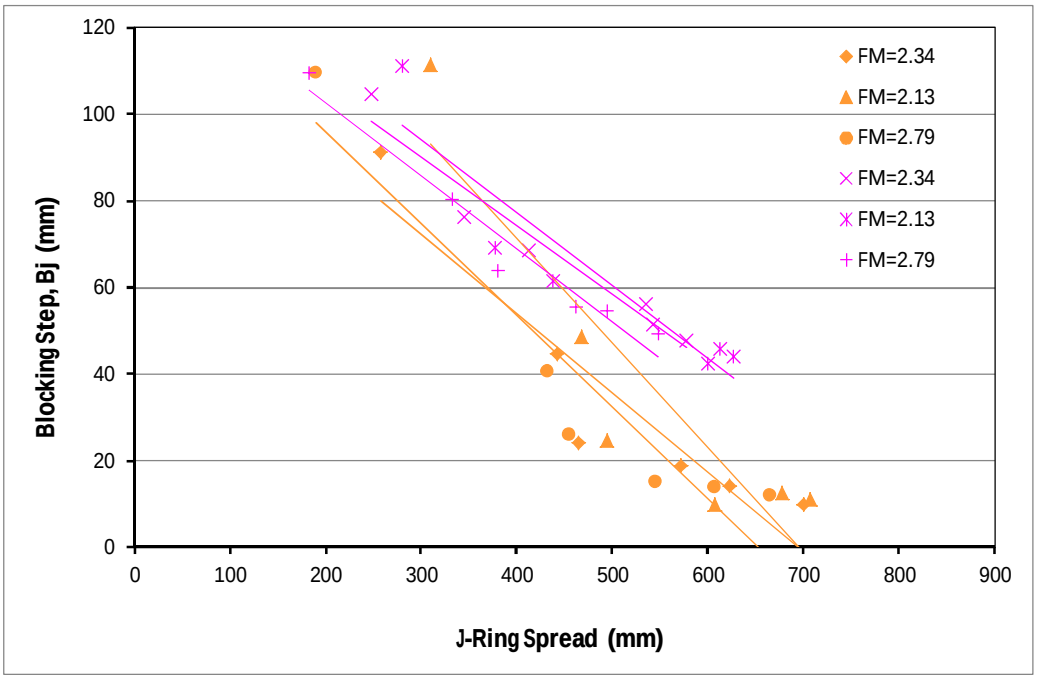

Fig.4.28 All of the measurement blocking step and J-ring spread of UHPFRC

4.2.5.5 Compressive test results on hardened UHPFRC properties

To investigate the effect of fineness modulus (FM) of conventional sands on the compressive strength properties UHPFRC, 26 mixes presented in Table 4.1 were investigated. The mix designs have been developed according to total water content in the mix. The total water content consists of the added water plus free water content in the SP. The main variables in the mix design are the fineness modulus, water and SP content. These test results are from the 100mm diameter and 200mm height cylinders cast according to the Table 4.4. In general, three cylinders were tested for each mix at various ages that is shown in Table 4.4 and the compressive strength test results were averaged three of the cylinders to get the final value that is presented in the Table 4.4. The results are presented in the Table 4.4 according to the each mix design with the corresponding days in terms of mean compressive strength, standard deviation, co-efficient of variation, standard error and the lower and upper 95% confidence interval of the compressive strength for each specimen. In general, it

can be observed from Table 4.4 that the compressive strength achieved from the UHPFRC test results ranged from 107MPa to 162MPa to the corresponding test age 7 to 90 days. It is also observed that the standard deviation of the tested specimens ranging from 0.389 to 14.963 with the corresponding co-efficient of variation 0.25% to 10.84%. Furthermore, the differences in compressive test results varied maximum 10.84% amongst the three specimens and the corresponding maximum standard error 8.639 of the specimen. The variation in results can be attributed to the minimal number of test specimens tested.

Table 4.4 UHPFRC compressive test results with conventional fine aggregate

Mixes	Days	Compressive Strength				95% Confidence Interval	
		Mean Strength, MPa	Standard Deviation, MPa	Coefficient of variation	Standard Error	Lower limit, MPa	Upper limit, MPa
1	7	117	3.027	0.0259	1.747	115.3	118.7
	28	139	10.804	0.0777	6.238	133.1	144.9
	56	149	7.089	0.0476	4.093	145.1	152.9
	90	141	4.631	0.0328	2.674	138.5	143.5
2	7	117	6.814	0.0582	3.934	113.3	120.7
	28	145	1.440	0.0099	0.832	144.2	145.8
	56	152	4.757	0.0313	2.747	149.4	154.6
	90	147	6.117	0.0416	3.532	143.6	150.4
3	7	112	4.208	0.0376	2.429	109.7	114.3
	28	147	1.440	0.0098	0.832	146.2	147.8
	56	143	4.648	0.0325	2.684	140.5	145.5
	90	146	6.228	0.0427	3.596	142.6	149.4
4	7	128	3.711	0.0290	2.143	126.0	130.0
	28	153	1.261	0.0082	0.728	152.3	153.7
	56	153	3.488	0.0228	2.014	151.1	154.9
	90	155	6.904	0.0445	3.986	151.2	158.8
5	7	120	12.890	0.1074	7.442	112.9	127.1
	28	149	4.501	0.0302	2.599	146.5	151.5
	56	148	8.910	0.0602	5.144	143.1	152.9
	90	146	1.282	0.0088	0.740	145.3	146.7
6	7	123	4.874	0.0396	2.814	120.3	125.7
	28	150	5.943	0.0396	3.431	146.7	153.3
	56	153	3.339	0.0218	1.928	151.2	154.8
	90	150	5.327	0.0355	3.076	147.1	152.9
7	7	107	4.859	0.0454	2.805	104.3	109.7
	28	136	7.513	0.0552	4.337	131.9	140.1
	56	138	14.963	0.1084	8.639	129.8	146.2
	90	143	4.125	0.0288	2.381	140.7	145.3

8	7	102	2.140	0.0210	1.235	100.8	103.2
	28	141	2.429	0.0172	1.402	139.7	142.3
	56	150	6.382	0.0425	3.685	146.5	153.5
	90	138	3.652	0.0265	2.109	136.0	140.0
9	7	107	1.710	0.0160	0.987	106.1	107.9
	28	141	9.439	0.0669	5.450	135.8	146.2
	56	153	6.260	0.0409	3.614	149.6	156.4
	90	141	3.019	0.0214	1.743	139.3	142.7
10	7	123	3.769	0.0306	2.176	120.9	125.1
	28	137	9.211	0.0672	5.318	131.9	142.1
	56	162	0.894	0.0055	0.516	161.5	162.5
	90	158	2.831	0.0179	1.634	156.4	159.6
11	7	130	6.183	0.0476	3.571	126.6	133.4
	28	143	3.248	0.0227	1.875	141.2	144.8
	56	160	2.940	0.0184	1.698	158.4	161.6
	90	150	5.376	0.0358	3.104	147.1	152.9
12	7	131	2.836	0.0216	1.637	129.4	132.6
	28	146	2.120	0.0145	1.224	144.8	147.2
	56	148	2.740	0.0185	1.582	146.5	149.5
	90	139	7.405	0.0533	4.275	134.9	143.1
13	7	112	4.807	0.0429	2.775	109.4	114.6
	28	138	0.892	0.0065	0.515	137.5	138.5
	56	149	7.075	0.0475	4.085	145.1	152.9
	90	153	10.563	0.0690	6.098	147.2	158.8
14	7	110	3.699	0.0336	2.136	108.0	112.0
	28	141	5.222	0.0370	3.015	138.1	143.9
	56	151	4.472	0.0296	2.582	148.5	153.5
	90	154	8.218	0.0534	4.745	149.5	158.5
15	7	110	2.176	0.0198	1.256	108.8	111.2
	28	138	1.543	0.0112	0.891	137.2	138.8
	56	153	2.140	0.0140	1.235	151.8	154.2
	90	143	5.795	0.0405	3.346	139.8	146.2
16	7	124	6.768	0.0546	3.907	120.3	127.7
	28	148	1.625	0.0110	0.938	147.1	148.9
	56	155	0.389	0.0025	0.225	154.8	155.2
	90	151	4.933	0.0327	2.848	148.3	153.7
17	7	119	2.166	0.0182	1.250	117.8	120.2
	28	148	5.903	0.0399	3.408	144.8	151.2
	56	152	4.778	0.0314	4.759	149.4	154.6
	90	151	0.431	0.0029	0.249	150.8	151.2
18	7	121	9.055	0.0748	5.228	116.0	126.0
	28	150	1.923	0.0128	1.110	148.9	151.1
	56	134	4.207	0.0314	2.429	131.7	136.3
	90	154	6.353	0.0413	3.668	150.5	157.5
19	7	120	4.985	0.0415	2.878	117.3	122.7
	28	150	1.626	0.0108	0.939	149.1	150.9
	56	153	3.673	0.0240	2.120	151.0	155.0
	90	146	1.019	0.0070	0.588	145.4	146.6
20	7	127	3.626	0.0286	2.093	125.0	129.0
	28	152	2.220	0.0146	1.282	150.8	153.2
	56	154	4.042	0.0262	2.334	151.8	156.2
	90	147	1.011	0.0069	0.584	146.4	147.6

21	7	130	1.011	0.0078	0.584	129.4	130.6
	28	153	4.131	0.0270	2.385	150.7	155.3
	56	156	4.412	0.0283	2.547	153.6	158.4
	90	149	2.653	0.0178	1.532	147.5	150.5
22	7	135	1.325	0.0098	0.765	134.3	135.7
	28	151	2.169	0.0144	1.252	149.8	152.2
	56	154	3.130	0.0203	1.807	152.3	155.7
	90	147	1.468	0.0100	0.848	146.2	147.8
23	7	131	3.568	0.0272	2.060	129.0	133.0
	28	148	1.784	0.0121	1.030	147.0	149.0
	56	151	2.543	0.0168	1.468	149.6	152.4
	90	144	2.695	0.0187	1.556	142.5	145.5
24	7	131	3.577	0.0273	2.065	129.0	133.0
	28	143	2.049	0.0143	1.183	141.9	144.1
	56	146	1.509	0.0103	0.871	145.2	146.8
	90	140	0.972	0.0069	0.561	139.5	140.5
25	7	116	3.756	0.0324	2.169	113.9	118.1
26	7	131	4.501	0.0344	2.599	128.5	133.5

Some observations can be seen according to the compressive strength test results. The lowest compressive strength of 7–days was found of 107MPa with a 95% confidence interval of 100.8 MPa to 103.2 MPa for the sand of FM of 2.34 with w:c = 0.17 and sp:c = 0.0565 and the highest compressive strength was 135MPa with a 95% confidence interval of 134.3MPa to 135.7MPa for the sand of FM of 2.34 with w:c = 0.19 and sp:c = 0.025. It is also seen that 28-days compressive strength of lowest value was observed 136.0MPa with a 95% confidence interval of 131.9MPa to 140.1MPa for the sand of FM of 2.34 with w:c = 0.1775 and sp:c = 0.045 and the highest compressive strength was 153MPa with a 95% confidence interval of 152.3MPa to 153.7MPa for the sand of FM of 2.13 with w:c = 0.165 and sp:c = 0.0384.

Figures 4.29 and 4.30 illustrate the influence of FM of conventional natural fine aggregate on the compressive strength gain of UHPFRC with time of each mix. In the plots, the same colour tics indicate mixes with the same FM and tics with the same shape indicate mixes with the same sp:c ratio for each mix corresponding days.

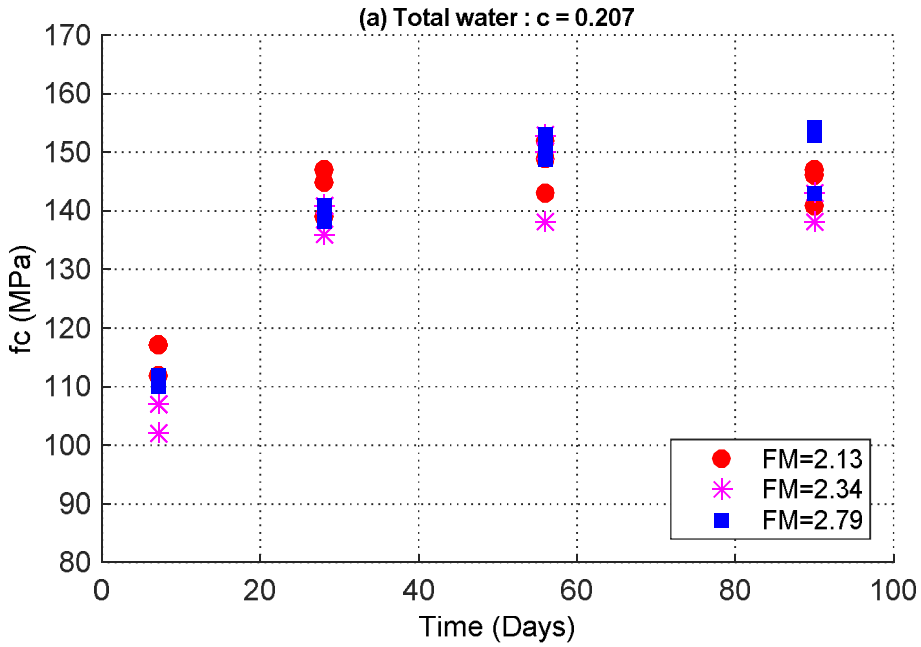

Fig.4.29 Compressive strength gain over time for mixes with conventional fine aggregate

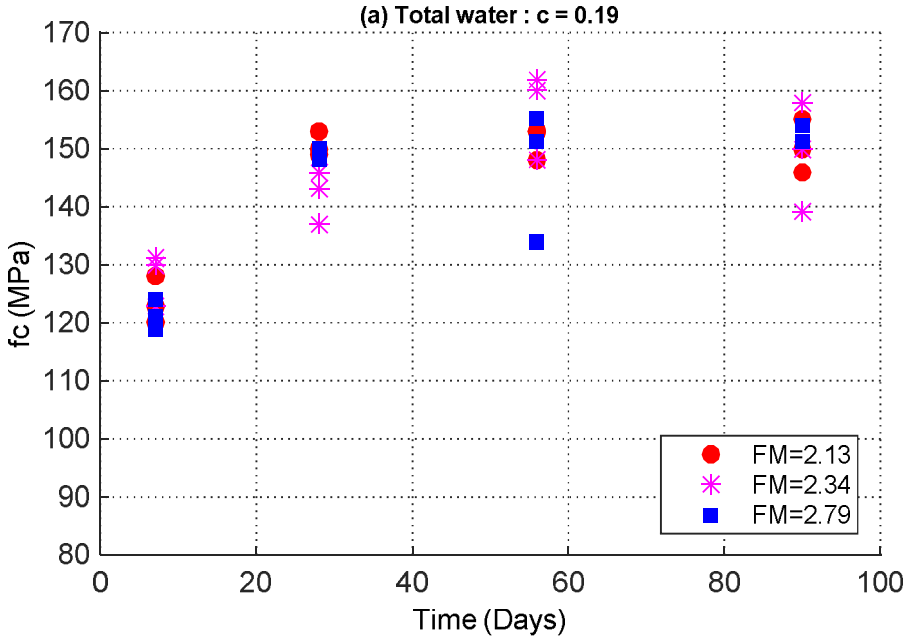

Fig.4.30 Compressive strength gain over time for mixes with conventional fine aggregate

It can be observed in Table 4.4 that the total water to cement ratio most strongly influence the compressive strength of the mixes and hence the results are divided into two plots in which the w:c ratio is constant. It can be seen from Figures 4.29 and

4.30 that most of the compressive strength gained at early age 7 days in all the mixes. In general, it can be estimated about 74% and 79% of their 56 and 90 days compressive strength (f_c) respectively. The 28-day compressive strength was in the range of 136-153MPa and there is marginal strength gains achieved at this stage for total w:c ratios. The increase in strength from 7 to 28 days was reached at a rapid rate before slowing markedly to 56 days beyond which the change in strength is relatively small, this is especially so for total w:c = 0.190 and for mixes with lower FM which indicates that there may have been insufficient free water for the hydration reaction to be completed fully. Similar finding reported by the Yang et al. (2009) in their research. They concluded that conventional natural sand can achieved continuous increase in compressive strength of UHPFRC until 56 days; however decrease in strength in some of the cases. It is seen that the compressive strength of UHPFRC by using conventional natural sand can attained similar strength to the silica sand. The compressive strength by using silica sand will discuss in the series – IV. The differences in the compressive strength amongst the conventional sand in UHPFRC results from the distribution of grain size of the materials where the most homogenous and concrete arises when the cement grains fill the voids between well graded sand and the silica fume fills the voids between the cement grains. This filling behaviour leads improved bonding of the constituents, resulting in higher compressive strength or higher load carrying capacity of the structural members.

It is also interesting to mention that the continuous increase in compressive strength observed until 56 day period, however in some cases a decrease in strength between day 56 and 90 occurs for both plots and is observed most significant in those mixes with the lowest total free w:c ratio and with a higher FM of sand mixes. After 56 days, the decrease of strength was ranged 4 to 8% for total w:c = 0.207 and 0.190 contents of the mix specimens. It was also observed that the compressive strength of

90 days was little increase from the 56 days period or remains unchanged of 56 days value. The similar observation also reported by the other researchers (Graybeal, 2007; Yang et al., 2009). This loss of strength can be attributed to the formation of internal micro cracks due to shrinkage, which is restrained primarily by the fibres, but also by the aggregate as suggested by the correlation between the loss of strength and FM. In general, it is also observed that the compressive strength achieved with total w:c = 0.19 mixes shows higher strength then the total water: c mixes = 0.207 this behaviour is more significant at early 7 days and medium period of 56 days. The decrease in strength for total w:c = 0.207 mixes is on average 11% and 4% of total w:c = 0.190 mixes for 7 and 56 days period respectively. This behaviour may be attributed to the combined effect of higher SP and water content in the mix which creates more air void and less homogeneity in the UHPFRC, resulting in decrease the compressive strength. It is concluded that UHPFRC conventional natural fine aggregate can achieved similar compressive strength to the silica sand at early age and also the long term period.

The influence of the sp:c ratio on the compressive strength of UHPFRC is shown in Figures 4.31 and 4.32 where the total w:c ratio is fixed and plots have been separated to observe the effect of the total w:c content in the mixes. Compressive strengths versus sp:c content are plotted for the tested days 7, 28, 56 and 90 with fineness modulus of sand which are represented by the circular, rectangular and cross shaped tics respectively.

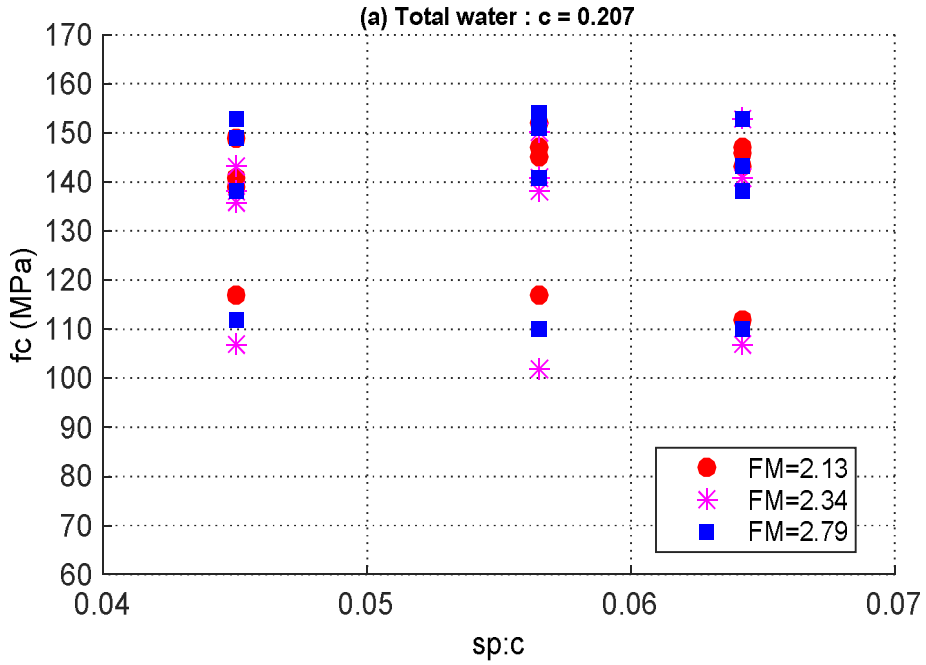

Fig.4.31 Influence of sp:c ratio of compressive strength

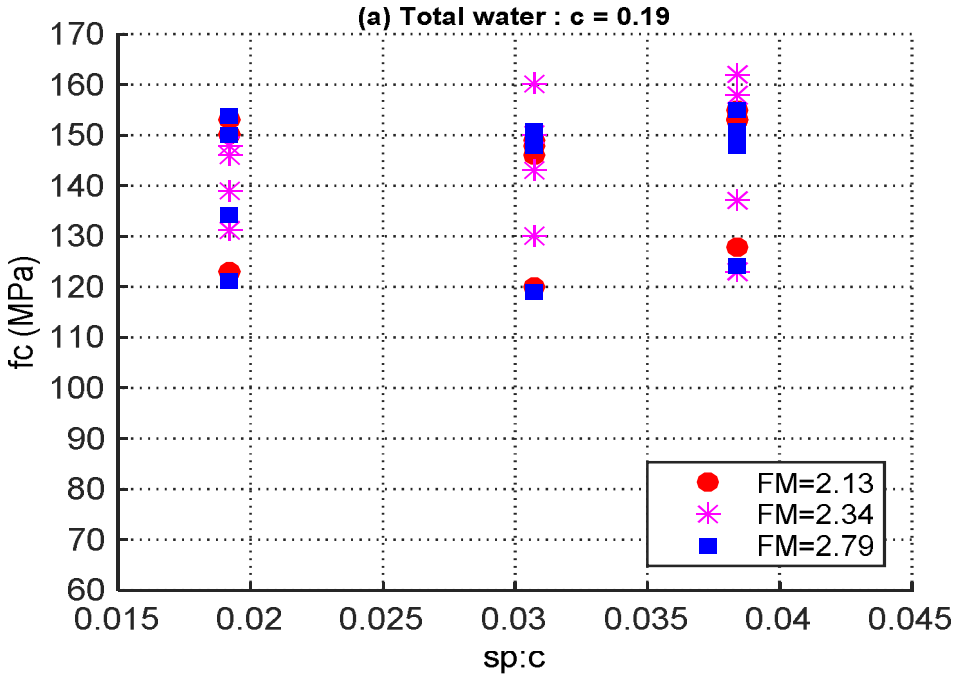

Fig.4.32 Influence of sp:c ratio of compressive strength

Initially considering the results in Figure 4.31 it can be seen that there appears to be a minor decrease in compressive strength with increasing sp:c ratios with the exception of the highest FM sand mixes. However, this behaviour is not observed in Figure

4.32 where total w:c ratios are lower, except for in the case of the highest FM. It is observed from the Fig.4.31 and Fig.4.32 that higher total w: c ratios mixes shows the maximum decrease in compressive strength then the lower total w: c ratios mixes for medium FM sand and it is around 11%.

The reduction in strength with increasing sp:c ratios can be attributed to the reduction in initial surface hydration of C_3S (Gagn et al., 1996; Odler & Becker, 1980) which is primarily responsible for reducing early age compressive strengths and hence the rate of strength gain. It can be also found from Fig.4.32 that as the sp:c content increases in lower total w:c ratio mixes the compressive strength increases as well for medium FM of sand (FM =2.79). This can be happen due to the more angular sand particle and excess hydration occurs at the early stage of curing. It is also observed that from the Figs.4.31 and 4.32 that with increasing or decreasing SP content in the total w:c = 0.207 and 0.190 mixes exhibit very quiet similar compressive strength except the early strength development. It seems that there are negligible effects of total water content in these mixes in the longer period.

Figures 4.33 and 4.34 show the clear effect of compressive strength as a function of the FM and the graphs are plotted 7, 28, 56 and 90 days test results with respect to total w:c and sp:c content which represents by the circular, rectangular and cross shaped tics. It is noted that both of the Figs.4.33 and 4.34 plotted and analyse the strength characteristics based on the two major dependent variables SP and FM and the third variable is the days.

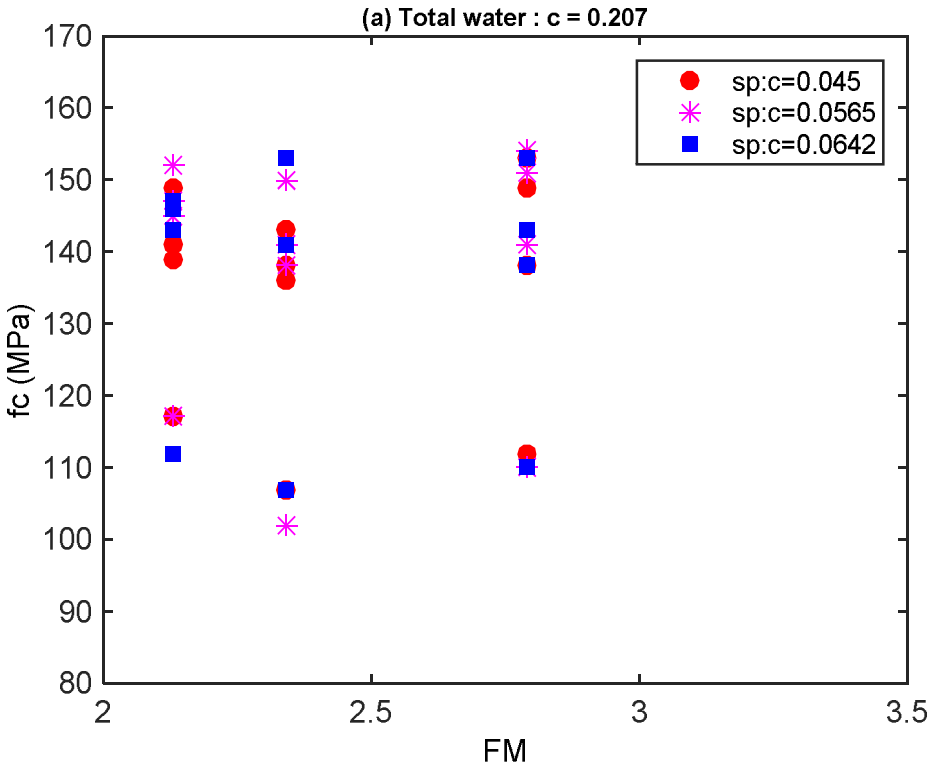

Fig.4.33 Influence of FM on compressive strength

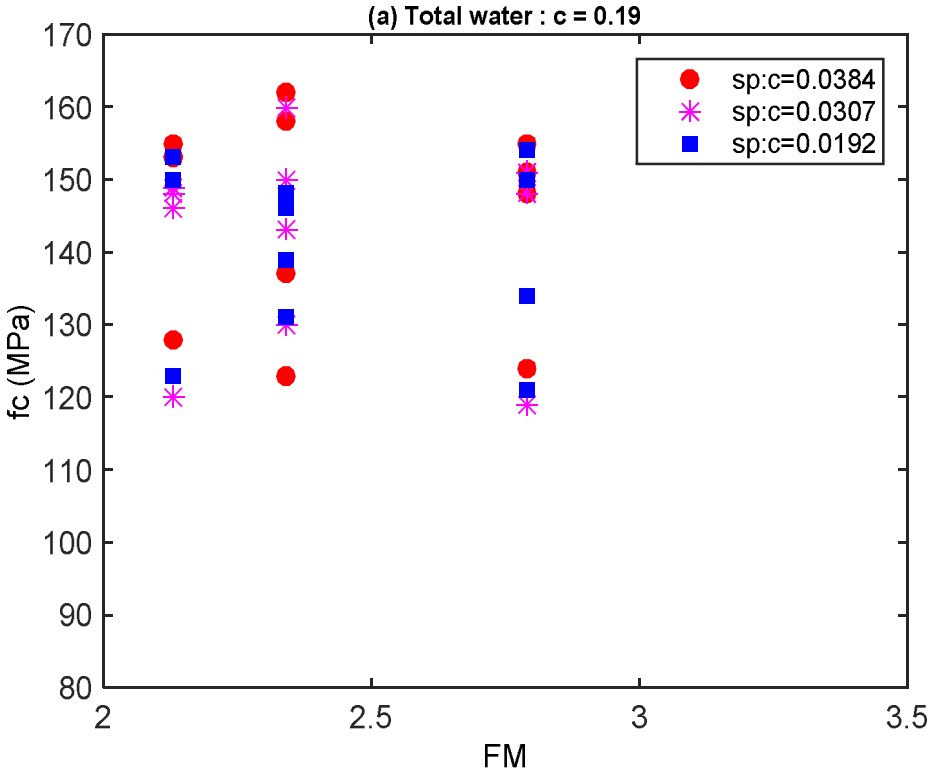

Fig.4.34 Influence of FM on compressive strength

It is seen from Fig.4.33 that there is a correlation of FM with compressive strength in the vertical scatter results, especially at the early ages. The mixes with medium FM sand appear lowest strength gain at higher total w:c ratios at the early age; consequently the compressive strength is observed quiet similar with medium FM sand and other sand at lower total w:c ratios. The difference in the compressive strength at the early ages between the sands type might be attributed the sand geometry and internal structure and excessive hydration at the early stage of curing (Yang et al., 2009).

It can be seen in Figure 4.33 and 4.34 from the vertical scatter results that there is a consistent and significant reduction in strength with increasing FM which appears to be independent of the mix design apart from in the case of very low w:c and sp:c ratios where a slight increase in strength occurs with FM. This suggests that there may be insufficient water for rapid hydration of the cement in these cases. As the rate of reduction in compressive strength is independent of the mix design, that is the total w:c and sp:c ratios, the reduction in strength with FM can be attributed to the packing density of the sand rather than the water requirement for hydration of the cement, that is the FM acts as a limit to strength rather than the w:c ratio.

The influence of sp:c ratio and FM on the compressive strength of UHPFRC has been identified in the previous section and the Figure 4.35 shows the variation of compressive strength in f_c with the sp:c ratio normalised by FM as this is expected to more clearly show the influence of sp:c. It can now be seen clearly in Figure 4.35 that the compressive strength is strongly correlated to the sp:c/FM ratios.

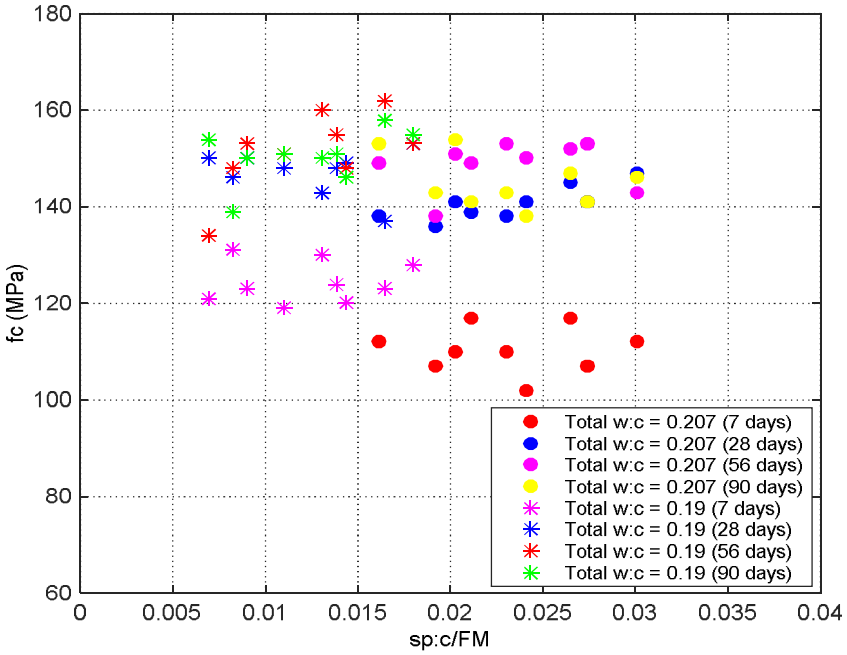

Fig.4.35 Influence of FM on fc

It can be seen from Fig.4.35 that total w:c =0.19 ratio mixes gained higher strengths then the total w:c =0.207 for each testing ages. This increase in strength can be attributed to the reduction in entrained air as the sp:c increases lead to the increase bond between cement paste and sand particle. In other words, the increase in SP results in increased instability of air voids and therefore an overall reduction in the entrained air, which can be expected to result in an increase in compressive strength of between 3 and 5% per percentage loss of entrained air (Neville, 1995; Safiuddin et al., 2008; Yang et al., 2009).

This finding is similar to that shown by Wille et al. (2011b) where the compressive strength of UHPFRC was defined directly as a function of entrained air, however in this case the definition has been extended to being in terms of FM which is significant as the FM is potentially more easily determined and hence should be available to all concrete technologist when undertaking the mix design.

4.3 Series – II: Coarse Aggregate as Partially Replaced with Fine Aggregate on UHPFRC

In the earliest series – I, UHPFRC mixes have been developed with three types of conventional sand as replacement of more expensive silica sand to reduce construction cost and attained similar strength and flow properties to the expensive silica sand. Concrete is a three phases composite material that consisted of hardened cement paste, aggregate skeleton and interfacial zone or bonding with the constituents. The coarse aggregate plays an important role on the mechanical properties in normal strength concrete; however in UHPFRC with enhanced cement paste and transition zone properties, the granular skeleton or pore structure can become the weakest point. The good bonding the concrete is enhanced by the suitable amount of coarse aggregate in the mix. So, it can be possible to consider potential use of coarse aggregate in the UHPFRC to improve mineralogical characteristic, proper texture; suitable flowability and gain early strength. A very few number of researches have been conducted on the influence of particle size, and different coarse aggregate (CA) to fine aggregate (FA) ratio to produce ultra-high performance fiber reinforced concrete (Ma et al., 2004; Wang et al., 2012; YANG et al., 2012). Wang et al. (2012) have investigated several CA to FA ratio to produce UHPFRC with a w/b of 0.14, 0.16 and 0.18. Although several studies reported on the mechanical and durability properties of UHPFRC with CA, however there is limited research to identify the optimum CA content in UHPFRC to achieve suitable flow and strength properties. Hence in this section mix designs are investigated to quantify the optimal ratio of CA to FA in order to achieve good flow and strength properties. The advantage of using coarse aggregate on UHPFRC is in further reducing material costs. To achieve fresh and hardened properties with incorporating coarse aggregate, the standardized procedure such as mix proportion, mixing, preparation, associated testing and result discussion are described in this section.

4.3.1 Materials and mix proportions

The basic proportions of the concrete mix a comprised of 1:1:0.266:0.175 ratios by weight of sulphate resisting cement (Type SR), coarse aggregates, fine aggregates, silica fume and steel fibres used for the mixes. The coarse aggregate grading was investigated to determine the influence of aggregate grading on the development of hardened properties of UHPFRC as shown in Fig.4.1. When selecting a mix design, it is always expected to compose the aggregates with maximum packing. The method described in ACI-211.1 (reapproved in 2002) states that the actual voids in compacted coarse aggregates are to be filled by sand, cement, silica fume and water. They also suggested that the coarse aggregate size of less than 12.5mm gives optimum packing in the mix. The smaller the coarse aggregate the larger is the aggregate surface to be enveloped by the cement paste. This attains to a high paste volume in UHPFRC to get a sufficient flow ability and optimum strength.

The bulk density of coarse aggregate used in this study was 1725kg/m^3. In all mixes, conventional washed river sand with FM of 2.34 was used instead of expensive silica quartz powder and silica quartz sand. The coarse aggregate was partially replaced with conventional sand in the mix to observe the behaviour of rheological and hardened properties of UHPFRC and compare the properties without CA mixes.

Initially, trial mixes were conducted, starting with the lowest CA to FA ratio, lower water and higher SP content i.e total water content 0.20675 in order to identify the upper limit at which the concrete was no longer workable due to the presence of coarse aggregate. To obtain the suitable mix proportion, 16 concrete mixtures were prepared with different CA/FA ratios by varying the key mixture parameters, namely SP and water content as presented in Table 4.5. According to the trial mixes in Table 4.5 it was observed that mix no.16 with total water content 0.190 shows the lowest

slump and that does not satisfy the UHPFRC requirement. Hence at this point the trial pour was stopped until the mix design composition of w:c = 0.1775 and sp:c = 0.045 with total water content 0.190. The compressive strength test of all trial mixes was determined at 7 days in order to identify optimal mixes for further investigation, at which point, the ratio of CA/FA = 0.82 was selected according to the optimum slump and strength of the mixes. Then, the three mixes with selected CA/FA have been conducted in the laboratory to investigate the influence of coarse aggregate with total water content 0.2075. Composition of UHPFRC mixture with CA/FA ratio is shown in Table 4.5.

The basic material including cement, fine aggregate, steel fiber, silica fume, SP were described in section 4.2.1 in series - I.

Table 4.5 Mix designs to investigate the influence of coarse aggregate

Mix number	CA:FA	w:c	sp:c	Total w:c
1-CA	0.82	0.1775	0.0450	0.20675
2-CA	0.82	0.170	0.0565	0.20675
3-CA	0.82	0.165	0.0642	0.20675
4-CA	1.00	0.165	0.0642	0.20675
5-CA	0.33	0.165	0.0642	0.20675
6-CA	3.00	0.165	0.0642	0.20675
7-CA	0.67	0.165	0.0642	0.20675
8-CA	0.54	0.165	0.0642	0.20675
9-CA	1.22	0.165	0.0642	0.20675
10-CA	1.50	0.165	0.0642	0.20675
11-CA	0.43	0.165	0.0642	0.20675
12-CA	1.86	0.165	0.0642	0.20675
13-CA	1.00	0.17	0.0565	0.20675
14-CA	0.33	0.17	0.0565	0.20675
15-CA	1.86	0.17	0.0565	0.20675
16-CA	1.50	0.17	0.0565	0.20675
17-CA	1.00	0.1775	0.045	0.20675
18-CA	1.00	0.165	0.0384	0.190

4.3.2 Mixing procedure

The mixing procedure is identical to that described in section 4.2.2 except that the coarse aggregate was included in the initial mixing of dry materials.

4.3.3 Specimen preparation and curing regimes

Specimen preparation and curing regime followed that discussed in part 4.2.3.

4.3.4 Test set-up and instrumentation

To determine rheological properties of UHPFRC with coarse aggregate addition, slump height, slump spread and j-ring spread measurements procedure were measured in an identical way to that covered in section 4.2.4. Test set-up and associated instrumentation and testing procedure were similar that described in section 4.2.4 to determine the hardened properties of UHPFRC with coarse aggregate. Figures 4.36 (a) and (b) presented the slump height measurement without and with fiber in the mixes; slump spread measurement is shown in Figures 4.36 (c) and (d), J-ring blocking step and J-ring spread measurement without fiber are illustrated in Figures 4.36 (e) and (f), and the measurement of J-ring blocking step and J-ring spread with fiber are depicted in Figures.4.36 (g) and (h).

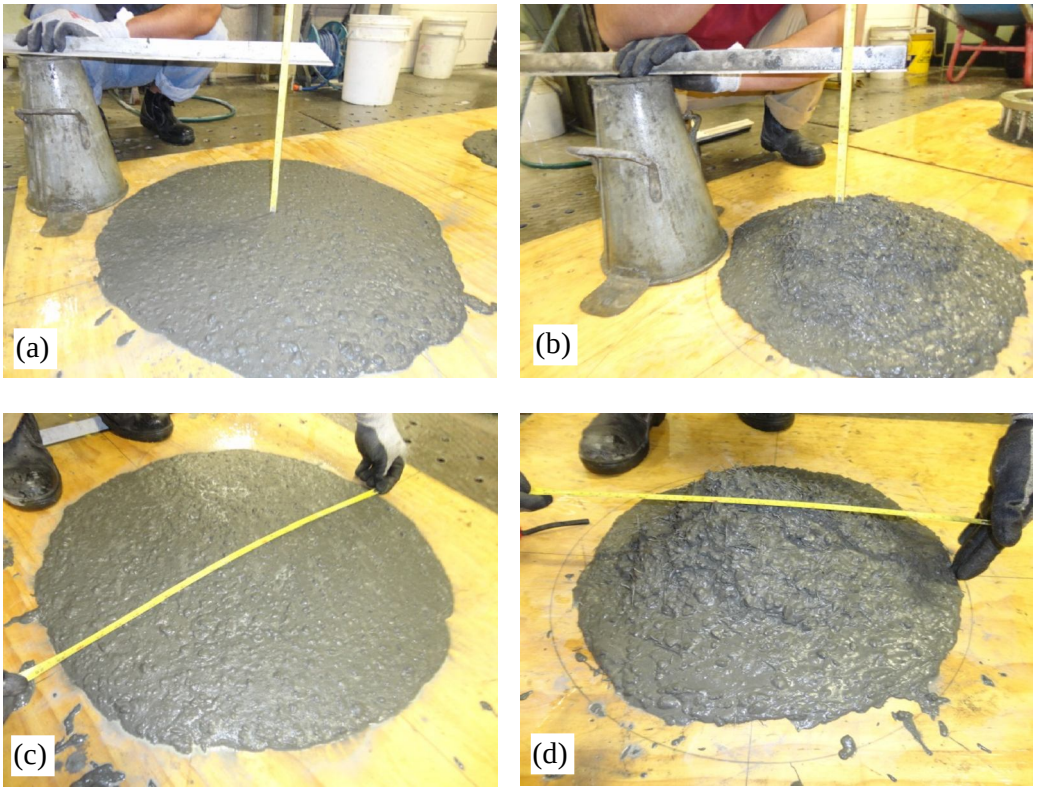

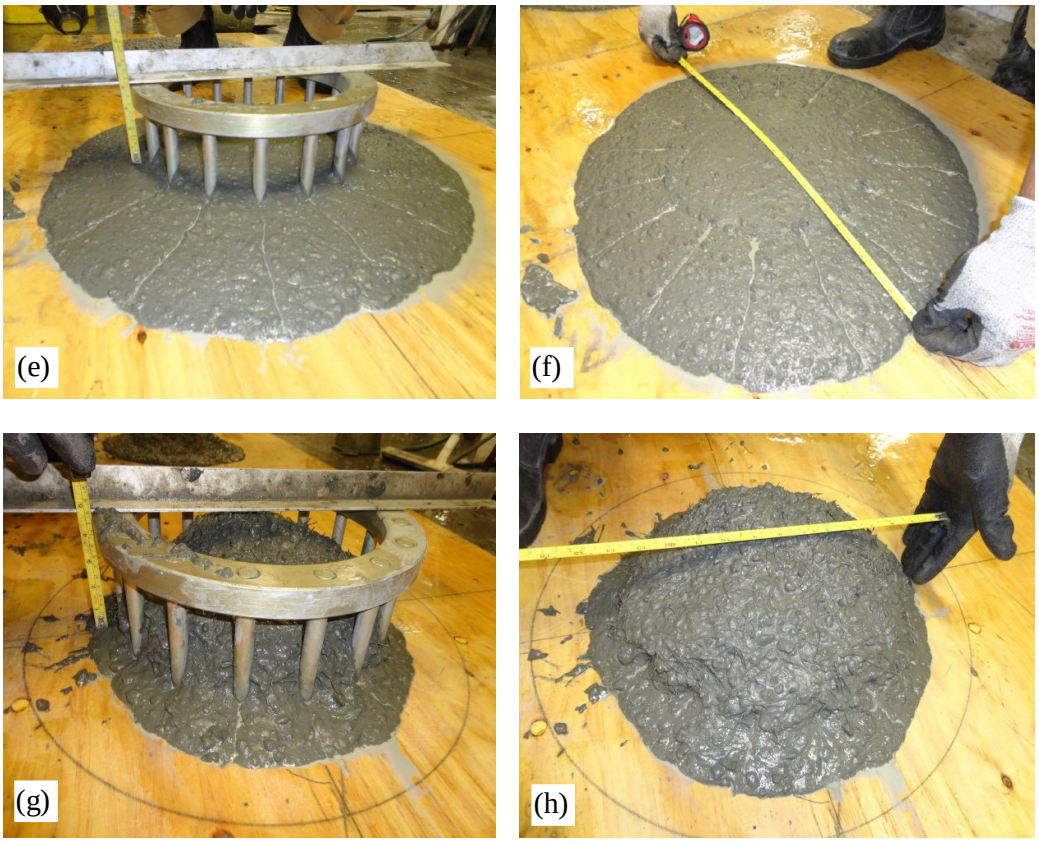

Fig.4.36 Measurement of (a) slump height without fiber (b) slump height with fiber (c) slump spread without fiber (d) slump spread with fiber (e) J-ring blocking step without fiber (f) J-ring spread without fiber (g) J-ring blocking step with fiber (h) J-ring spread with fiber

4.3.5 Test results and discussion

4.3.5.1 Influence of coarse aggregate on rheological properties of UHPFRC

The optimum CA to FA ratio was achieved from the trial mixes of UHPFRC with lower water and higher SP content. Finally, three mixes were selected based on the standard slump spread and 7-days strength characteristics values of UHPFRC and conducted the large amount of mixes with optimum CA to FA ratio. In this section, the influence of coarse aggregate on the rheological properties of UHPFRC was investigated including slump height, slump flow and J-ring blocking step and J-ring spread. The red color line in the graph indicates the mixes with fiber and the blue color line in the graph demonstrate without fiber addition in the mixes. The influence of coarse aggregate on the slump test of UHPFRC without and with fiber addition

and other influencing variable such as SP and water is depicted in the following Fig.4.37 and Fig.4.38 respectively.

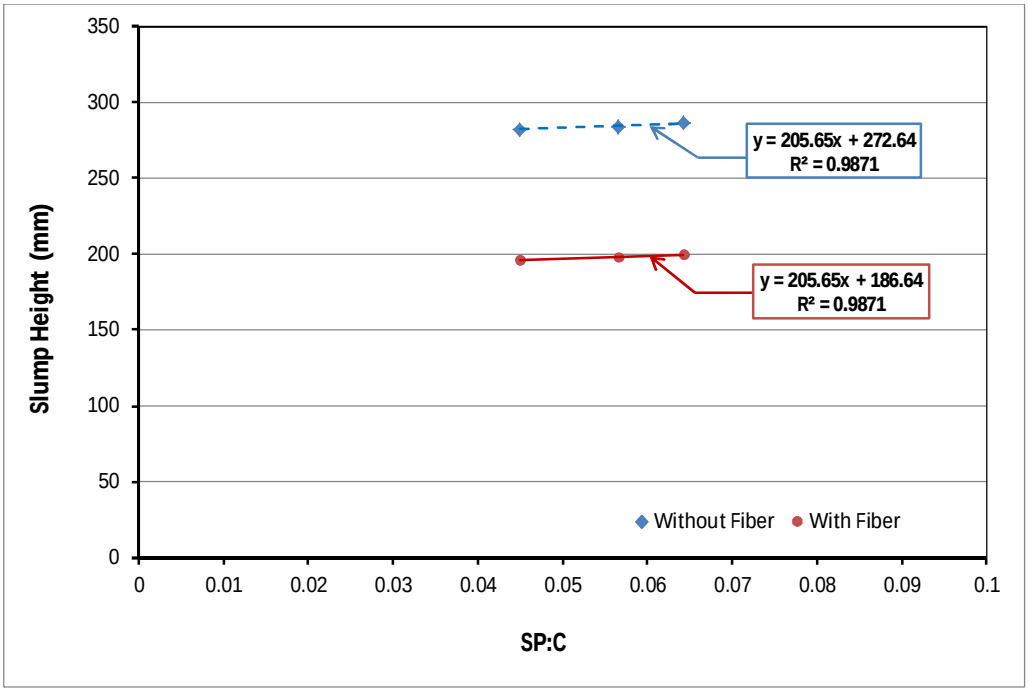

Fig.4.37 Slump versus superplasticizer (SP) content

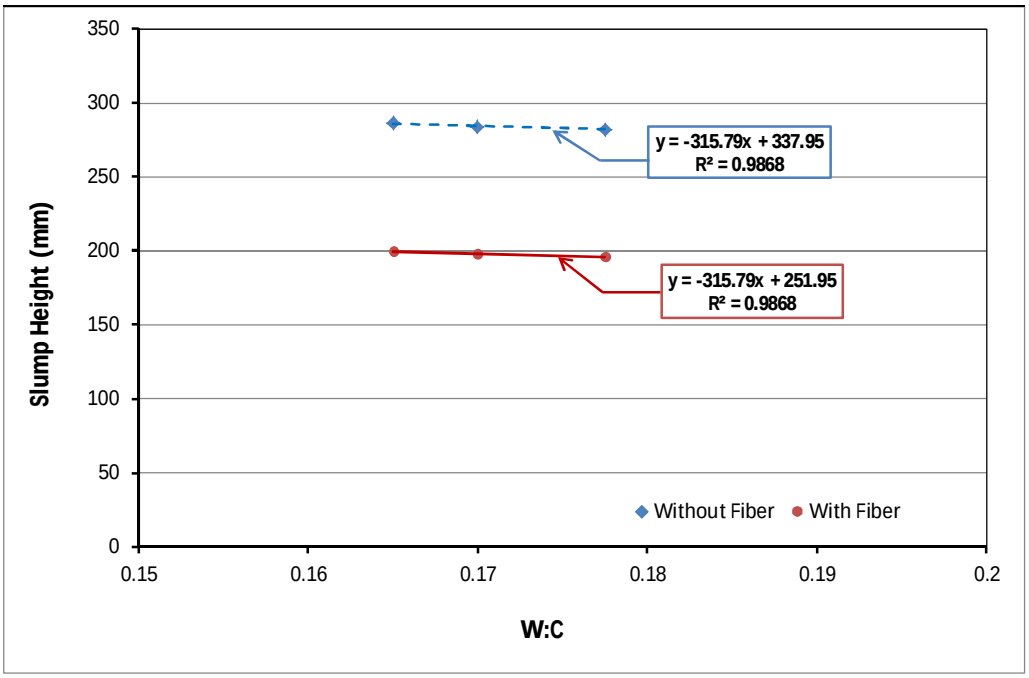

Fig.4.38 Slump versus water content

It is observed from Fig. 4.37 and Fig. 4.38 without and with fiber mixes that as the SP content increases the concrete gains the slump although the water-cement content decreases. It is also seen from both Figures that the trend line shows similar behaviour. It can be seen that with fiber addition there is a significant decrease of slump, however this behaviour was not observed without coarse aggregate addition from the previous mix. This suggests that the fibres are interacting detrimentally with the coarse aggregate to reduce flowability. The decrease of slump due to coarse aggregate content can also be attributed to the larger size of particle which predominantly decrease the fluidity of the mix resulted in increase the viscosity of the cement paste.

The slump spread and spread time test of UHPFRC with coarse aggregate in its fresh state achieved with and without the use of fiber shown in Fig. 4.39 to Fig 4.41. The test was done according to the slump test mentioned in ASTM-C1611/C1611M-09b (2009). This test measures two parameters; filling ability by measuring the horizontal spread and the spread time of concrete until 500mm spread is reached (T_{50}) is a calculates of the speed of spread time.

Figure 4.39 observed that the increasing of SP content is little increased of slump spread with and without fiber; consequently slump spread is decreasing with increasing the water content in the mixes as refer to Fig.4.40. It can also be seen in Figs.4.39 from trend lines that the flow of the concrete with and without fiber shows quiet similar slopes; however the opposite trend follow when water amount increased for slump spread refer to Fig.4.40. This behaviour demonstrate that the coarse aggregate attributed large size of particle and large surface area than other constituents of the mixes resultant in decreased the fluidity of the mixes and increased the viscosity of the cement paste. This behabiour is more pronounced when

the fiber added with the mixes. There is a small variation of the mixes due to the greater absorption capacity of coarse aggregate that interact with aggregate resultant in prevented increase of the spread.

The spread attained 595mm-715mm before fiber addition and the flow obtained 442.5mm-602.5mm after fiber addition. It was observed in Fig.4.41 that the flow ability is decreased with increasing the time without and with fiber mixes. It is also seen that the coarse aggregate with fiber have taken more time to reach the 500mm spread circle line. It means that the concrete was sticky and not highly workable when the coarse aggregate added with mix of UHPFRC and it is more significant with fiber mixes. However, the spread obtained with the coarse aggregate addition in the mixes is acceptable as standard spread value when compare with conventional fine aggregate mixes. It can be concluded that the coarse aggregate, water and SP retained by the concrete constituents and make the flow slower (Yang et al., 2009).

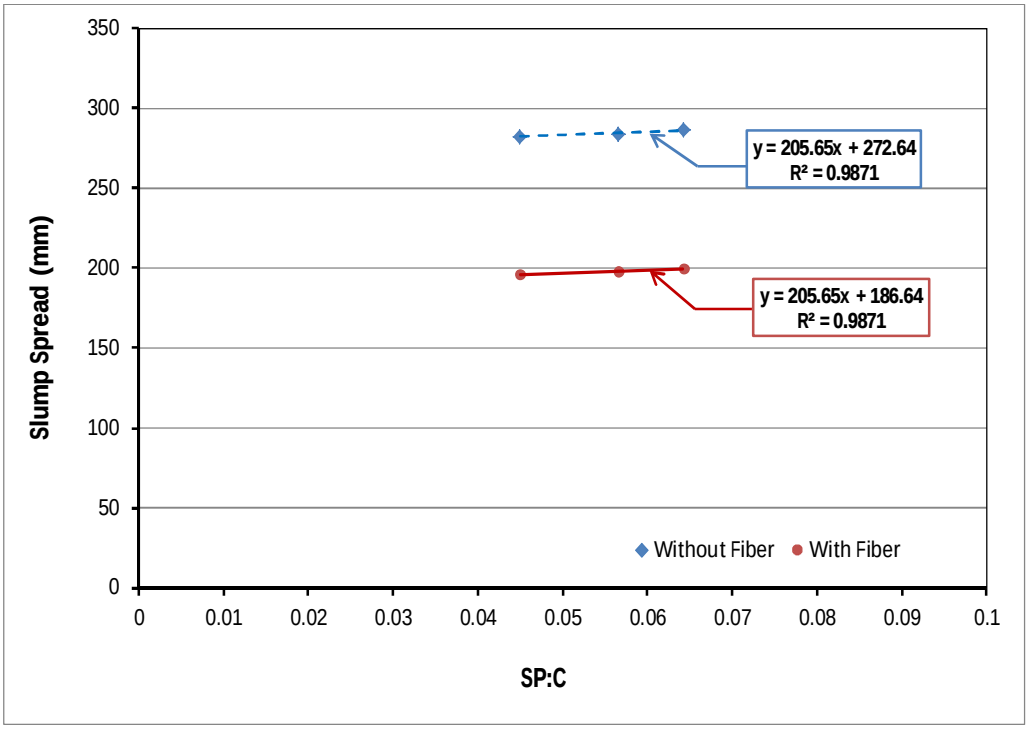

Fig.4.39 Slump spread versus superplasticizer (SP) content

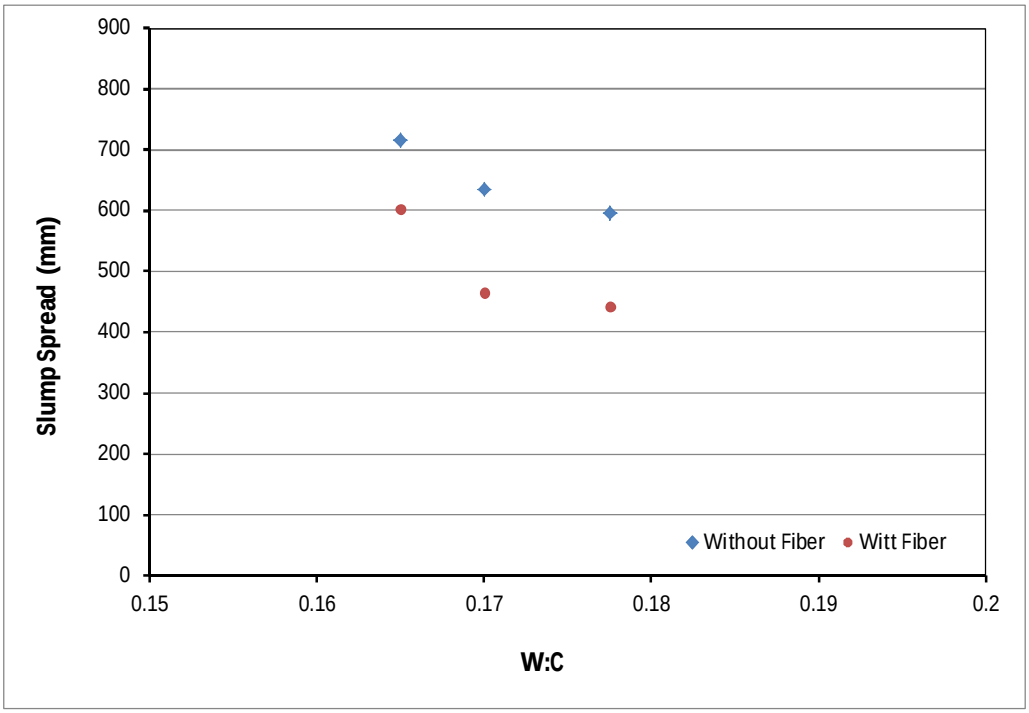

Fig.4.40 Slump spread versus water content

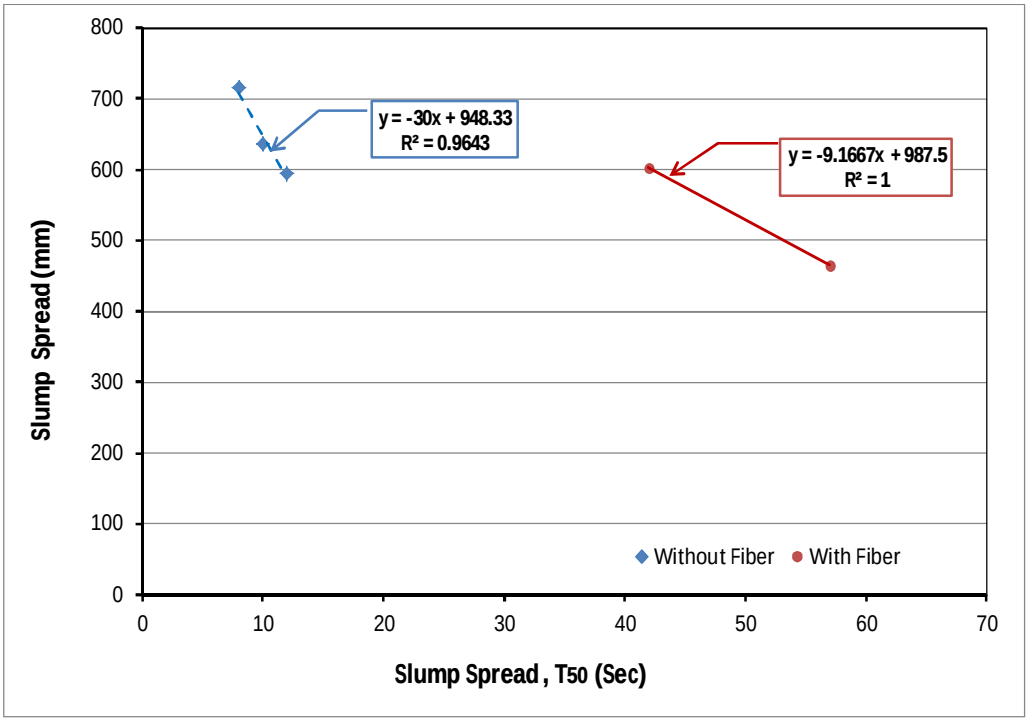

Fig.4.41 Slump spread versus slump spread time, T_{50}

The j-ring spread of UHPFRC with coarse aggregate in its fresh state obtained without and with the use of fiber shown in Fig.4.42 to Fig.4.46. The J-ring spread diameters of all mixes were in the range 617.5-577.5mm and 487.5-372.5mm without and with fiber respectively. It can be seen from Figure 4.42 that the fresh concrete passing ability is increased with increases of SP content for both without and with fiber cases; however the j-ring spread is decreasing with increasing of water content refer to Fig.4.43. It indicates that the present of SP content in the UHPFRC mixes is more susceptible function to make fluidity of the mixes rather than water content increase or decrease. On the other hand, the j-ring passing ability decreased a significantly with the introduction of fibers and coarse aggregate to the mix compare with conventional fine aggregate and decreased from slump spread test. This behaviour attributed of larger size of particle and the interaction between the fiber and the coarse aggregate which act together to create blocking and also the spread further prevented through the J-ring steel reinforcement.

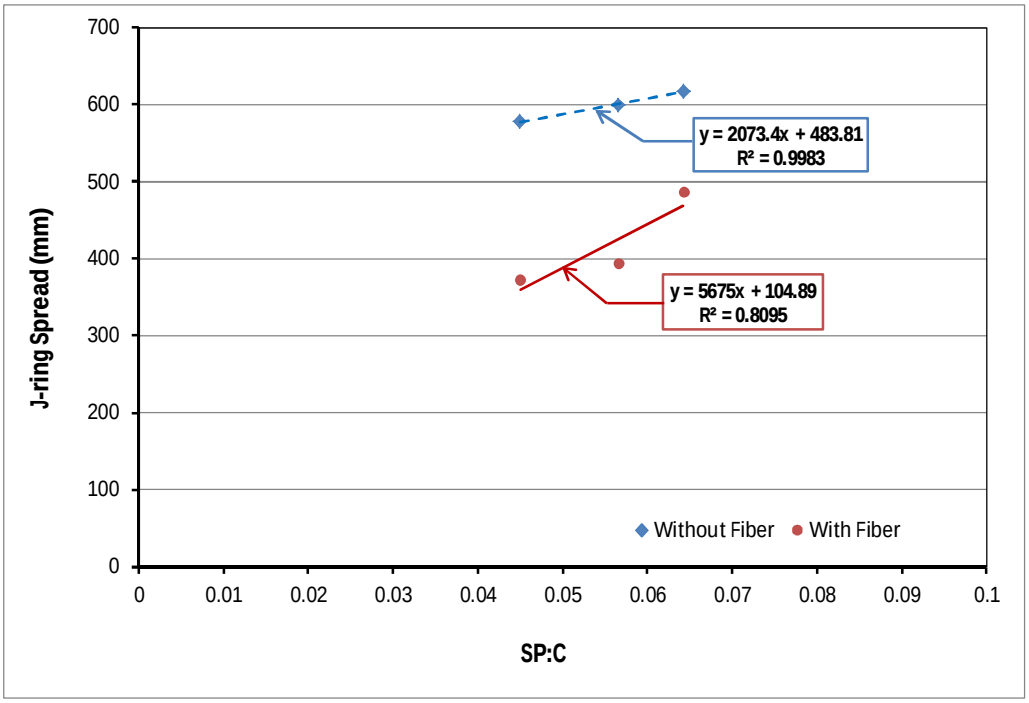

Fig.4.42 J-ring spread versus superplasticizer content

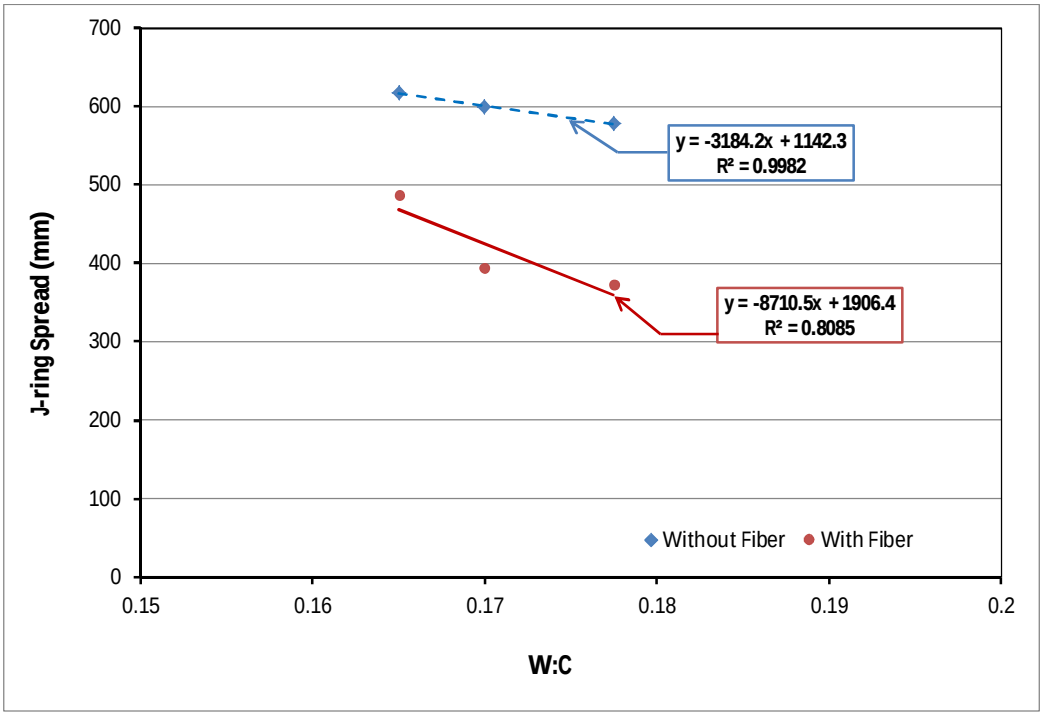

Fig.4.43 J-ring spread versus water content

Plot of j-ring spread time (T_{50j}) versus J-ring spread are illustrated in Figs.4.44. It is seen that J-ring spread is decreasing with increasing of j-ring time and this behaviour is more significant with fiber mixes. It is interesting to mention that there are no j-ring time values in the graph; it reveals that the coarse aggregate and fiber together makes the spread slower through the J-ring steel reinforcement. It is stronger with fiber mixes and the spread did not reach the 500mm circle so that no values appear in the graph. Similar behaviour is noticed when plotted the j-ring and spread time in a same graph and the slump spread time shows lower then j-ring spread to reach 500mm circle without fiber case refer to Fig.4.45. The increase in spread time is attributed to the larger surface area of coarse aggregate which absorbed more water and makes the flow sticky. It is important to notice that with the same content SP and water content, slump spread is always exhibits higher values than the j-ring spread as illustrated in Fig.4.46. In both test, the similarity observed that the spread values decreased with fiber mixes.

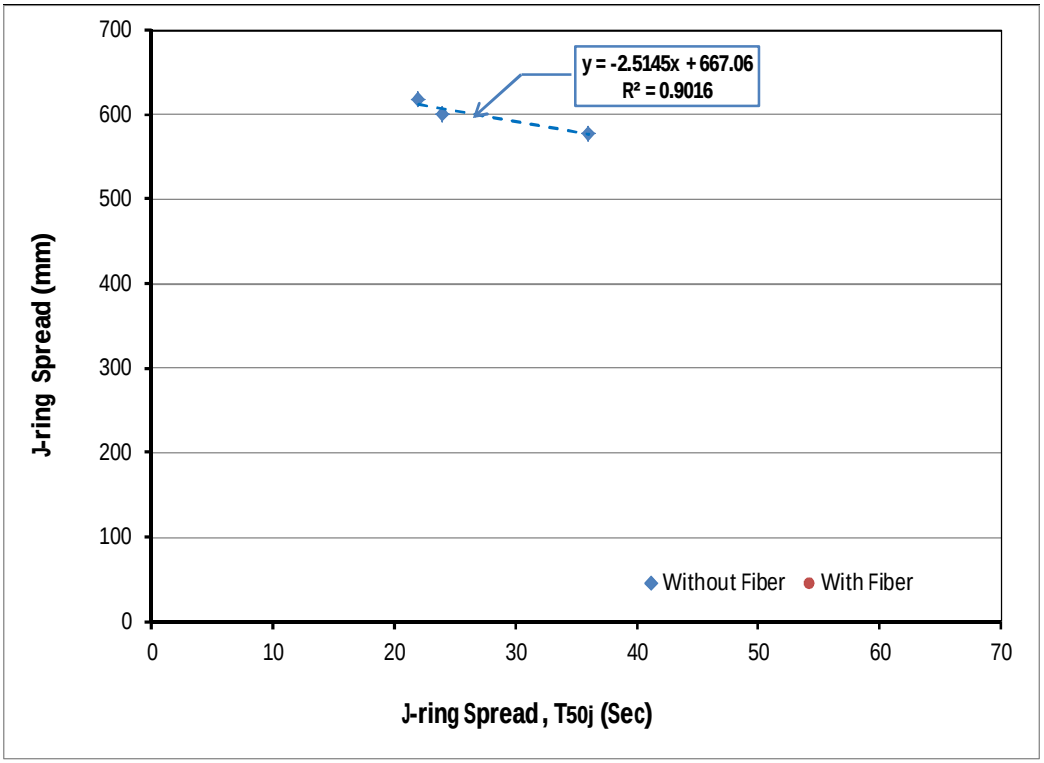

Fig.4.44 J-ring spread versus slump spread time, T_{50}

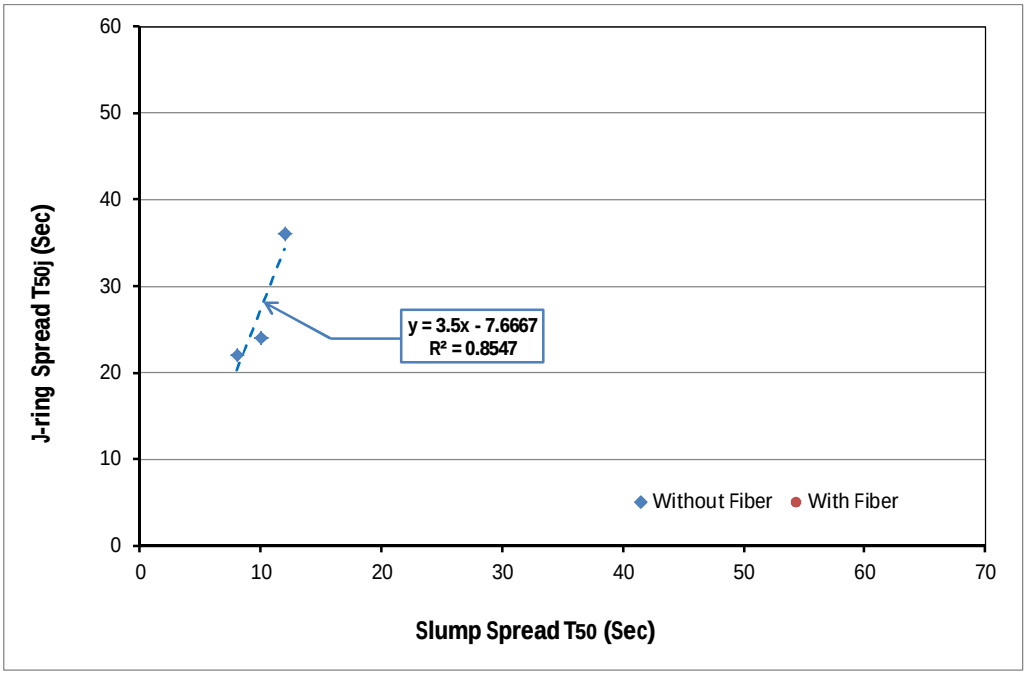

Fig.4.45 J-ring spread time versus slump spread time

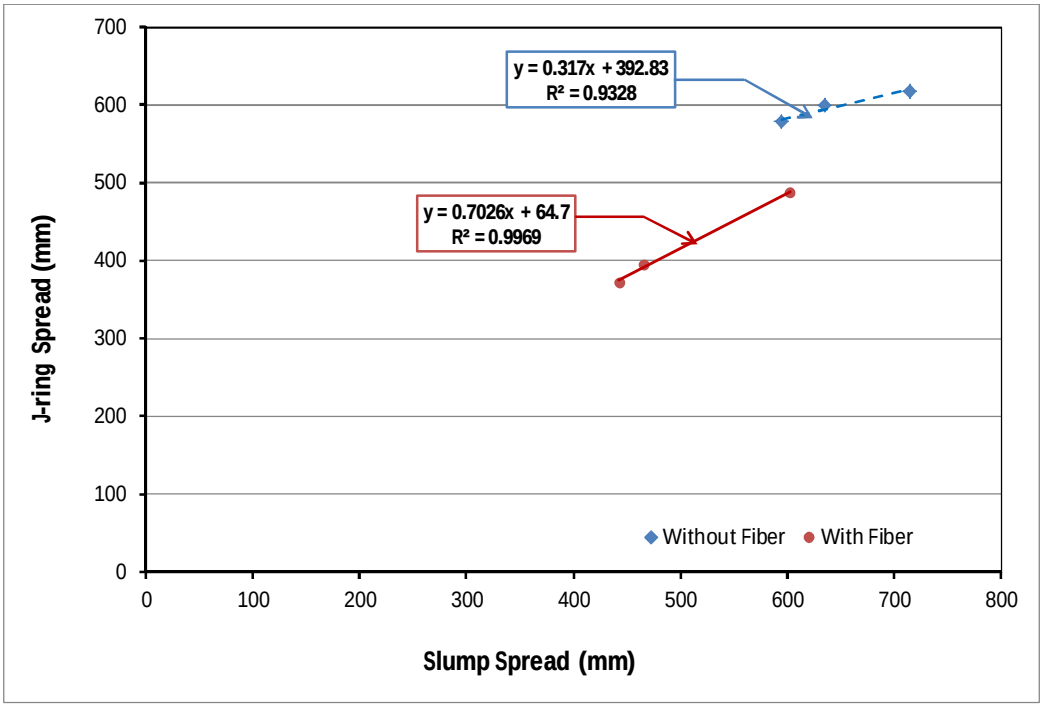

Fig.4.46 J-ring spread versus slump spread

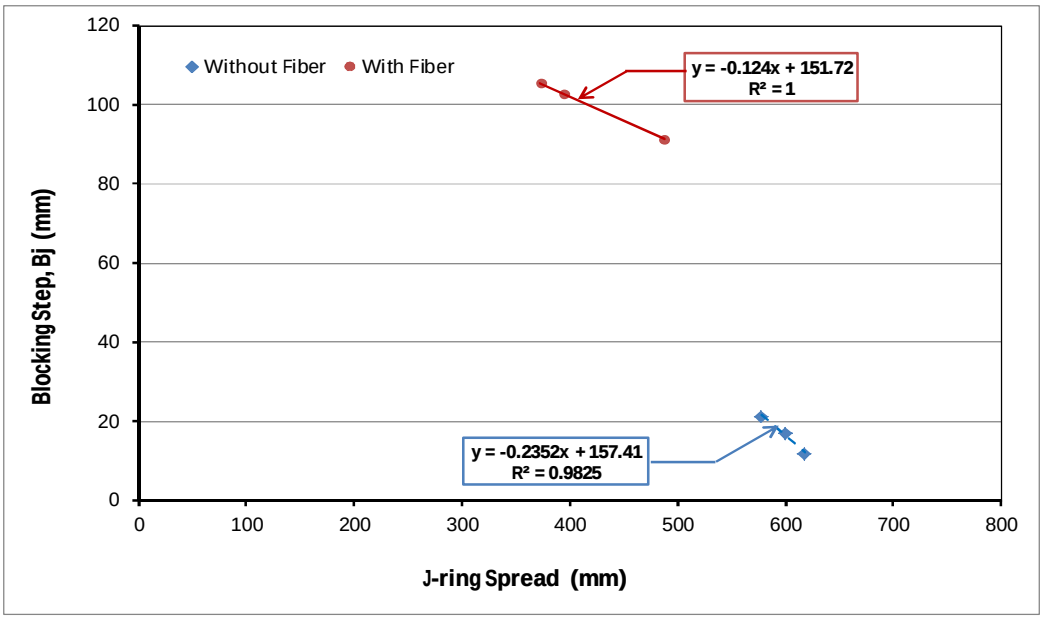

Fig.4.47 Blocking step versus J-ring spread

Blocking steps measures the restriction of deformability of the spread in the mix through the narrow steel reinforcement. It is seen in Fig.4.47 that the trend lines shows much more scatter results without and with fiber mixes with coarse aggregate

addition. It is also observed that blocking steps are higher with fiber mix and lower at without fiber mix. It is also noticed that when the blocking step increased j-ring spread decreased with and without fibers mixes. Blocking step is more pronounced with fiber mixes. It demonstrates that the fiber content and coarse aggregate act together in preventing the spread of the mixes.

The relative change in slump spread after the addition of fibers for mixes with coarse aggregate is shown in Figure 4.48, where it can be seen that for mixes with high w:c ratios the addition of CA has a positive or negligible effect for CA:FA ratios less than 0.5. For CA:FA ratios greater than 0.5 substantial reductions in slump spread occur, particularly for low w:c ratios mixes. When the CA:FA ratio of the mixes exceeds 1.5, the decreasing of slump is not much more significant. Moreover, the relative slump spreads of fresh UHPFRC mixes are much closer when it falls between 80 and 100%. This behaviour can be expected as the higher levels of CA prevent uniform distribution of the fibres which can result in fibre balling.

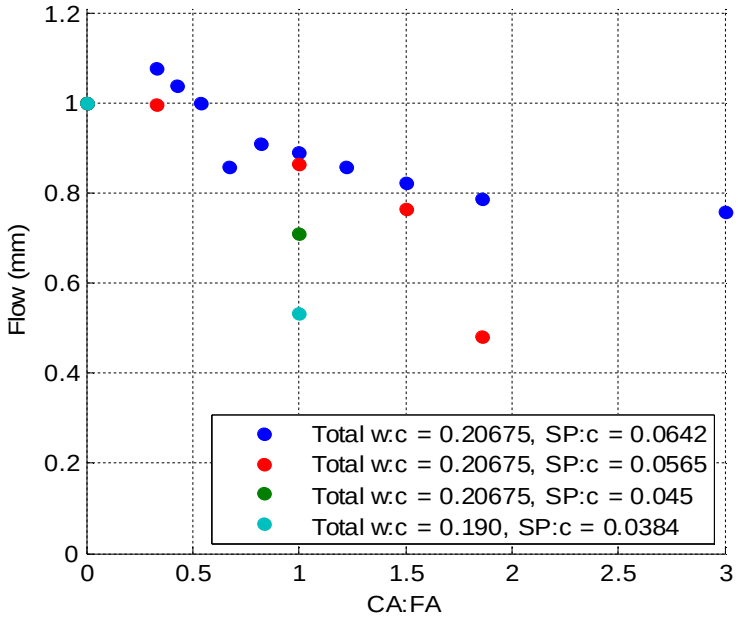

Fig.4.48 Change in concrete flowability with CA addition

4.3.5.2 Influence of coarse aggregate on hardened properties of UHPFRC

In order to quantify the influence of coarse aggregate on the compressive behaviour of UHPFRC a series of 18 trial mixes as listed in Table 4.6 were conducted to identify the optimal CA:FA ratio. It should be noted that these trials were carried out with the same total w:c and sp:c ratios as the mixes without coarse aggregate for comparison purposes and in all trial mixes only 7 day strengths were measured. A summary of the strength results is presented in Table 4.6. Three cylinders were tested for each mix at various ages that is shown in Table 4.6 and the compressive strength test results were averaged three of the cylinders to get the final value that is presented in the Table 4.6. The results are presented in the Table according to the each mix design with the corresponding days in terms of mean compressive strength, standard deviation, co-efficient of variation, standard error and the lower and upper 95% confidence interval of the compressive strength for each specimen. In general, it can be observed from Table 4.6 that the compressive strength achieved from the UHPFRC test results ranged from 110MPa to 148MPa to the corresponding test age 7 to 90 days for the different CA:FA ratios mixes.

Table 4.6 Compressive strength of UHPFRC with coarse aggregate

Mix	CA:FA	Day	Compressive Strength				95% Confidence Interval	
			Mean Strength MPa	Standard Deviation MPa	Coeff. of variation	Stand. Error	Lower limit, MPa	Upper limit, MPa
1	0.82	7	121	5.487	0.0453	3.168	118.0	124.0
		28	145	5.030	0.0347	2.904	142.2	147.8
		56	147	8.827	0.0600	5.096	142.2	151.8
		90	139	3.322	0.0239	1.918	137.2	140.8
2	0.82	7	115	1.088	0.0095	0.628	114.4	115.6
		28	144	2.884	0.0200	1.665	142.4	145.6
		56	148	9.365	0.0633	5.407	142.9	153.1
		90	138	2.992	0.0217	1.728	136.4	139.6
3	0.82	7	117	1.492	0.0128	0.861	116.2	117.8
		28	147	4.267	0.0290	2.464	144.7	149.3
		56	144	10.670	0.0741	6.160	138.1	149.9

		90	135	4.303	0.0319	2.484	132.6	137.4
4	1.00	7	116	0.810	0.0070	0.468	115.6	116.4
5	0.33	7	120	0.720	0.0060	0.416	119.6	120.4
6	3.00	7	115	0.450	0.0039	0.260	114.8	115.2
7	0.67	7	110	2.881	0.0262	1.664	108.4	111.6
8	0.54	7	114	5.042	0.0442	2.311	111.2	116.8
9	1.22	7	111	4.321	0.0389	2.495	108.6	113.4
10	1.50	7	113	0.721	0.0064	0.416	112.6	113.4
11	0.43	7	119	0.524	0.0044	0.302	118.6	119.2
12	1.86	7	115	0.431	0.0037	0.249	114.7	115.2
13	1.00	7	113	0.540	0.0048	0.312	112.7	113.3
14	0.33	7	116	0.720	0.0062	0.416	115.6	116.4
15	1.86	7	114	1.981	0.0174	1.144	112.9	115.1
16	1.50	7	115	0.901	0.0078	0.520	114.5	115.5
17	1.00	7	121	1.621	0.0134	0.936	120.1	121.9
18	1.00	7	129	3.781	0.0293	2.183	126.9	131.1

To more clearly show the influence of coarse aggregate, Figure 4.49 shows a comparison of the 7 day compressive strengths with aggregate normalised against the strength of identical mixes without coarse aggregate. It can be observed that in all the UHPFRC mixes the addition of coarse aggregate led to an increase in 7 day compressive strength, in some cases of up to 14% for medium SP content mix.

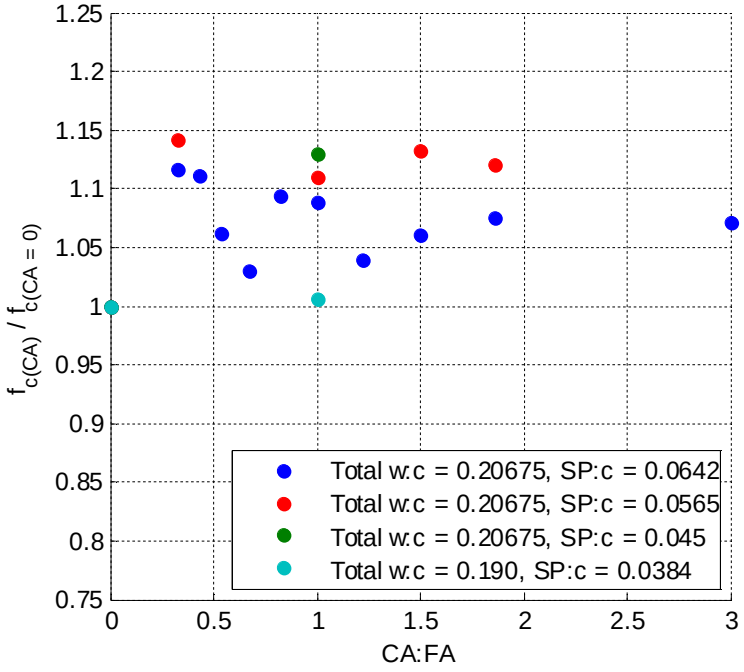

Fig.4.49 Increase in 7 day compressive strength due to CA addition

Further looking at Figure 4.49 it can be noted that the greatest and most consistent improvement in strength occurs when the CA:FA ratio is less than 0.5 which suggests within this range the greatest compaction of the coarse aggregate skeleton with the mortar phase is possible, it should however be noted that this conclusion is based on a limited data set and further investigations are required to identify the optimal CA:FA ratio.

Based on the results of the trial mixes with coarse aggregate, mixes 1, 2 and 3 were considered for further study including tracking the gain in compressive strength over time; the results of which are shown in Figure 4.50. It can be noted that while the influence of coarse aggregate led to an increase in early age strength by day 90, the strength of mixes with coarse aggregate had dropped to as low as 93% of the strength of the mix without coarse aggregate. This reduction in strength can be attributed to increased restrain of shrinkage of the mortar phase by the coarse aggregate resulting in increased micro-cracking (Hobbs, 1974).

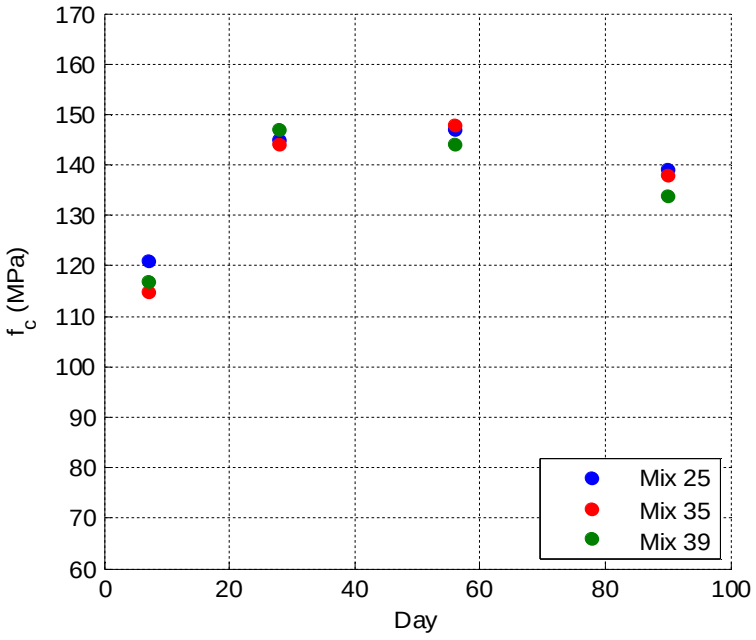

Fig.4.50 Compressive strength gain over time for mixes with CA

In general, from Figure 4.49 and Figure 4.50 it can be seen that there is potential to incorporate coarse aggregate into UHPFRC mixes but its inclusion requires consideration of not only the w:c but also the CA:FA ratio when conducting mix design and that further research is required in reducing the shrinkage of the cement paste when coarse aggregate is involved in the UHPFRC production.

4.4 Series – III: Granulated Lead Smelter Slag (GLSS) as Fine Aggregate Replacement on UHPFRC

The influence of coarse aggregate as partially replaced with fine aggregate was investigated for ultra-high performance fiber reinforced concrete (UHPFRC) in the earliest series – II. In this series, the effect of granulated lead smelter slag (GLSS) on fresh and hardened properties of UHPFRC were investigated as fine aggregate replacement. In present scenario, a rapid growth and innovation development increases the demand for sustainable building materials in the construction industry. It creates a global issue in the sustainable development to compose the concrete materials which are competitive from both economic and environment perspective. Natural resources in worldwide are depleting, in contrast there is substantial increase in the generation of industrial wastes during manufacturing process which could have a promising use in the construction industry as alternative material for partial or full substitution of either a cementitious material or fine aggregates.

Granulated lead smelter slag is a by-product of heavy metal extraction obtained during lead smelting process in the industry. It was estimated 3.9 million tonnes of lead produces in 2009 in the world and the production of each ton of metallic lead generates as a by-product material around 100-350kg that is known as granulated lead smelter slag (de Andrade Lima & Bernardez, 2011; Ogundiran et al., 2013) . Several studies have been conducted on the use of granulated blast furnace slag as

aggregate in high strength concrete (Al-Jabri et al., 2009; Khanzadi & Behnood, 2009; Wu et al., 2010), and the few studies have focused on the utilization of GGBFS in reactive powder concrete (Yazıcı et al., 2010; Yazıcı et al., 2008) and very few number of researches investigated on ultra-high performance concrete with GBFS (Ambily et al., 2015; Randl et al., 2014; Urbonas et al., 2013). It was found that small number of studies conducted on chemical synthesis and characterization of GLSS materials, however there are no studies in the literature concerning the incorporation of granulated lead smelter slag in UHPFRC. In this test series, the possibility of using GLSS into manufacture of UHPFRC was investigated, this was done to offset the environmental impact of the high volumes of cement used. Furthermore being a waste material GLSS is a low cost material thus its inclusion can lead to cost savings cost. In this study GLSS although has been shown to have some supplementary cementing capabilities, due to the large particle size, here it is investigated as an alternative material for full substitution of fine aggregate.

4.4.1 Materials and mix proportions

The basic material selection was same in this section mixes as briefly described in section 4.2.1. In this investigation, conventional fine aggregate (sand) were fully replaced by GLSS. GLSS has similar gradation of particle sizes as sand shown in Fig.4.1 and it is granular in nature with a black glassy appearance refer to Fig.4.51.

Fig.4.51 Granulated lead smelter slag (GLSS) used in UHPFRC

The constituents of UHPFRC mix a comprised of 1:1:0.266:0.175 ratios by weight of sulphate resisting cement (Type SR), fine aggregate (total of granulated lead smelter slag), silica fume and steel fibres (Dramix-3D). Mix design of UHPFRC with SP and water is presented in Table 4.7. In these mixes a GLSS with a bulk density of 1350kg/m^3 was used in this investigation.

Table 4.7 Mix designs of UHPFRC to investigate the influence of GLSS

Mix number	FM	W:C	SP:C	Total W:C
1-FA	4.01	0.1775	0.045	0.20675
2-FA	4.01	0.17	0.0565	0.20675
3-FA	4.01	0.165	0.0642	0.20675
4-FA	4.01	0.1775	0.0192	0.190
5-FA	4.01	0.17	0.0307	0.190
6-FA	4.01	0.165	0.0384	0.190

4.4.2 Mixing procedure

An identical mix procedure to that described in section 4.2.2 was followed.

4.4.3 Specimen preparation and curing regimes

Specimen preparation and curing regime was similar as discussed in part 4.2.3. The only exception of this concrete is the demoulding procedure. All of the specimens of each mix were demoulded after 48 hours due to the softness nature of the concrete after 24 hours of ambient curing.

4.4.4 Test set-up and instrumentation

To determine rheological properties of UHPFRC incorporating GLSS, slump height, slump spread and j-ring flow properties were measured. Measurement of slump height, slump spread, j-ring spread and j-ring blocking step is depicted in Figs.4.52 (a) and (b) to Figs.4.52 (g) and (h) without and with fiber mixes. Test set-up and instrumentation were the similar as mentioned in the section 4.2.4 to investigate the rheological and hardened properties of UHPFRC with GLSS.

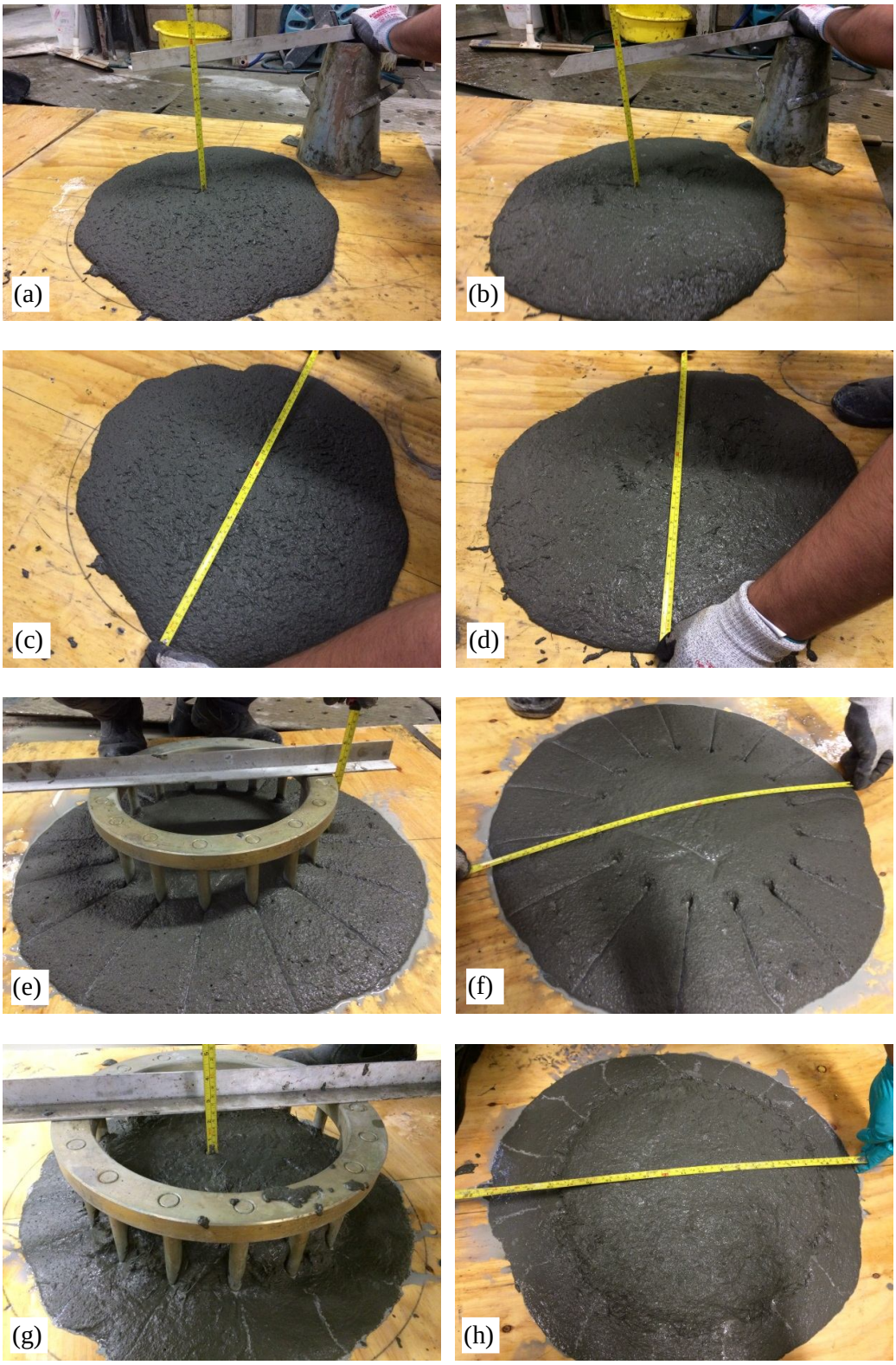

Fig.4.52 Measurement of (a) slump height without fiber (b) slump height with fiber (c) slump spread without fiber (d) slump spread with fiber (e) J-ring blocking step without fiber (f) J-ring spread without fiber (g) J-ring blocking step with fiber (h) J-ring spread with fiber

4.4.5 Test results and discussion

4.4.5.1 Influence of granulated slag on rheological properties of UHPFRC

Influence of granulated slag on the rheological properties of UHPFRC was investigated including slump height, slump flow and J-ring blocking step and J-ring spread. The influence of granulated slag on slump test of UHPFRC without and with fiber addition and other influencing variable such as SP and water is presented in the following Fig.4.53 and Fig.4.54 respectively. Six mixes were conducted with GLSS to observe the workability and strength behaviours. It is observed from Fig.4.53 and Fig.4.54 without and with fiber mixes that as the SP content increases the concrete gains the slump although the w:c content decreases. It can be seen that with fiber and slag addition there is a decrease of slump, however this behaviour was not observed without slag addition from the previous mix. The decrease of slump due to slag content is attributed to the larger size of particle than the sand which predominantly decreases the fluidity of the mix resulted in increased viscosity of the cement paste.

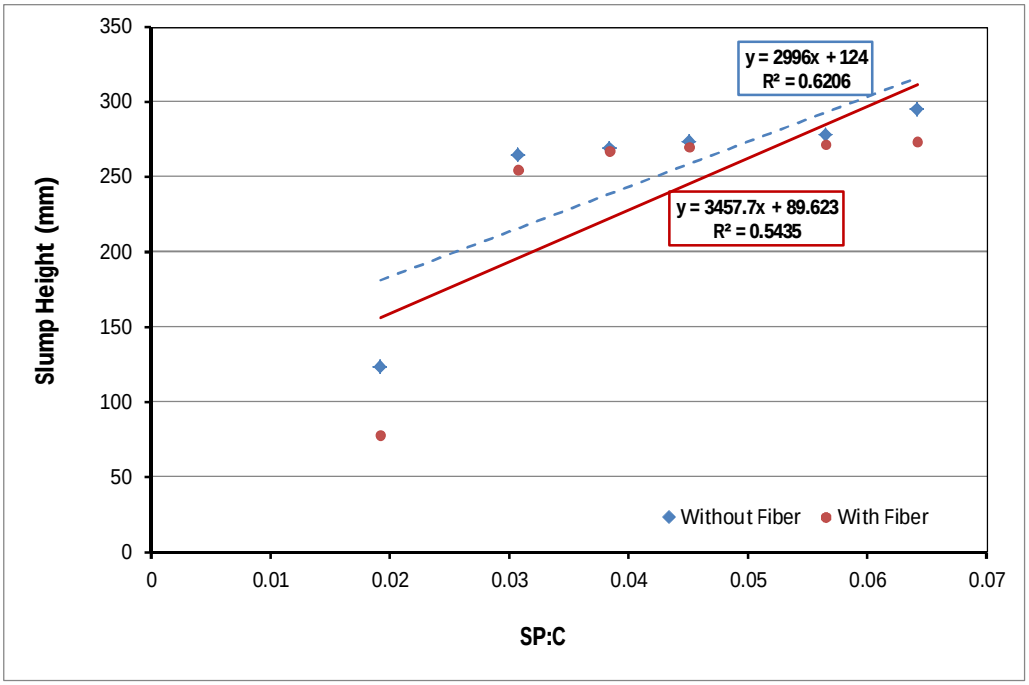

Fig.4.53 Slump spread versus superplasticizer (SP) content

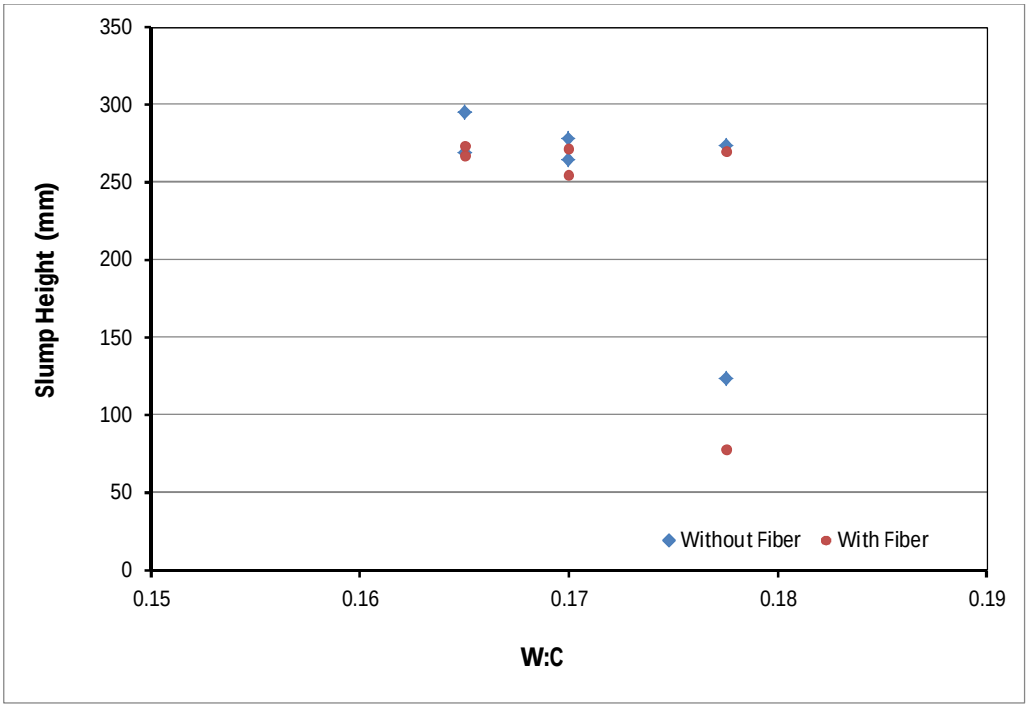

Fig.4.54 Slump spread versus water content

The slump spread and spread time test of UHPFRC with granulated slag in its fresh state achieved with and without the use of fiber shown in Fig.4.55 to Fig.4.57. The test was done according to the slump test mentioned in ASTM-C1611/C1611M-09b (2009). The spread attained 285mm-782mm before fiber addition and the flow obtained 305mm-720mm after fiber addition. The slump spread is increasing with increasing the SP content for without and with fiber cases; however with increasing water content the spread is decreased refer to Fig.4.56 and shows quite similar values. This can be happened because of the fluidity nature of SP than the water resultant in increased spread. The slump spread with fiber mixes are little bit lower than without fiber mixes. With the addition of fibres with GLSS attributed to the increase in internal surface area which produces higher cohesive forces in combined and resultant in decrease the spread of UHPFRC. It can be seen in Figs.4.55 from trend lines that the spread of the concrete with and without fiber shows quite similar

slopes. It indicates that the fresh concrete was sticky and not highly workable, which is followed quite similar behaviour to the coarse aggregate addition in UHPFRC.

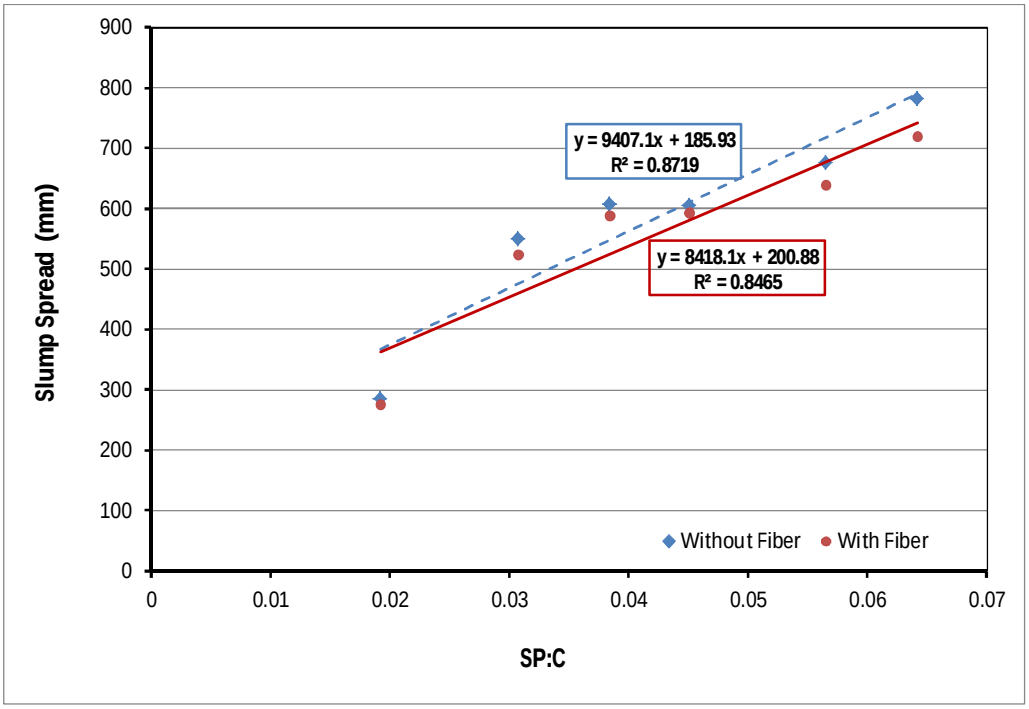

Fig.4.55 Slump spread versus superplasticizer (SP) content

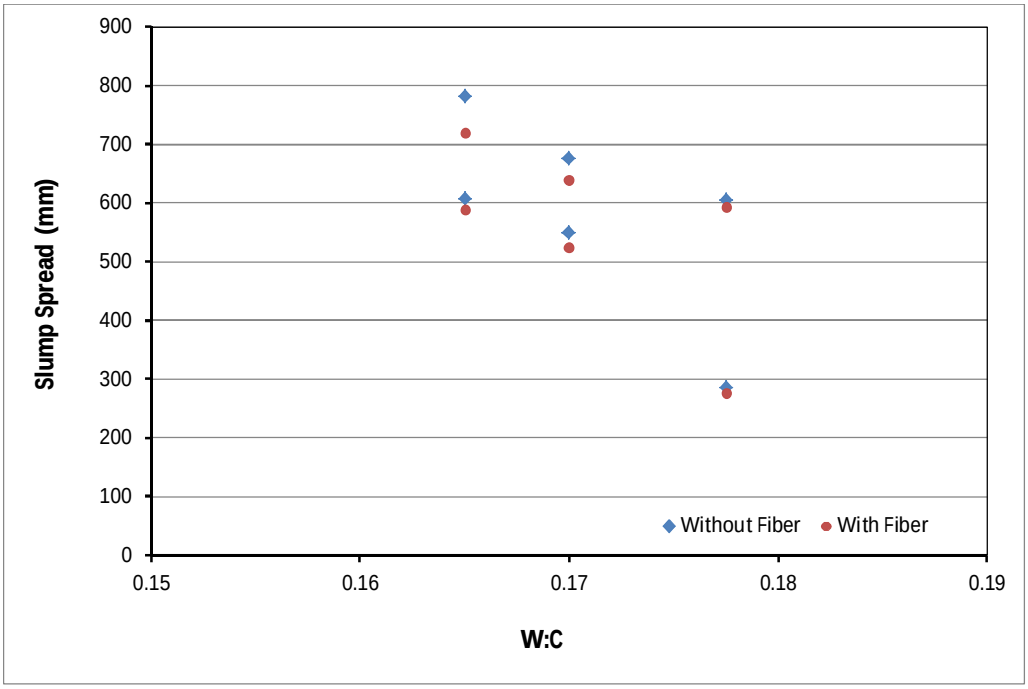

Fig.4.56 Slump spread versus superplasticizer content

Slump spread time (T_{50j}) with slump spread is depicted in Fig.4.57. The results indicate the direct relation between the slump spread and the spread time of fresh UHPFRC. It can be seen that slump spread decreased with increasing the spread time and the trend lines shows very quite similar behavior without and with fiber mixes. It is important to notice that slump spread time with fiber took greater time then without fiber mixes, except the lowest slump spread time more than 15sec. This behaviour is significant with fiber mixes and attributed to the granulated slag and fiber act together which predominantly increase the internal surface area that produces higher cohesive forces followed in decreased the slump spread with increase the slump spread time of UHPFRC.

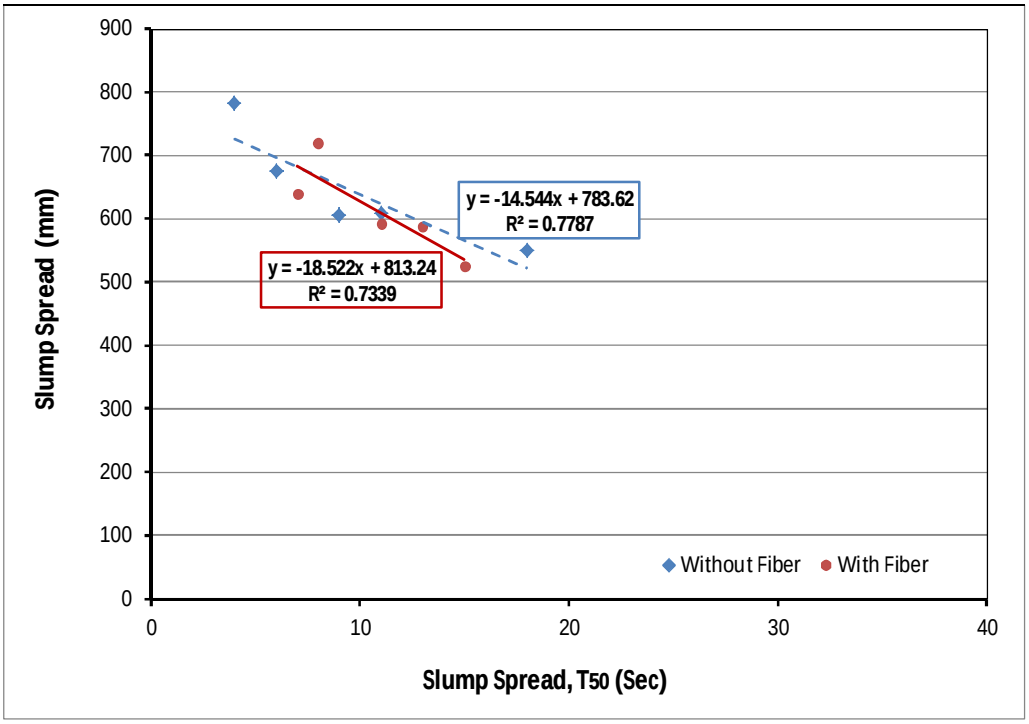

Fig.4.57 Influence of time (T_{50}) on slump spread measurement

The j-ring spread of UHPFRC with granulated slag in its fresh state obtained without and with the use of fiber shown in Fig.4.58 to Fig.4.60. The J-ring spread diameters of all mixes were in the range 262.5-770.5mm and 227.5-570mm without and with

fiber respectively. It is observed that fresh concrete passing ability is increasing with the increases of SP content for both without and with fiber cases; consequently the j-ring spread decreased with increasing the water content in the mixes refer to Fig. 4.59. This behaviour is more pronounced with fiber mixes and it demonstrates the granulated slag and fiber working together and created higher cohesive forces with higher surface area to prevent the flowing of concrete through the narrow steel reinforcement. Furthermore, this also indicates the stiffer flow due to coarser slag addition in the mixes. This behaviour attributed of larger size of particle than sand and fiber acts together to create blocking or prevent the flow through the J-ring steel reinforcement. Plot of j-ring spread time (T_{50j}) versus J-ring spread are illustrated in Figs.4.60. It is important to notice that J-ring spread time with fiber mixes shows much more greater values then without fiber mixes. It is interesting to mention that the j-ring spread time increasing without and with fibers mixes; however j-ring spread values are quite similar at the final stage.

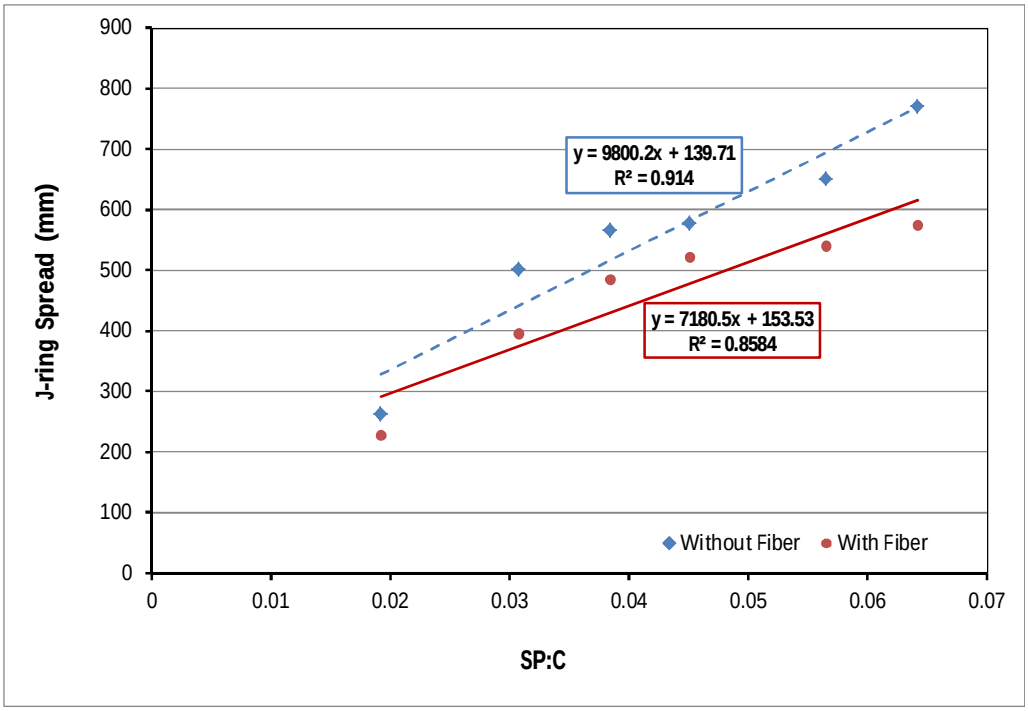

Fig.4.58 Slump spread versus superplasticizer content

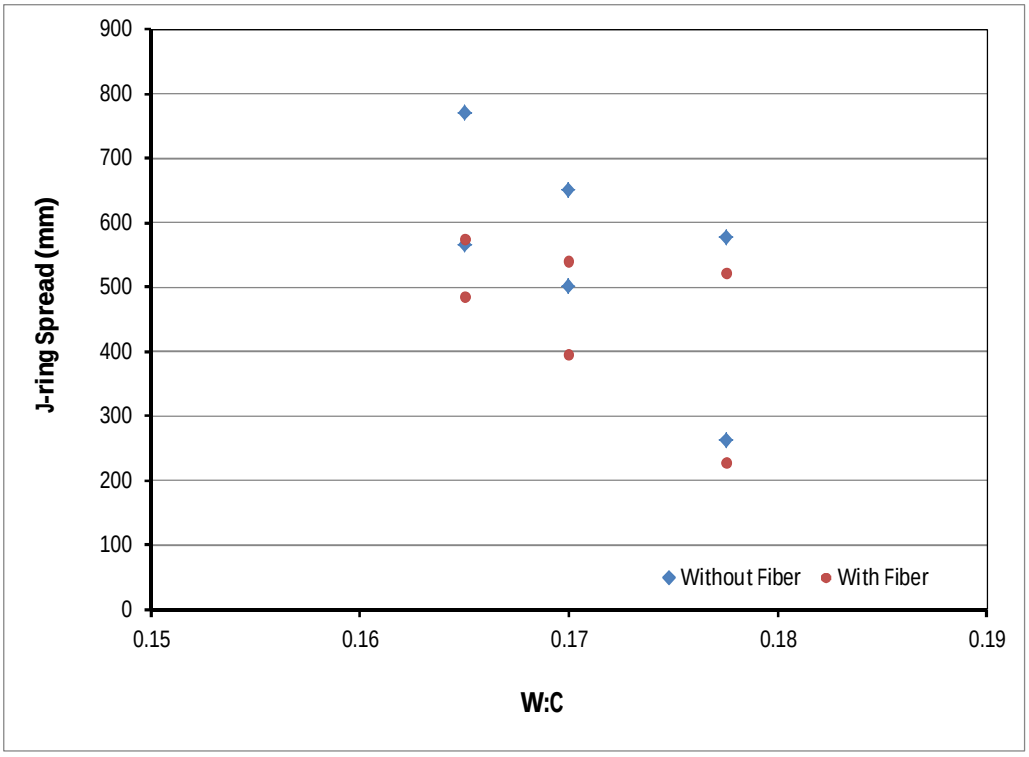

Fig.4.59 Slump spread versus water content

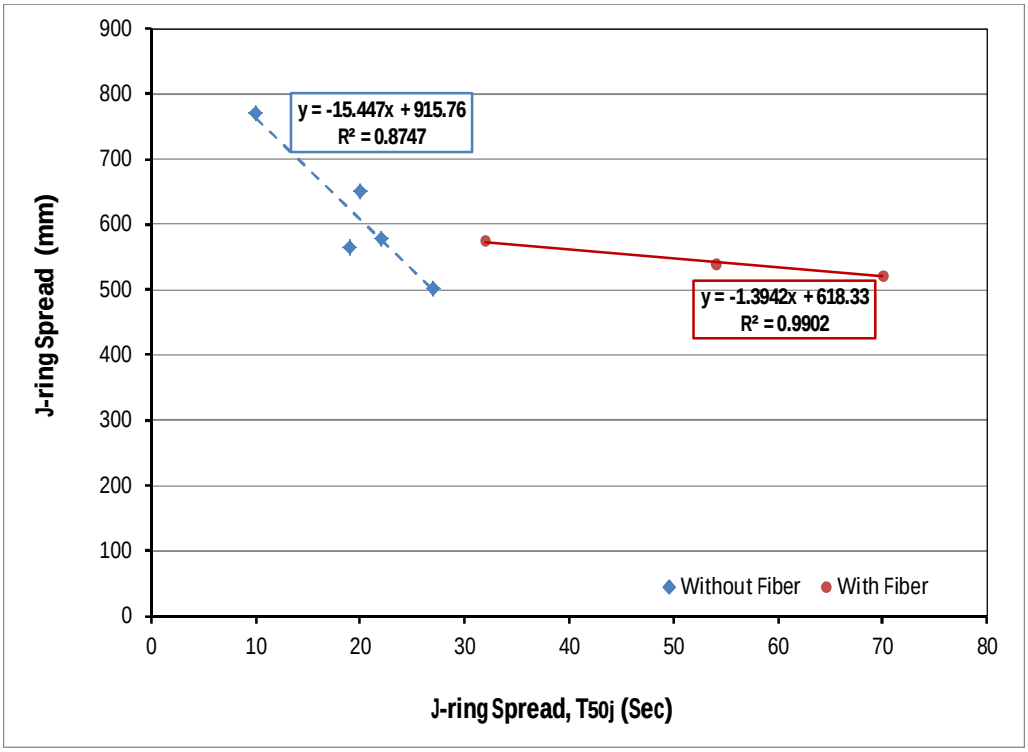

Fig.4.60 Influence of time (T_{50}) on spread measurement

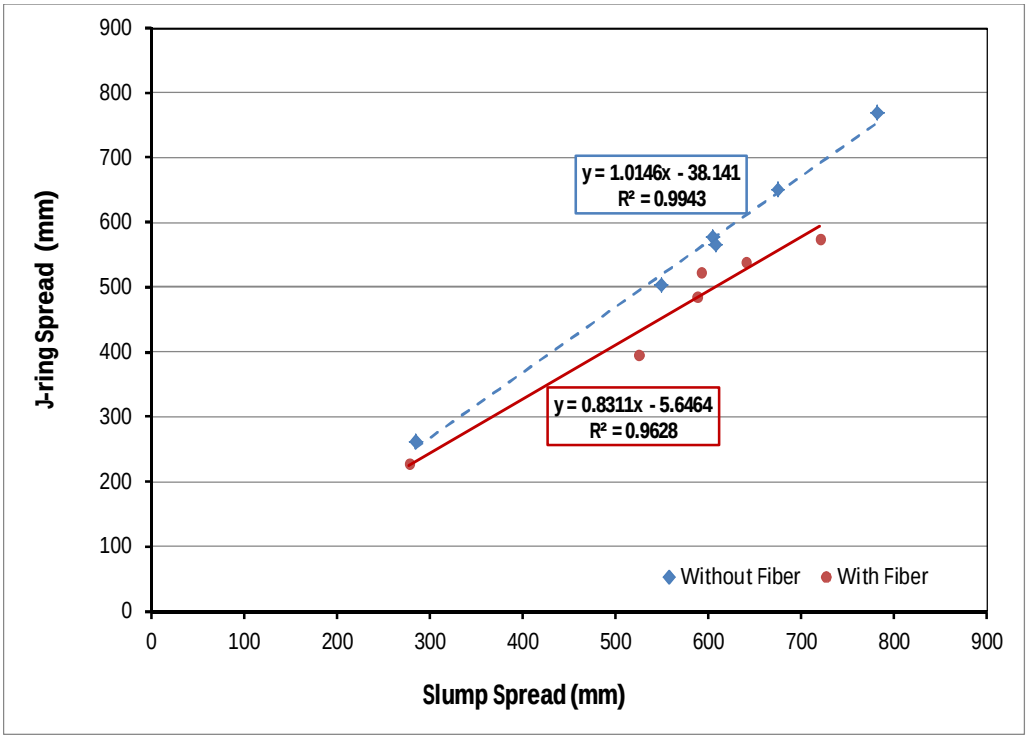

Fig.4.61 J-ring spread versus slump spread

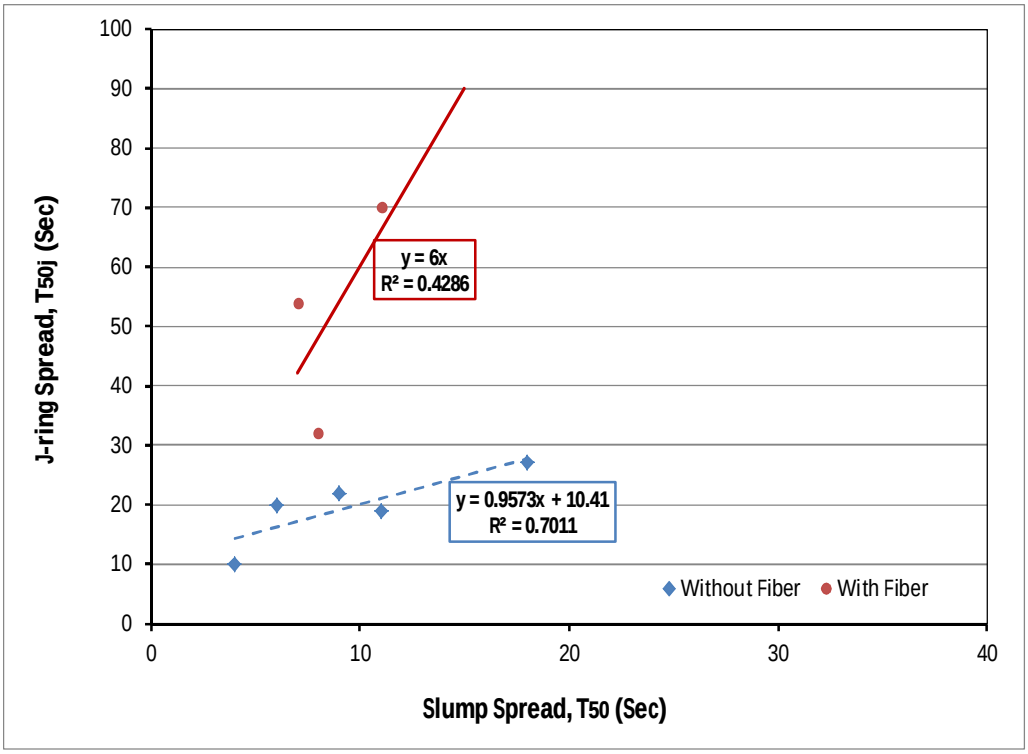

Fig.4.62 Influence of J-ring time and slump spread time

Figure 4.61 shows the J-ring spread with slump spread results trend lines without and with fiber mixes. The trend line exhibit similar slope and the slump spread noticed the higher values then j-ring spread. Similar finding is observed when plotted the j-ring and spread time in a same graph. It is mentioned that the j-ring spread is taken more time with fibers mixes; however it shows quite similar time without fiber mixes. It can be seen that the j-ring spread time exhibits higher time then slump spread refer to Fig.4.62. It attributed to the larger surface area created by coarse aggregate and hooked end fiber that demonstrated high cohesive force and friction between them resultant in decreased the spread and increase the spread time.

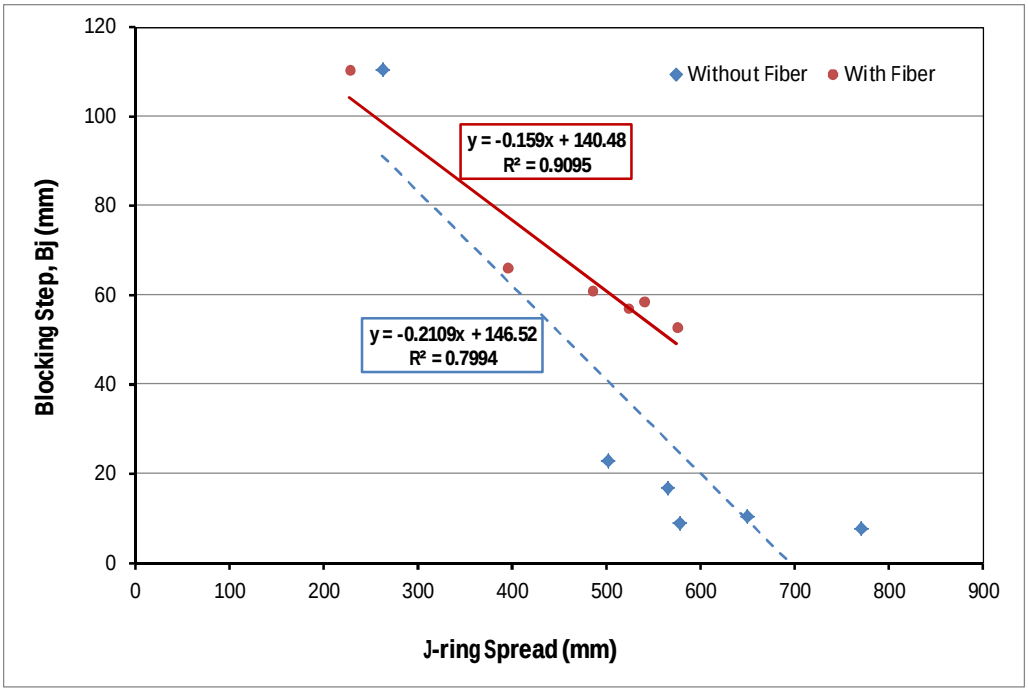

Fig.4.63 Blocking step versus J-ring spread

The two trend lines shows much more scatter results without and with fiber mixes as illustrated in Fig.4.63. Blocking steps measure the restriction of deformability of the spread of mix through j-ring test. With an increase the blocking step, the j-ring spread of the UHPFRC decreases sharply with and without fibers mixes. The

difference between them is quite obvious without fiber mixes when especially higher spread required with lower blocking step. However, the mixes with fiber content achieved optimum j-ring spread with medium blocking step. It attributed to the increase in the internal surface area that produces higher cohesive forces between the fibres and concrete constituents. Hence, it can be demonstrated that when the fibres and GLSS are included, the cohesive forces are higher, and resultant in decreased the j-ring spread of UHPFRC.

4.4.5.2 Influence of slag on hardened properties of UHPFRC

To investigate the effect of granulated slag on the compressive strength properties of UHPFRC from the 6 mixes are presented in Table 4.8. Initially, several trial pour has been conducted first in the laboratory with higher SP and water content then started the mixes from more moist to the driest mixes according to the SP and water content. The first three mixes were developed with total water content 0.20675 and another three mixes total water content were 0.190. The total water content consists of the water plus free water content in the SP. These test results are from the 100mm diameter and 200mm height cylinders cast according to the Table 4.8. Three cylinders were tested for each mix at various ages that is shown in Table 4.8 and the compressive strength test results were averaged three of the cylinders to get the final value that is presented in the Table 4.8. The results are presented in the Table 4.8 according to the each mix design with the corresponding days in terms of mean compressive strength, standard deviation, co-efficient of variation, standard error and the lower and upper 95% confidence interval of the compressive strength for each specimen. In general, it can be observed from Table 4.8 that the compressive strength achieved from the UHPFRC test results ranged from 83MPa to 139MPa to the corresponding compressive strength test age 7 to 90 days.

Table 4.8 Compressive strength of UHFRPC with GLSS

Mixes	Days	Compressive Strength				95% Confidence Interval	
		Mean Strength, MPa	Standard Deviation, MPa	Coefficient of variation	Standard Error	Lower limit, MPa	Upper limit, MPa
1	7	91	2.358	0.0259	1.361	89.7	92.3
	28	128	2.675	0.0209	1.544	126.5	129.5
	56	139	1.960	0.0141	1.132	137.9	140.1
	90	131	0.530	0.0040	0.306	130.7	131.3
2	7	83	4.874	0.0587	2.814	80.3	85.7
	28	121	5.777	0.0477	3.335	117.8	124.2
	56	134	3.394	0.0253	1.959	132.1	135.99
	90	131	1.134	0.0087	0.655	130.4	131.6
3	7	97	2.683	0.0277	1.549	95.5	98.5
	28	126	3.382	0.0268	1.952	124.1	127.9
	56	132	0.964	0.0073	0.557	131.5	132.5
	90	129	2.376	0.0184	1.372	127.7	130.3
4	7	103	2.225	0.0216	1.285	101.8	104.2
	28	129	1.915	0.0148	1.106	127.9	130.1
	56	136	2.302	0.0169	1.329	134.7	137.3
	90	131	3.964	0.0303	2.289	128.8	133.2
5	7	105	2.528	0.0241	1.460	103.6	106.4
	28	128	3.570	0.0279	2.061	126.0	130.0
	56	134	3.019	0.0225	1.743	132.3	135.7
	90	130	4.470	0.0344	2.581	127.5	135.7
6	7	118	5.202	0.0441	3.004	115.1	120.9
	28	131	2.710	0.0207	1.565	129.5	132.5
	56	136	2.437	0.0179	1.407	134.7	137.3
	90	131	2.987	0.0228	1.724	129.4	132.6

Figures 4.64 to 4.66, it can be seen that the use of granulated slag as a replacement for conventional geological sands does not alter the behaviour of the resultant UHPFRC that which would be expected by increasing the coarseness of the filler. It is interesting to notice that with an increasing the curing days the compressive strength enhanced up to 56 days for both total water content mixes as shown in Figs. 4.64 and 4.65, exceptional observed in decreased the strength at 90 days period. That is, the increased coarseness of fine aggregate leads to a reduction in the packing density, the shrinkage crack induced on the concrete surface in long term period and hence reduced compressive strength for a given w:c.

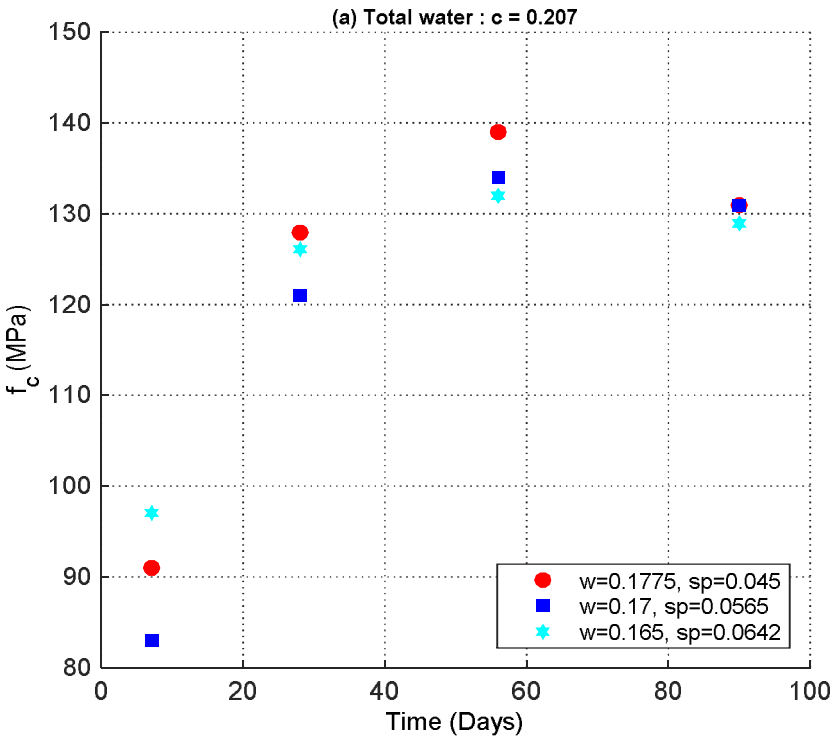

Fig.4.64 Compressive strength gain versus time with slag addition

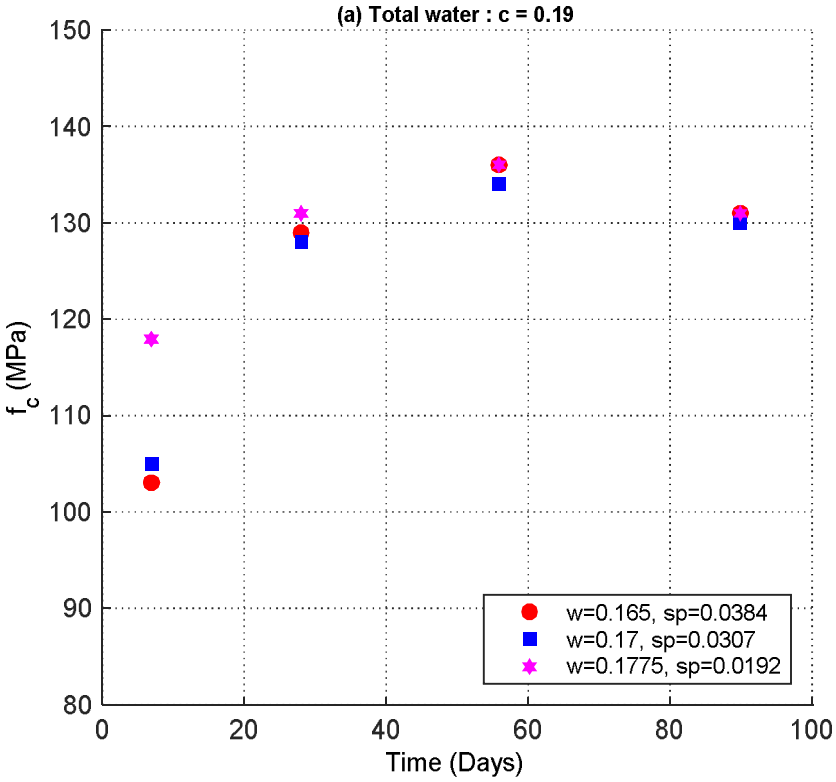

Fig.4.65 Compressive strength gain versus time with slag addition

Moreover, the early strength exhibits higher value for the total water content 0.190 mixes and it attributed to the less water present in the constituents and the interface between the concrete matrix, GLSS and fibres become denser resultant in increased the strength. It can also be seen that the early strength lower are obtained in mixes utilising a GLSS particularly in mixes with higher ratios of SP refer to Fig.4.66. Moreover, with the same fibre content with GLSS, the compressive strengths are shows quite similar values for all of the curing ages except for the early strength result. It is seen from the results that the highest compressive strength was achieved 139MPa with GLSS which is 7-10% less than the UHPFRC produced with conventional sand. Moreover, it is clear that the compressive strength of UHPFRC with GLSS is still comparable to the UHPFRC produced with conventional. This result suggests that there is potential to utilise granulated slag as a filler material in produce high performance fiber concrete where ultra-high strengths are not required in construction industry.

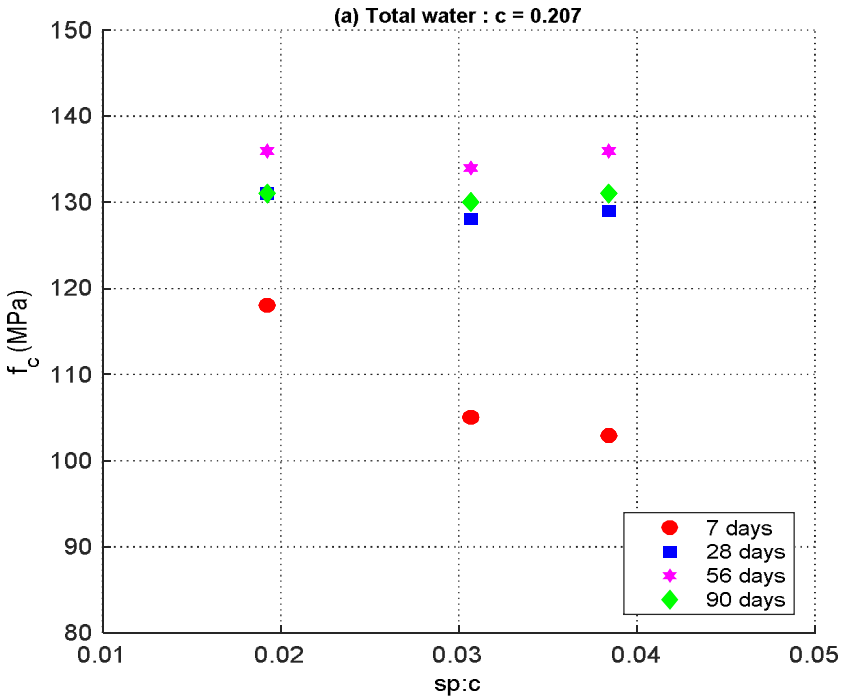

Fig.4.66 Compressive strength gain versus superplasticizer with slag addition

4.5 Series – IV: Expensive Silica Sand as Fine Aggregate on UHPFRC

The fresh and hardened properties of UHPFRC using conventional materials and industrial by-products have been investigated in series III. In this section the hardened behaviour of UHPFRC with expensive silica sand as a fine aggregate is investigated. The basic composition of ultra-high performance fiber reinforced concrete consists of silica powder and silica quartz sand. In the last decades, a significant effort has been conducted to investigate the physical and mechanical behaviour of UHPFRC in the construction industry (Batoz & Behloul, 2009). Numerous research has been conducted on UHPFRC mix design in varies ways (Graybeal & Davis, 2008; Habel et al., 2008; Wille et al., 2011b; Yu et al., 2014; Yu et al., 2015), several researches have conducted on the mechanical behaviour of UHPFRC with different types and configurations of instrumentation to capture the descending (softening) branch (Hassan et al., 2012; Prabha et al., 2010), some of the researchers examined the material efficiency and cost effective approach on UHPFRC (Wille & Boisvert-Cotulio, 2015) and several researches on the application and optimizing UHPFRC in the construction industry (Perry & Seibert, 2008; Vicenzino et al., 2005; Wille et al., 2011a).

Despite all this research, there is still need for substantial research effort on UHPFRC mix design and its fresh and hardened properties to understand the full behaviour of UHPFRC. In this series, the aim of using silica sand was to provide an efficient mix design on UHPFRC and compare the behaviours with conventional sand UHPFRC. The benefit of using silica sand on UHPFRC is to achieve a cement matrix as dense as possible resulting in reduced micro-cracks and capillary pores in the concrete. These requirements are obtained by enhancing the homogeneity with fine quartz silica sand. To acquire hardened properties with silica sand and silica

quartz sand, the standardized procedure such as mix proportion, mixing, preparation, associated testing and result discussion are described in this section.

4.5.1 Materials and mix proportions

Two concrete mix proportions are investigated in this series, which is 1:0.5:0.5:0.266:0.175 and 1:0.25:0.28:0.64:0.25:0.175 mix of cement: silica fume: silica sand 60G (silica powder) and silica sand 30/60 (silica quartz). Silica sand with a bulk density of 1450kg/m^3 was used in this investigation and the grain size curve is shown in Fig.4.1. The mix design of expensive fine aggregate (silica powder and silica quartz sand) as illustrated in Table 4.9.

Table 4.9 Mix designs to investigate the influence of expensive fine aggregate

Mix number	w:c	sp:c	Total w:c
1	0.20	0.05	0.2325
2	0.19	0.035	0.21275
3	0.193	0.0356	0.2161
4	0.1775	0.050	0.210
5	0.1775	0.060	0.2165
6	0.165	0.100	0.2300
7	0.165	0.060	0.2040
8	0.185	0.03375	0.2069
9	0.20	0.03375	0.2219
10	0.195	0.03375	0.2169

4.5.2 Mixing procedure

In this series, two types of mixes were performed with different constituent's amount. For the first mix, all of the dry components that is the cement, silica fume, silica sand 60G and silica sand 30/60 were mixed first for 1 minute in the 80L concrete mixer until it observed that all of the constituents were well combined. Similarly, the second mix, silica sand 400G and silica sand 18/40, cement and silica fume were mixed for 1 minute. The edges of the mixture at the bottom surface were checked for both mixes whether any constituent particle stacks around the mixture or not. The rest of the mixing procedure is same as described in section 4.2.2.

4.5.3 Specimen preparation and curing regime

Specimen preparation and curing regime is similar as discussed in part 4.2.3.

4.5.4 Test set-up and instrumentation

Test set-up and instrumentation is the similar as mentioned in the section 4.2.4 to investigate the strength behaviours of UHPFRC with including expensive silica powder and silica quartz sand.

4.5 Test results and discussion

To investigate the effect silica sand on the compressive strength properties of UHPFRC 10 mixes as presented in Table 4.10 were investigated. The mix design was developed according to total water content in the mix. Strength test results were determined the 100mm diameter and 200mm height cylinders cast according to the Table 4.10. Three cylinders were tested for each mix at various ages and the results are summarised in Table 4.10. It should be noted that the compressive strength test results are the average of three individual test results. Further in Table 4.10 for each testing time the mean compressive strength, standard deviation, co-efficient of variation, standard error and the lower and upper 95% confidence interval of the compressive strength is given. In general, it can be observed from Table 4.10 that the compressive strength achieved from the UHPFRC test results ranged from 90MPa to 162MPa to the corresponding test age 7 to 90 days.

Table 4.10 Compressive strength of UHPFRC with silica sand

Mixes	Days	Compressive Strength				95% Confidence Interval	
		Mean Strength, MPa	Standard Deviation, MPa	Coeff. of variation	Standar -d Error	Lower limit, MPa	Upper limit, MPa
1	7	101	1.170	0.0116	0.676	100.4	101.6
	28	148	1.080	0.0073	0.624	147.4	148.6
	56	159	1.261	0.0079	0.728	158.3	159.7
	90	154	1.261	0.0082	0.728	153.3	154.7

2	7	128	0.360	0.0028	0.208	127.8	128.2
	28	152	0.991	0.0065	0.208	151.5	152.5
	56	162	1.710	0.0106	0.572	161.1	162.9
	90	157	2.881	0.0183	0.988	155.4	158.6
3	7	115	0.810	0.0070	0.468	114.6	115.4
	28	152	1.801	0.0118	1.040	151.0	153.0
	56	161	0.900	0.0056	0.520	160.5	161.5
	90	156	2.251	0.0144	1.299	154.8	157.2
4	7	114	0.721	0.0063	0.416	113.6	114.4
	28	133	1.080	0.0081	0.624	132.4	133.6
	56	150	2.522	0.0168	1.456	148.6	151.4
	90	145	0.900	0.0062	0.520	144.5	145.5
5	7	90	1.891	0.0210	1.092	89.0	91.0
	28	125	0.720	0.0058	0.416	124.6	125.4
	56	139	3.961	0.0285	2.287	136.8	141.2
	90	135	1.890	0.0140	1.091	134.0	136.0
6	7	109	0.631	0.0058	0.364	108.7	109.3
	28	150	0.991	0.0066	0.572	149.5	150.3
	56	158	4.501	0.0285	2.599	155.5	160.5
	90	153	2.700	0.0176	1.559	151.5	154.5
7	7	119	11.534	0.0969	6.659	112.7	125.3
	28	145	3.073	0.0212	1.774	143.3	146.7
	56	152	7.856	0.0517	4.353	147.7	156.3
	90	147	2.654	0.0181	1.532	145.5	148.5
8	7	115	1.676	0.0146	0.968	114.4	115.9
	28	140	3.184	0.0227	1.838	138.3	141.7
	56	152	1.661	0.0109	0.959	151.1	152.9
	90	147	3.321	0.0226	1.917	145.2	148.8
9	7	106	1.145	0.0108	0.661	105.4	106.6
	28	129	7.468	0.0579	4.312	124.9	133.1
	56	138	2.863	0.0207	1.653	136.4	139.6
	90	135	2.490	0.0184	1.437	133.6	136.4
10	7	111	4.239	0.0382	2.447	108.7	113.3
	28	134	1.470	0.0110	0.849	133.2	134.8
	56	145	3.820	0.0263	2.205	142.9	147.1
	90	141	2.042	0.0145	1.179	139.9	142.1

Figures 4.67 and 4.68 illustrate the influence of curing time (7, 28, 56 and 90days) and SP content on the compressive strength of UHPFRC of each mix with expensive silica sand. In the plots, the Figure 4.67 represents the all silica sand with same colour and the colour and tics with the same shape indicate mixes with the same sp:c ratio for each mix corresponding days in Figure 4.68. It can be seen from Fig.4.67 that with increasing the days the compressive strength is increased; except 90 days strength which is decreased in small percentage. It can be attributed to the shrinkage

formed on the UHPFRC specimen for long time curing. Similar observations found for the conventional material utilising to produce UHPFRC. It is noticed that the highest strength obtained with the moderate amount of SP in the mix; however the higher amount of SP decreased the strength refer to Fig.4.68. It may be happened due to the more fluidity nature of SP and voids formed in the mixes that lead to the change of the internal skeleton of the UHPFRC resultant in decreased the strength.

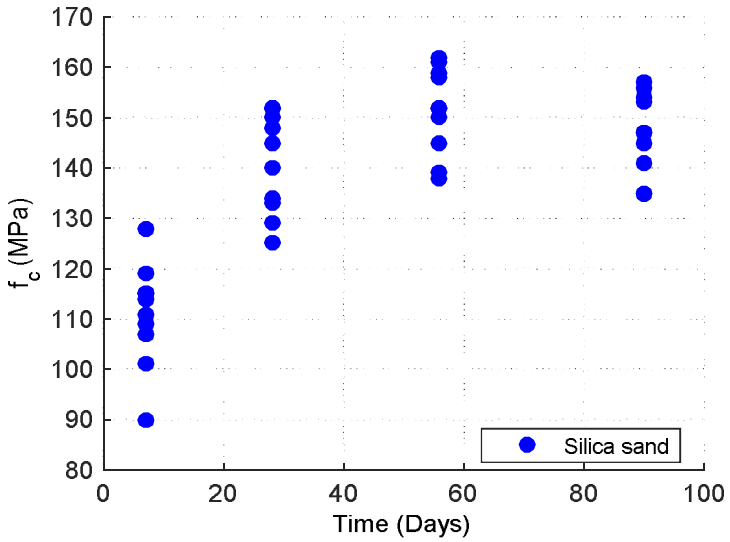

Fig.4.67 Influence of time on the compressive strength of UHPFRC with silica sand

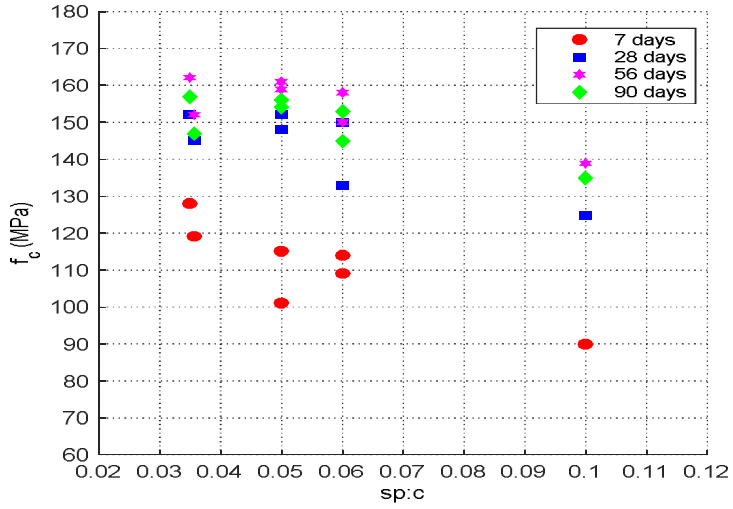

Fig.4.68 Influence of sp:c on the compressive strength of UHPFRC with silica sand

4.6 Series – V: Conventional Sand and Expensive Silica Sand as Fine Aggregate on UHPFRC with Heat Curing

In this series, the effect of heat curing on hardened properties of UHPFRC manufactured with conventional sand and expensive silica sand is investigated in the laboratory. UHPFRC shows high functionality due to the active participation of the silica fume pozzolanic reaction and the hydration of cement paste. Curing is an important in that it allows more water to be take part in the hydration process of cement paste thus leading to increased compressive strength (Haque, 1990). There are several curing methods which may be used to further enhance the hydration process and to gain the early age strength characteristics. Hot water or boiling water curing is one of these techniques with its use leading to high early age strengths; reduce curing time as well as enhanced final strength of concrete. With heat treatment of concrete extensive researches have been investigated on the hardened behaviour of UHPFRC under low and high steam pressure curing (Graybeal & Hartmann, 2003; Park et al., 2015; Yazici, 2007), few investigations conducted on heat curing or heat treatment at low and high temperature (Askar et al., 2012; Bumanis et al., 2015; Graybeal & Davis, 2008; Safi et al., 2014) and some studies carried out on thermal treatment of UHPFRC (Prem et al., 2013; Toropovs et al., 2013). In this series, the aim of heat curing was to enhance early strength and observe the strength behaviours with curing age through the pozzolanic reaction and hydration of cement in UHPFRC such that there is a reduction of pore size which will lead to increased strength and durability characteristics.

In this section, when investigating heat curing of UHPFRC with conventional and expensive silica sands, the standard procedures for mix proportion, mixing of constituents, preparation of specimen, associated test set-up and instrumentation, and the result discussion followed in previous series were under taken separately.

4.6.1 Materials and mix proportions

Two concrete mix proportions consist of 1:1:0.266:0.233 and 1:0.5:0.5:0.266:0.233 were considered for conventional and expensive silica sand ratios of this series of mixes. First mix was conducted with conventional river washed sand with FM=2.34 and the second mix was done with silica sand 60G and silica sand 30/60. Silica sand with bulk density of 1450kg/m^3 was used in this investigation. The mix of expensive silica powder, silica sand and conventional sand as illustrated in Table 4.11 and the grain size curve is shown in Fig.4.1. The mix design of UHPFRC specimens were cured by ambient and heat treatment method.

Table 4.11 Mix designs to investigate the suitable mix for hot and ambient curing

Mix Number	w:c	SP:c	Total w:c
1-Hot & Ambient Cure	0.165	0.0850	0.20675
2-Hot & Ambient Cure	0.170	0.0565	0.20675

4.6.2 Mixing procedure

In this series, two types of mixes were conducted with river washed sand and silica sand as fine aggregate in the mixes. For the first mix, all of the dry components that is the cement, silica fume, silica sand 60G and silica sand 30/60 were mixed for 1 minute in the 80 litres capacity of concrete mixer until it observed that all of the constituents were well combined. For the second mix, washed river sand, cement and silica fume were mixed first for 1 minute. Then, the machine was stopped and edges of the machine around the surface especially at the bottom surface were checked accurately. The rest of the mixing procedure is same as described in section 4.2.2.

4.6.3 Specimen preparation and curing regimes

Specimen preparation up to filling of steel moulds is similar as discussed in part 4.2.3. The rest of the preparation technique of UHPFRC specimens for heat and ambient curing are discussed in the this section. All of the heat cure specimens were

prepared according to Australian Standard AS1012.9 (Australia, 1999). After the filling of cylinders steel moulds, specimens were stored in ambient laboratory conditions for temperature for 3-6 hours. After that, specimens were capped within the mould using steel plate and placed in the curing tank such that a clearance of at least 50mm was provided between adjacent moulds and between moulds and the side walls of the tank to provide adequate circulation of the water in the tank. The level of the water was adjusted in the tank around 25mm above the top of the specimens. The initial temperature of the water was between 10^0C and 30^0C. The lid of the tank was then closed and the temperature of the water increased to 82^0C in first 2hrs and maintained it for a further 14 hrs. Thereafter the moulds were removed from the tank and allowed it to cool in air for at least 1 hour and in the following hour all of the specimens were demoulded in the laboratory. After that, the specimens were capped in accordance with AS1012.9 (Australia, 1999) and again immersed the specimens in water at temperature of 23^0C for a period of not less than 2 hours from the time of immersion. First set of specimens were tested between 23 hours and 27 hours from the time of batching based on standard of AS1012.9 (Australia, 1999).

4.6.4 Test set-up and instrumentation

To investigate Test set-up and instrumentation is the similar as described in the section 4.2.4 investigates the strength behaviours of UHPFRC with expensive silica sand and river washed sand by heat and ambient curing method.

4.6.5 Test results and discussion

To investigate the effect of heat and ambient cured with silica and river washed sand conventional sand on the compressive strength properties of UHPFRC from the two mixes are presented in Table 4.12. The mix design has been developed according to total water content in the mix. The total water content consists of the water plus free

water content in the SP. These test results are from the 100mm diameter and 200mm height cylinders cast according to the Table 4.12. In general, three cylinders were tested for each mix at various ages that is shown in Table 4.12 and the compressive strength test results were averaged three of the cylinders to get the final value that is presented in the Table 4.12.

The results are presented in the Table 4.12 according to the each mix design with the corresponding days in terms of mean compressive strength, standard deviation, co-efficient of variation, standard error and the lower and upper 95% confidence interval of the compressive strength for each specimen. In general, it can be observed from Table 4.12 that the compressive strength achieved from the UHPFRC test results ranged from 140MPa to 154MPa for heat cured and 98MPa to 139MPa for ambient cured to the corresponding test age 7 to 90 days.

Table 4.12 UHPFRC compressive test results with conventional fine aggregate

Mixes	Days	Compressive Strength				95% Confidence Interval	
		Mean Strength, MPa	Standard Deviation, MPa	Coefficient of variation	Standard Error	Lower limit, MPa	Upper limit, MPa
	3	140	8.507	0.0608	4.912	135.3	144.7
	7	145	2.192	0.0151	1.265	143.8	146.2
1-Hot	14	147	3.467	0.0236	2.002	145.1	148.9
Cure	28	150	2.543	0.0170	1.468	148.6	151.4
	56	154	0.964	0.0063	0.557	153.5	154.5
	90	151	2.058	0.0136	1.188	149.9	152.1
1-	7	100	2.617	0.0262	1.511	98.6	101.4
Amb.	14	124	6.218	0.0501	3.590	120.6	127.4
Cure	28	139	5.367	0.0386	3.099	136.1	141.9
	3	139	1.325	0.0095	0.765	138.3	139.7
	7	144	7.159	0.00497	4.133	140.1	147.9
2-Hot	14	147	2.437	0.0166	1.407	145.7	148.3
Cure	28	149	2.720	0.0183	1.570	147.5	150.5
	56	151	1.110	0.0074	0.641	150.4	151.6
	90	149	2.720	0.0183	1.570	147.5	150.5
2-	7	98	3.948	0.0403	2.279	95.8	100.2
Amb.	14	120	5.737	0.0478	3.312	116.9	123.1
Cure	28	138	2.420	0.0175	1.397	136.7	139.3

It is clearly seen from Fig.4.69 that heat or water boiling curing methods enhanced the compressive strength at early age strength (Askar et al., 2012; Toropovs et al., 2013) and improves the microstructure of concrete. The early 7 days age strength has increased remarkably on average 94% of its ultimate strength by heat curing and also increased of about 40% than the ambient curing. This behaviour is attributed to the pozzolanic reaction and hydration of cement occur quickly resultant in provoked the changes of micro-structural skeleton such that there is a reduction of pore size which will lead to increased strength and durability characteristics. Consequently, the ambient cured specimen's strength follows the natural strength curve of UHPFRC. It is also very interesting to notice that the ultimate compressive strength is followed the similar behaviour of other series not changed for mixes with silica and washed river sand by heat curing. This is suggested that heat curing method could be potential where early age strength necessary to facilitate the construction work.

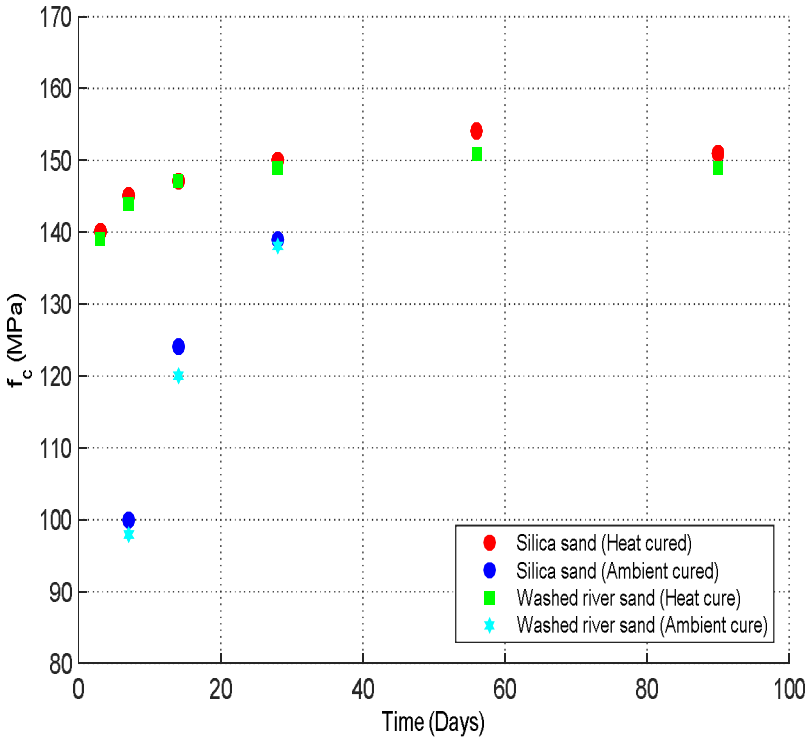

Fig.4.69 Strength vs time of silica and washed river sand by heat curing

4.7 Stress-strain relationship of UHPFRC for all of the mixes

Figure 4.70 shows the 90 day axial and lateral stress strain relationships of UHPFRC for each of the mix design series which prepared with three types of conventional fine aggregate (sand), ground granulated lead smelter slag, coarse aggregate addition respectively. The different colour line in the Fig.4.70 indicates different types of mix series with respect to the FM which discussed in the series I, II and III.

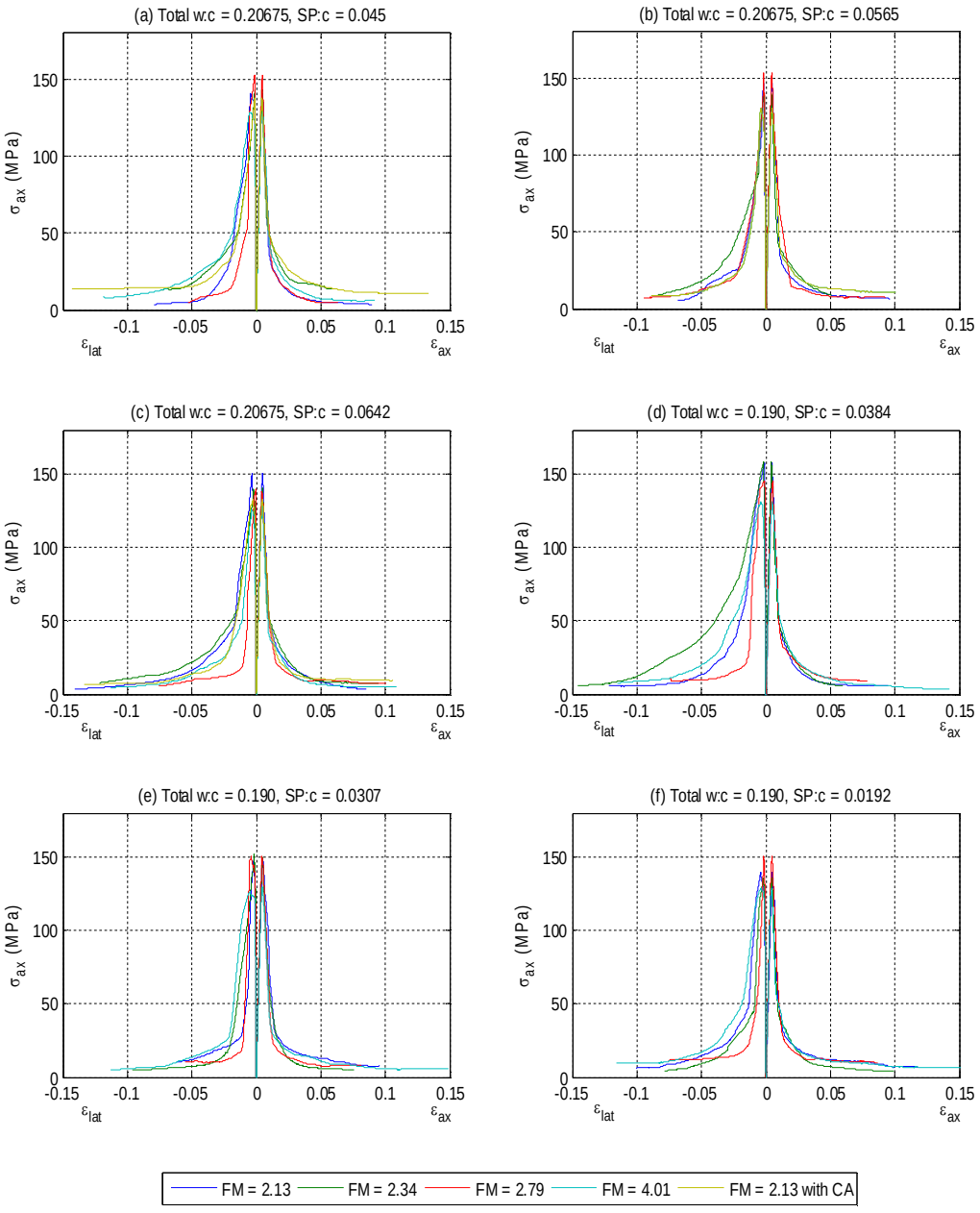

Fig.4.70 90 days axial and lateral stress strain relationships

From Figure 4.70 it can be seen that the material behaved in a linear fashion until the peak stress was achieved. This is followed by a relatively rapid reduction in strength until a stable stress plateau which gives the material substantial ductility. It can also be noted that the material undergoes significant stable dilation during softening indicating it may be efficiently confined.

As the stress strain relationship for each mix is similar in shape, the axial and lateral stress strain relationship for each mix is shown normalised by the peak stress and strain at peak stress $\varepsilon_0$in Figure 4.71. Through this normalisation it can be seen that there is relatively little scatter in the axial stress strain relationship but significant scatter in the lateral stress strain relationship on the falling branch which is due to the difficulty in capturing the total dilation due to wedge sliding (Chen et al. 2014).

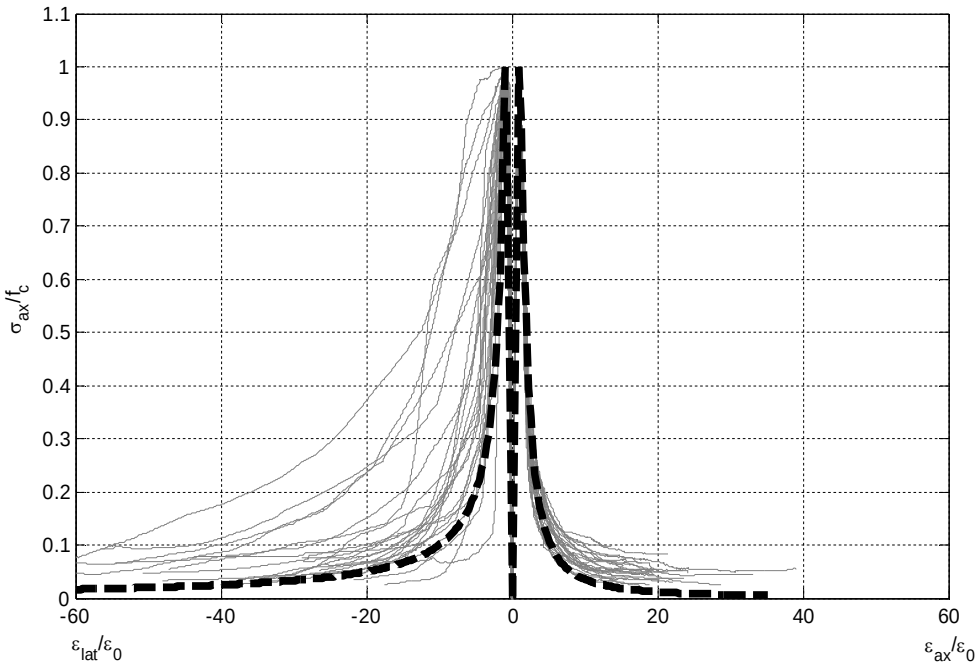

Fig.4.71 Normalised axial and lateral stress strain relationships

Based on the normalised stress strain relationships, for use in analysis a lower bound description of axial stress strain relationship can be described by:

$$\sigma_{ax} = E_c \varepsilon_{ax}; \varepsilon_{ax} \leq \varepsilon_0 \qquad \text{Equation (4.1)}$$

$$\sigma_{ax} = \frac{f_c}{1 + \left(\frac{\varepsilon_{ax}}{\varepsilon_0} \right)^{1.5}}; \varepsilon_{ax} > \varepsilon_0 \qquad \text{Equation (4.2)}$$

$$\sigma_{ax} = \frac{E_c}{\gamma} \varepsilon_{lat}; \varepsilon_{ax} \leq \varepsilon_0 \qquad \text{Equation (4.3)}$$

$$\sigma_{ax} = \frac{f_c}{1 + \gamma \left(\frac{\varepsilon_{lat}}{\varepsilon_0} \right)}; \varepsilon_{ax} > \varepsilon_0 \qquad \text{Equation (4.4)}$$

Which is shown as the heavy dashed line in Figure 4.71 and in which the elastic modulus E_c, strain at peak stress $\varepsilon_0$and Poisson's ratio γ for each mix is presented in Table 4.13.

Table 4.13 Mechanical properties of mix designs

Mix number	f_c (MPa)	E_c(MPa)	ε_0	γ
1-FA	141	36100	0.00472	0.300
2-FA	147	35800	0.00910	0.355
3-FA	150	35000	0.00485	0.358
4-FA	140	30100	0.00484	0.220
5-FA	148	35000	0.00508	0.206
6-FA	158	37300	0.00468	0.191
7-FA	143	38400	0.00439	0.264
8-FA	140	36900	0.00434	0.238
9-FA	140	36200	0.00478	0.370
10-FA	136	35600	0.00428	0.240
11-FA	150	36700	0.00476	0.232
12-FA	158	40900	0.00448	0.462
13-FA	153	37300	0.00452	0.270

14-FA	153	38000	0.00445	0.447
15-FA	138	37600	0.00427	0.131
16-FA	151	10200	0.00484	0.222
17-FA	151	37800	0.00427	0.189
18-FA	145	37900	0.00514	0.120
19-FA	129	36300	0.00474	0.305
20-FA	130	35500	0.00470	0.284
21-FA	128	33900	0.00460	0.348
22-FA	129	35500	0.00426	0.228
23-FA	130	33600	0.00449	0.277
24-FA	131	35200	0.00496	0.272
25-CA	133	37100	0.00432	0.168
35-CA	138	36000	0.00444	0.170
39-CA	138	38200	0.00450	0.190

4.8 Summary

In this chapter, the experimental investigation has been carried out on UHPFRC utilising conventional material and methods. The following major finding can be outlined from the first part of the research:

To produce UHPFRC specialist materials such as expensive silica sand and complex manufacturing procedures increases the cost of UHPFRC. Due to this reason, UHPFRC is still very limited application taking place in the construction industry. So, it is of great concern to achieve of similar strength and workability of UHPFRC utilising conventional materials and methods that lead to less cost of production.

From the overall experimental investigation, it can be observed that UHPFRC could be manufactured with conventional materials and methods and without the need to specialist curing regime. The experimental results revealed that sufficient compressive strength and workability was obtained such that the materials proposed could be used in the construction industry.

UHPFRC can achieved the compressive strength in the ranges of 130-160MPa with conventional mixing and curing regimes. It has also showed very good workability which is the requirement of UHPFRC. Experimental results and observations demonstrate that a strong inverse correlation obtained between the fineness modulus of the fine aggregate and the compressive strength. The addition of a small quantity of coarse aggregate which is less than CA: FA = 0.5 does not lead to a reduction in workability that the economy of the mix can be improved through coarse aggregate addition and also the early age strength is higher than without coarse aggregate.

UHPFRC with expensive silica sand the compressive strength was obtained in the range of 90MPa to 162MPa to the corresponding test age 7 to 90 days. The result reveals that the UHPFRC with conventional fine aggregate shows quiet similar compressive strength and so it could be a alternative to reduce the cost of UHPFRC. The early strength of heat curing was achieved almost 94% of its ultimate strength; however it was increased very small in the long run. It can be seen that theoretical axial and lateral stress-strain curves developed gave a reasonable prediction of the experimental results and the experimental investigation observed that the lateral deformation is on average 60-73% smaller than then axial deformation for UHPFRC.

CHAPTER 5

EXPERIMENT ON SIZE EFFECT WITH COMPRESSIVE DUCTILITY OF UHPFRC

Ultra-High Performance Fiber Reinforced Concrete (UHPFRC) has gained increasing attention in the construction industry, particularly in applications where high ductility is required, for example where resistance to seismic or blast loading is essential (Steinberg, 2009; Wu et al., 2009; Yi et al., 2012). Hence the focus of this chapter is on experimentally quantifying the ductility of UHPFRC with varying fibre types and quantities in order to show the influence of fibres on ductility. The first part of the chapter gives an overview of the rheological properties of the mix investigated, followed by the presentation of test results on the ductility behaviour of UHPFRC concrete with different amounts and types of fibers. Importantly in this chapter a large-volume of tests results are presented to derive the ductility response of UHPFRC concrete including an investigation into size effects and its impact on the axial and lateral stress-strain response. Finally, test results are compared and discussed with regard to the main variables: fiber amount; types of fibre; and the sizes and shapes of the specimens.

5.1 Introduction

In recent years, research has been carried out to investigate both the mix design methodology and the structural performance of UHPFRC before and after softening of RC elements under concentric loading (Graybeal, 2007; Wille et al., 2011; Yang et al., 2010; Yoo & Yoon, 2015; Yu et al., 2014). UHPFRC has been found to show a good ductility response under concentric loading. A small amount of research has been conducted in recent years on UHPFRC to determine the ductility behaviour with different methods of testing and instrumentation (Wille et al., 2014; Wille et al.,

2012). Ductility is the ability to undergo large deformations before failure. With regards to safety, ductility of structures may be as an important phenomenon as their strength. This is the benefit to the users of the structure as it provides a warning prior to final failure of the structures allowing occupants time to take preventive measure. Therefore, a substantial research has been carried out on the rotation capacity of structures constructed from conventional concrete but in general most guidance in national codes of practice are empirically based and show significant scatter (Oehlers et al., 2010). The introduction of new types of materials such as high performance concrete therefore requires renewed research attention in this area.

It has been identified recently that the rotation capacity of a plastic hinge is size dependent due to concrete softening (Bigaj & Walraven, 2002; Carpinteri et al., 2009; Chen et al., 2013). Advanced numerical techniques such as the segmental approach (Chen et al., 2013; Haskett et al., 2009; Visintin et al., 2012a; Visintin et al., 2012b), which will be further discussed in chapter 6 have been developed to incorporate the mechanics of size dependency and hence the main major challenge of quantifying the ductility of UHPFRC members is to quantify the descending or softening branch. As is recognised that the major contribution to the overall deformation of concrete whilst softening is due to localised sliding along softening wedges (Chen et al., 2013). It is essential that the total deformation along the entire specimen height is recorded such that the total local behaviour is measured. That is in order to capture the descending or softening branch, appropriate instrumentation to capture platen to platen deformation is required (Chen et al., 2013). Additionally due to the high compressive strength of UHPFRC, which may be in excess of 150MPa, an appropriate loading rate should be selected before the testing and this may lead to long test times.

Existing test results on the ductility of UHPFRC some of the researcher did not measure the deformation platen to platen of UHPFRC and hence test results are only valid on the ascending branch (Graybeal, 2007). To address this issue, Hassan et al. (2012) and Prabha et al. (2010) has been invented suitable test methods to capture the softening branch of UHPFRC. Hassan et al. (2012) used the circular ring with LVDT's around the specimen to measure the elastic deformation and two LVDT's placed platen to platen that parallel to the specimen to measure the softening branch. Prabha et al. (2010) used two LVDT's between the platens in two opposite sides of the specimen for measurement of axial post peak softening deformation.

The influence of fibre type, volume and length of ductility has been a topic of intense study recently and this is necessitated by the range of fibre types available. A review of these studies follows.

The structural performance of UHPFRC with different fiber length has been studied by Yoo et al. (2015) who concluded that an increase in fiber length and twisted steel fibers led to the improvement of post-peak and ductility responses. The effect of different macro steel fibers with volume content 0-1.5% on the flexural response of hybrid UHPFRC was studied by Kim et al. (2011). They found that longer hooked end and twisted steel fibers with 1.5% fiber content exhibit better flexural strength, deflection capacity and energy absorption capacity than other fibers. Sbia et al. (2014) showed that the optimum reinforcement system, which comprised Polyvinyl alcohol (PVA) and Carbon nanofiber (CNF) of 0.37 and 0.047 volume percentage of UHPFRC improved the flexural strength, deflection capacity and compressive strength. Reactive powder concrete was studied by Al-Jubory (2013) with different types and volume fractions of 1-2% steel fibers. He concluded that both types of

fibers have shown good performance in terms of both the higher strength and ductility due to the higher volume fraction of fiber.

In addition to fibre type and volume specimen shape and size is known to influence compressive strength and ductility. For example much research has investigated the relationship between various cylinder and cube sizes on the compressive strength of concrete (Del Viso et al., 2008; Graybeal & Davis, 2008; Lubell & A.S., 2011). For standard concrete with mixture designs at normal compressive strength levels, it was observed that cube specimens gave higher compressive strength than the cylinders with strength increases of around 10% (Del Viso et al., 2008); however the difference between cube and cylinder strength has been shown to decrease as concrete compressive strength increases. When comparing different sizes of specimens, researchers have demonstrated that, at normal strength levels, the smaller specimens tend to present higher compressive strengths, with strengths decreasing up to 13% when the specimen sizes doubled (Lubell & A.S., 2011). This result has been theorized to be due to larger specimens having a greater likelihood of containing elements of low strength.

Further research by Kazemi and Lubell (2012) compared the influence of specimen size and shape (that is, cubes and cylinders) on the compressive strength of UHPFRC with V_f= 2% of short steel fibers. This research showed that smaller specimen sizes had higher compressive strengths than larger specimens but no clear relationships were established between the peak compressive strength of cylinder and cube samples of different sizes as the fiber volume fraction changed. The results of flexural tests show that the flexural tensile strength of UHPFRC decreases as the prism height increases. This suggests that the cracking and peak flexural tensile strength, as well as the strain-hardening behaviour, are affected by the specimen size

and the fiber content. The use of short steel fibers in UHPFRC significantly improves its flexure toughness. These and other similar concretes are generally classified as UHPFRC, with very high compressive strengths, usable pre- and post-cracking tensile strengths, and significantly improved durability properties as compared with conventional concretes. However, the influence of specimen size as well as their corresponding toughness properties has not been well established and needs further research. In addition to the mechanical properties outlined previously, the rheological properties of a UHPFRC mixture can be influenced by the mix proportions, the fiber volume fraction, and the energy imparted by the mixer.

In this section, the size effect of specimens with different fiber content and amount is investigated. Also, the influence of fiber on the ductility response is determined. This size dependent phenomenon of specimens will be incorporated in the next chapter to determine the rotation capacity of plastic hinges in UHPFRC members.

5.2 Experimental Methodology

A testing program was developed to investigate the influence of specimen size and shape on the compressive strength and ductility of UHPFRC. The main parameters investigated are the fiber type, fiber volume, and variations in specimen sizes and shapes. The amount of fiber ranged from 0 to 3% and while fiber type was varied with each type having differing end anchorage had, diameters and lengths. The fibres investigated had a proprietary names of Dramix 3D, 4D and 5D and are available from Bekaert Ltd in South Australia. Also reported in this chapter is the variation of crack pattern due to the specimen size and shape on UHPFRC as this has implications for the modelling of the formation of concrete softening wedges in flexural beams and columns (Chen et al., 2013; Visintin & Oehlers, 2012; Visintin et al., 2012a).

5.2.1 Materials and mix proportion

The mix proportions were selected in this experimental section according to the basic mix design from Chapter 4. The mix proportions of the concrete by weight are 1:1:0.266:0.175 of sulphate resisting cement (Type SR), fine aggregate, silica fume and steel fibres. After fixing the cement, silica fume and fine aggregate ratio the water and SP content was varied to get the suitable UHPFRC mix. Washed river sand with FM 2.34 was used in all of the mixes instead of expensive silica sand to produce UHPFRC in this research. The basic composition of the ultra-high performance concrete is given in Table 5.1. This was used to investigate the influence of fiber amount and fiber type on the ductility performance of UHPFRC.

Table 5.1 Basic composition of UHPFRC mixture

Mix	Material constituents					
	Cement	Sand	Silica fume	Steel fibers	Water	Superpl-asticizer
	Amount, kg/m^3					
1	920	920	245	161	163	41.4

The mix constituents used in this experimental investigation is the same as described in Chapter 4 with the only difference being the variation of steel fibers for the selected mix proportion. The different properties of steel fiber are described in this section. All of the steel fibers (Dramix-BG) were cold drawn, hooked end wire supplied by the Bekaert Ltd in South Australia. Mixes with each steel fiber type were made with 0, 1, 2 and 3% volume-fraction. Table 5.2 shows the different steel fiber properties received from the manufacture data sheet. Fig.5.1 (a), (c) and (e) shows the steel fibers used in the mix design. Figures 5.1 (b), (d) and (f) show a schematic of each fibre with dimensions.

Table 5.2 Types and properties of steel fibers

Properties	3D Fiber	4D Fiber	5D Fiber
Tensile Strength (MPa)	1345	1500	2300
Young Modulus (MPa)	210	210	210
Length of fiber (mm)	36	60	64
Diameter (mm)	0.55	0.9	0.9
Aspect ratio	65	66	70

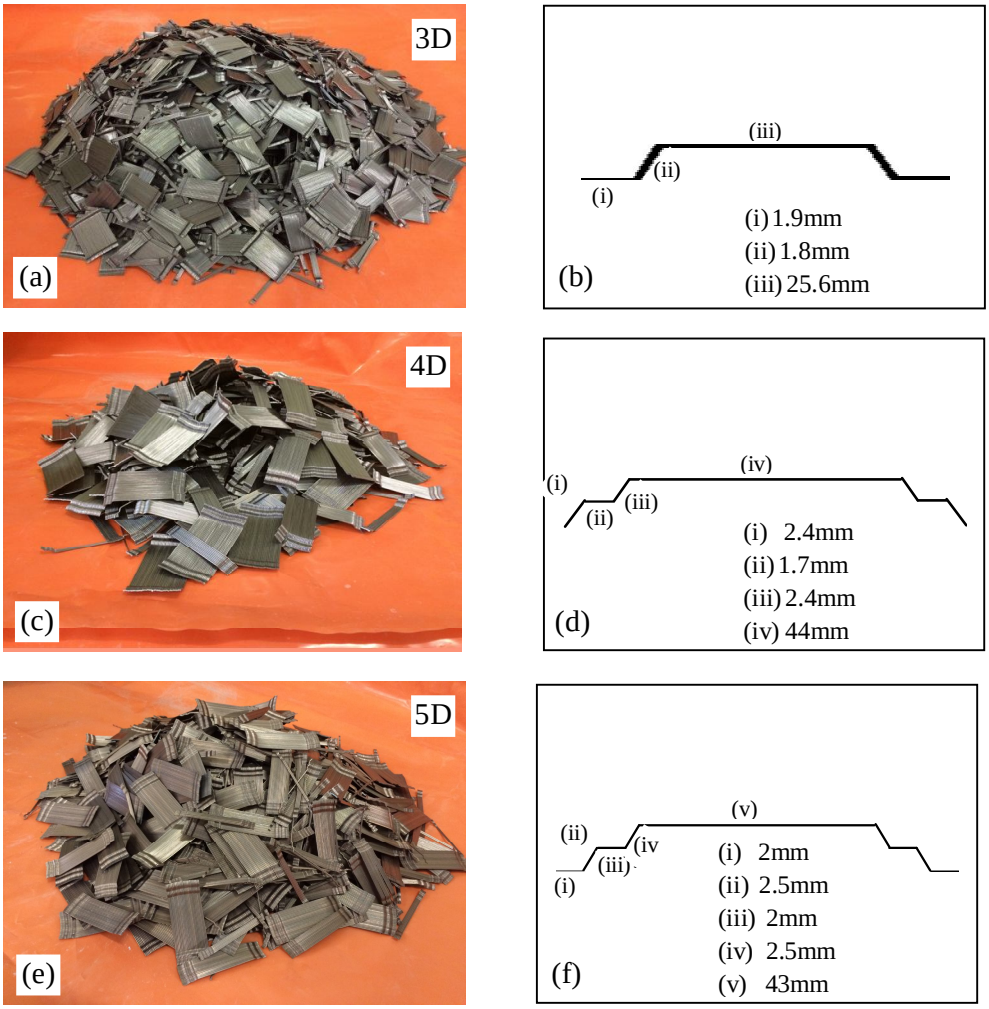

Fig.5.1 (a), (c) and (e) Steel fiber used in UHPFRC (b), (d) and (f) Single part of fiber (31, 60 and 63mm length respectively)

5.2.2 Design of specimen

An efficient experimental investigation has been carried out to produce a material model which can be incorporated into a numerical model for the evaluation of the

rotation capacity of plastic hinges of UHPFRC beam elements. This experimental investigation carried out has mainly concentrated to investigate the size and shape effect with the variation of amount of fiber and type on the post-peak softening branch of the stress-strain relationship of UHPFRC. At the softening region, the failure of the specimen results in the increase of contraction with a decrease in load. The experimental program aims also to evaluate the failure or crackpattern of concrete under compression. All of these criteria finally affect the measure of ductility of specimens, which is size dependent. For this purpose, the scope of the experimental test series has three major influencing factors: specimen size and shape, steel fiber reinforcement amount and fiber type.

The deformation behaviour is normally independent based on the specimen size and shape and the failure of the specimens affect the overall performance. Based on the above concepts, the experimental program was divided into four test series according to the specimen size and shape and fiber amount and typeas illustrated in Table 5.3. The specimen quantity of each series is presented in Table 5.4.

Table 5.3 Experimental design

Specimen designation	Fiber (%)	Test series	Fiber type	Specimen dimension			
				L	W	H	D
S-100x200-3D-0	0	1	3D	-	-	200	100
S-100x200-3D-1	1	1	3D	-	-	200	100
S-100x200-3D-2	2	1	3D	-	-	200	100
S-100x200-3D-3	3	1	3D	-	-	200	100
S-100x200-4D-0	0	1	4D	-	-	200	100
S-100x200-4D-1	1	1	4D	-	-	200	100
S-100x200-4D-2	2	1	4D	-	-	200	100
S-100x200-4D-3	3	1	4D	-	-	200	100
S-100x200-5D-0	0	1	5D	-	-	200	100
S-100x200-5D-1	1	1	5D	-	-	200	100
S-100x200-5D-2	2	1	5D	-	-	200	100
S-100x200-5D-3	3	1	5D	-	-	200	100
S-100x400-3D-0	0	2	3D	200	100	400	-

S-100x400-3D-1	1	2	3D	200	100	400	-
S-100x400-3D-2	2	2	3D	200	100	400	-
S-100x400-3D-3	3	2	3D	200	100	400	-
S-100x400-5D-0	0	2	5D	200	100	400	-
S-100x400-5D-1	1	2	5D	200	100	400	-
S-100x400-5D-2	2	2	5D	200	100	400	-
S-100x400-5D-3	3	2	5D	200	100	400	-
S-100x400-4D-0	0	3	4D	-	-	400	100
S-100x400-4D-1	1	3	4D	-	-	400	100
S-100x400-4D-2	2	3	4D	-	-	400	100
S-100x400-4D-3	3	3	4D	-	-	400	100
S-100x300-4D-0	0	4	4D	-	-	300	100
S-100x300-4D-1	1	4	4D	-	-	300	100
S-100x300-4D-2	2	4	4D	-	-	300	100
S-100x300-4D-3	3	4	4D	-	-	300	100

Table 5.4 Specimen quantities

Series	Size	Specimen Quantities					
		0%	1%	2%	3%	Series	Total
1	100x200	9	9	9	9	36	84
2	100x400	6	6	6	6	24	
3	100x400	3	3	3	3	12	
4	100x300	3	3	3	3	12	

Each series consisted of 0% fiber content (control) group as well as groups to investigate fiber content ranged from 1 to 3%. It is worth mentioning that the final behaviour of each test series was taken to be the average of three specimens, this was done to allow for variation between tests, which is particularly important in UHPFRC as variation in fibre volume and orientation in each sample tested can lead to increased scatter of results. Test series 1 was comprised of 36 cylinder specimens with dimension of 100x200mm with the three different types of fiber that is either 3D, 4D or 5D fibres such that the influence of fibre type could be identified. Test series 3 and 4 consisted of 12 specimens each with 4D fibers but of dimension 100x400mm and 100x300mm respectively such that the influence of specimen slenderness could be investigated. Rectangular prisms were investigated in test series

2 encompassing the dimension of 100x200x400mm with two different types of fiber and the prism with a edge length of 200mm thus allowing for the influence of specimen shape to be investigated. It should be noted that in Table 5.3 the specimen is designated using the following procedure: the first letter “S” refers to specimens; the second set of characters, for example “100x200” refers to the dimension of the specimen, third set of characters, for example “3D” indicates the fiber type and the last letter for example “0” refer to the fiber percentage. Each specimen dimension indicates the length (L), width (W), height (H) and diameter (D). To analyse the specimens test series, concrete peak strength, strain, final deformation, were recorded using a computerised data logger and crack pattern and failure behaviours were obtained by the photographs.

5.2.3 Specimen preparation

As the mixing procedure was discussed in detail in Chapter 4 only details relevant to the study outlined in Table 5.3 will be provided here.

A pan mixer of 80 litres capacity was used in the manufacture of the concrete. The mixer consisted of three concentric rotating steel paddles. It was observed that the mixer could easily rotate the UHPFRC constituents with 1% and 2% volume-fraction of fiber of the mix; however the volume-fraction of 3% fiber mix could not be mixed satisfactorily. The fibers balled around the machine paddles stopping the rotating the paddles. Balling of the fibers around the mixing paddles resulted in non-uniform distribution of the fibres with 3% fiber volume fraction and to compensate for this additional vibration of samples was required for these mixes when casting in moulds as shown in Figure 5.2(a).

Rheological properties were measured with varying fiber amounts and types as soon as mixing were completed and prior to casting in moulds as shown in Figure 5.2(b). Rheological properties measured according to (ASTM-C143/C143M-12, 2012; ASTM-C1611/C1611M-09b, 2009; ASTM-C1621/C1621M-09a, 2009) and include: slump, slump flow and time, J-ring flow and time and blocking step. These were recorded for each mix with different volume fractions of fiber. The spread value was measure in parallel and perpendicular directions to the flow.

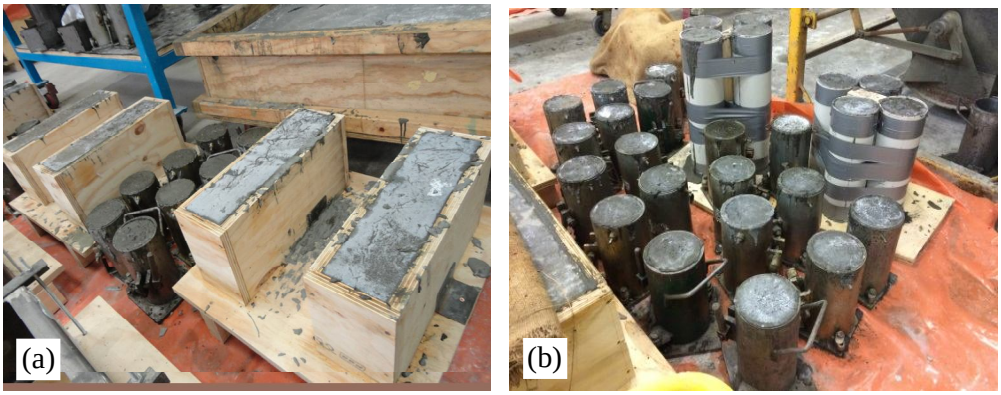

Fig.5.2 Preparation of specimen (a) 3D and 5D fiber types (b) 4D fiber type

It should be noted that the the curing and grinding procedure were the same as described in the Chapter 4 and the laboratory temperature was at around 20 ± 5^{0}C in summer season and 12 ± 5^{0}C in winter season.

5.2.4 Test set-up and instrumentation

All test procedures to determine the rheology of the concrete including slump cone measurement, slump flow and J-ring flow test procedures were undertaken as described in the test set-up and instrumentation section in Chapter 4.

All concrete specimen compression strength tests for all of the series were conducted according to the standard (ASTM-C39/C39M-12, 2012). A Seidner Compression Testing Machine with maximum capacity 3000kN was used to determine the compressive strengths. The specimens were tested up to their peak strength under

load control after that under deflection control. The basic load configuration and test set-up was constant throughout the testing. The loads were applied on the top surface of 100mm diameter cylinders and 100x200x400mm prisms. The load application rate was maintained at 50kN/min in the ascending branch and 0.1mm/min after the peak load was obtained (descending branch) for all of the specimens. An Amsler Compressive Testing Machine with a maximum load capacity of 5000kN was used to determine the stress-strain behaviour and maximum strength of all UHPFRC 56 day old specimens. Figures 5.3(a) to (d) show the UHPFRC specimen test set-up and instrumentation, test chamber and computer recorded data system.

Fig.5.3 Rectangular UHPFRC specimens set-up and instrumentation (b) Cylindrical UHPFRC specimens set-up and instrumentation (c) Test chamber for UHPFRC specimens (d) Computer record data system

All of the other compression testing was undertaken at 7, 28, and 90 days in order to quantify the compressive strength gain over time. At day 56, specimens were instrumented with 4 Linear Variable Displacement Transducers (LVDTs) to measure the total platen to platen axial deformation and 3-LVDTs equally spaced laterally at mid-height to measure the total lateral dilation. For cylindrical specimens, two axial strain gauges were used to measure the axial strain due to concentric loads and three lateral strain gauges were used to measure the strain. For rectangular specimens, four axial strain gauges were used at four faces of the specimens to measure the axial strain due to concentric loads and four lateral strain gauges were used to measure the lateral strain.

5.3 Test results and analysis

At first, the measured rheological properties of the UHPFRC with different fiber types and amounts are described and compared amongst them in this section. The rheological properties determined are the slump height, flow ability and passing ability of UHPFRC. After that, compressive strength properties of UHPFRC with various curing ages are discussed and then the compressive ductility test results is presented and discussed. Finally, the measured ductility test results are compared to evaluate the influence of fiber content and type on size effect behaviours.

5.3.1 Rheological properties of UHPFRC

In order to determine the rheological properties, the different amounts of different fibers on the slump height, slump flow (flowability) and j-ring flow (passing ability) were conducted in the laboratory. All the measured diameter of the flow spread had approximately circular shape in parallel and perpendicular position of ply wood board. It can be clearly seen from Fig.5.4 to Fig.5.6 that the slump height, slump

flow and J-ring flow decreases with increasing fiber volume fraction in the UHPFRC mixes. It is apparent from these Figures that flow was most significantly reduced for the 3D fibres and least reduced for 5D fibers. It is noticed from Fig.5.4 and 5.5 that slump height and slump flow 2% fiber volume fraction show similar results to that of a fibre volume fraction of 1% for all fiber type mixes, indicating that the influence of fibre addition in this range has a negligible influence on the measurement of these rheological properties. However, 3% fiber volume fraction exhibits lowest flow, especially the 3D fiber type which can easily differentiate from other fiber flow. It may cause due to the same mass of fiber in the mix resultant in higher amount of 3D fiber present in the same volume of concrete mix which can increase the cohesive forces between the fibres and the matrix that leads to reduce the flow spread. Moreover, the stiff concrete matrix formed and it changed the structure of the granular skeleton and push apart particle that are relatively large than with fiber length that leads to reduce of flow for short fiber.

Further investigating flow in the presence of the j-ring it can be seen in Figure 5.6 that flow around reinforcement is significantly reduced with increasing fibre volumes fraction. It can be clearly seen that the j-ring flows of the designed UHPFRC are larger than 500 mm for 5D and 4D for 1 and 2% fiber volume fraction; however it fluctuate around 400-300mm for all types of fiber for 3% fiber volume fraction. The fluctuated flow of 3D fiber attributed to an interlocking of fibres may occur if reinforcement spacing is small and this may have design and construction implications. Fig.5.7 illustrates the relationship between the slump and j-ring flow for all fibre types and volume fraction were investigated. The consistent linear relationship between the slump flow and the J-ring flow regardless of fibre type and volume fraction suggests that the change in fibre type and volume fraction did not have a significant influence on the interaction of the UHPFRC with the J-ring.

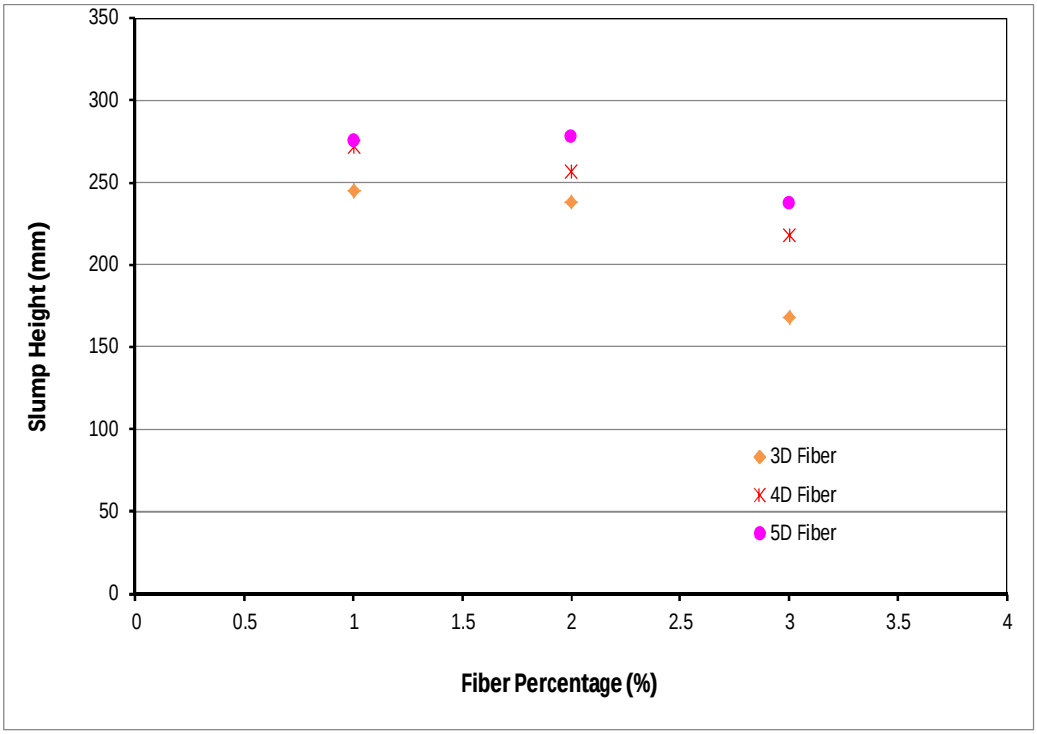

Fig.5.4 Slump height versus fiber amount

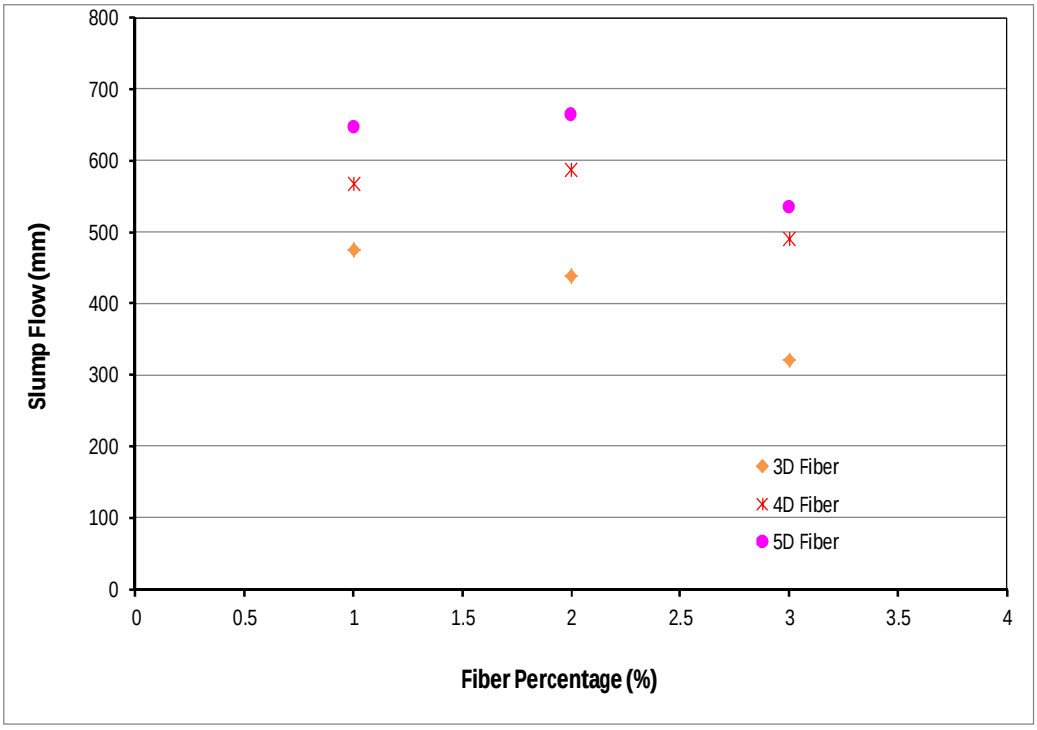

Fig.5.5 Slump flow versus fiber amount

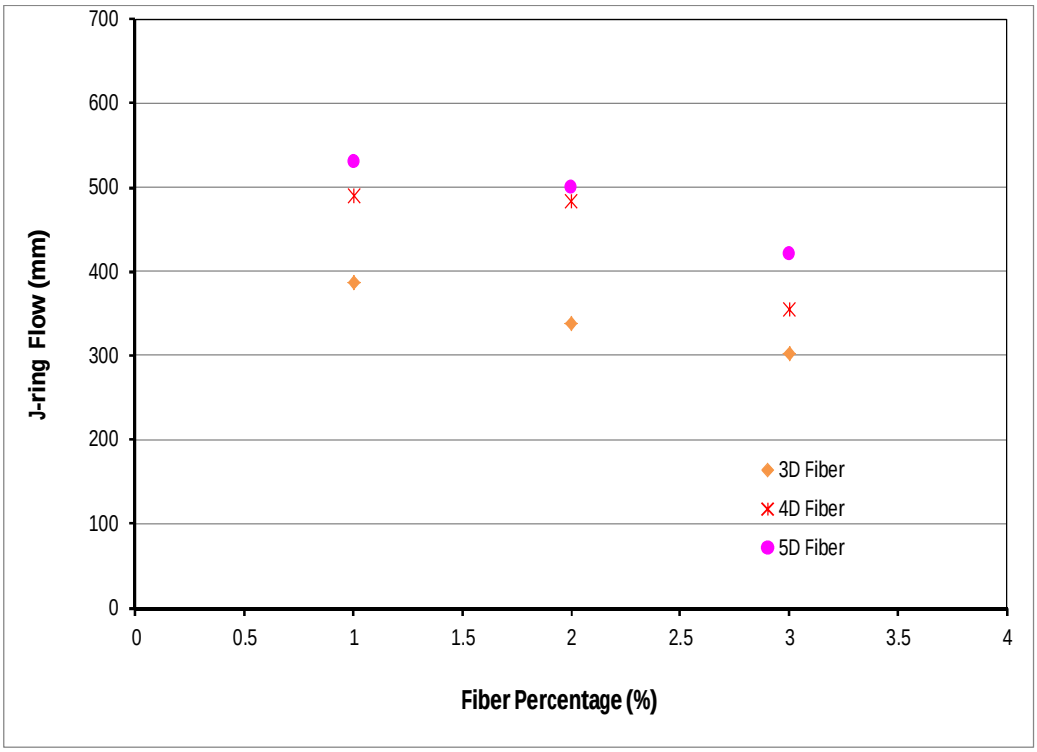

Fig.5.6 J-ring flow versus fiber amount

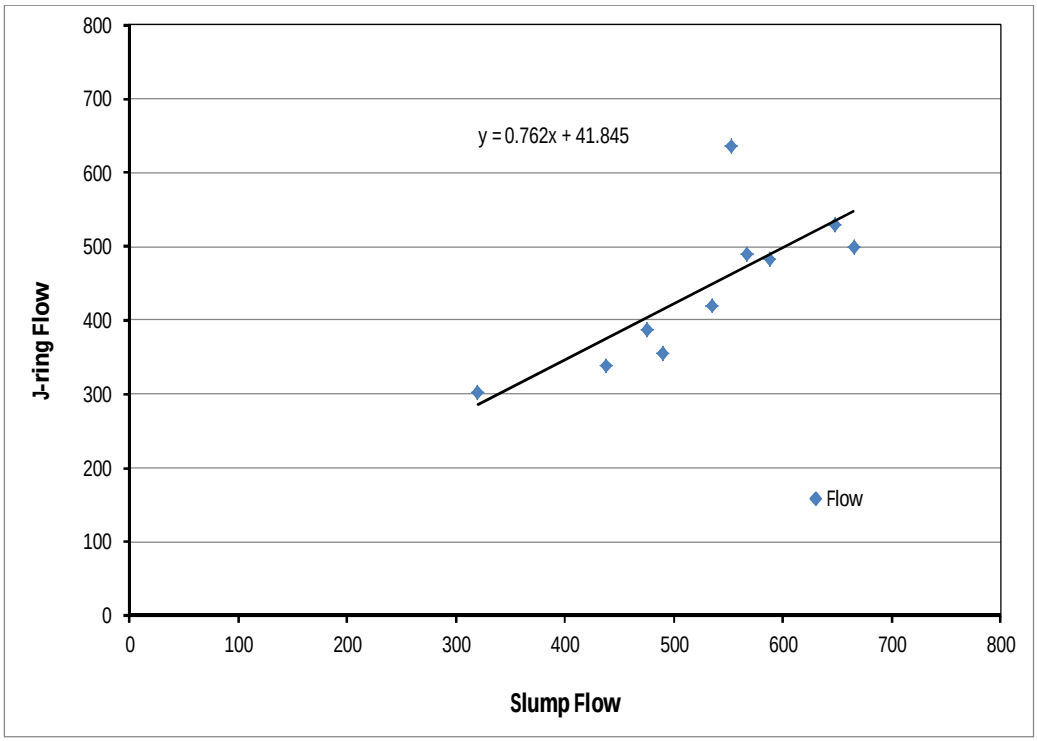

Fig.5.7 J-ring flow versus slump flow

Slump and j-ring flow with time is shown in Fig.5.8 and Fig.5.9. It is observed that 5D fiber flow time is less than the 4D fiber types. There are no time values observed in Fig.5.8 for 3D fiber and in Fig.5.9 for 3D and 4D fibers. It indicates that the flow did not exceed the circle of 500mm on plywood and also it very much less than longest fiber. It may be because in a certain mass of fibres which was added there are more fibres and due to the much number of fibres in a given volume they are interlocking, cohesive forces and end anchorage of fibers each other with concrete matrix to prevent the flow especially in the J-ring when passing through the reinforcement. Following the opposite trend, the longest fiber mix was observed more flowable than other types of fiber and takes less time to spread as refer to Fig. 5.8. However, the flowing time of 5D fiber through j-ring has taken around 6-7 times higher than slump flow to exceed 500mm circle of plywood. It can be concluded that it has a great potential to use in design based on the requirement of the flowability in the structural applications in construction industry.

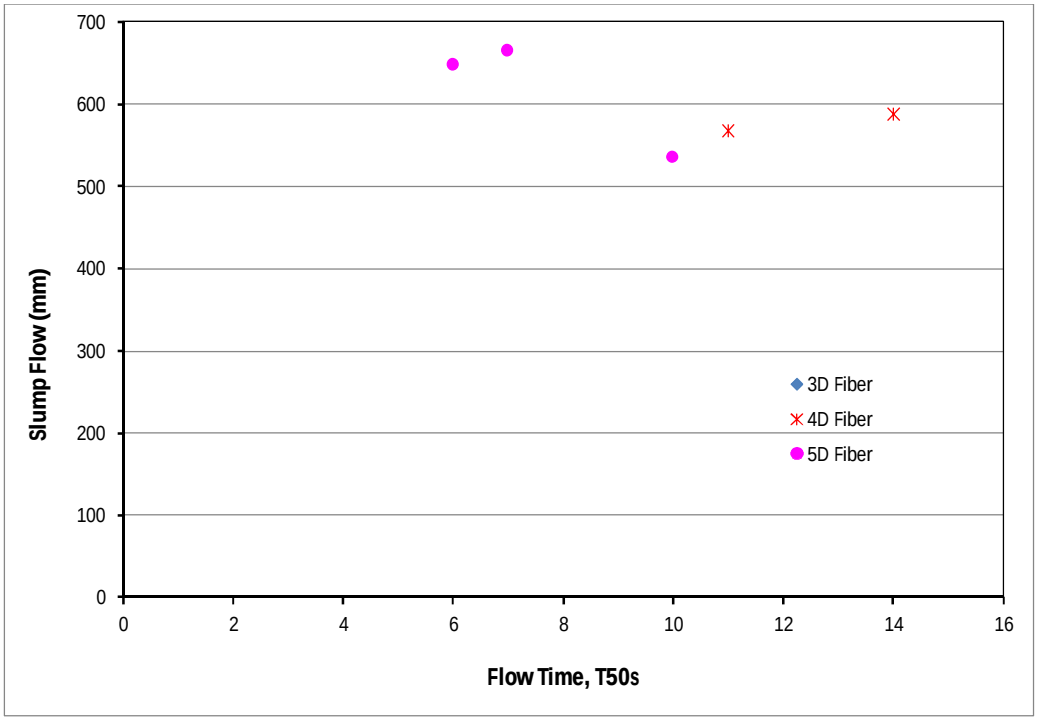

Fig.5.8 Slump flow versus flow time

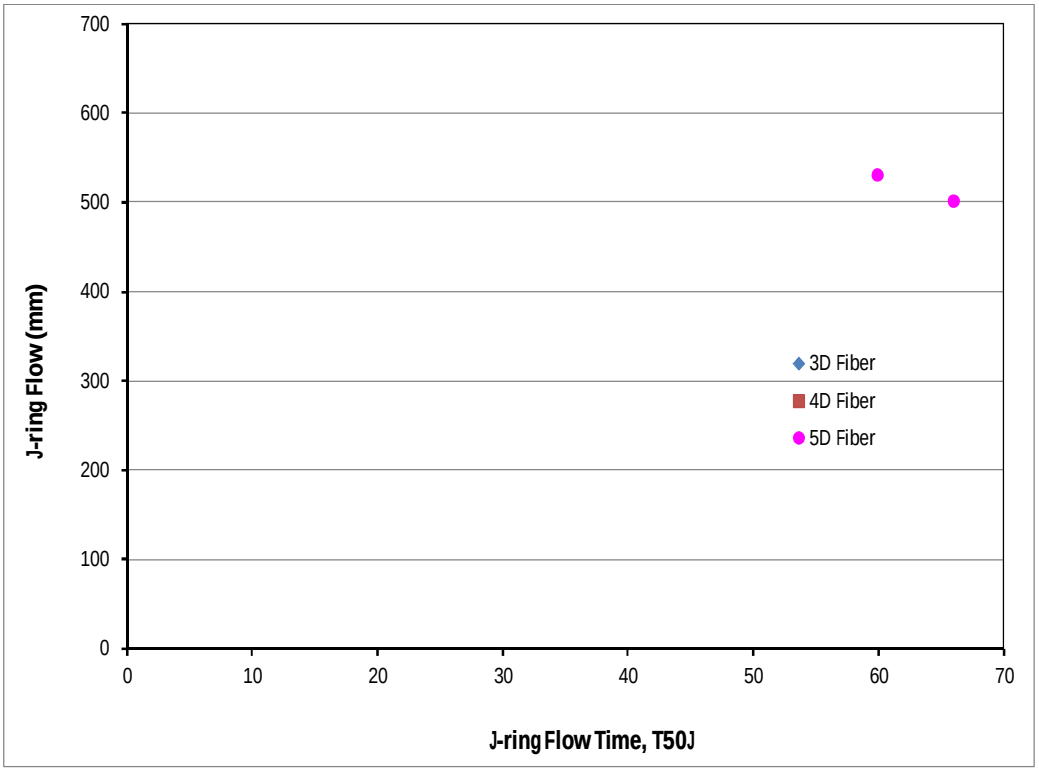

Fig.5.9 J-ring flow versus flow time

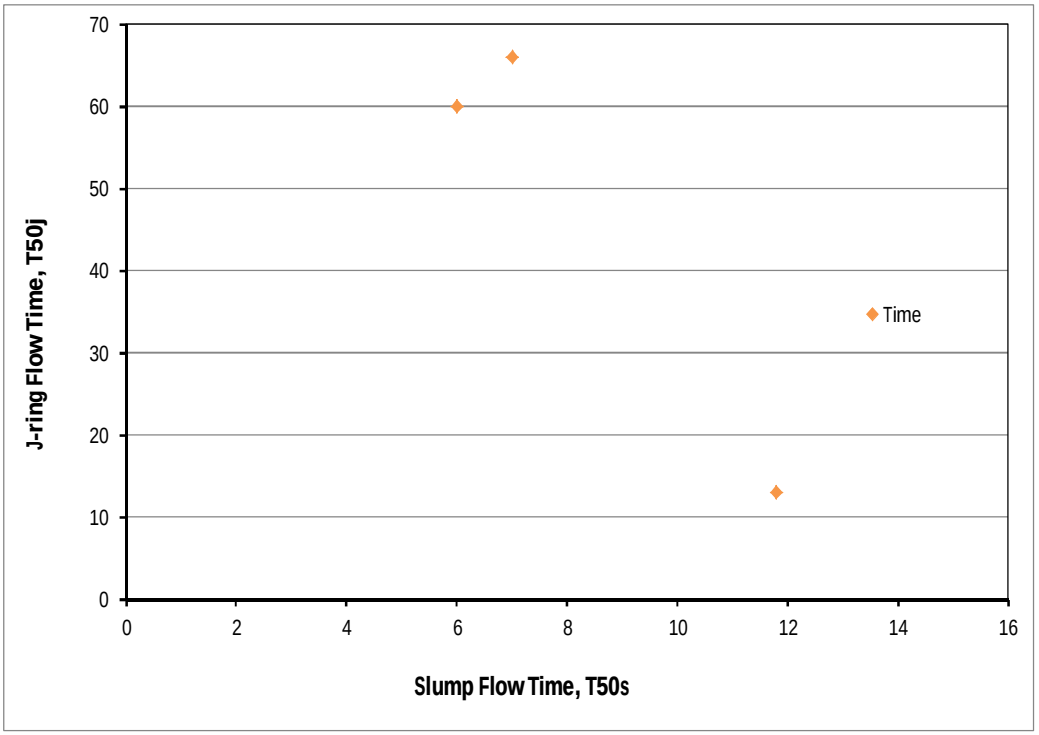

Fig.5.10 J-ring flow versus slump flow time

Fig.5.10 presented the comparison of j-ring flow and slump flow time curve. From this Figure it can be noticed that there is a difference in flowability and passing ability time and J-ring flow required much more time than the slump flow. It may occur due to the more interlocking, and higher cohesive force produced by the fiber in concrete matrix and it make stronger when passing through the steel reinforcement. This behaviour gives us the information about the flow rate through the spacing of reinforcement or without reinforcement where it necessary in the construction site structural applications

Blocking steps means the restriction of deformability of the flow in the mix. Blocking step measures the height difference between the center of concrete and the outermost concrete of the J-ring. It is also expected from the blocking step measurement that whether the passing ability of concrete flow through steel reinforcement is poor or high. Blocking step has a great influence in the structural applications where the concrete flow rate measure with and without steel reinforcement. Blocking step measurement with j-ring flow and different fiber volume fraction of 3D, 4D and 5D fiber types is illustrated in Fig.5.11 and 5.12. It is seen that with an increasing fiber volume fraction of different fiber blocking step is increased, it is quite obvious for higher volume fraction of 3D fiber. The behaviour of 3D fiber blocking step attributed to the same mass of fibres included in the mix and there are more fibres present in a same volume of mix. It is important to notice that 4D fiber exhibits medium blocking step that is in between 3D and 5D fibers. This behaviour reveals the interlocking due to medium length and end anchorage. Therefore it might be concluded that high fiber and smallest fiber increased blocking step and that is followed similar behaviour with j-ring flow results.

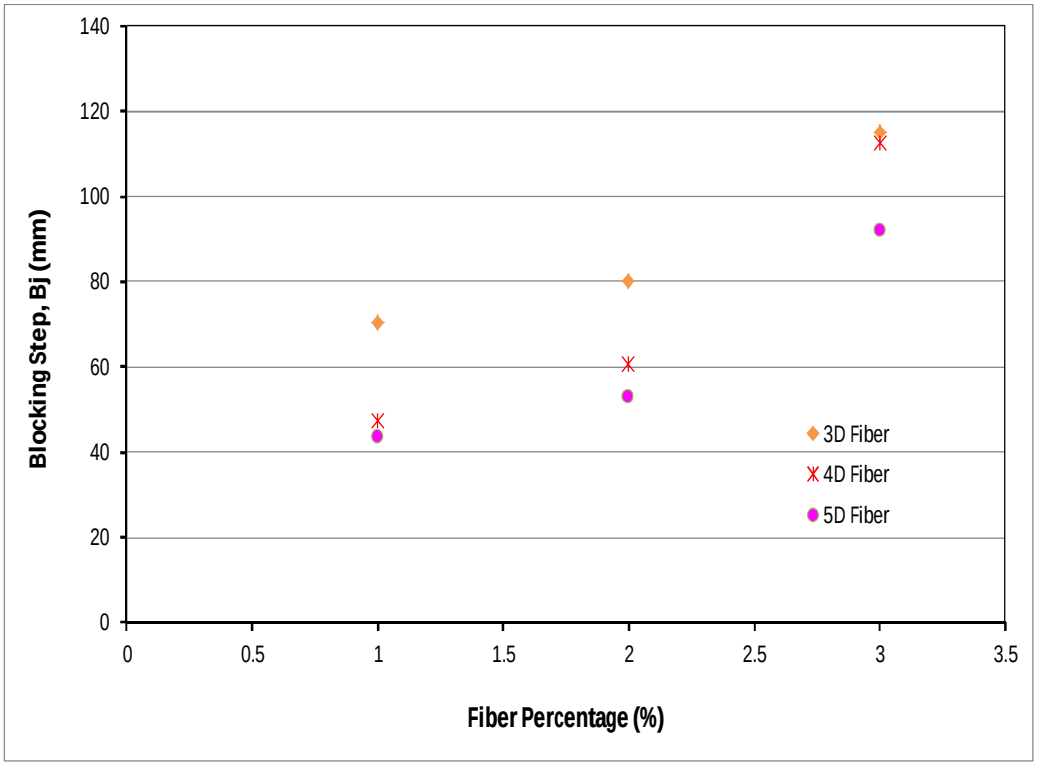

Fig.5.11 Blocking step versus fiber percentage

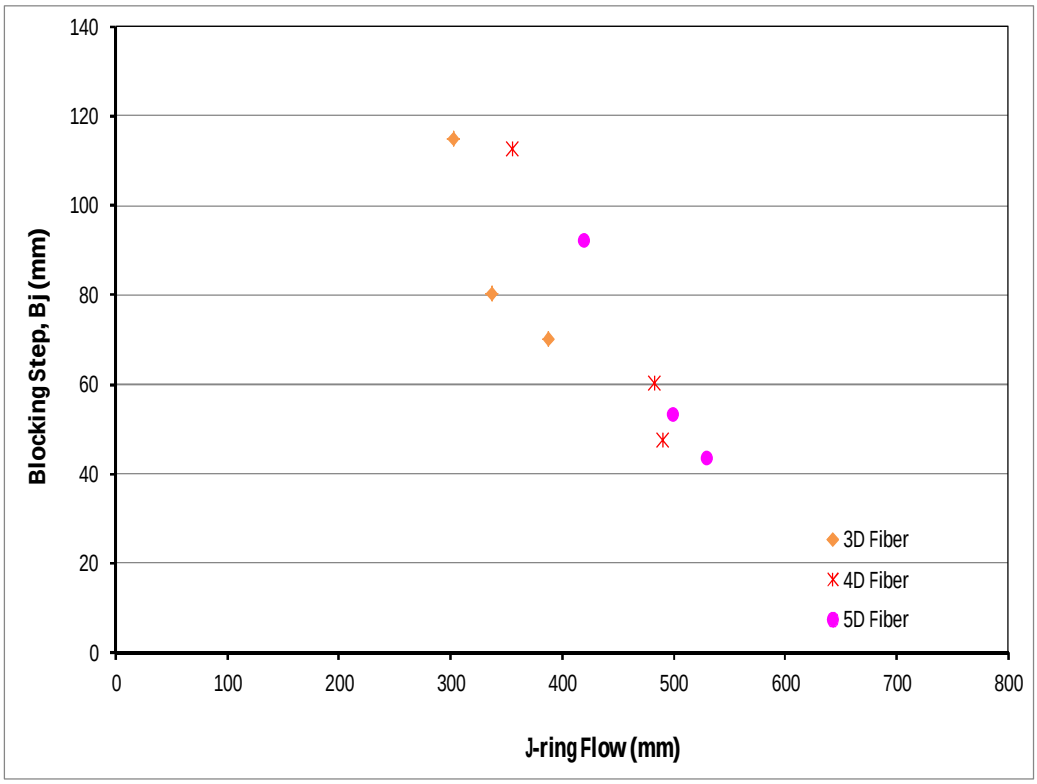

Fig.5.12 Blocking step versus j-ring flow

5.3.2 Compressive behaviour of UHPFRC with curing age

In Chapter 4 it was identified that the strength of UHPFRC is highly time dependent and that the strength of UHPFRC may regress over time due to restraint of shrinkage by the fibres. Thus in this chapter the influence of varying fibre type and content of compressive strength gain is investigated. In Table 5.5, the compressive strength of all 100x200mm cylinders is given at days 7, 28, 56 and 90. The results given are the mean of three identical test specimens at each time stepand in Table 5.5 results are divided according to the fiber type and quantity. To show the variation in individual tests along with the mean strength thestandard deviation, co-efficient of variation, standard error and the lower and upper 95% confidence interval of the compressive strength is also provided.

In general, it can be seen from Table 5.5 that the compressive strength obtained from the UHPFRC test results ranged from 100MPa to 160MPa for different fiber types and fiber volume fraction. It is also observed that the standard deviation of the tested specimens ranges from 0.709 to 14.652 with the corresponding co-efficient of variation 0.52 % to 12.63%. It can be observed that the difference in compressive test results varies by a maximum 12.63% amongst the three specimens corresponding to a maximum standard error of 8.459. This magnitude of this error can be attributed to the relatively small number of test specimens of each type used to determine the compressive strength. The lowest compressive strength of 7–days was found of 100MPa with a 95% confidence interval of 98.8 MPa to 101.2MPa for the 0% fiber volume fraction in the mixes. It is also noticed that with the inclusion of 1% fiber volume fraction, lowest compressive strength was obtained around 103MPa with a 95% confidence interval of 100.2MPa to 105.8MPa for the 5D fiber type and the highest compressive strength was achieved 160MPa with a 95% confidence interval of 159.1MPa to 160.9MPa for the 4D fiber type with 3% fiber volume fraction.

Table 5.5 Compressive strength of UHPFRC with different fiber type and amount

Fiber Type	Fiber %	Day	Compressive Strength				95% Confidence Interval	
			Mean Strength, MPa	Standard Deviation, MPa	Coefficient of variation	Standard Error	Lower limit, MPa	Upper limit, MPa
0D	0	7	100	2.265	0.0226	1.308	98.8	101.2
		28	111	1.789	0.0161	1.033	110.0	112.0
		56	116	14.652	0.1263	8.459	108.0	124.0
		90	112	13.450	0.1201	7.765	104.6	119.4
3D	1	7	116	5.730	0.0494	3.308	112.9	119.1
		28	120	1.131	0.0094	0.653	119.4	120.6
		56	128	4.748	0.0371	2.741	125.4	130.6
		90	142	5.160	0.0363	2.979	139.2	144.8
3D	2	7	118	6.720	0.0569	3.880	114.3	121.7
		28	137	0.709	0.0052	0.409	136.6	137.4
		56	146	10.445	0.0715	6.030	140.3	151.7
		90	139	1.281	0.0092	0.740	138.3	139.7
3D	3	7	122	7.186	0.0589	4.149	118.1	125.9
		28	139	7.478	0.0538	4.317	134.9	143.1
		56	151	5.479	0.0363	3.164	148.0	154.0
		90	149	2.407	0.0162	1.390	147.7	150.3
4D	1	7	110	3.683	0.0335	2.127	108.0	112.0
		28	116	0.972	0.0084	0.561	115.5	116.5
		56	137	19.024	0.1389	10.983	126.6	147.4
		90	147	3.885	0.0264	2.243	144.9	149.1
4D	2	7	113	1.254	0.0111	0.724	112.3	113.7
		28	146	0.515	0.0035	0.297	145.7	146.3
		56	155	11.460	0.0739	6.616	148.7	161.3
		90	148	0.989	0.0067	0.571	147.5	148.5
4D	3	7	120	2.335	0.0195	1.348	118.7	121.3
		28	149	1.556	0.0104	0.898	148.1	149.9
		56	160	1.612	0.0101	0.931	159.1	160.9
		90	158	6.494	0.0411	3.749	154.4	161.6
5D	1	7	103	5.150	0.0500	2.974	100.2	105.8
		28	112	5.101	0.0455	2.945	109.2	114.8
		56	122	1.960	0.0161	1.131	120.9	123.1
		90	137	3.204	0.0234	1.850	135.2	138.8
5D	2	7	105	10.372	0.0988	5.988	99.3	110.7
		28	121	14.723	0.1217	8.500	112.9	129.1
		56	131	9.684	0.0739	5.591	125.7	136.3
		90	127	1.348	0.0106	0.778	126.3	127.7
5D	3	7	111	3.507	0.0316	2.025	109.1	112.9
		28	127	2.421	0.0191	1.398	125.7	128.3
		56	138	0.867	0.0063	0.500	137.5	138.5
		90	136	3.098	0.0228	1.789	134.3	137.7

Comparisons of compressive strength with curing age for different types and volume fraction of fibers are shown in Fig.5.13 and Fig.5.14. It is important to notice that from Fig.5.13 in general compressive strength of UHPFRC gradually increases up to a peak around 160MPa at 56 days for 4D fiber before regressing slightly at day 90 for all types and volume fraction of fiber. The difference of strength between fiber types with same volume fraction is relatively small, exceptional observed for 0% and 1% fiber mixes. Moreover, the rate of gain compressive strength was observed with increasing fiber amount for each curing days each fiber type; however the gain of strength shows highest value with 3% fiber volume fraction at 56 days period. This behaviour could be attributed to the combined effect of 4D fiber in resisting the crack development and mixture with 4D fiber is more homogeneous leads to increase the strength compared to 3D and 5D fibers. Consequently, decreasing the strength at 90 days suggest that the increased shrinkage effect with higher fibre volumes results in increased cracks leading to a decrease in strength.

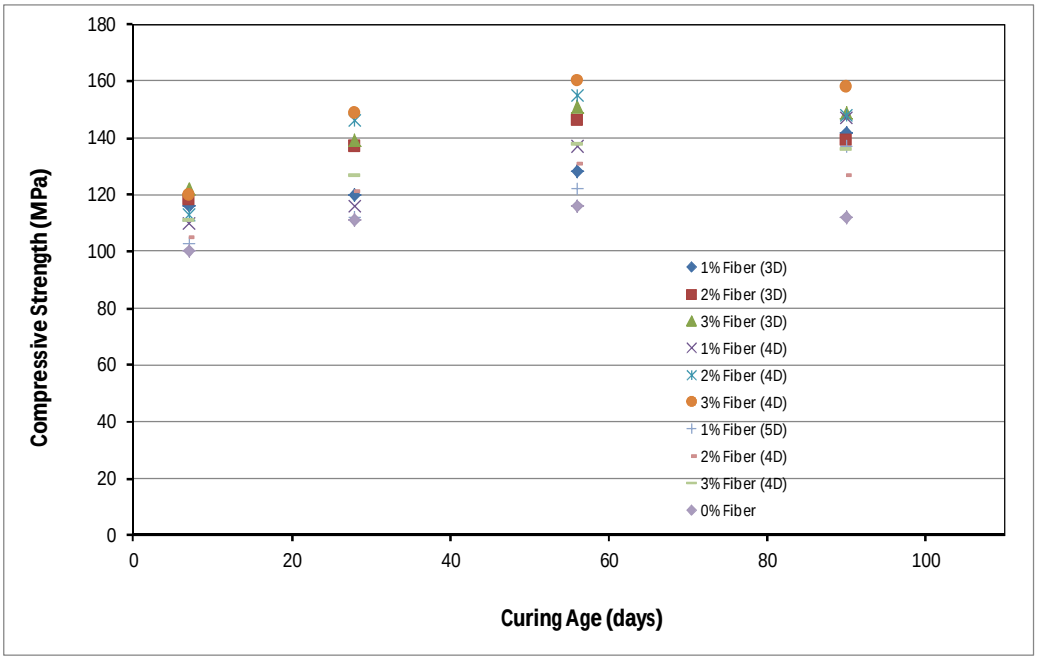

Fig.5.13 Comparison of compressive strength with curing age for different types of fiber type and amount

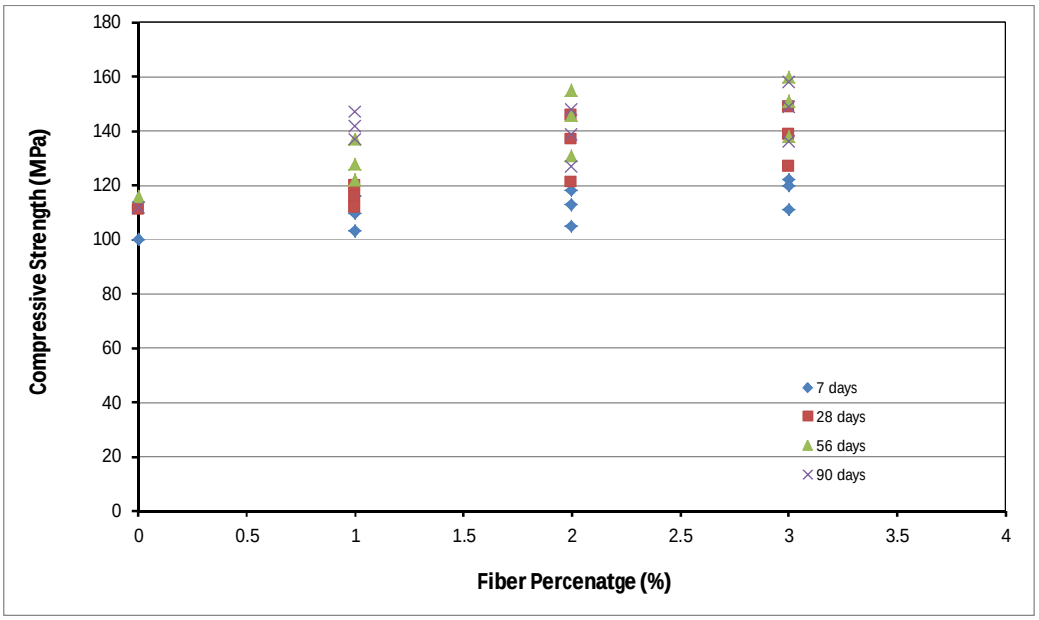

Fig.5.14 Comparison of compressive strength with fiber percentage with curing age

Further, the compressive strength compare separately as a normalised stress with the different fiber type is presented in Fig.5.15 and Fig.5.16. The fiber of 3D is considered as reference strength and then 4D and 5D fiber strength compare with the reference fiber type.

While the compressive strength up to an age of 56 days is observed increase with increasing fiber volume, by day 90 the lowest fibre volumes have the greatest compressive strength for all fibre types. This trend suggests that the increased restraint to shrinkage provided by the higher fibre volumes results in increased micro-cracking leading to a greater reduction in strength.

The strength comparison amongst the fiber type is shown in Fig.5.15 and Fig.5.16. It is seen that following the 28 days to 90 days test the 4D fiber achieved the highest strength followed by the 3D fibers, whilst 5D fiber shows the lowest strength at all time period considered. Due to the increased end anchorage of the fibres with more homogeneity that work together, it was expected that the 4D and 3D fibres would

lead to improved performance over the 5D fibres. As a consistent mass of fibres was added to the mix, the increased size of the 5D fibres means that overall there may be significantly less fibres present in any given volume of concrete. Thus the reduction in strength with the 5D fibres may be due to the reduced number of fibres.

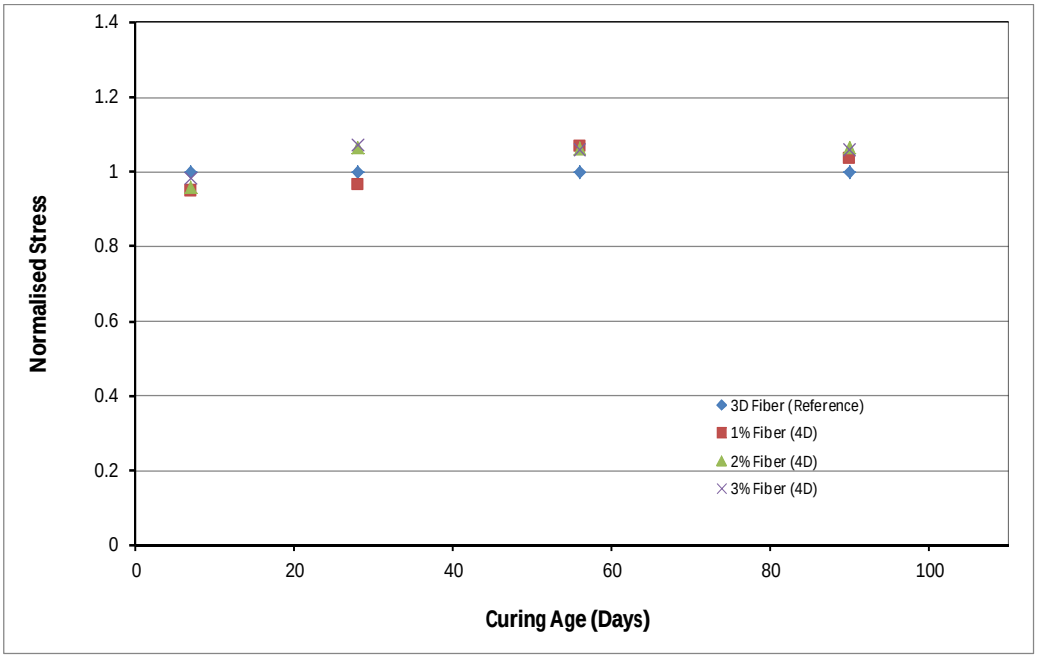

Fig.5.15 Strength comparison with curing age for different fiber type

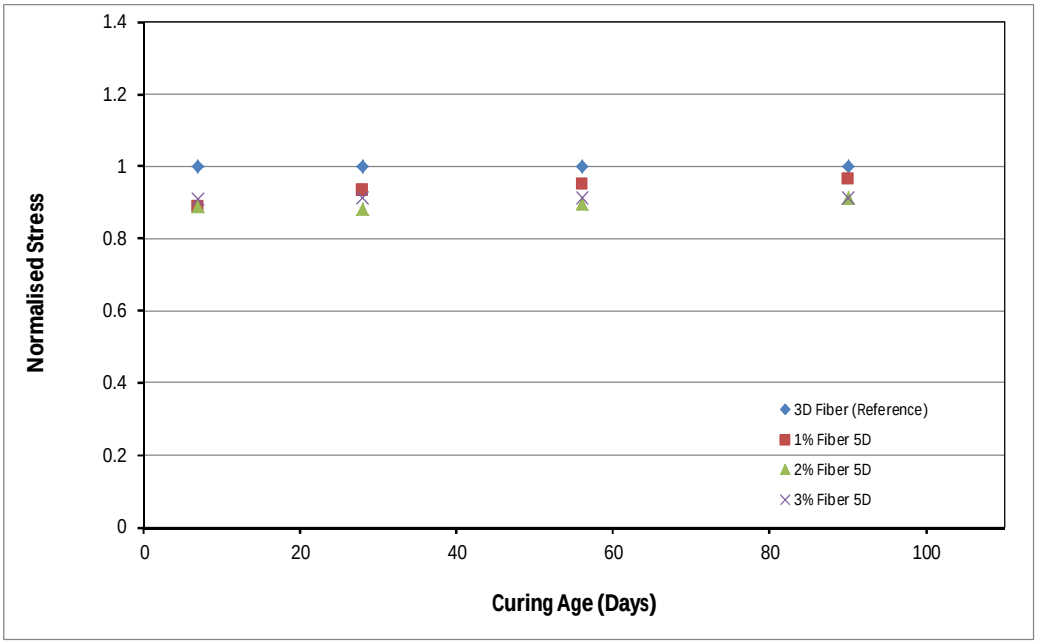

Fig.5.16 Strength comparison with curing age for different fiber type

5.3.3 Axial behaviours of UHPFRC under concentric loading

Axial stress-strain experimental results including secant stiffness, peak strength, peak strain, failure strength and failure strain of different fiber type and amount of UHPFRC are presented in Table 5.6. In general, it can be seen from Table 5.6 that the secant stiffness calculated from the UHPFRC test results ranged from 34009MPa to 41651MPa for different fiber types and volumes. It can be also seen that the highest peak strength of the tested specimens ranges from 117 to 160 with the corresponding peak strain 0.0036 to 0.0045 for test series 1. It is also observed that the highest failure stain obtained of 0.2238 for 5D fiber with 3% fiber volume fraction and the lowest failure strain captured of 0.084 for 3D fiber with 1% fiber volume fraction. This behaviour can be attributed to the relatively longer fiber and less fiber content in the mix when compare to the weight. The peak strength and ultimate failure strain reduce to 8.1% and 51% respectively; when the specimen size make it double for the same volume fraction of fiber and type.

Table 5.6 Axial stress-strain results of UHPFRC

Specimen designation	Fib-er %	Test series	Fiber type	Secant Stiff. (MPa)	Peak Strength (MPa)	Peak Strain	Failure Strength (MPa)	Failure Strain
S-100x200-3D-0	0	1	3D	34009	117	0.0036	106	0.009
S-100x200-3D-1	1	1	3D	32702	127	0.0044	6.060	0.0846
S-100x200-3D-2	2	1	3D	35491	146	0.0044	4.831	0.1125
S-100x200-3D-3	3	1	3D	37109	150	0.0046	7.576	0.1315
S-100x200-4D-0	0	1	4D	34009	117	0.0036	106	0.009
S-100x200-4D-1	1	1	4D	35002	137	0.0042	6.683	0.101
S-100x200-4D-2	2	1	4D	37246	155	0.0044	4.394	0.148

S-100x200-4D-3	3	1	4D	37461	160	0.0045	7.234	0.187
S-100x200-5D-0	0	1	5D	34009	117	0.0036	106	0.009
S-100x200-5D-1	1	1	5D	29874	121	0.0049	6.3625	0.1315
S-100x200-5D-2	2	1	5D	35496	133	0.0044	7.7263	0.1808
S-100x200-5D-3	3	1	5D	35861	138	0.0043	5.7772	0.2238
S-100x400-3D-0	0	2	3D	34009	117	0.0036	106	0.009
S-100x400-3D-1	1	2	3D	38006	115	0.0043	2.994	0.0467
S-100x400-3D-2	2	2	3D	41651	133	0.0042	5.088	0.0569
S-100x400-3D-3	3	2	3D	39041	139	0.0042	4.967	0.0667
S-100x400-5D-0	0	2	5D	34009	117	0.0036	106	0.009
S-100x400-5D-1	1	2	5D	30189	112	0.0044	1.351	0.0787
S-100x400-5D-2	2	2	5D	27385	122	0.0045	5.262	0.0938
S-100x400-5D-3	3	2	5D	30022	128	0.0047	5.249	0.1091
S-100x400-4D-0	0	3	4D	34009	117	0.0036	106	0.009
S-100x400-4D-1	1	3	4D	35516	126	0.0040	0.981	0.0660
S-100x400-4D-2	2	3	4D	37280	142	0.0040	1.948	0.0797
S-100x400-4D-3	3	3	4D	34192	147	0.0044	2.819	0.0918
S-100x300-4D-0	0	4	4D	34009	117	0.0036	106	0.009
S-100x300-4D-1	1	4	4D	38024	124	0.0035	0.6288	0.0923
S-100x300-4D-2	2	4	4D	38962	141	0.0036	2.476	0.1098
S-100x300-4D-3	3	4	4D	40584	142	0.0037	1.469	0.1322

Following the Table 5.6, typical compressive axial and lateral stress-strain responses of the UHPFRC are shown in Fig.5.17 to Fig.5.23 for test series 1 to 4 specimens. The associated testing and instrumentation procedure was described in the previous section for fiber type and volume fraction of UHPFRC including size effects. The axial deformation measured by the LVDT's between platen to platen and the lateral deformation measured with LVDT's around the specimen at mid height.

It should be noted that all of the test series specimen stress-strain curves were processed by first removing bedding down from the test raw data. It is worth mentioning that each curve represents individual fiber amount and type of fiber and also each curve is represents the average of three UHPFRC specimen test results. The right side curves of the graph represent axial behaviours and the left side of the graph illustrated lateral responses of the UHPFRC specimens.

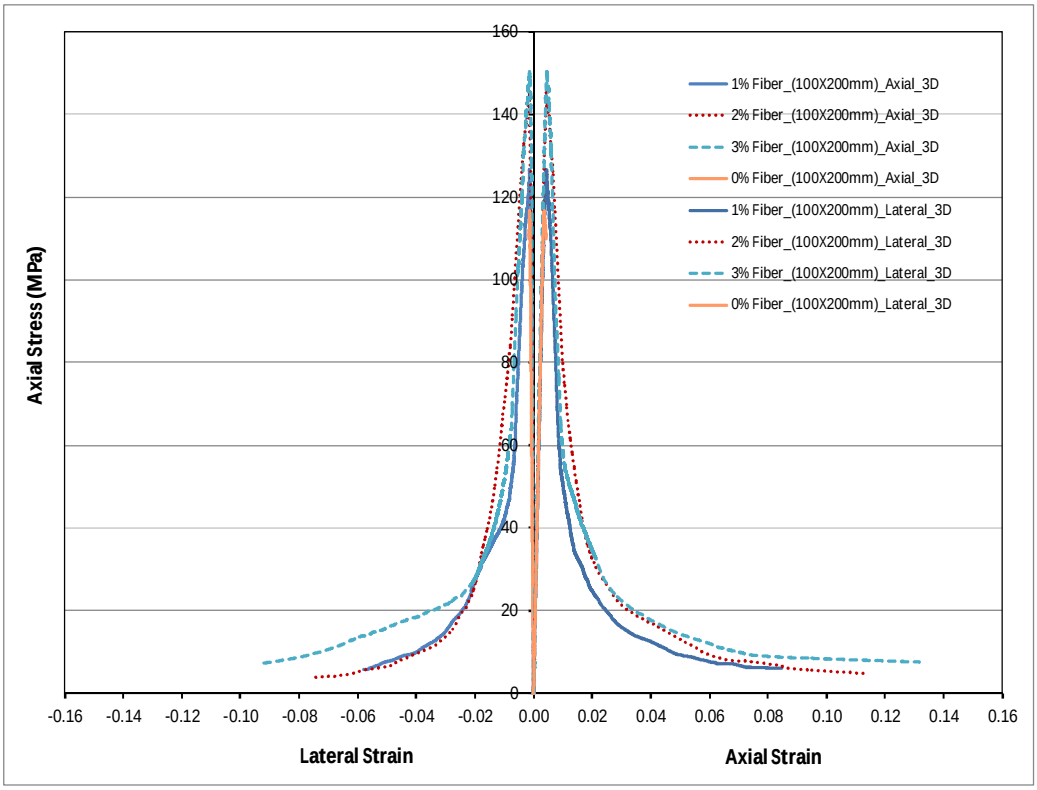

Fig.5.17 Axial and lateral stress-strain response of 3D fiber with different amount

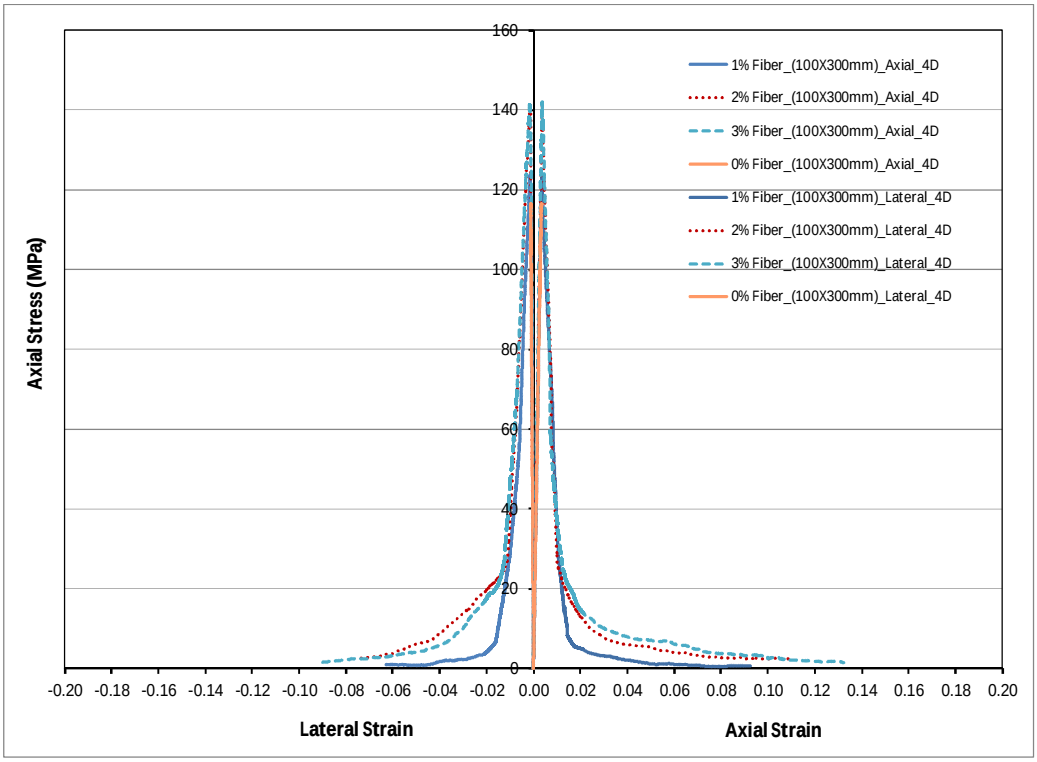

Fig.5.18 Axial and lateral Stress-strain response of 4D fiber with different amount

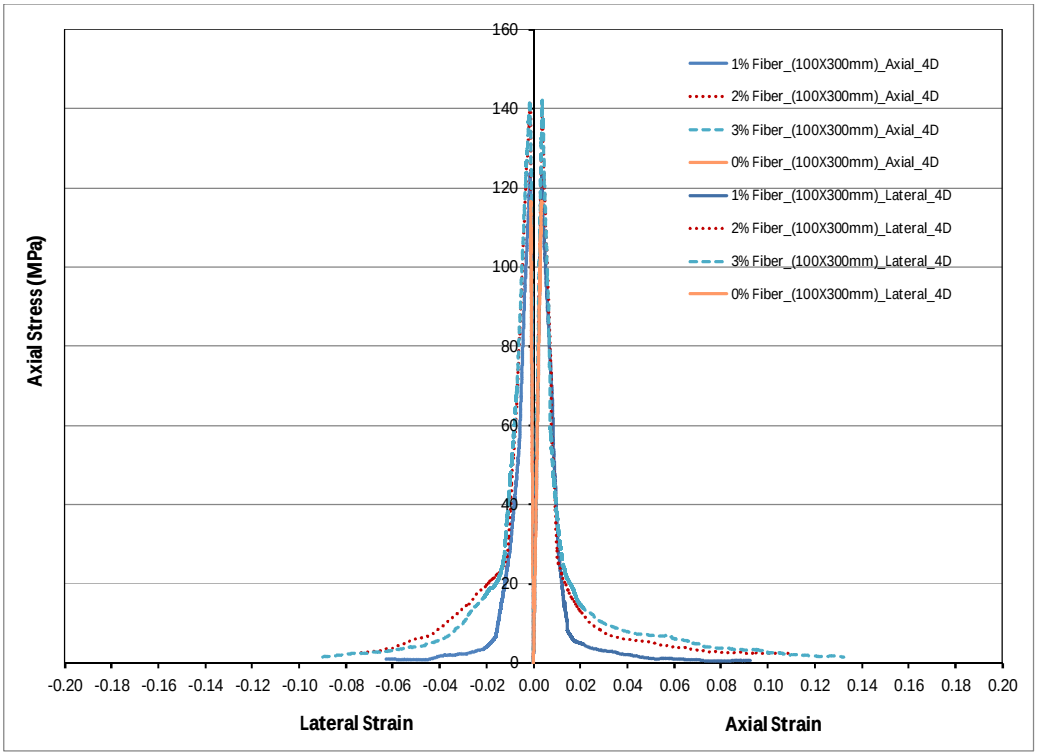

Fig.5.19 Axial and lateral Stress-strain response of 4D fiber with different amount

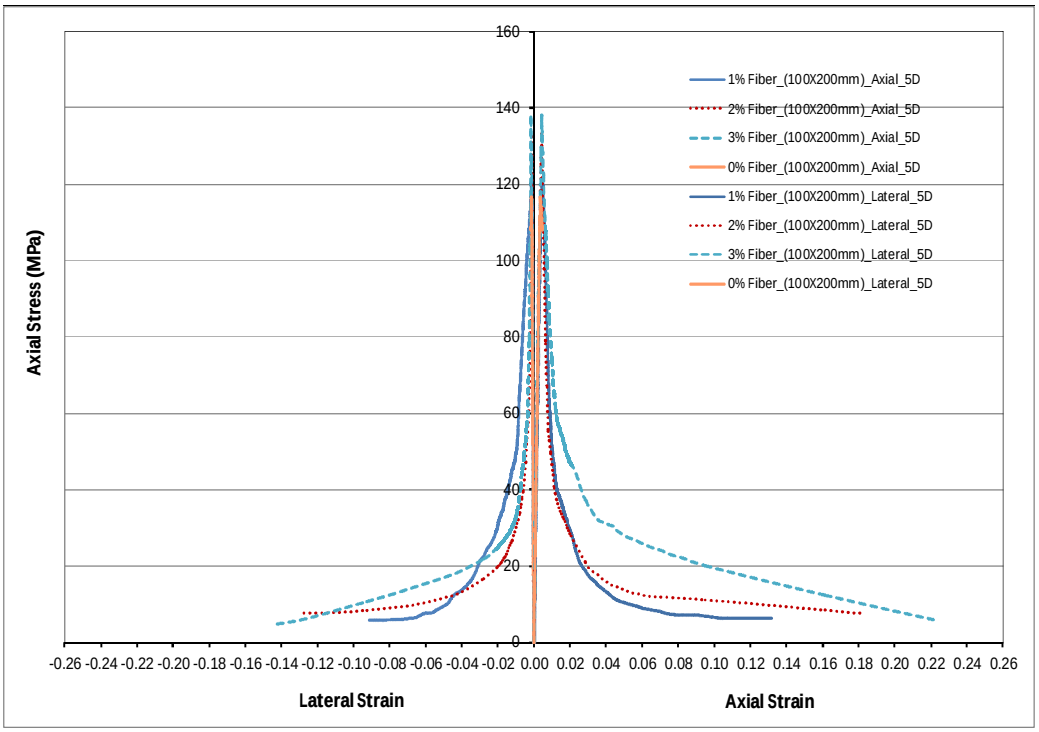

Fig.5.20 Axial and lateral Stress-strain response of 5D fiber with different amount

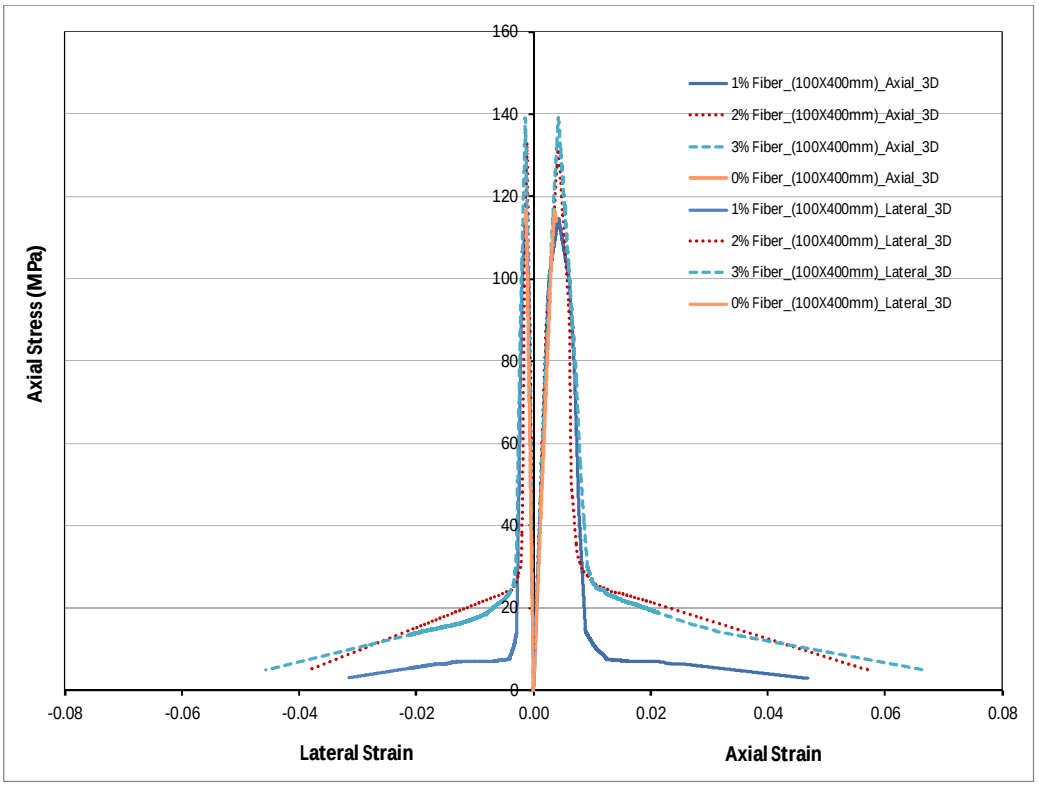

Fig.5.21 Axial and lateral Stress-strain response of 3D fiber with different amount

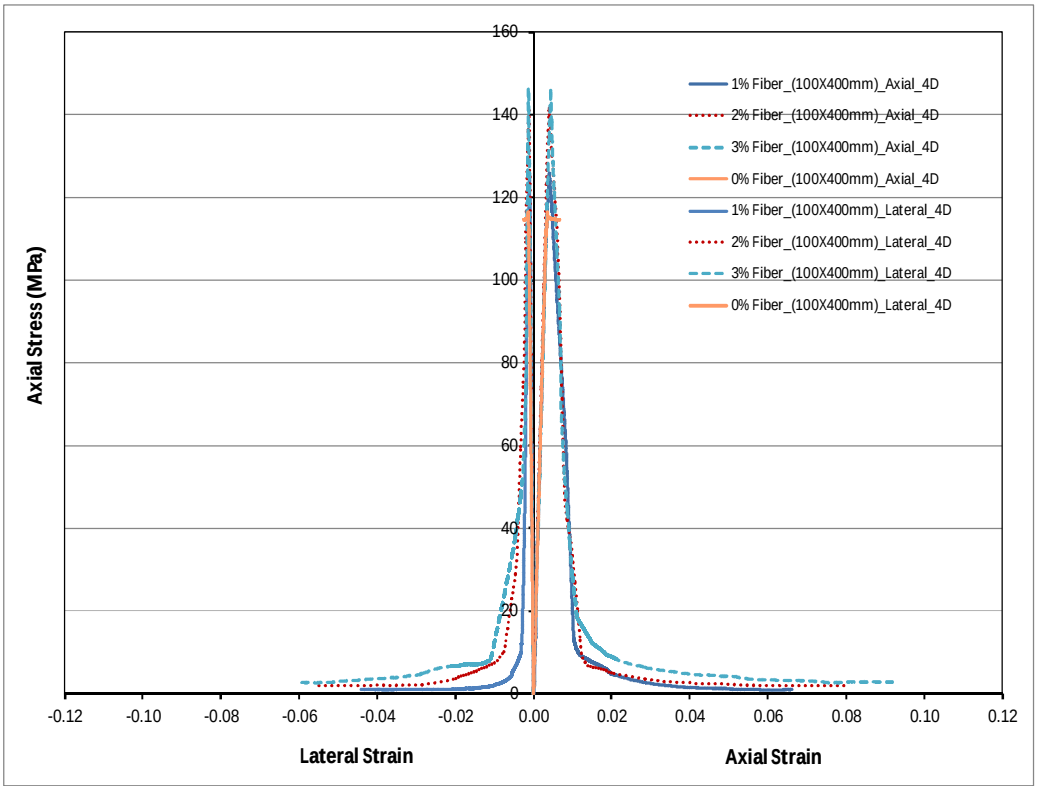

Fig.5.22 Axial and lateral Stress-strain response of 4D fiber with different amount

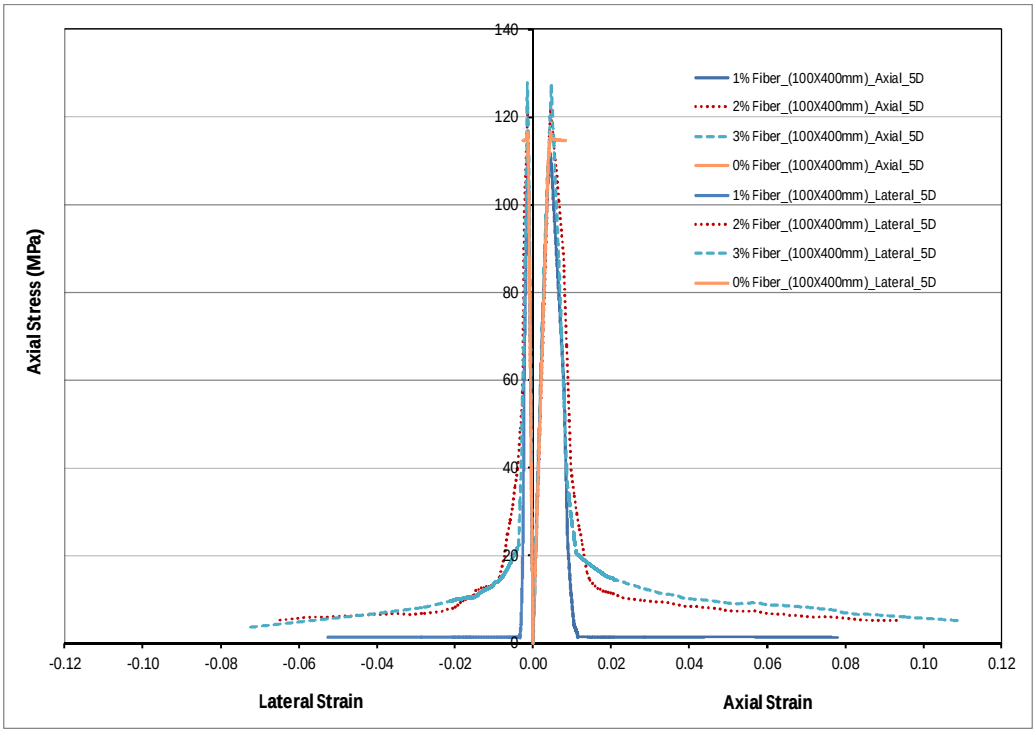

Fig.5.23 Axial and lateral Stress-strain response of 5D fiber with different amount

The specimens with 0% fiber mixture observed brittle behaviour for all types of fibers with a sudden drop in the load-carrying capacity of at a peak strain of 0.43%. Similar finding also reported by Kazemi and Lubell (2012) with 0% fiber content specimen. Conversely the specimens containing fibres exhibited ductile post-peak responses in both axial and lateral behaviours. This ductility occurs because the steel fibers partially restrained the lateral expansion and prevent uncontrolled sliding along inclined sliding planes allowing for larger axial deformations. It is seen from the Fig.5.17 to Fig.5.23 that slope of the ascending branch appears to be similar nature and linear for all types of fibers amount and types, but the slope of the post-peak softening branch decreases as fiber volume fraction increases, represents greater overall energy absorption capacity (Kazemi & Lubell, 2012). It was observed that the lateral deformation is on average 58-78% smaller than then axial deformation for different fiber type and amount the entire UHPFRC specimens.

5.3.3.1 Influence of specimen size on axial response of UHPFRC in compression

To show the influence of specimen size on the ductility of UHPFRC the compressive axial stress-strain responses of 100x200mm, 100x300 and 100x400 prisms and cylinder of test series 1 to 4 with fiber volume fractions of 0, 1, 2 and 3% as presented in Table 5.6 are shown in Fig.5.24 to Fig.5.34 for different types of fiber. A laboratory test program was conducted at the University of Adelaide to determine ductility responses of UHPFRC including size effects. Each curve represents the average of three specimens corresponding to a different specimen size, fibre type or fibre content. Again the raw data has been processed by removing any bedding down at the beginning of the test. The axial contraction measured platen to platen by the four LVDT's at four corner of the loading platform. Then, the average of values of four curves is then taken as the overall deformation for the given test specimen.

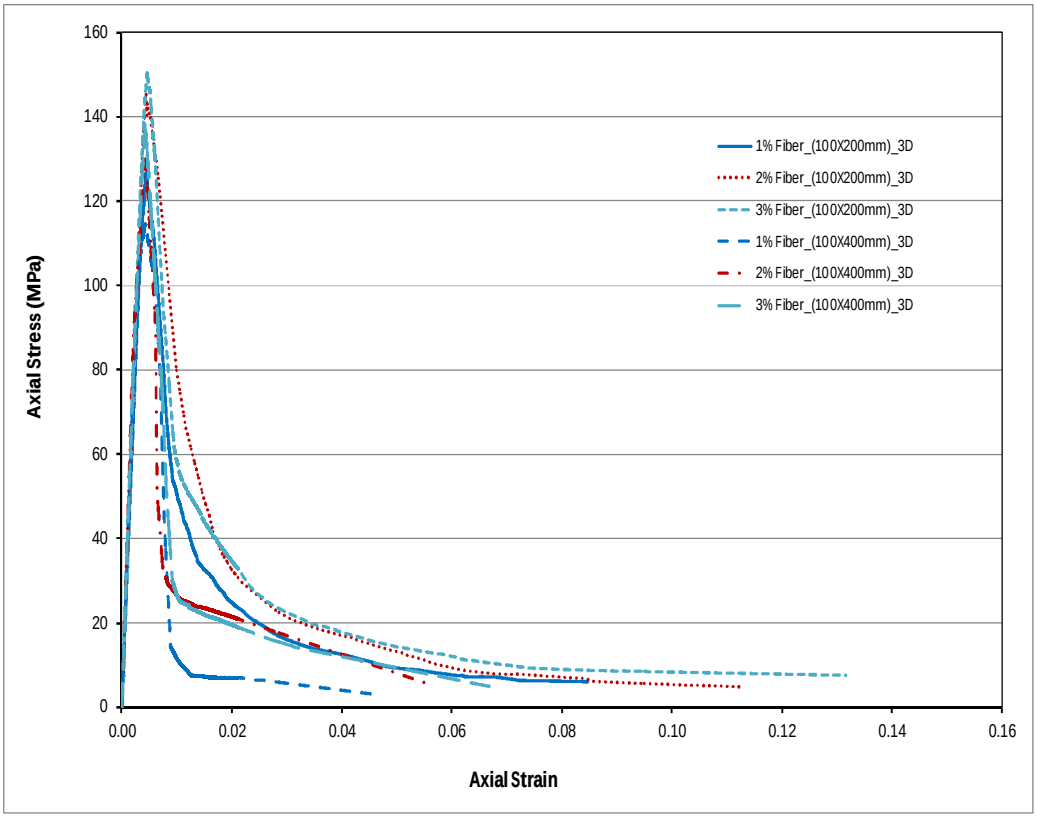

Fig.5.24 Influence of size on axial stress-strain response of 3D fiber with different fiber amount

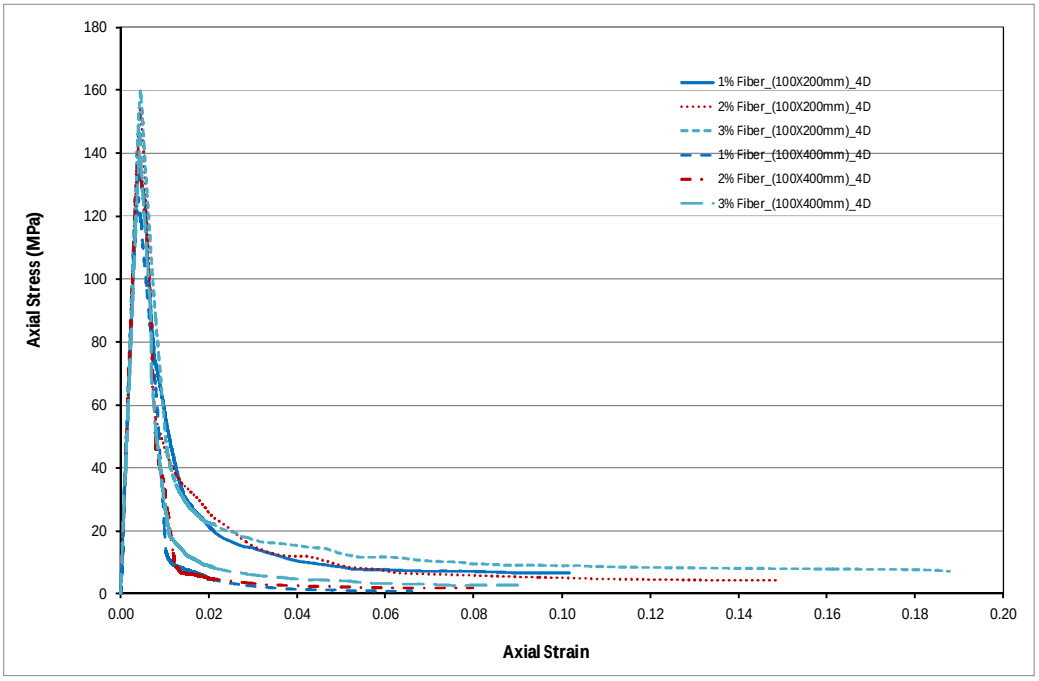

Fig.5. 25 Influence of size on axial stress-strain response of 4D fiber with different amount

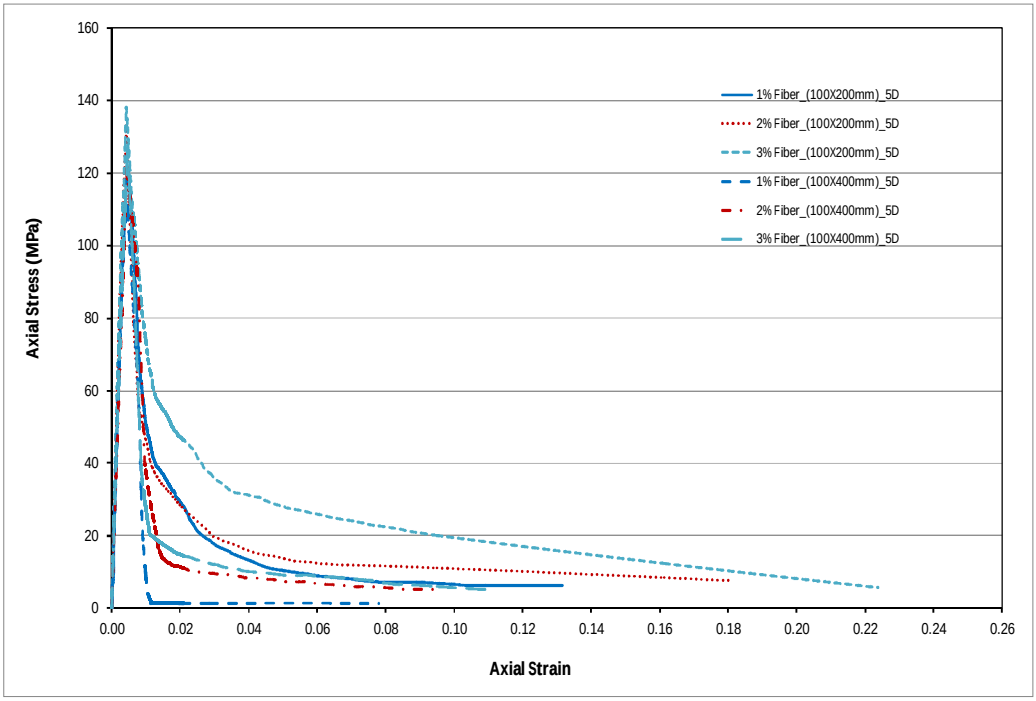

Fig.5.26 Influence of size on axial stress-strain response of 5D fiber with different amount

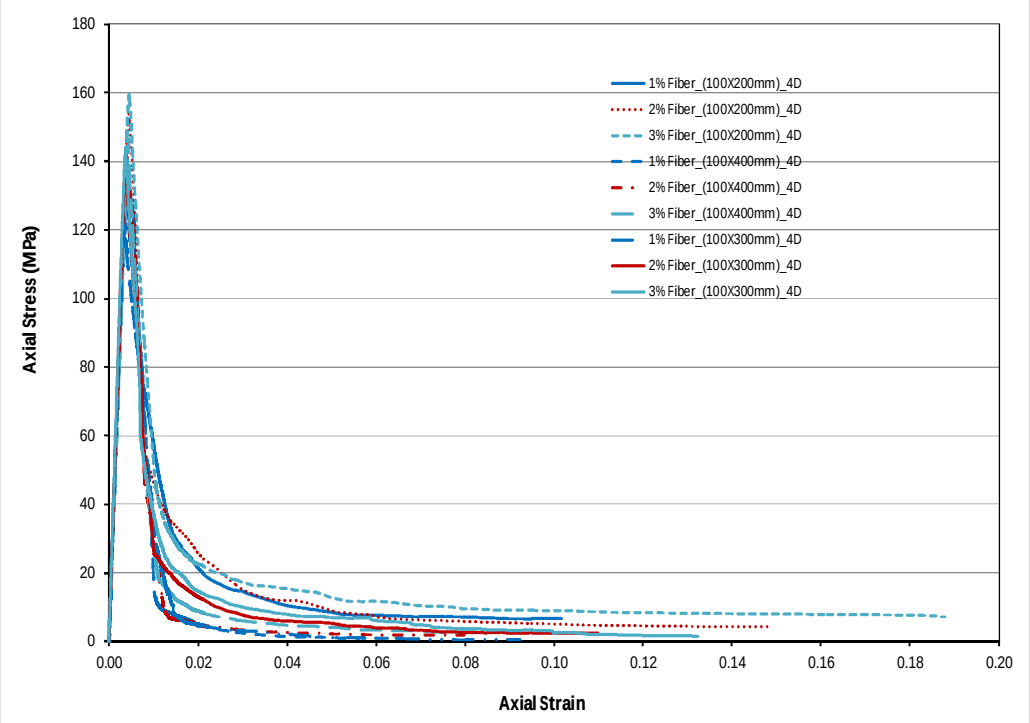

Fig.5.27 Influence of size on axial stress-strain response of 4D fiber with different amount

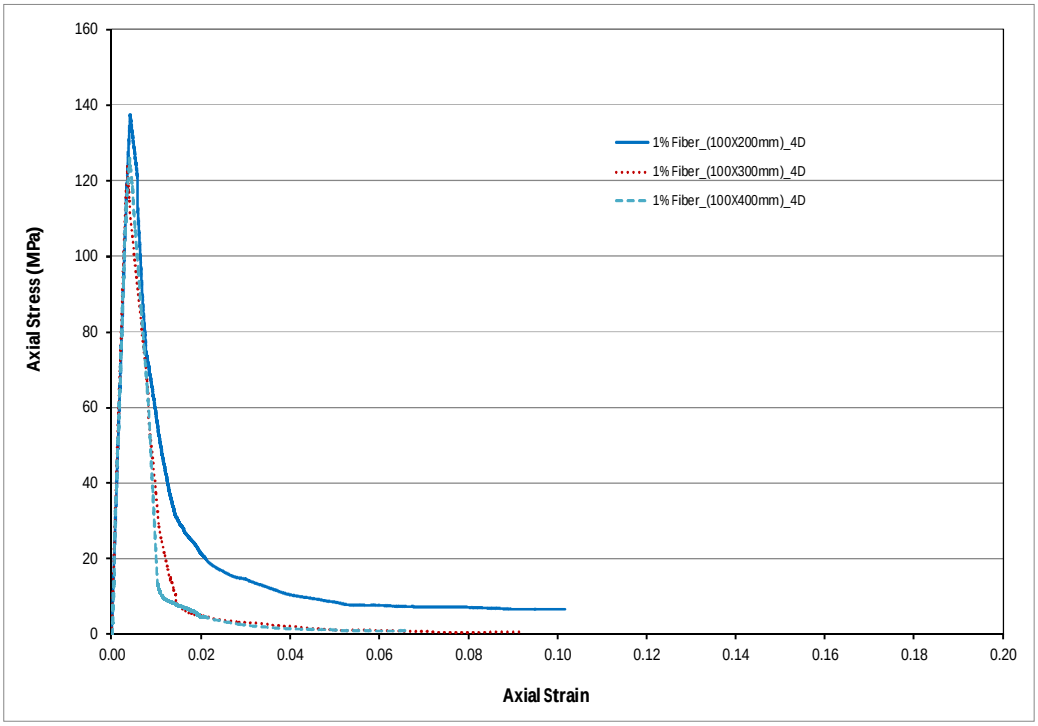

Fig.5.28 Influence of size on axial stress-strain response of 4D fiber with 1% fiber content

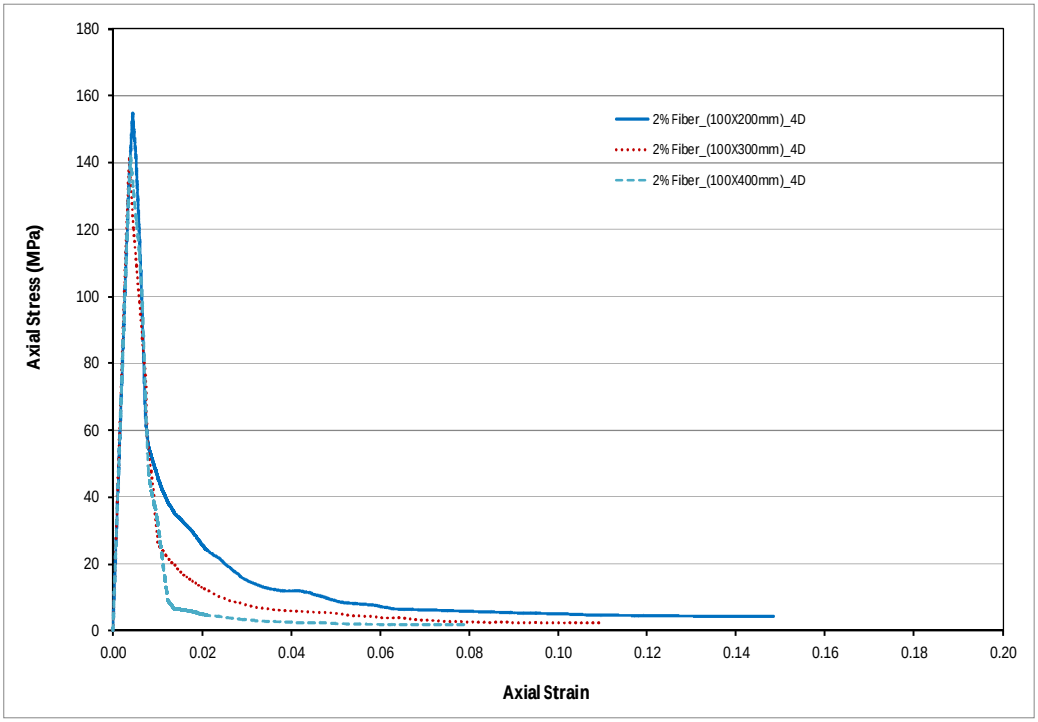

Fig.5.29 Influence of size on axial stress-strain response of 4D fiber with 2% fiber content

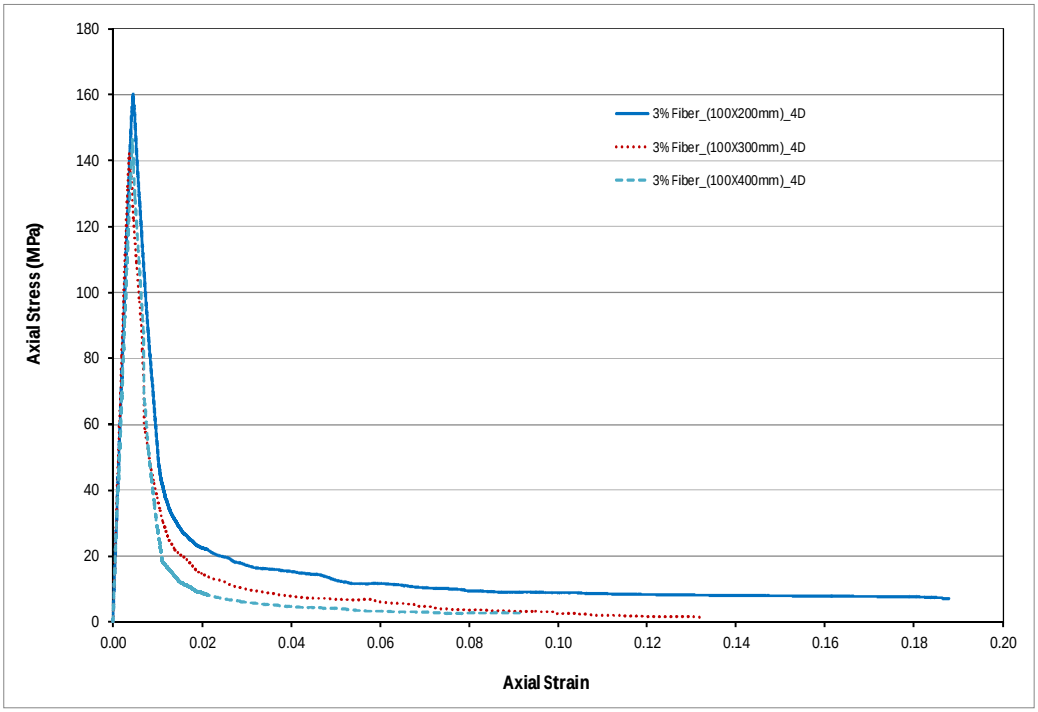

Fig.5.30 Influence of size on axial stress-strain response of 4D fiber with 3% fiber content

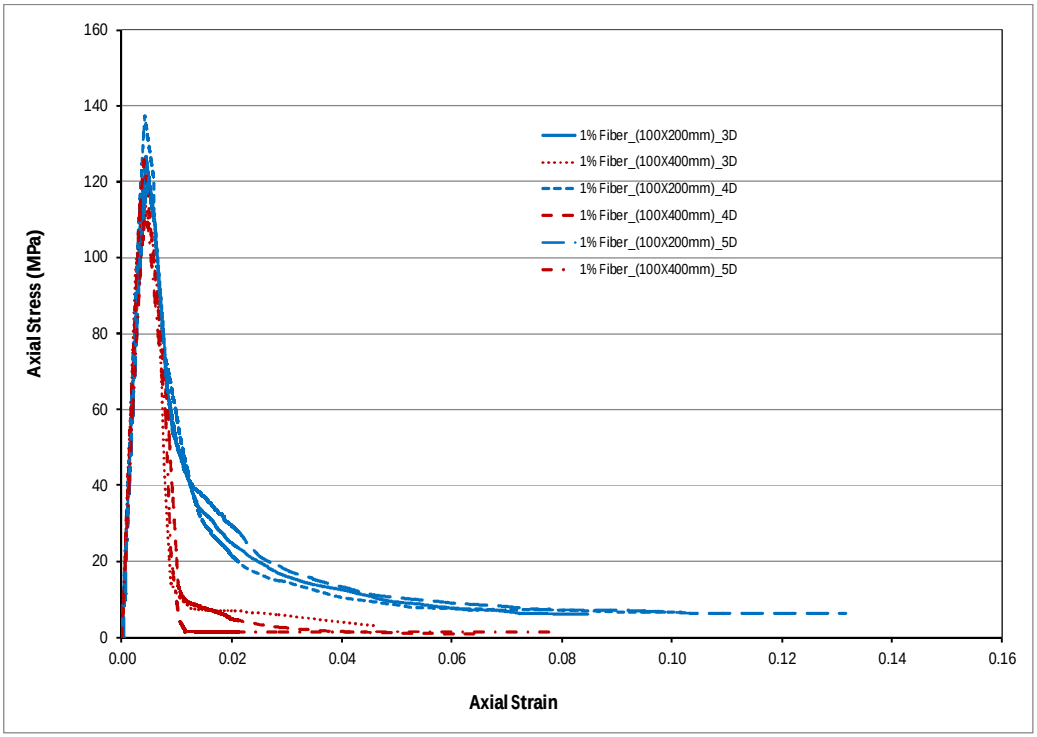

Fig.5.31 Influence of size on axial stress-strain response of different fiber with 1% fiber content

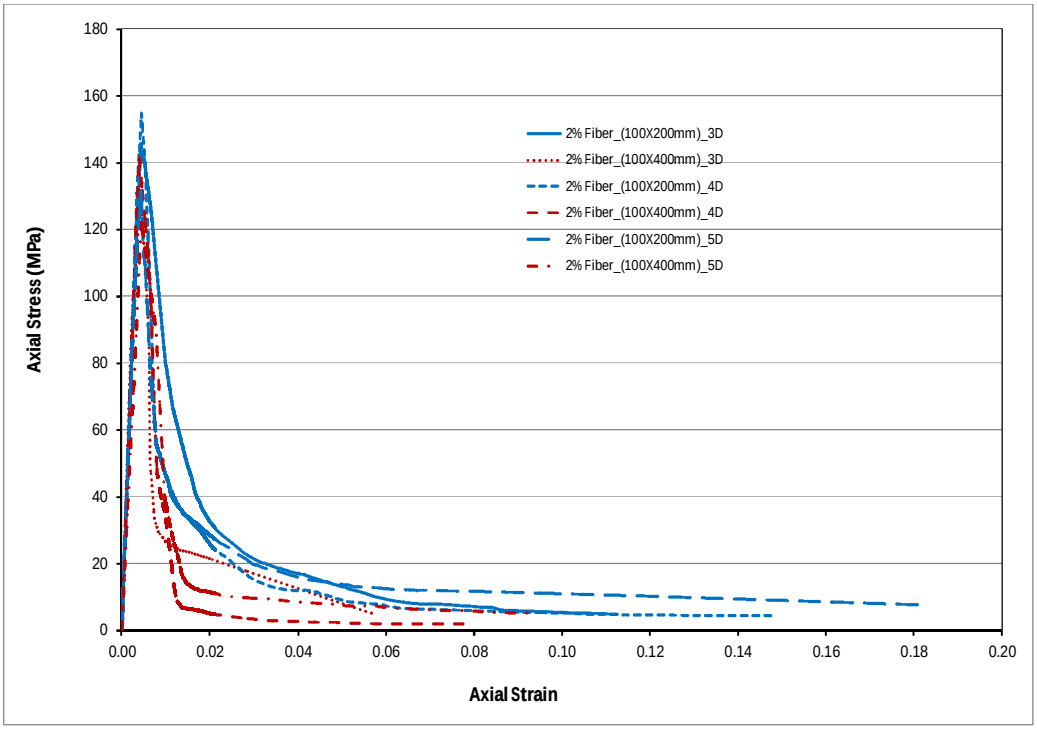

Fig.5.32 Influence of size on axial stress-strain response of different fiber with 2% fiber content

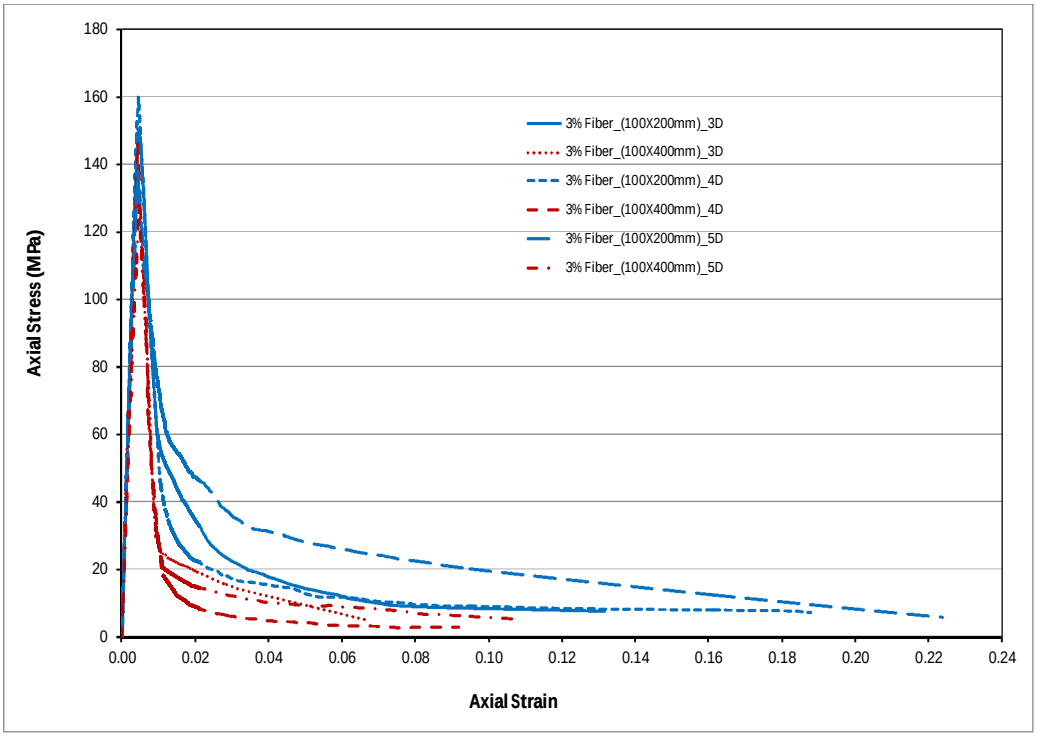

Fig.5.33 Influence of size on axial stress-strain response of different fiber with 3% fiber content

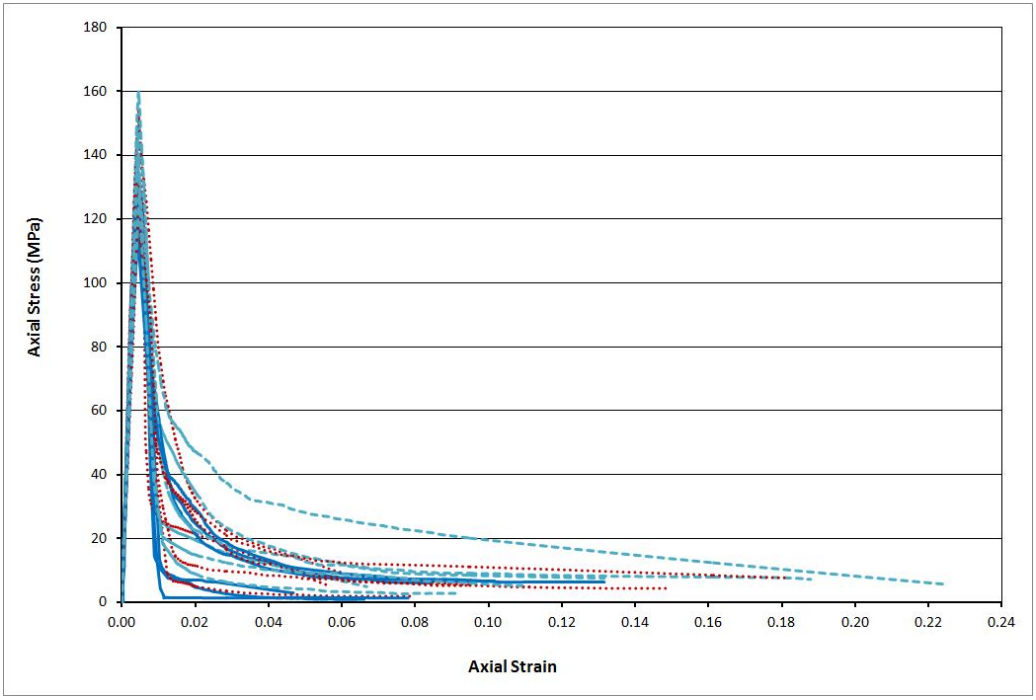

Fig.5.34 Influence of size on axial stress-strain response of different fiber and content

The influence of axial size effects of UHPFRC as shown in Fig.5.24 to Fig.5.34 is crucial for extrapolation of test results from laboratory specimen to the real structural engineering members. It is interesting to mention from all of the Figures that an increasing the size or increase the slenderness of the specimens, the UHPFRC shows a snap back or more brittle nature and the axial size effect is clearly apparent from Figures 5.24 to 5.27. The axial size effects of the specimens are observed in terms of peak strength and ductility responses with the variation of fiber types and amount.

It is also seen from Figures 5.28 to 5.33 that the peak strength decreases as the specimen size or slenderness of the specimen increases. The mix with fiber volume-fraction 1 and 3%, a 9.55% and 7.47% decrease at the peak compressive strength was observed when doubling the specimen size for 3D fiber, 8.36% and 8.57% decreased peak strength for 4D fiber and 7.58% and 7.45% decreased the peak for 5D fibers.

Lubell and A.S. (2011) found that compressive strength decreased up to 9.8% for 3% fiber content specimen when the size make doubled. It is also clearly observed that reduction of strain due to size effect is significantly affecting the UHPFRC specimens. The specimen with slenderness (*l/d =2*) exhibits an ultimate strain of more than double that of the specimen with slenderness (*l/d =4*).

Significantly the specimen shape does not affect the compressive strength and strain observed from the test results and thus the results of a cylinder test are applicable for application to any shape members. As an indication of the magnitude of the size-effect in Fig.5.34 represents the comparison of size effect for all of the specimens with different fiber types and amount.

5.3.3.2 Influence of size effect on lateral response of UHPFRC in compression

The compressive lateral stress-strain responses of 100x200mm, 100x300 and 100x400 UHPFRC prisms and cylinder specimens of test series 1 to 4 with fiber volume fractions of 0, 1, 2, and 3% as presented in Table 5.6 are illustrated in Fig. 5.35 to Fig.5.45 for 3D, 4D and 5D fibers. Each curve represents the average of three corresponding specimens. In each test the lateral dilation was measured by three LVDT's at mid height around the diameter of the specimen. The average of values of three curves is the initial curve for each specimen. The similar finding of axial size effect is observed in lateral size effect for UHPFRC specimen. It worth mention that the increasing the size of the specimens, the UHPFRC exhibit brittle nature after post-peak stage. The more clear size effect in terms of peak strength and ductility behaviour is observed in Fig.5.38 due to one more size considered for 4D fibers. The peak strength decreases as the specimen size or slenderness of the specimen increases as follows the similar trend of axial size effect ductility responses of specimens. The overall comparison of lateral size effect is shown in Fig.5.45.

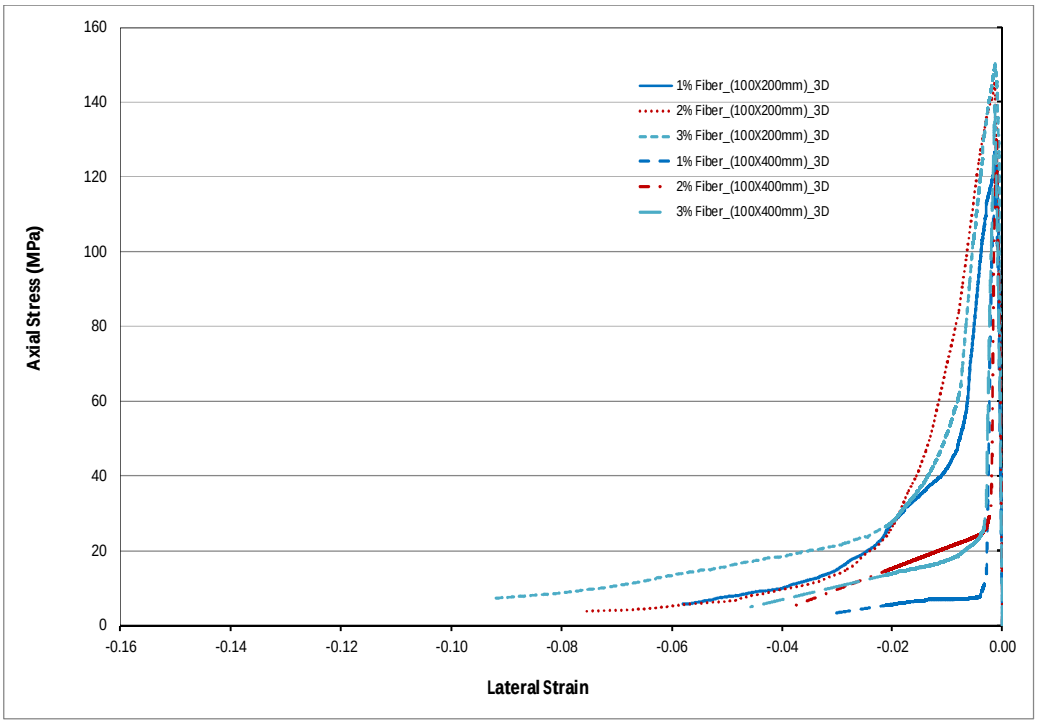

Fig.5.35 Influence of size on axial stress-strain response of 3D fiber with different amount

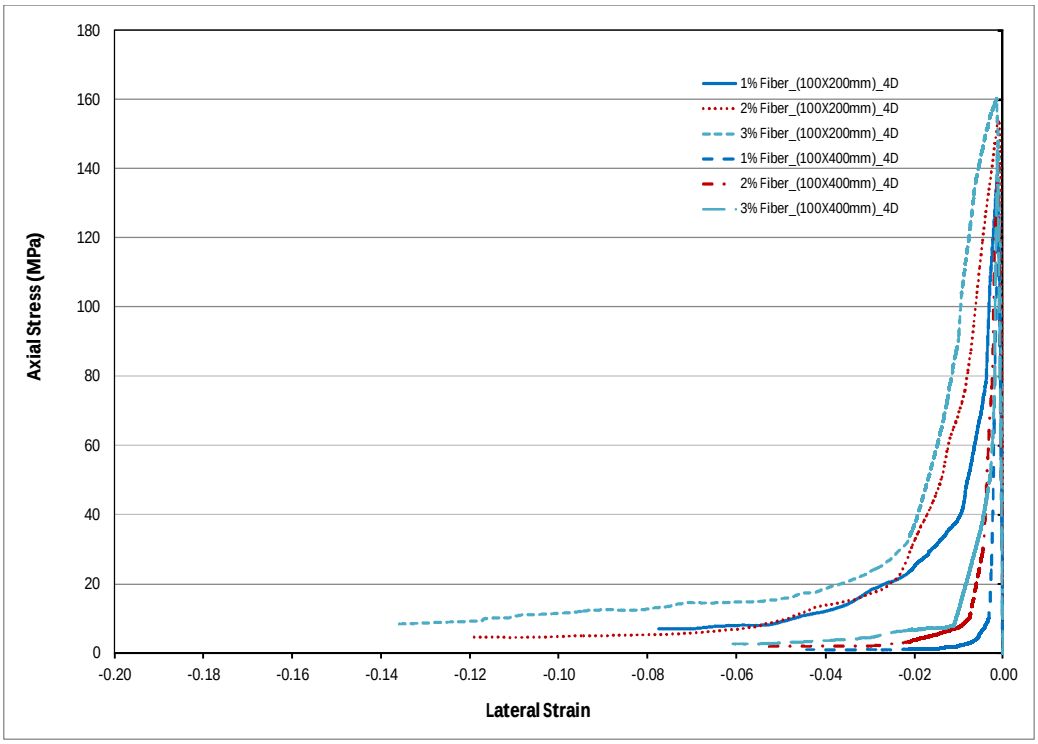

Fig.5.36 Influence of size on axial stress-strain response of 4D fiber with different amount

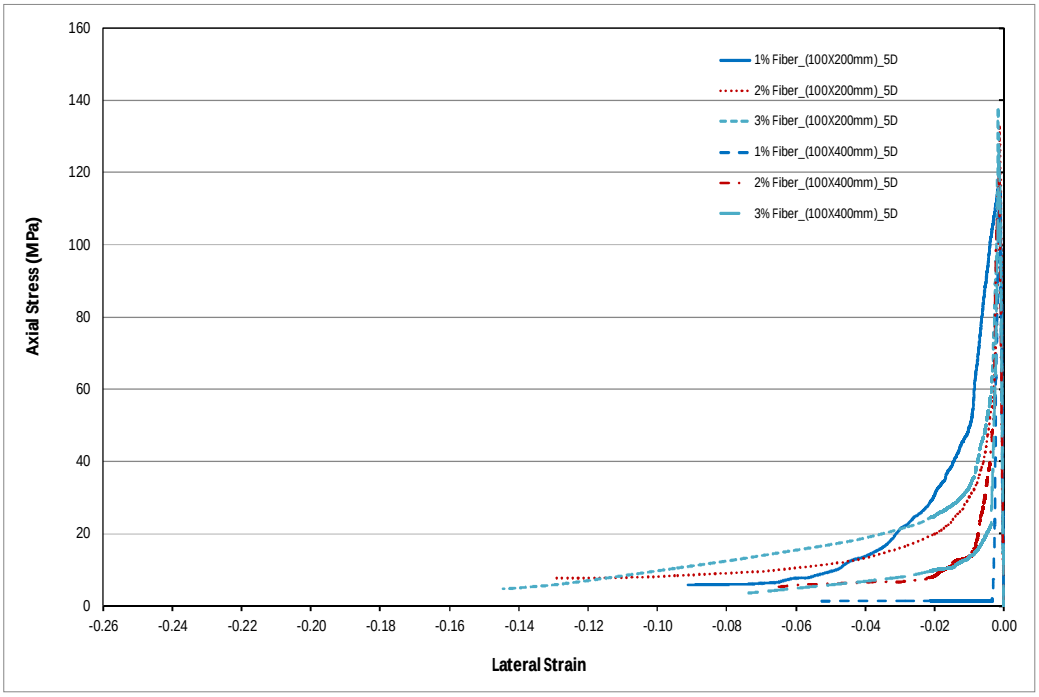

Fig.5.37 Influence of size on axial stress-strain response of 5D fiber with different amount

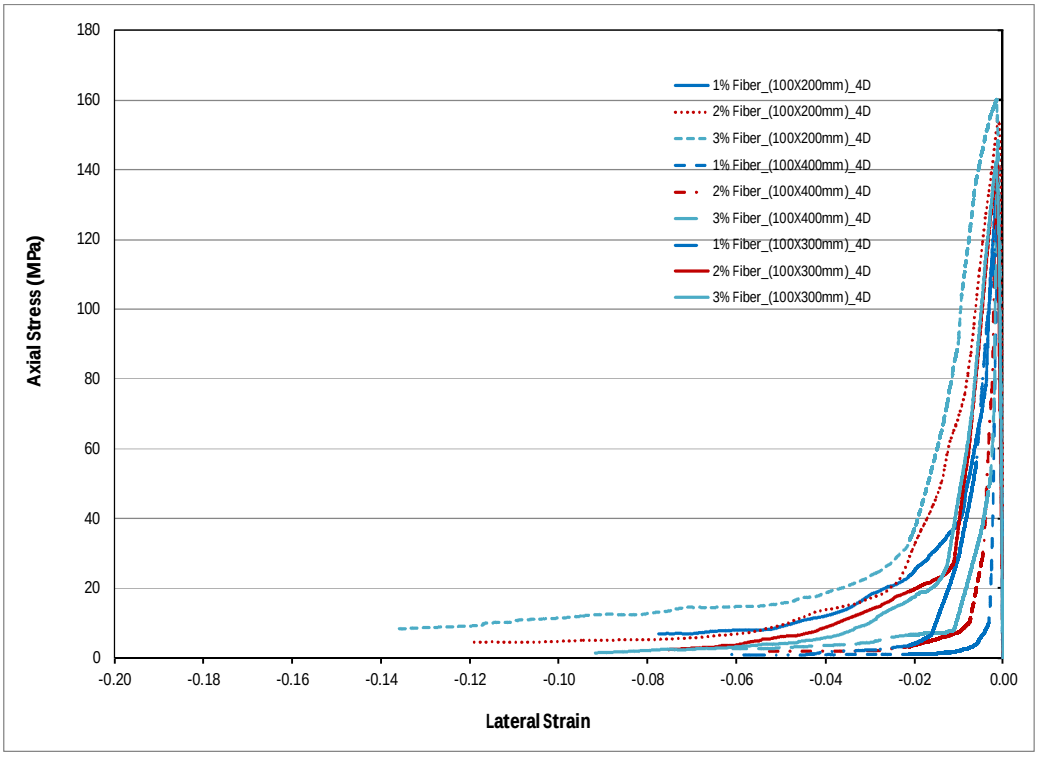

Fig.5.38 Influence of size on axial stress-strain response of 4D fiber with different amount

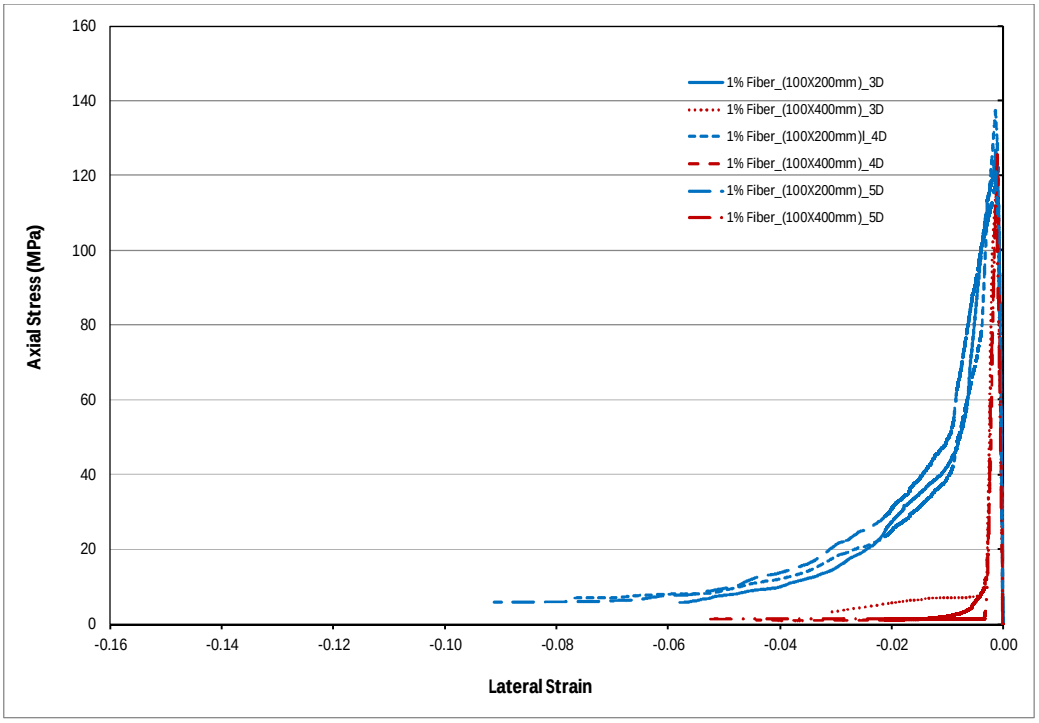

Fig.5.39 Influence of size on lateral stress-strain response of different fiber with 1% fiber content

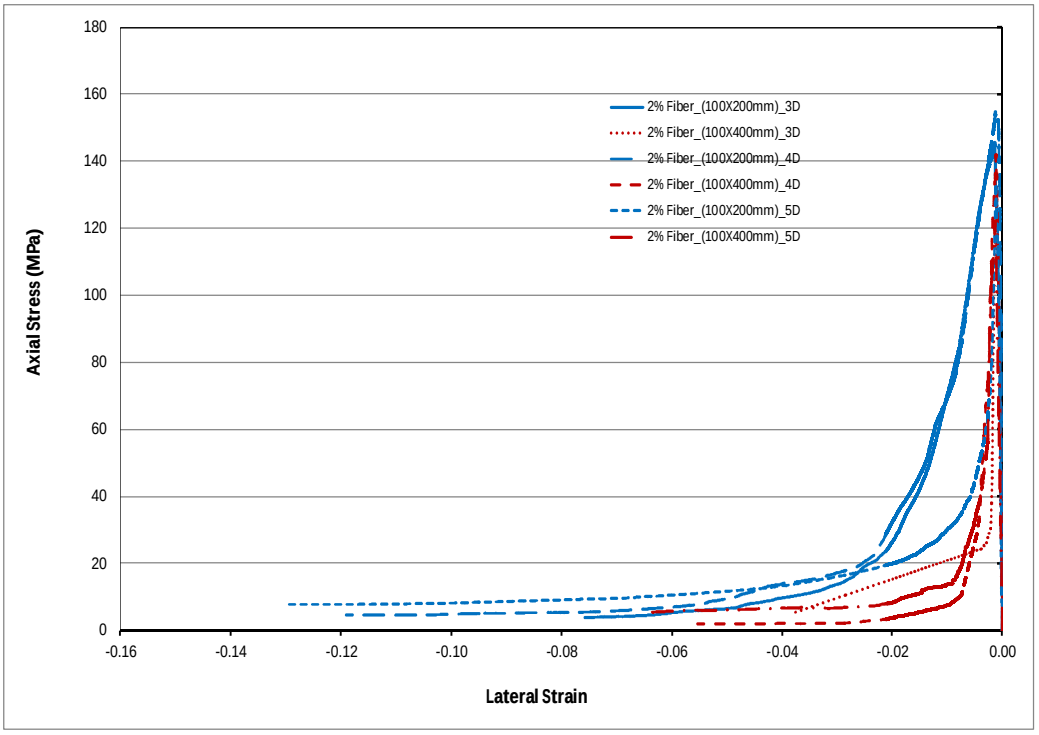

Fig.5.40 Influence of size on lateral stress-strain response of different fiber with 2% fiber content

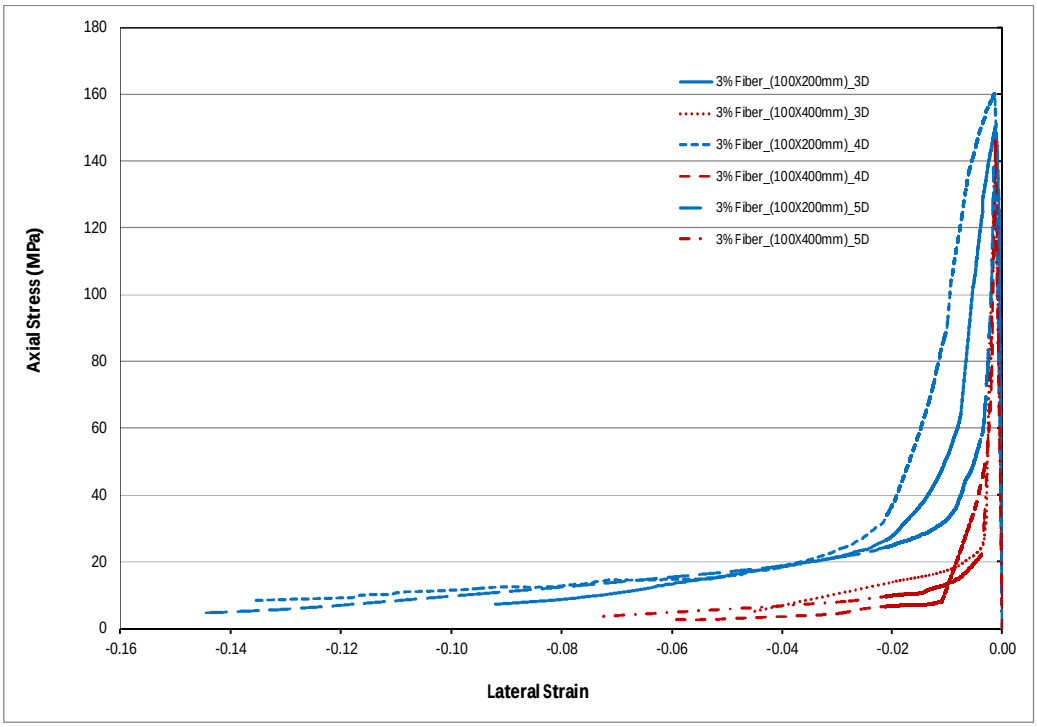

Fig.5.41 Influence of size on lateral stress-strain response of different fiber with 3% fiber content

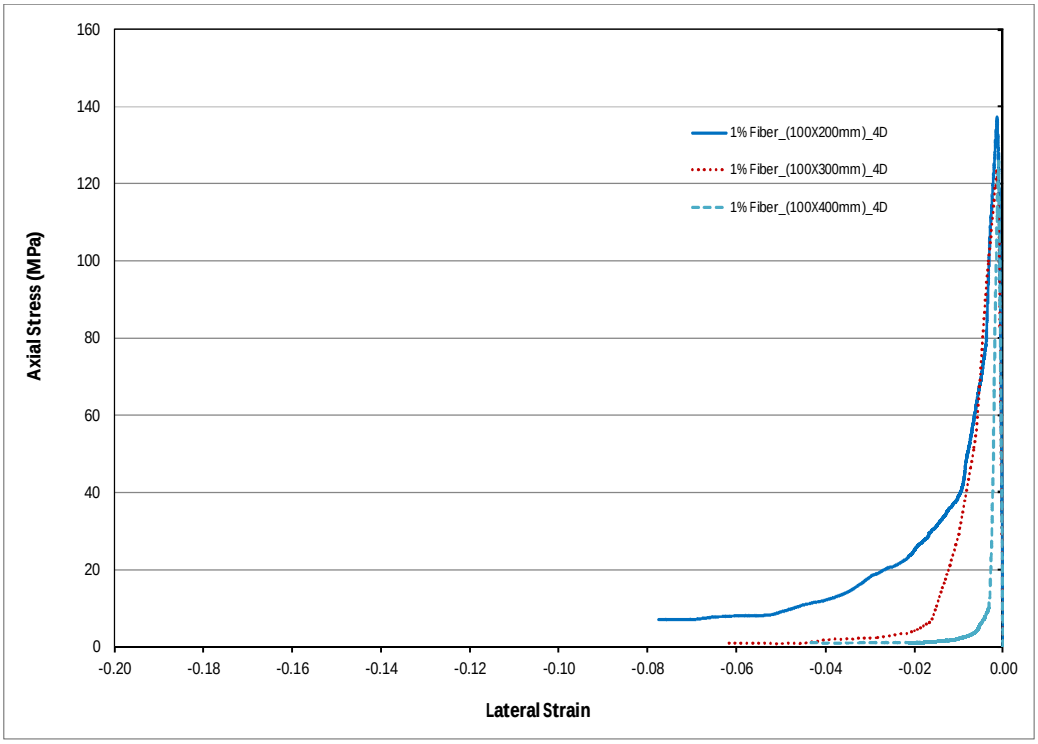

Fig.5.42 Influence of size on lateral stress-strain response of 4D fiber with 1% fiber content

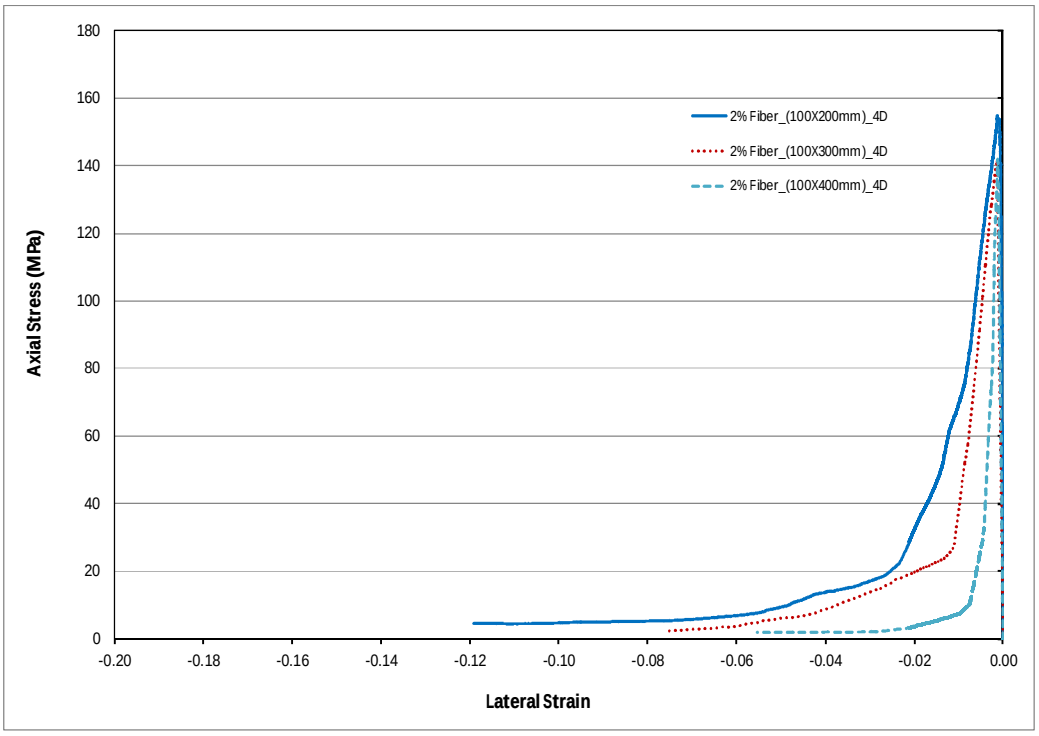

Fig.5.43 Influence of size on lateral stress-strain response of 4D fiber with 2% fiber content

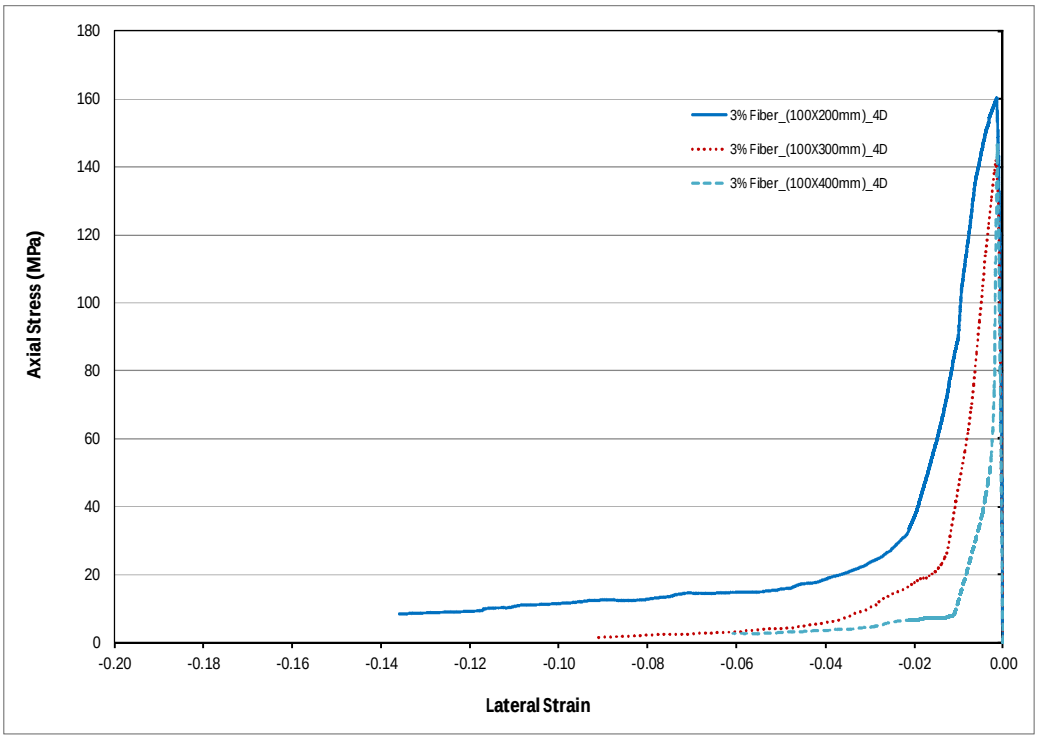

Fig.5.44 Influence of size on lateral stress-strain response of 4D fiber with 3% fiber content

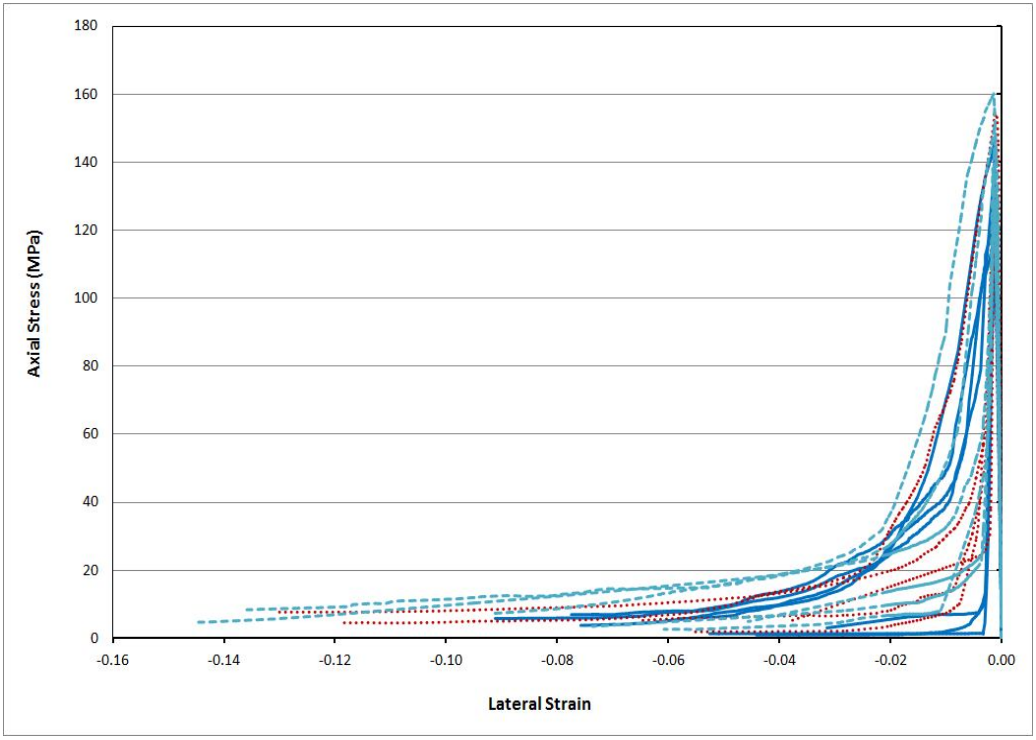

Fig.5.45 Influence of size on lateral stress-strain response of different fiber and content

5.3.3.3 Influence of fiber on axial response of UHPFRC in compression

The influence of fibers on compressive axial stress-strain responses of 100x200mm, and 100x400 UHPFRC prisms and cylinder specimens of test series 1 to 3 with fiber volume fractions of 0, 1, 2, and 3% as presented in Table 5.6 are shown in Fig.5.46 to Fig.5.53 for 3D, 4D and 5D fibers. Test program was carried out at the University of Adelaide to determine influence of fiber on ductility responses of UHPFRC. Each curve represents the average of three corresponding specimens curve those tested with different amount and type of fiber. The raw data has been analysed by ignoring bedding down that produce beginning of the test. The axial contraction was measured platen to platen distance by the four LVDT's at four corner of the loading platform. After that, the average of values of four axial curves is considered as the overall deformation for the given test of UHPFRC specimens.

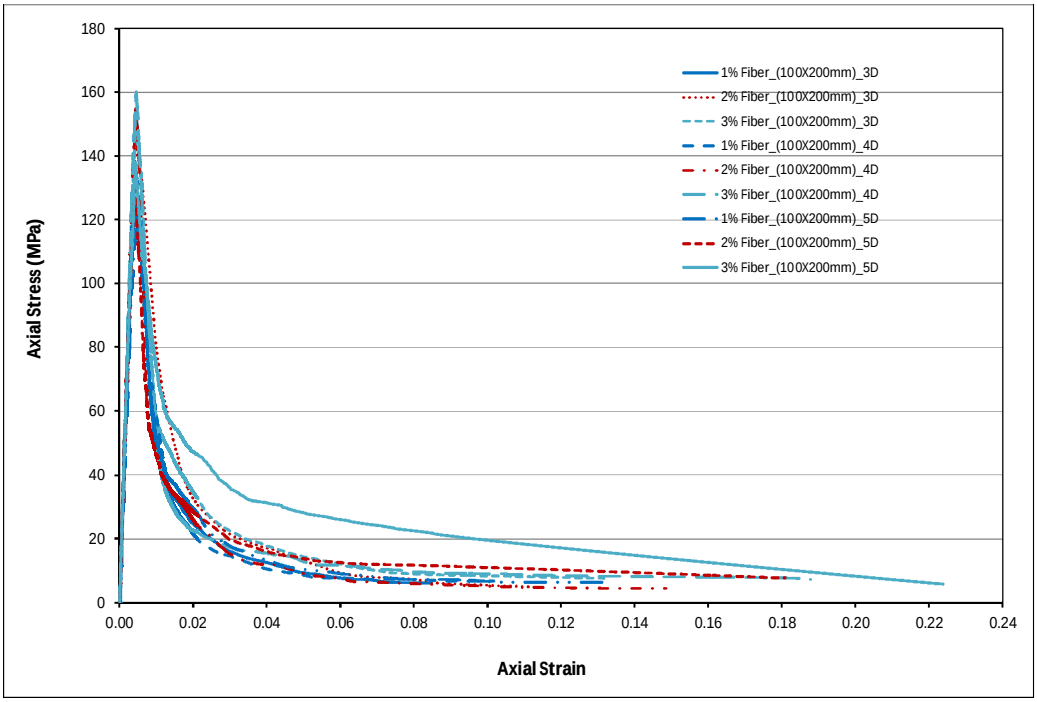

Fig.5.46 Influence of fiber on axial stress-strain response of 3D fiber with different content

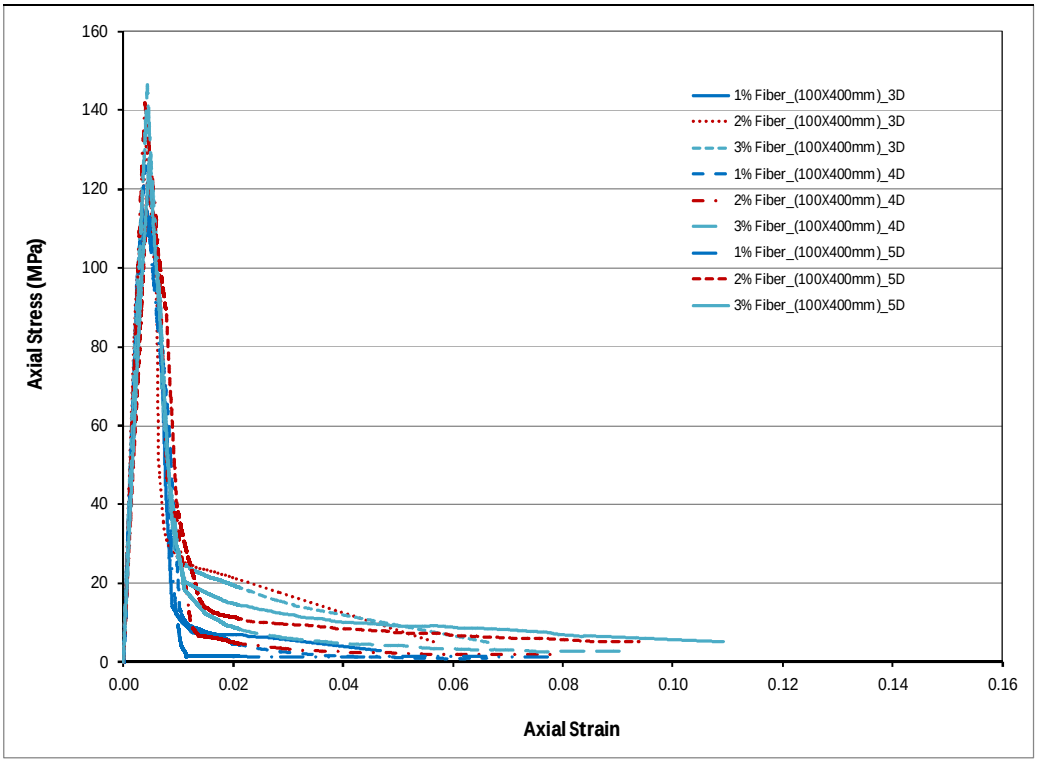

Fig.5.47 Influence of fiber on axial stress-strain response of 3D fiber with different content

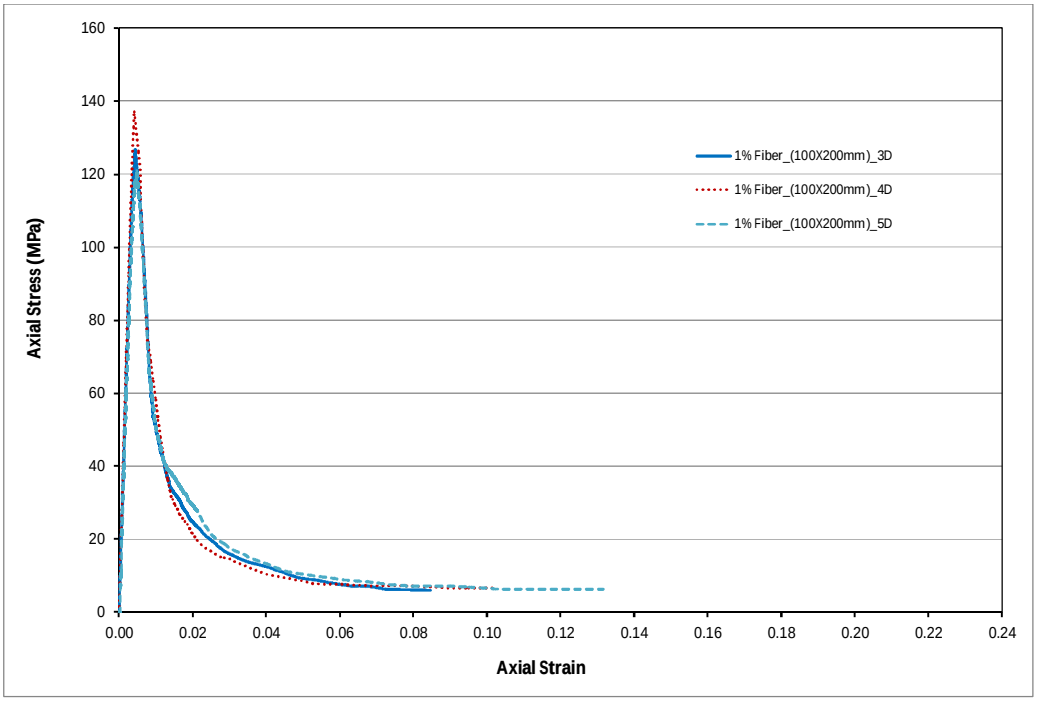

Fig.5.48 Influence of fiber on axial stress-strain response of different fiber with 1% fiber content

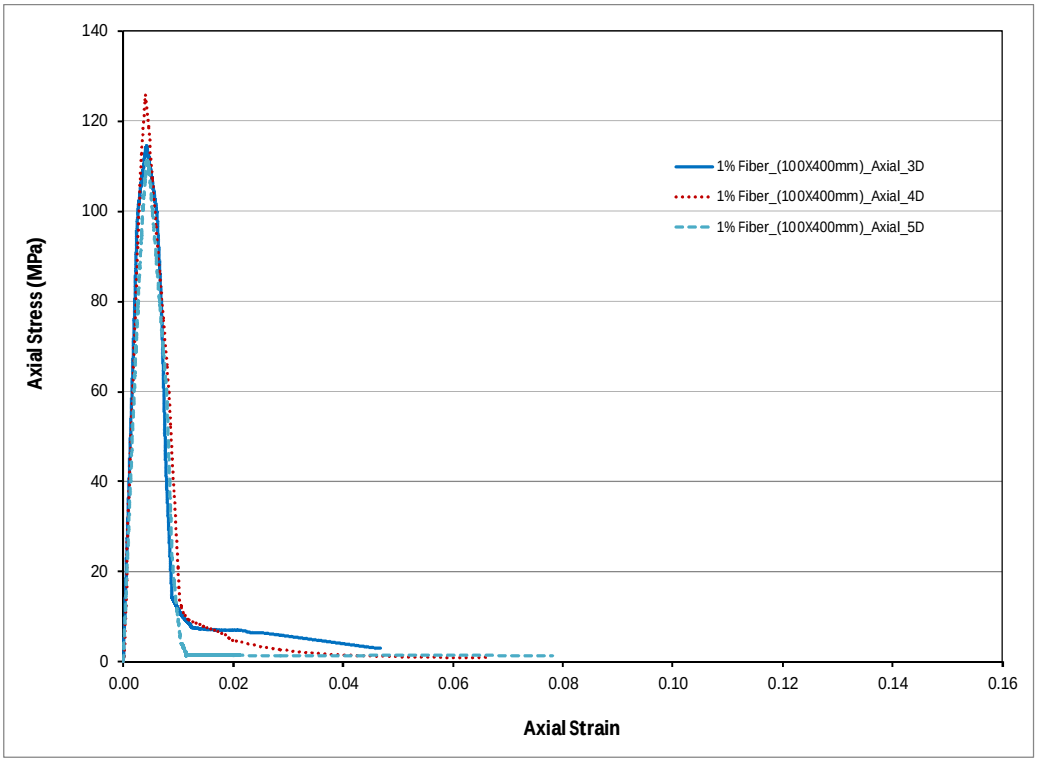

Fig.5.49 Influence of fiber on axial stress-strain response of different fiber with 1% fiber content

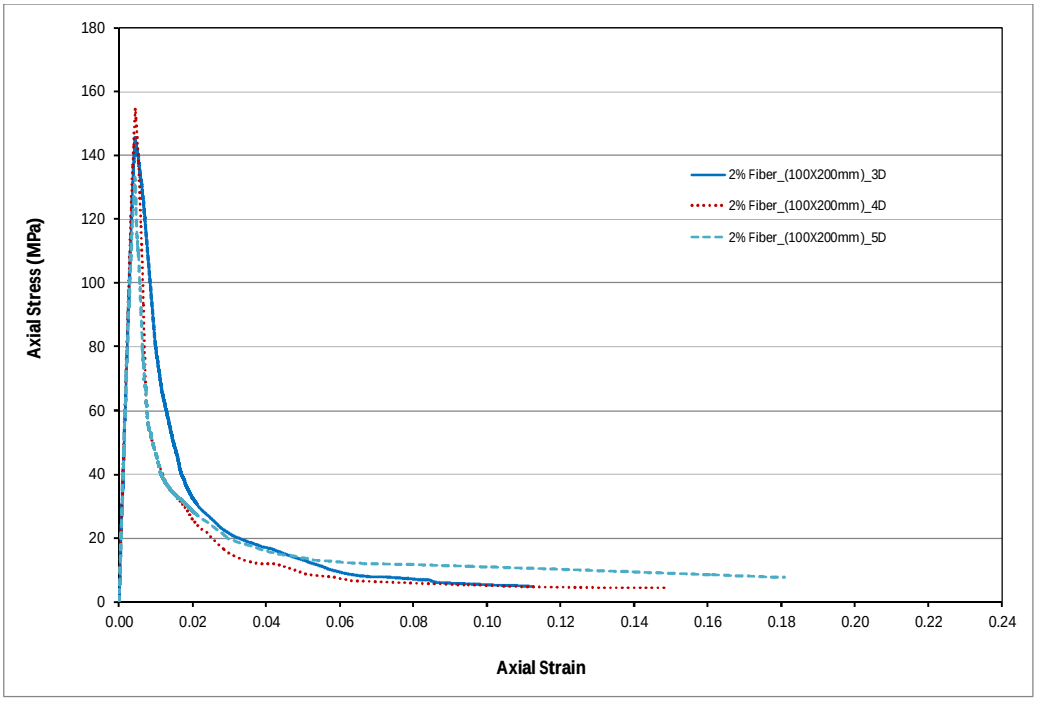

Fig.5.50 Influence of fiber on axial stress-strain response of different fiber with 2% fiber content

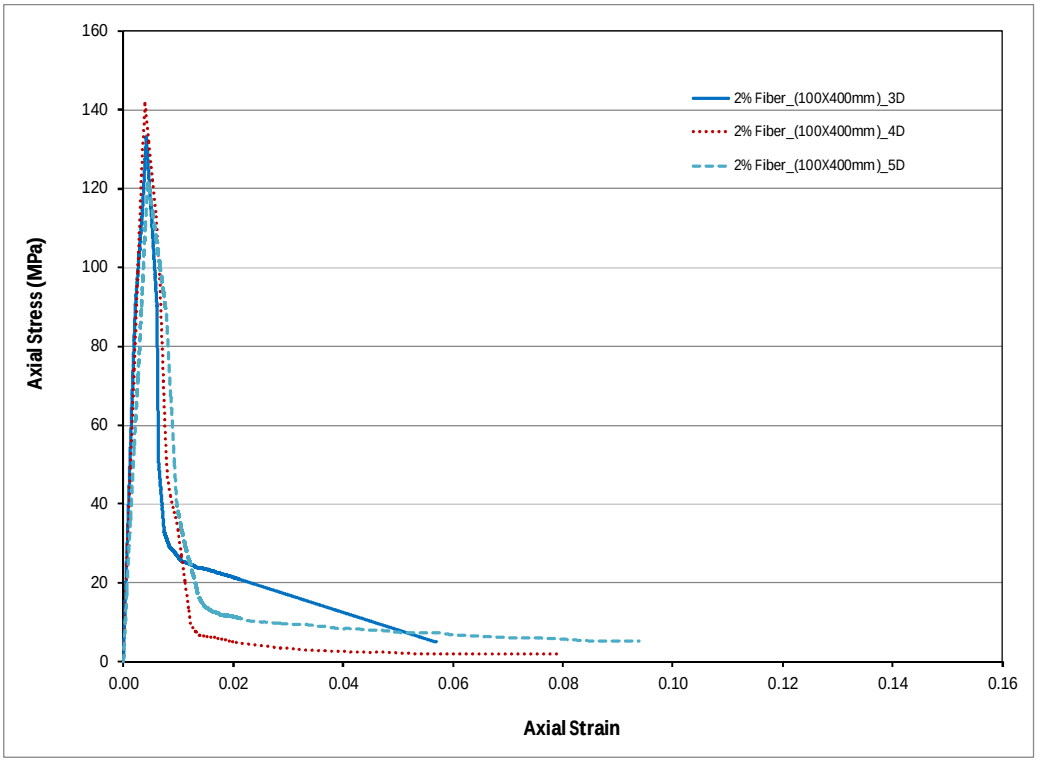

Fig.5.51 Influence of fiber on axial stress-strain response of different fiber with 2% fiber content

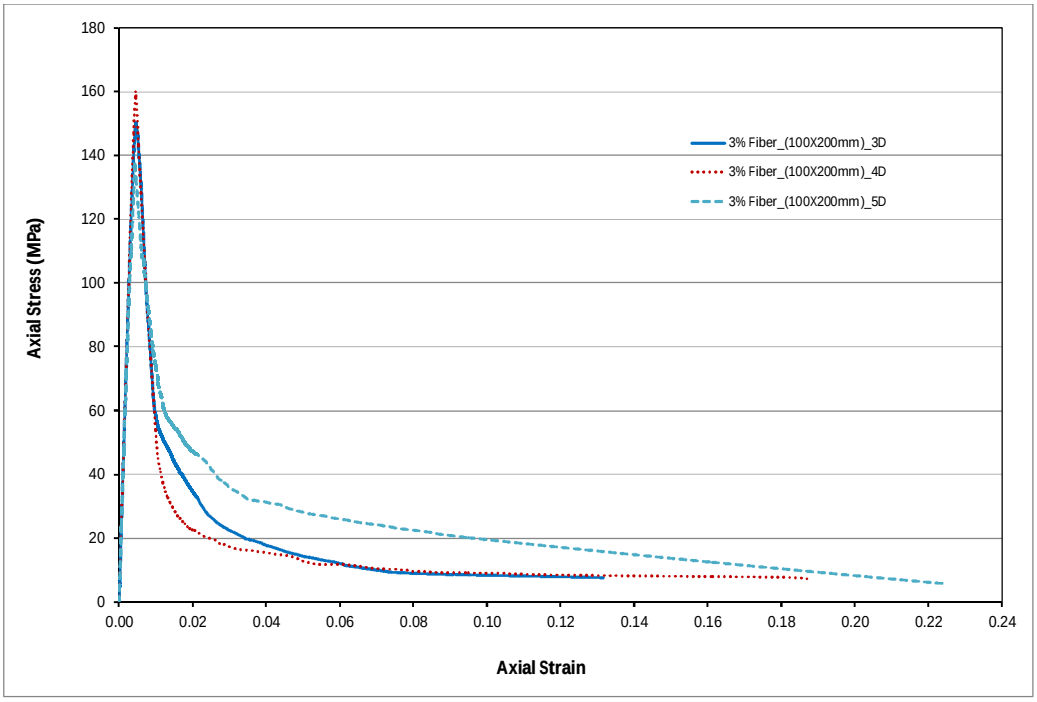

Fig.5.52 Influence of fiber on axial stress-strain response of different fiber with 3% fiber content

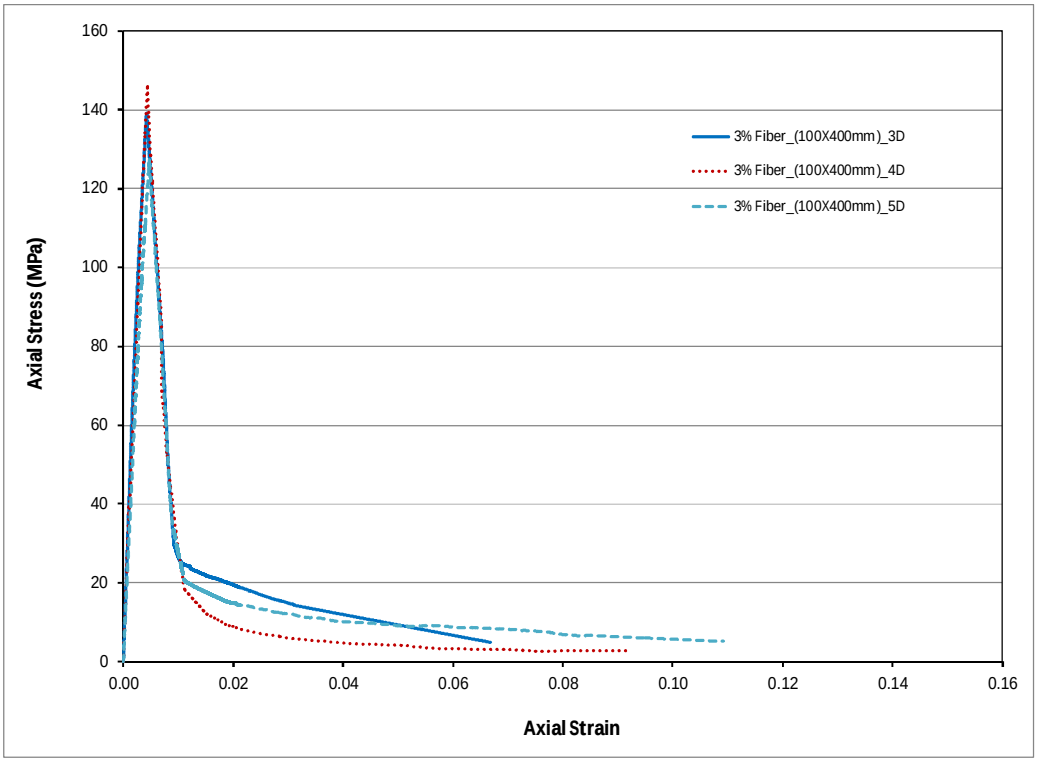

Fig.5.53 Influence of fiber on axial stress-strain response of different fiber with 3% fiber content

It is observed from Figures 5.46 and 5.47 that the amount of fiber content significantly affects the post-peak behaviour for all types of fiber specimen and the Figure 5.48 to Figure 5.53 represent clearly the fiber effect with same content but different type of fiber. Moreover, lowest fiber content exhibit lowest deformation observed at the descending branch and also higher fiber content shows large deformation by means of higher ductility response. It is also noticed that the longest fiber (5D) shows higher deformation than other two types of fibers, however it attain lower peak strength then other fibers. This suggests that there are less 5D fibres crossing a given crack due to the increased mass of an individual 5D fibre. The increase in strain can be attributed to the increased length and anchorage of the 5D fibres thus delaying failure and increasing axial strains.

5.3.3.4 Influence of fiber on lateral response of UHPFRC in compression

The influence of fiber on compressive lateral stress-strain responses of 100x200mm, and 100x400 UHPFRC prisms and cylinder specimens of test series 1 to 3 with fiber volume fractions of 0, 1, 2, and 3% as presented in Table 5.6 are shown in Fig.5.54 to Fig.5.61 for 3D, 4D and 5D fibers. Each curve represents the average of three corresponding specimens curve those tested with different amount and type of fiber.

In each test the lateral deformation was measured by three LVDT's at mid height around the diameter of the specimen. The average of values of three curves is the initial curve for each specimen. Similar finding observed as axial fiber influence in Figures 5.54 and 5.55 that the amount of fiber content significantly affects the post-peak behaviour for all types of fiber UHPFRC specimens. The more clear comparison of fiber effects in terms of peak strength, peak strain and ductility responses are observed on lateral test results in Figures 5.56 to 5.61.

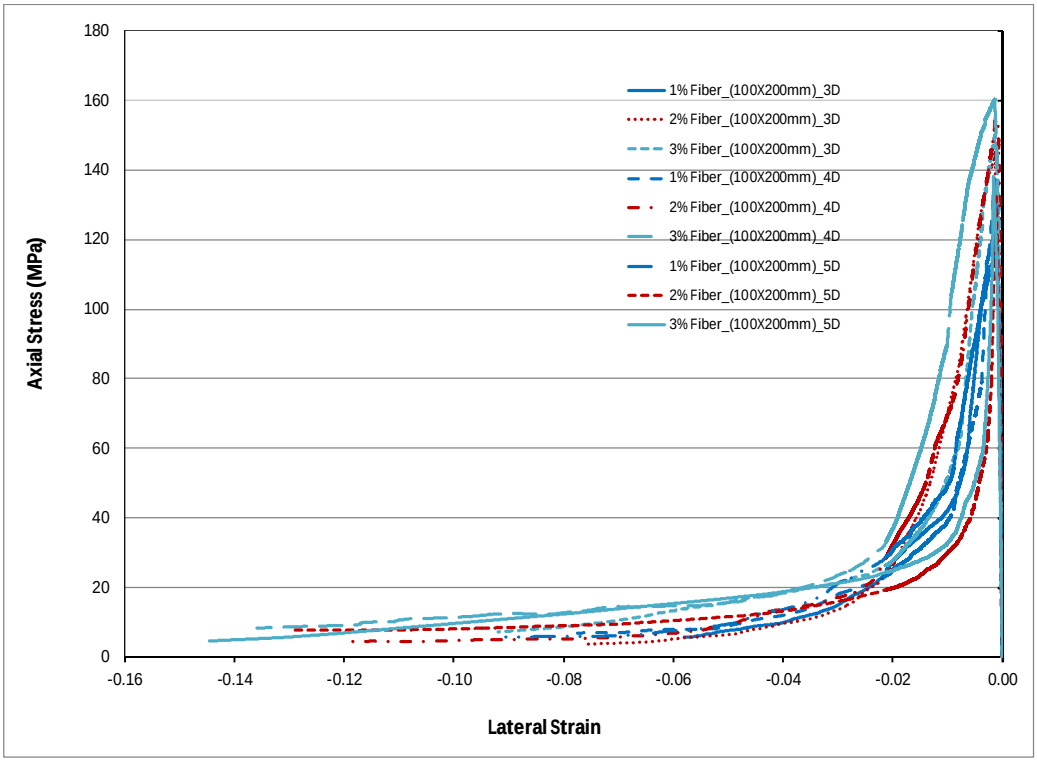

Fig.5.54 Influence of fiber on lateral stress-strain response of different fiber with different content

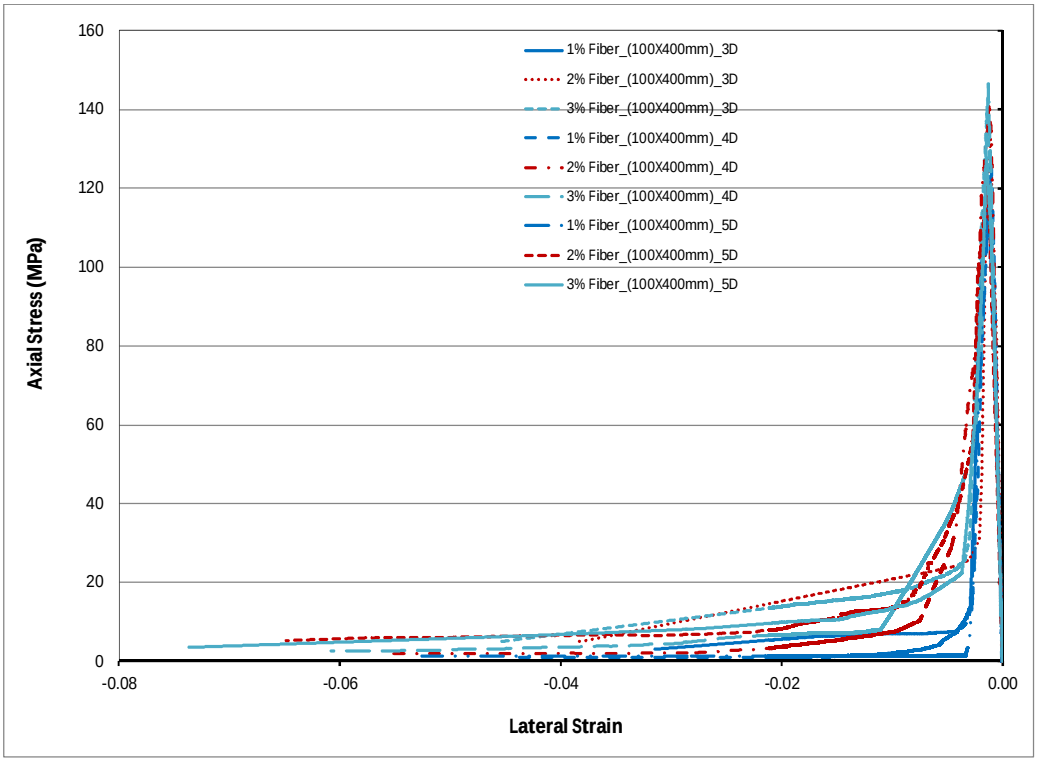

Fig.5.55 Influence of fiber on lateral stress-strain response of different fiber with different content

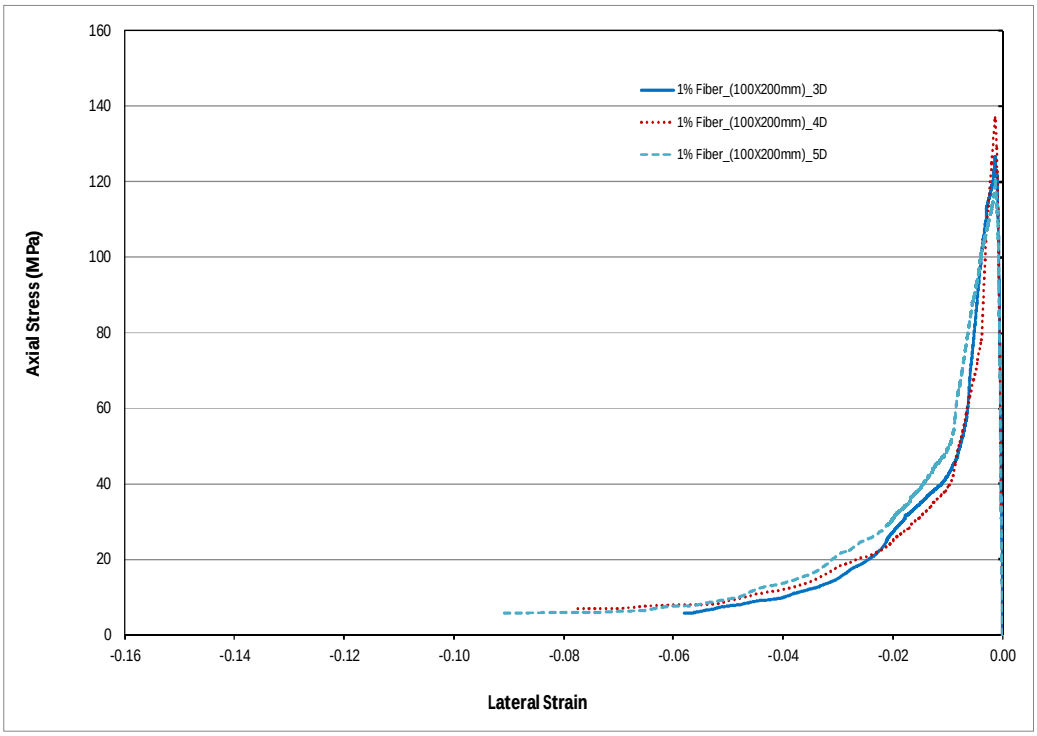

Fig.5.56 Influence of fiber on lateral stress-strain response of different fiber with 1% fiber content

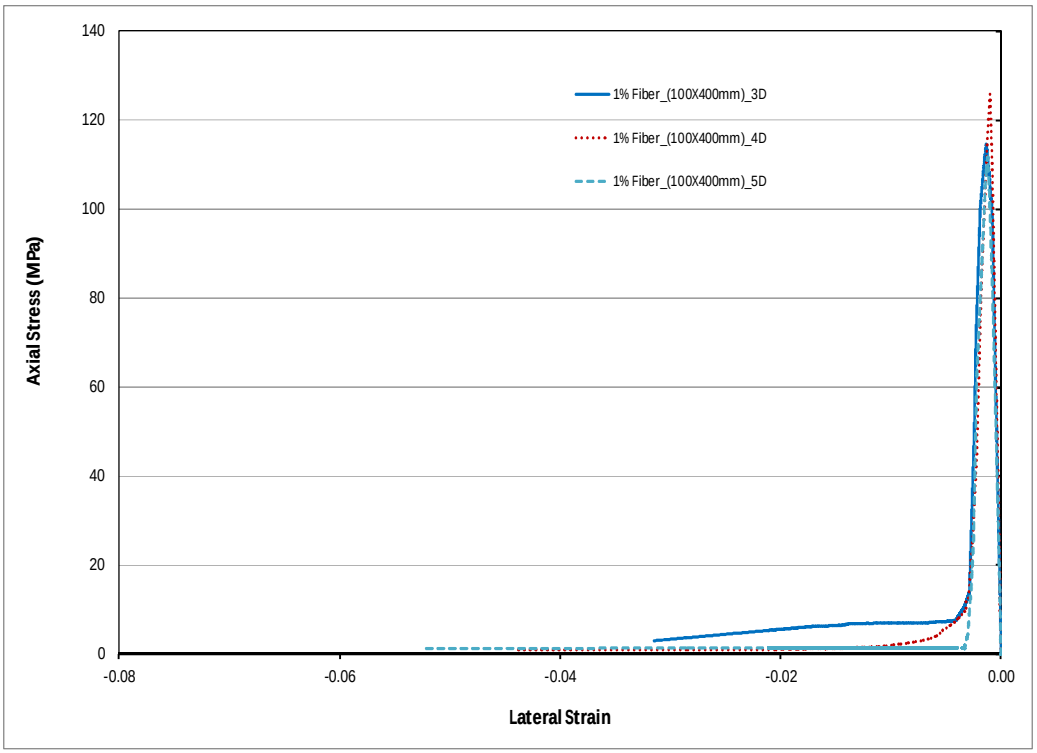

Fig.5.57 Influence of fiber on lateral stress-strain response of different fiber with 1% fiber content

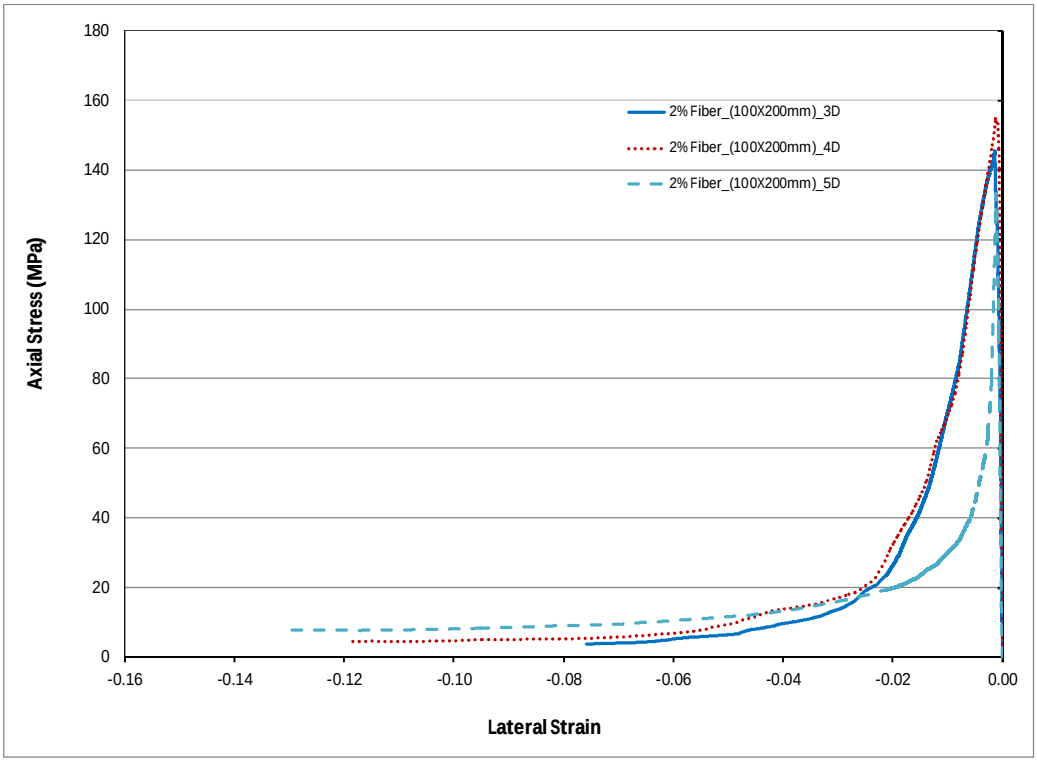

Fig.5.58 Influence of fiber on lateral stress-strain response of different fiber with 2% fiber content

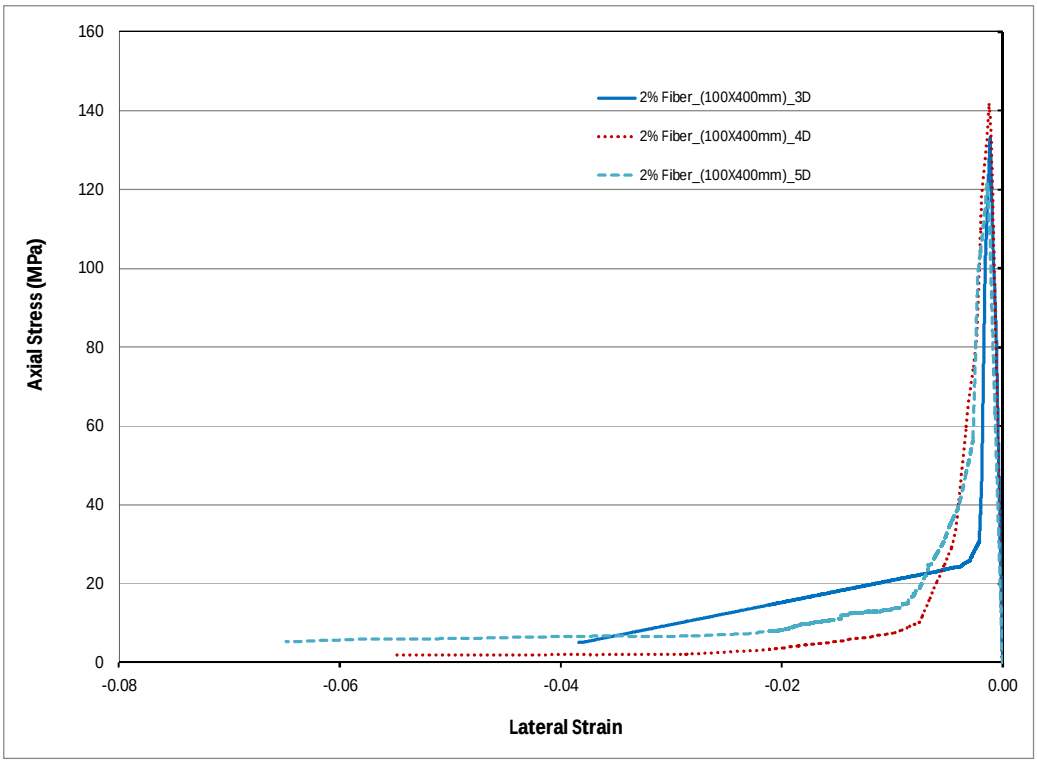

Fig.5.59 Influence of fiber on lateral stress-strain response of different fiber with 2% fiber content

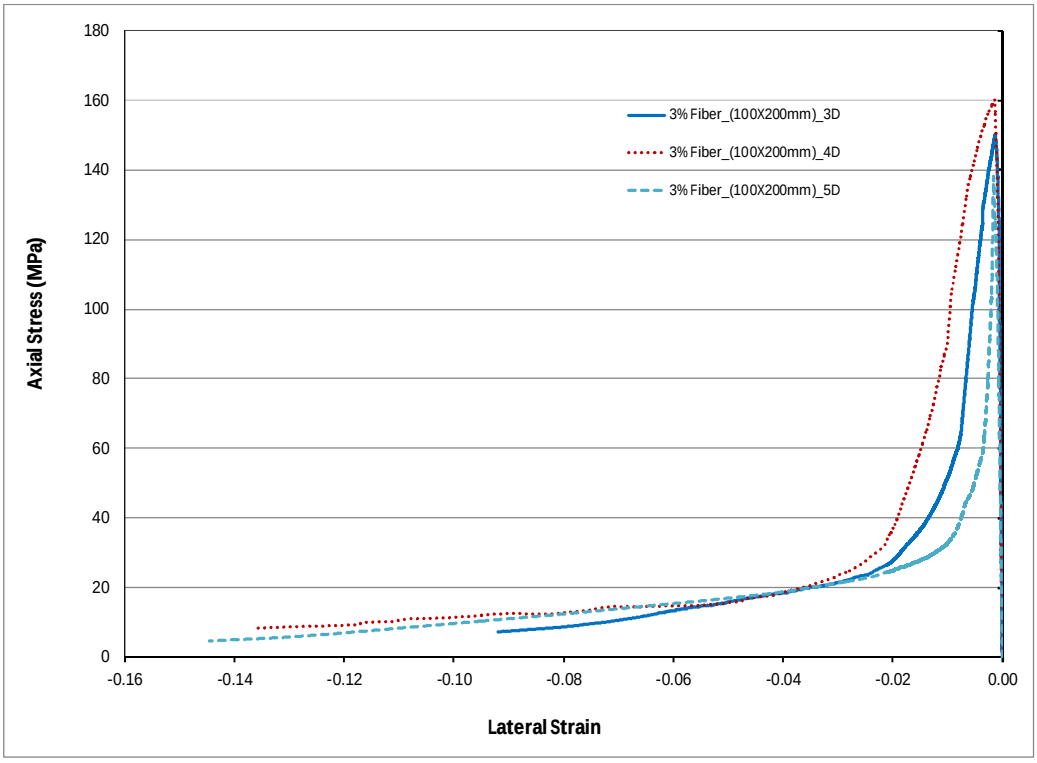

Fig.5.60 Influence of fiber on lateral stress-strain response of different fiber with 3% fiber content

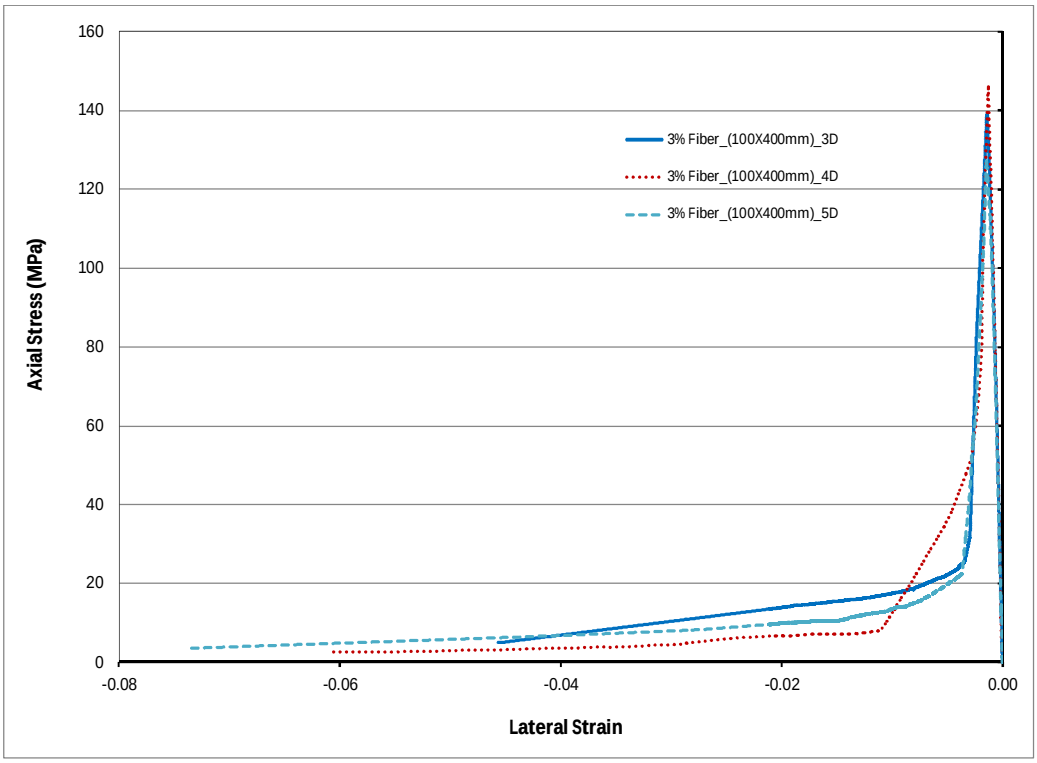

Fig.5.61 Influence of fiber on lateral stress-strain response of different fiber with 3% fiber content

5.3.3.5 Crack pattern and failure modes of UHPFRC specimens

All of the test series failure modes and crack pattern were observed during the uniaxial compression test and recorded via high-resolution photographs which allow for the identification of failure mode either through the formation of a single or circumferential sliding plane (Visintin et al., 2015) of concrete specimen.

The failure modes are presented for each of the test series of each percentage of fiber and type. Test series with fiber types and amount were presented before in Table 5.6. Following the Table 5.6 failure modes and crack pattern of each specimen will be presented and discussed here. All failure patterns of each percentage fiber content specimens are compared well and also compare with the control specimens with 0% fiber content especially at the top and bottom surfaces and the form of wedge on the specimen surface. Test series 1 and test series 2 are the same diameter specimen but different in height and fiber types. Test series 2 and test series 3 are the identical height of specimens but different in the dimension and fiber type.

It can be seen that Figure 5.62 shows the final failure modes and crack pattern of S-100x200-3D-0, S-100x200-3D-1, S-100x200-3D-2 and S-100x200-3D-3 concrete cylinder specimens for test series 1. The left side of top is the 0% fiber specimen and the right side of top is the 1% fiber specimen. Similarly, the bottom left and bottom right are the 2% and 3% fiber specimens respectively. It can be observed that all of the specimens except control specimen show almost single failure plane of shear friction wedge formation. The control specimen's failure pattern was observed reasonably well-formed cone shaped and preserved its bottom surface. It has been observed clearly from Fig.5.62 that single failure plane wedge formation occur along the specimen surface for 2% and 3% fiber content of specimens and likely to undergo ductile failure mode; however 1% fiber content specimen's observed the

wedge at the bottom plane but crack almost occur along the whole specimens that exhibit brittle failure mode. The behaviour is attributed to the more number of fibers present which interlocking fiber each other and make the homogeneity of concrete matrix leads to form single failure wedge formation for 2 and 3% fiber content.

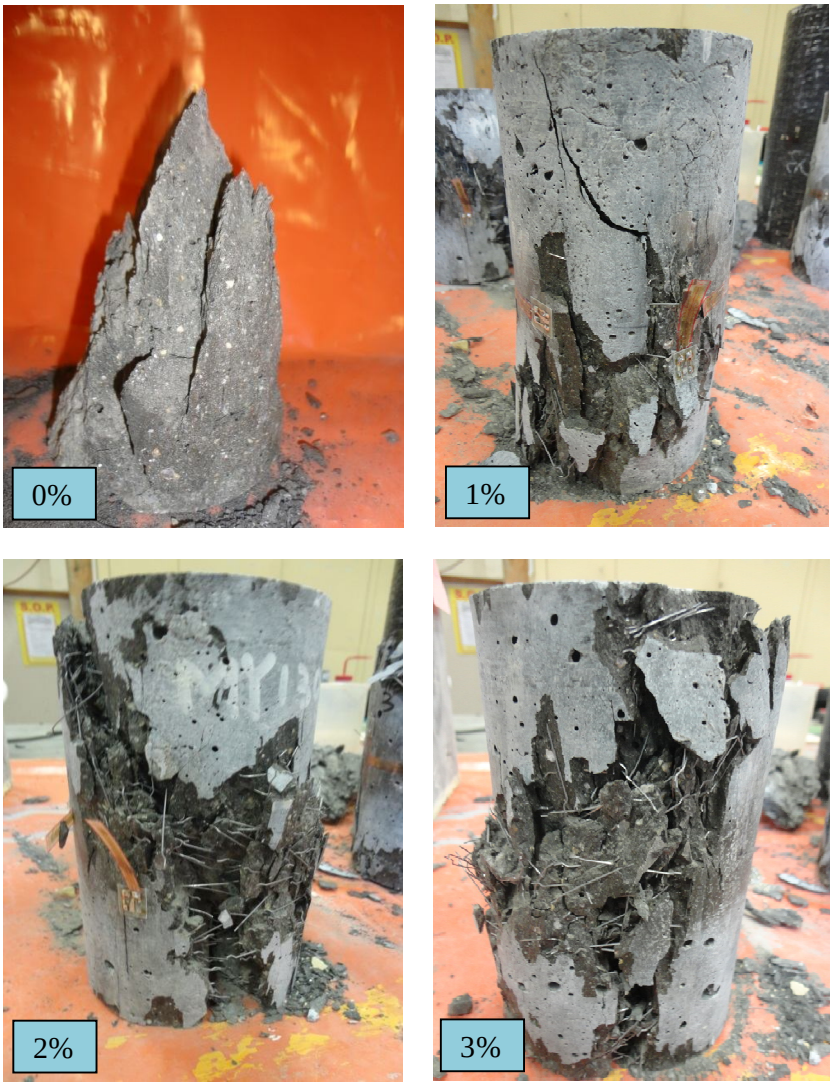

Fig.5.62 Failure pattern of 3D fiber specimens (Test series -1)

Failure modes and crack patterns for specimens of S-100x200-4D-0, S-100x200-4D-1, S-100x200-4D-2 and S-100x200-4D-3 of test series 1 are shown in Figure 5.63. The left side of top is the 0% fiber specimen and other percentage of fiber specimens are marked on the surface. It can be seen that all of the specimens except control

specimen show single failure plane of friction or single wedge formation. The control specimen exhibits brittle failure mode with well formed cone shaped; however the specimen with different fiber volume fraction corresponds to ductile failure characteristics with wedge formation along the surface of specimen. The wedge formation behaviour is attributed to the combined effect of fiber with homogeneity of concrete matrix that leads to create single plane wedge formation. It is also noticed that core concrete does not show any substantial crashing after peak; therefore, the specimens took a substantial load and deformation until failure.

Fig.5.63 Failure pattern of 4D fiber specimens (Test series -1)

Failure modes and crack pattern depicted in Figure 5.64 for the concrete cylinder specimens of S-100x200-5D-0, S-100x200-5D-1, S-100x200-5D-2 and S-100x200-5D-3 for test series 1. The left side of top is the 0% fiber specimen and other percentage of fiber specimens are marked on the surface. It can be seen that all of the specimens except control specimen show single failure plane of friction or single wedge formation entire length of the specimens. The control specimen demonstrates brittle failure mode with single cone shaped consequently fiber specimens depicted ductile nature. The wedge formation attributed to the interlocking fiber each other and homogeneity matrix formed along the surface that leads to create single wedge.

Fig.5.64 Failure pattern of 5D fiber specimens (Test series -1)

Failure modes and crack patterns are shown in Figure 5.65 for the test series 2 prism specimens. The concrete prisms of S-100x400-3D-0, S-100x400-3D-1, S-100x400-3D-2 and S-100x400-3D-3 failed with an explosive sound with undergo ductile characteristics except control one. The left side of top is the 0% fiber specimen and other percentage of fiber specimens are marked on the prism surface. It can be seen that all of the specimens except control specimen show a single failure plane of friction or single wedge formation along the length of the specimens. Wedge formation is more clearly visualised for 1 and 3% fiber content; however the formation of wedge length is more than half length of specimen of 2% fiber content.

Fig.5.65 Failure pattern of 3D fiber specimens (Test series -2)

The concrete prisms of S-100x400-5D-0, S-100x400-5D-1, S-100x400-5D-2 and S-100x400-5D-3 also failed with an explosive sound with ductile failure behaviour for test series 2 of 5D fiber type. Failure modes and crack pattern is presented in Figure 5.66 for these test series of the concrete prism specimens. The left side of top is the 0% fiber specimen and other percentage of fiber specimens are marked on the prism surface. It can be seen that all of the specimens except control specimen show single failure plane of friction or single wedge formation along the length of the specimens. The wedge formation behaviour is attributed to the interlocking of fiber each other and makes the homogeneity matrix that leads to create single wedge formation.

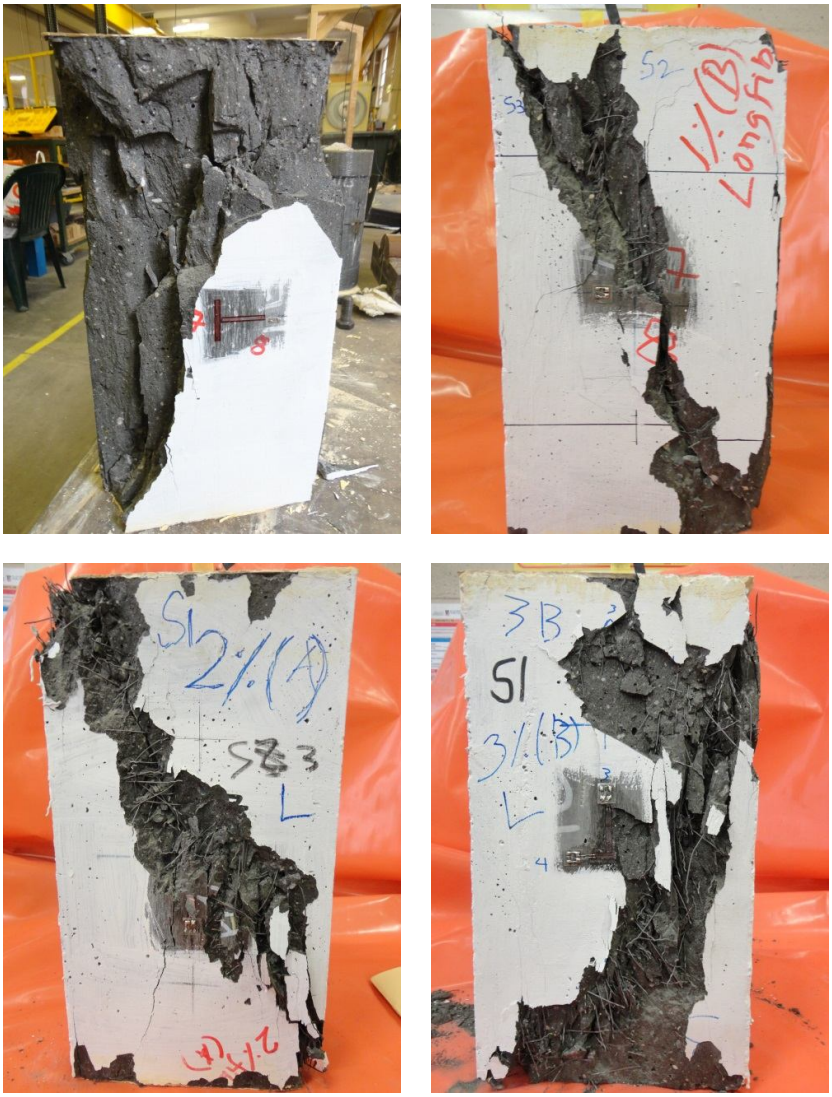

Fig.5.66 Failure pattern of 5D fiber specimens (Test series -2)

The concrete cylinder of S-100x400-4D-0, S-100x400-4D-1, S-100x400-4D-2 and S-100x400-4D-3 failed with an explosive sound for test series 3 of 4D fiber type. Failure modes and crack pattern are presented in Figure 5.67 for the series of the concrete cylinderspecimens. The left side of top is the 0% fiber specimen and other percentage of fiber specimens are marked on the prism surface. It can be seen that all of the specimens except control specimen show single failure plane of friction or single wedge formation along the length of the specimens. Wedge formation is clearly observed along the length for 1% and 2% fiber specimen and wedge form almost half length of the specimen for fiber percentage 3% specimens.

Fig.5.67 Failure pattern of 4D fiber specimens (Test series -3)

The concrete cylinder of S-100x300-4D-0, S-100x300-4D-1, S-100x300-4D-2 and S-100x400-3D-3 failure mode and crack pattern are illustrated in Figure 5.68 for test series 4 of 4D fiber type. The left side of top is the 0% fiber specimen and other percentage of fiber specimens are marked on the prism surface. It can be observed that all of the specimens except control specimen show single failure plane of friction or single wedge formation along the length of the specimens. The control specimen exhibits brittle nature of failure with single well cone shaped; however the fiber specimens show ductile single wedge formation entire specimen and it attributed to the homogeneity of concrete matrix formed with interlocking fiber each other.

Fig.5.68 Failure pattern of 4D fiber specimens (Test series -4)

5.4 Summary

Based on the size effect and ductility results of UHPFRC presented in this chapter, the major outcomes are as follows:

The inclusion of different steel fiber type and amount is very effective in increasing the strength and ductility behaviours of UHPFRC. It can be seen from the test results the post-peak responses of stress-strain curves with different steel fiber and types are dependent on the size of specimen. It was shown that doubling the height of the specimen tested significantly reduced the ductility of UHPFRC and that this behaviour was dependent on both fibre volume fraction and fibre type. The fiber content and types significantly affects the post-peak responses of UHPFRC specimens. For each type of fibers, it has been shown that increasing the fiber content leads to improved ductility. These results can be utilised to predict any other size of specimen behaviour with different fiber content and types.

Failure modes and crack patterns were found to be influence by the shape and fiber content of the specimens. Most of the cylindrical specimen observed a single failure plane on the surfaces from the mid height; however the rectangular prism specimen single failure plane observed from top to bottom height of the specimen. This behaviour is more pronounced with higher fiber content specimens. It can provide the warning before failure of the structural with ductility.

CHAPTER 6

SEGMENTAL ANALYSIS ON ULTRA-HIGH PERFORMANCE FIBER REINFORCED CONCRETE

This Chapter presents a new methodology for the quantification of the member ductility of ultra-high performance fibre reinforced concrete (UHPFRC) beams based on the segmental approach which has been developed at The University of Adelaide (Visintin & Oehlers, 2012; Visintin et al., 2012a; Visintin et al., 2012b). In order to apply the segmental approach a size dependent compressive stress strain relationship for UHPFRC is required. This is developed based on the test results presented in Chapter 5.

The structure of this chapter is as follows: initially a size dependent stress strain relationship for UHPFC is quantified from the test results presented in Chapter 5. Following this, the segmental moment rotation approach is developed for UHPFRC. The segmental approach is then used to demonstrate the influence of fiber amount and type on the rotation capacity of RC beams.

6.1 Introduction

Concrete is one of the most commonly used construction material around the world. In the design of a reinforced concrete structure ductility is arguably more important than strength in that it allows for the absorption of energy from external inputs such as earthquake loads and it ensures structures fail in the safest possible manner providing prior warning of collapse. The most common measurement of ductility is the quantification of the rotation of plastic hinges and an accurate definition of hinge rotation for conventional concrete is one of the longest standing research questions in structural engineering (Bigaj & Walraven, 2002; Carpinteri et al., 2009; Chen et al.,

2013; Lopes & Bernardo, 2003; Oehlers et al., 2008a) and a comparison of code approaches as found significant scatter in predictive models.

It has been argued by (Oehlers et al., 2008a; Visintin & Oehlers, 2012) that the reason for the scatter in approaches and the long standing nature of the research problem lies in the fundamental complexity of reinforced concrete. The rotation of a plastic hinge is dependent on the partial interaction mechanisms in the tension region which control the formation of cracks, crack widths, tension stiffening at all load levels and de-bonding of reinforcement (Oehlers et al., 2011; Oehlers et al., 2008b; Visintin et al., 2012b); while in the compression region the partial interaction mechanism of shear friction controls the formation and sliding behaviour of softening wedges (Visintin et al., 2012b).

Research has shown that the addition of fibres to concrete can increase its material ductility (Hassan et al., 2012) as well as its flexural ductility that is the ability to rotate at hinges (Yang et al., 2010). This chapter quantifies the moment-rotation (M/θ) of RC members made with ultra-high performance fibre reinforced concrete (UHPFRC). The chapter starts by illustrating how to quantify the stress-strain relationship of UHPFRC using the test results from Chapter 5 which had a range of sizes and fibre densities. The concrete compressive stress strain relations are given in a size dependent form that is suitable for any size of RC beam. It is then shown how the size dependent stress strain relationship can be used within the segmental moment rotation framework to quantify the moment-rotation behaviour of a reinforced UHPFRC beam in hinge region.

6.2 Quantifying the Stress-Strain Behaviour from the Ductility Test Results

6.2.1 Idealisation of axial stress-strain relationship

The stress-strain relationship of UHPFRC can be obtained directly from the test on concentrically loaded cylindrical or prismatic specimens a schematic view of which is given in Fig.6.1. The application of stress σ_{ax} in Fig.6.1 causes an axial deformation of the specimen D over its height L_{def} and the variation in axial deformation with applied stress is shown in Figure 6.2.

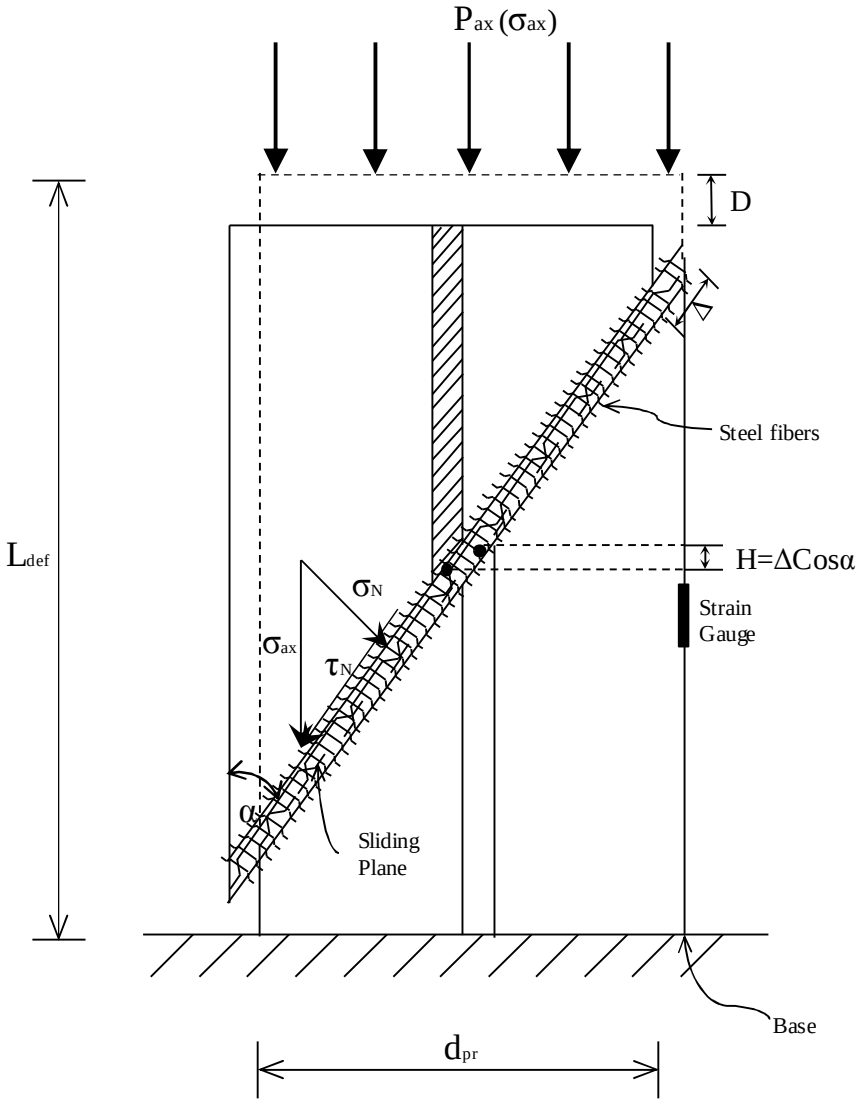

Fig.6.1 Deformation in a compression test

On application of the initial load, on the ascending branch OA up to the peak concrete strength f_c the deformation D can be considered a material deformation as given by the strain ε_{mat} recorded from strain gauges. That is

$$D = \varepsilon_{mat} L_{def} \qquad \text{Equation (6.1)}$$

In this stage non-linearity of the stress-deflection relationship in Fig.6.2 may occur due to the formation of micro-cracks. During the formation of micro-cracks fibres are engaged across the crack effectively providing passive confinement to the specimen such that in UHPFRC material non-linearity is small to negligible in the ascending region. As micro-cracking is spread throughout the whole specimen in this stage any non-linearity on the ascending branch OA can be considered to be a material property.

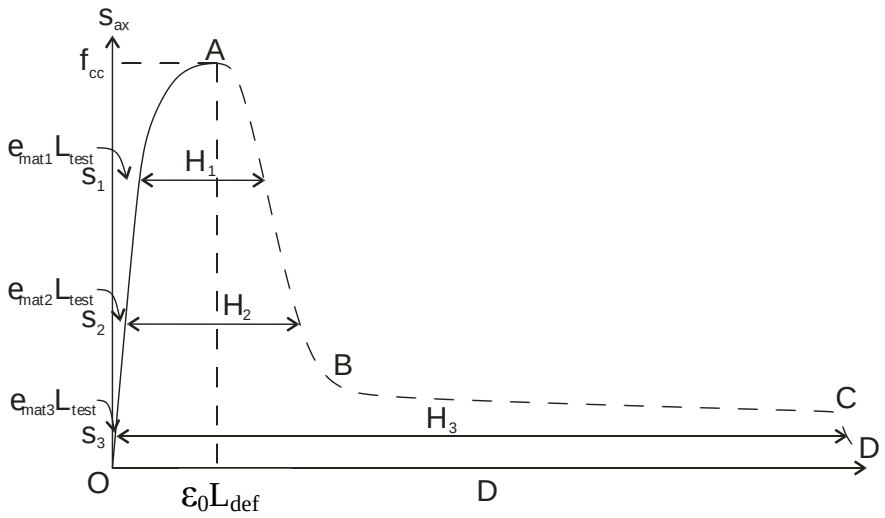

Fig.6.2 Variation of axial deformation with applied stress

Upon further loading a single sliding plane forms at an angle α in Figure 6.1 at the weakest zone in the concrete, which for short specimens is typically at mid height away from the end regions which many be confined by the loading platens. It should be noted that the location and the angle of formation of the single sliding plane was

recorded from the test results for UHPFRC and varied between 21 and 34 degrees for 1 and 3% fiber volume fraction respectively. For conventional concrete the angle at which a sliding plane forms has been quantified by (Balmer 1949; Cusson and Paultre 1995; Van Mier and Man 2009) and is within the range of 26 degrees.

In the descending branch of the stress-deflection relationship in Figure 6.2 the axial deformation due to sliding is taken as H in Figure 6.1 and can be determined geometrically such that the total deformation is

$$D = \varepsilon_{mat} L_{def} + H \qquad \text{Equation (6.2)}$$

It is therefore a matter of defining the non-material or local deformation H. The local deformation H can be obtained from experimentally determined shear friction material properties for example those in Figure 6.3 (Chen et al., 2015) which define the relationship between the normal stress σ_N, shear stress τ_N crack opening h_{cr} and slip H in Figure 6.1.

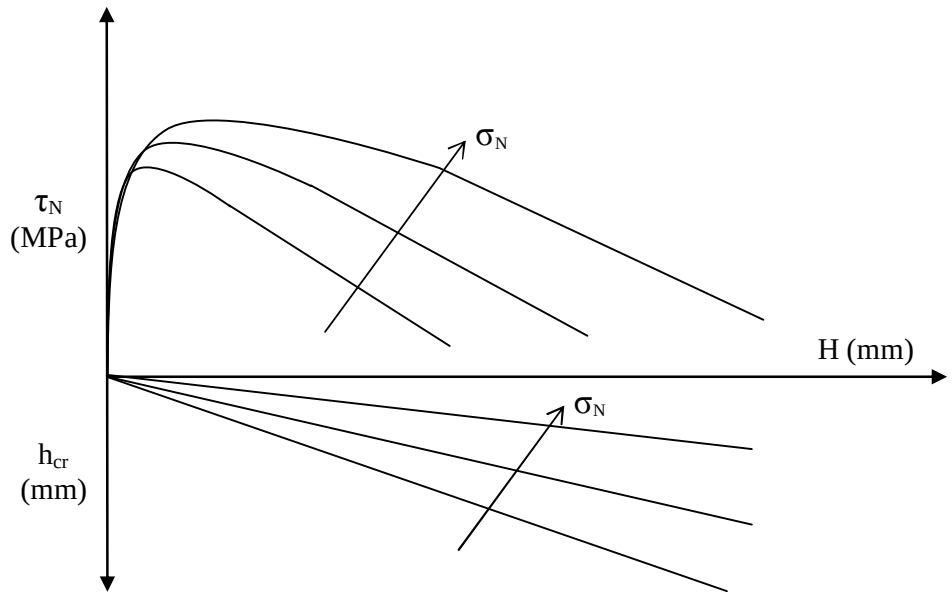

Fig.6.3 Shear friction material properties

A convenient alternative to the fundamental application of shear friction theory using the shear friction properties in Figure 6.3 is to use the shear friction mechanism indirectly to quantify a size dependent stress strain relationship from test results as follows.

Dividing the abscissa D in Figure 6.2 by the total length of the test specimen L_{def} gives an equivalent total stress-strain relationship OABC in Figure 6.4 which comprise both material and non-material deformations, that is

$$\varepsilon = \varepsilon_{mat} + \frac{H}{L_{ef}} \qquad \text{Equation (6.3)}$$

If the size of the test specimen in Figure 6.1 was doubled such that the total height was now $L_{def} = 2L_{test}$ the ascending branch of the stress strain relationship would remain unchanged as this is a size dependent material property by the equivalent strain due to sliding H would be halved shown as OADE in Figure 6.4. Hence it can be seen that using the shear friction approach and experimentally determine the load deflection behaviour for a single sized specimen allows for the definition of a universal size dependent stress strain relationship.

A stress train relationship using the shear friction concepts presented above will now be developed for UHPFRP using the test results in Chapter 5. In the development of this material model, behaviour is delineated into three stages.

Stage 1 is purely material strain based, Stage 2 is both material and shear-friction strain based, and Stage 3 is for all intents and purposes shear-friction strain based. Each stage from the Fig.6.4 represents:

Stage-1: Ascending branch-material strain based deformation

Stage-2: Descending branch – material + SF deformation

Stage-3: Plastic zone – predominating SF deformation

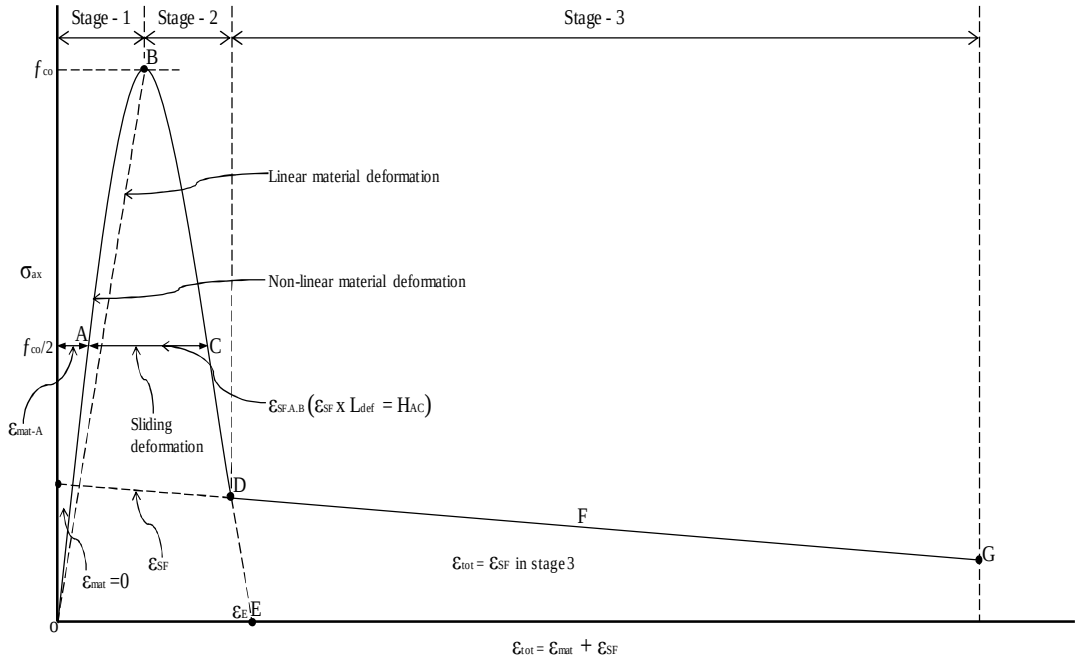

Fig.6.4 Idealised compression stress-strain relationship

The key points of the axial stress strain relationship in Fig.6.4 including the: secant stiffness, peak strength, peak strain, sliding deformation, Failure strength and deformation limit are summarised in Table 6.1 for differing fibre types and fibre densities. In Table 6.1 each series of tests consisted of a 0% fiber content control group as well as two other groups in which the fibre content ranged from 1 to 3%. It is worth mentioning that three specimens have been tested for each series each individual percentage of fiber content. The averages of three specimens result are the final behaviour of each test series. Test series 1 was comprised of 36 cylinder specimens with dimension of 100x200mm with the three different types of fiber, test series 3 consisted of 12 specimens with one type of fiber and one type of fiber of 12 specimens consisted for test series 4. Rectangular prisms were investigated in test series 2 encompassing the dimension of 100x200x400mm with two different types of fiber and the prism with a edge length of 200mm. The first letter “S” of specimen

designation in Table 6.1 refers to the specimens; the second series of numbers“100x200” refers to the dimension of the specimen, third for example“3D” indicates the fiber types and the last number, for example “0” refer to the fiber percentage.

Table 6.1 Axial stress-strain compressive ductility test results of UHPFRC

Specimen designation	Fiber %	Test series	Fiber type	Secant Stiff. (MPa)	Peak Strengt-h (MPa)	Peak Strain	Sliding def. (H_{AC}-mm)	Failure Strengt-h (MPa)	Deformat-ion Limit (H_G-mm)
S-100x200-3D-0	0	1	3D	34009	117	0.0036	0	106	1.868
S-100x200-3D-1	1	1	3D	32702	127	0.0044	1.305	6.060	16.934
S-100x200-3D-2	2	1	3D	35491	146	0.0044	1.753	4.831	22.510
S-100x200-3D-3	3	1	3D	37109	150	0.0046	1.334	7.576	26.314
S-100x200-4D-0	0	1	4D	34009	117	0.0036	0	106	1.8686
S-100x200-4D-1	1	1	4D	35002	137	0.0042	1.3276	6.683	20.3348
S-100x200-4D-2	2	1	4D	37246	155	0.0044	0.9833	4.394	29.694
S-100x200-4D-3	3	1	4D	37461	160	0.0045	1.2498	7.234	37.574
S-100x200-5D-0	0	1	5D	34009	117	0.0036	0	106	1.8686
S-100x200-5D-1	1	1	5D	29874	121	0.0049	1.36	6.3625	26.3
S-100x200-5D-2	2	1	5D	35496	133	0.0044	1.09	7.7263	36.16
S-100x200-5D-3	3	1	5D	35861	138	0.0043	1.734	5.7772	44.76
S-100x400-3D-0	0	2	3D	34009	117	0.0036	0	106	3.7372
S-100x400-3D-1	1	2	3D	38006	115	0.0043	2.372	2.994	18.708
S-100x400-3D-2	2	2	3D	41651	133	0.0042	1.877	5.088	22.788
S-100x400-3D-3	3	2	3D	39041	139	0.0042	2.288	4.967	26.708
S-100x400-5D-0	0	2	5D	34009	117	0.0036	0	106	3.7372
S-100x400-5D-1	1	2	5D	30189	112	0.0044	2.464	1.351	31.228
S-100x400-	2	2	5D	27385	122	0.0045	2.663	5.262	37.548

5D-2									
S-100x400-5D-3	3	2	5D	30022	128	0.0047	1.789	5.249	43.668
S-100x400-4D-0	0	3	4D	34009	117	0.0036	0	106	3.7372
S-100x400-4D-1	1	3	4D	35516	126	0.0040	2.5399	0.981	26.4296
S-100x400-4D-2	2	3	4D	37280	142	0.0040	2.1617	1.948	31.9096
S-100x400-4D-3	3	3	4D	34192	147	0.0044	1.9296	2.819	36.7496
S-100x300-4D-0	0	4	4D	34009	117	0.0036	0	106	2.8029
S-100x300-4D-1	1	4	4D	38024	124	0.0035	1.9876	0.6288	27.711
S-100x300-4D-2	2	4	4D	38962	141	0.0036	1.7056	2.476	32.961
S-100x300-4D-3	3	4	4D	40584	142	0.0037	1.5675	1.469	39.66

First consider the definition of Stage 1 in Fig.6.4 which is purely a strain based material property. The experimentally derived ascending portion of the stress strain relationship for each test dimension are summarised in Figs.6.5 to 6.7.

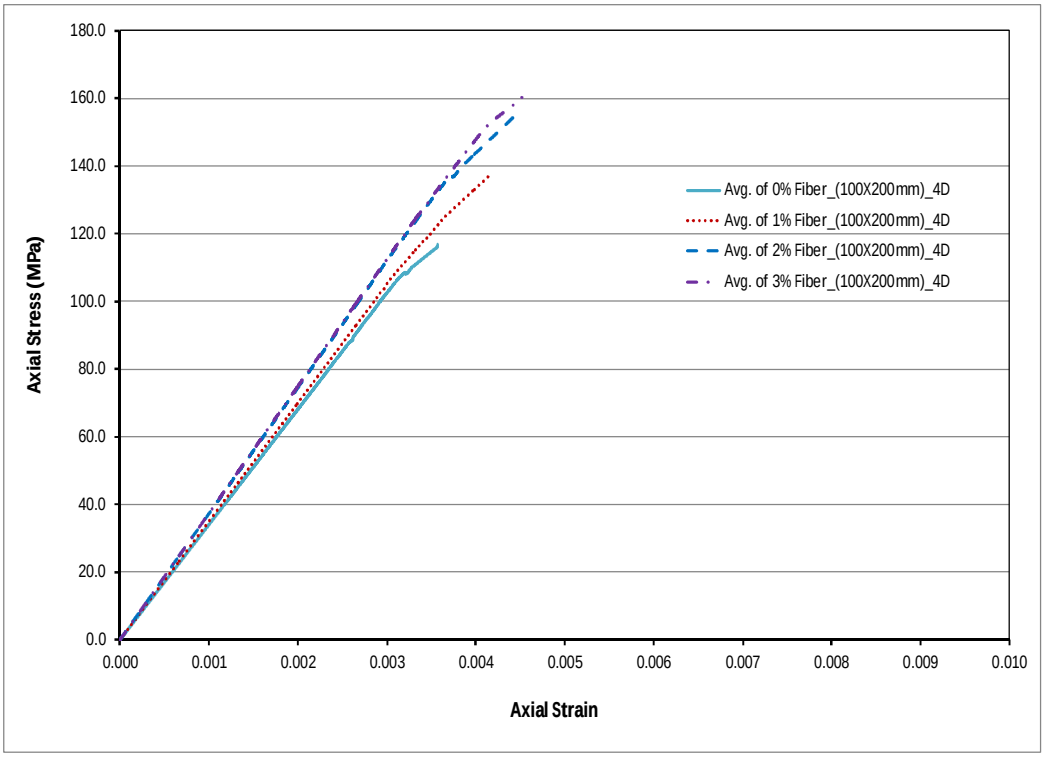

Fig.6.5 Experimental values of Stage 1 ascending branch for 100x200mm specimen

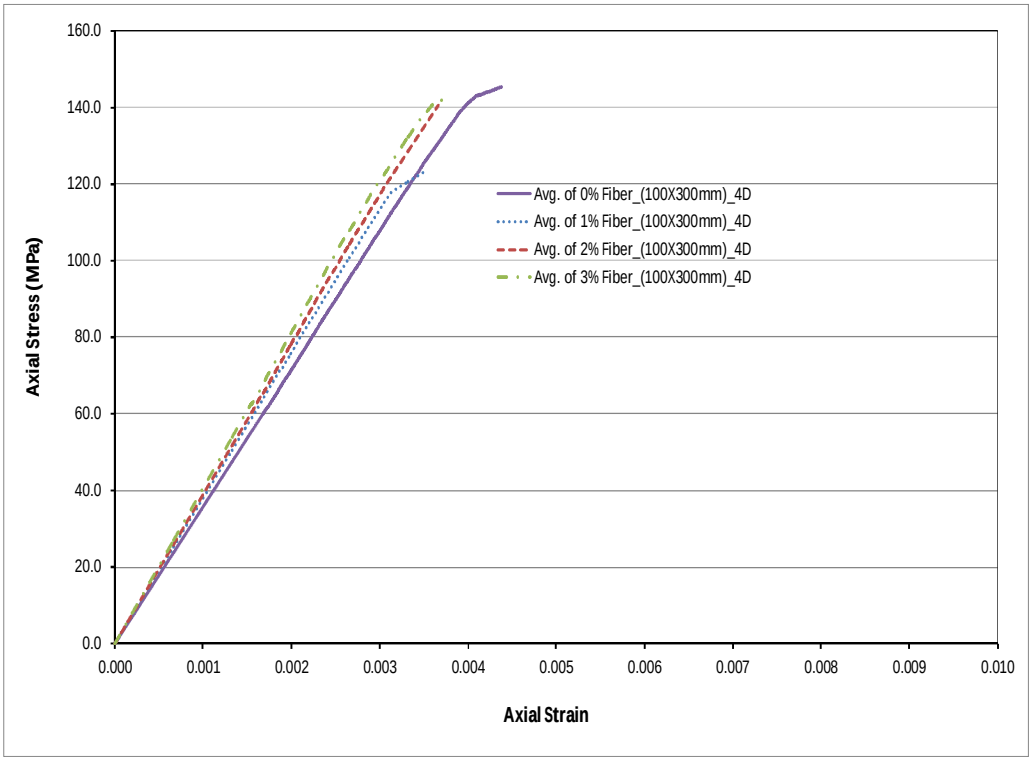

Fig.6.6 Experimental values of Stage 1 ascending branch for 100x300mm specimen

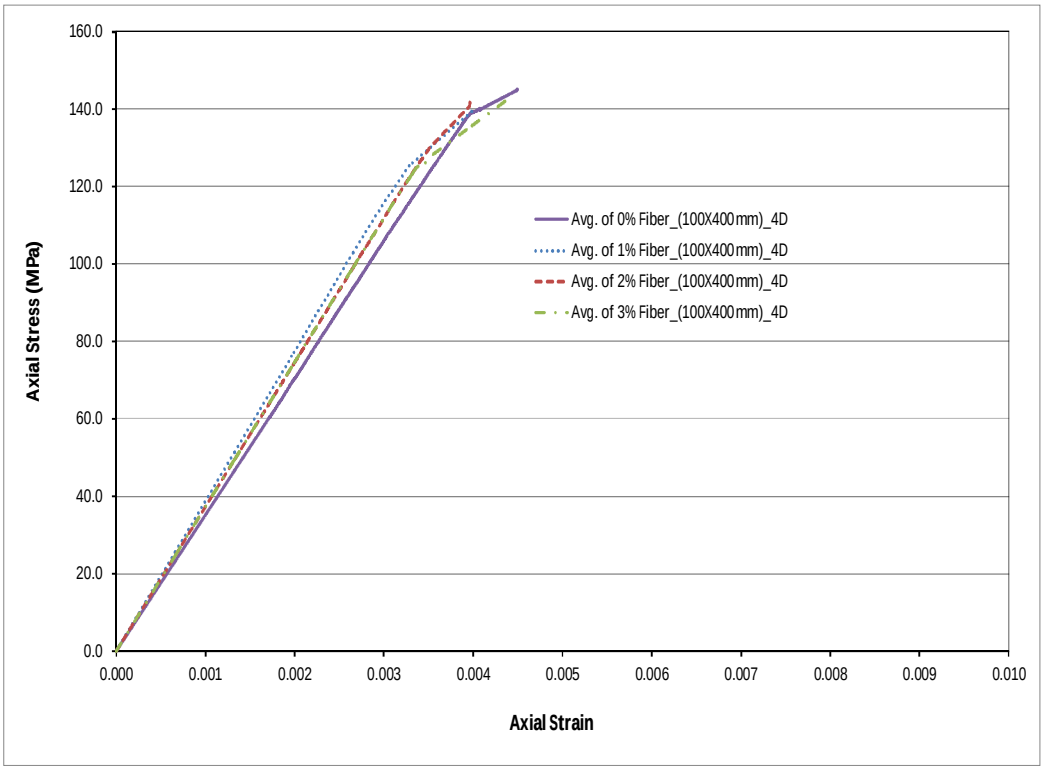

Fig.6.7 Experimental values of Stage 1 ascending branch for 100x400mm specimen

It can be observed from Figs.6.5 to 6.7 that all of the specimens show essentially a linear variation in Stage 1. Using the stress strain relationships in Stage 1 the secant stiffness of UHPFRC for each fibre type and quantity has been determine and the variation with fibres presented in Figs.6.8 to 6.11.

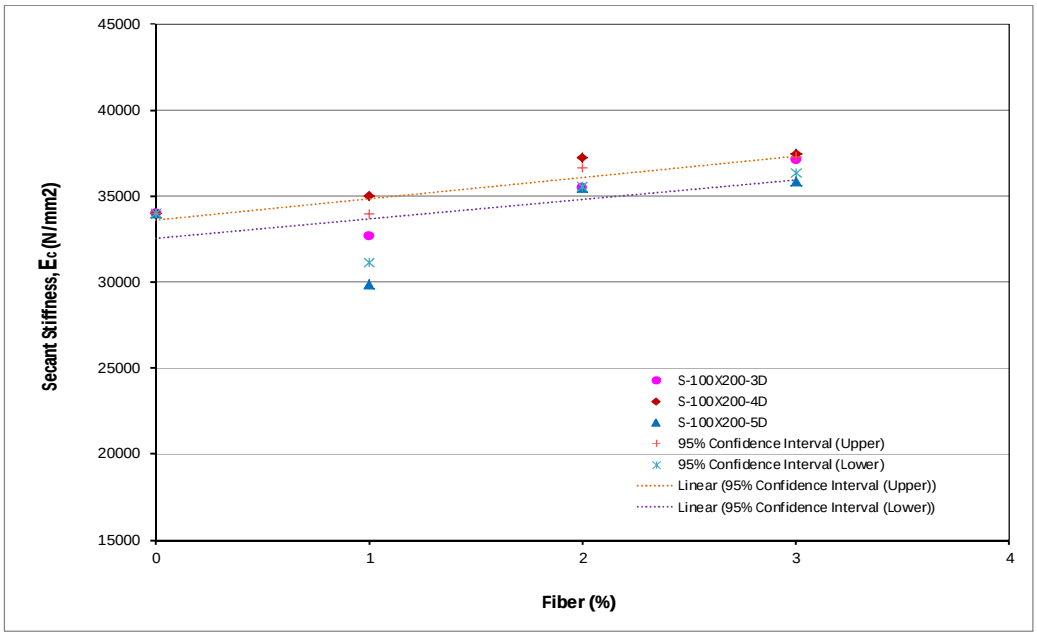

Fig.6.8 Quantification of secant stiffness for test series – 1 specimens

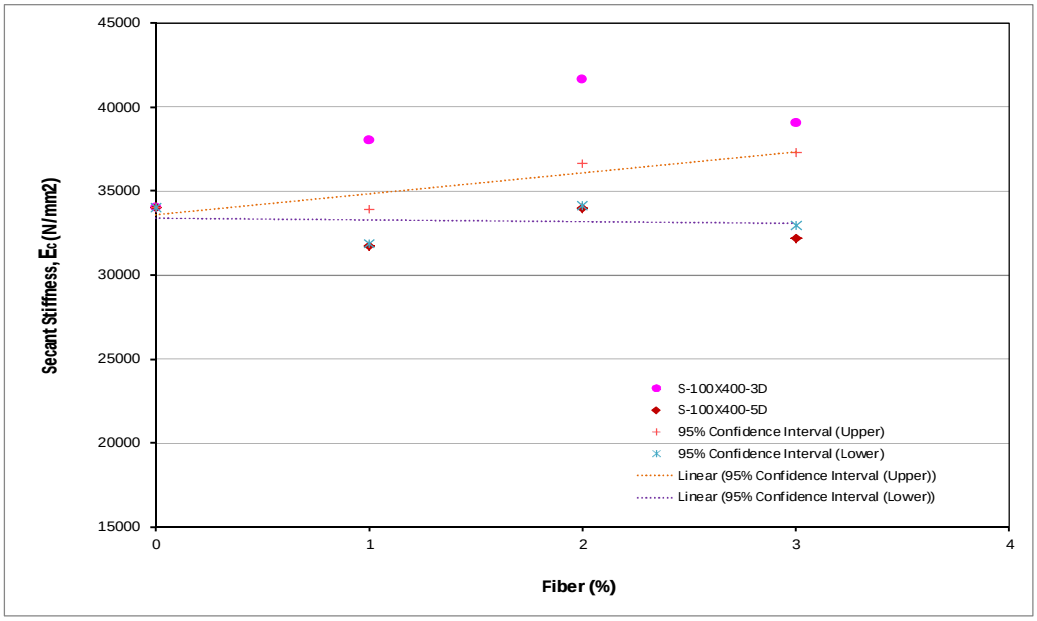

Fig.6.9 Quantification of secant stiffness for test series – 2 specimens

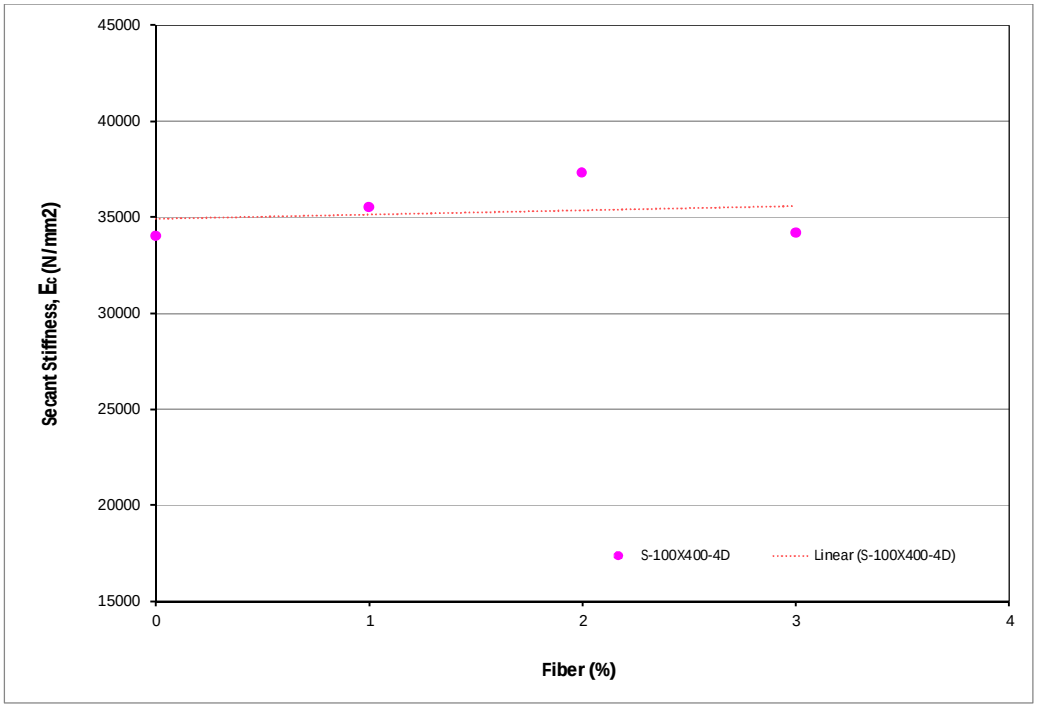

Fig.6.10 Quantification of secant stiffness for test series – 3 specimens

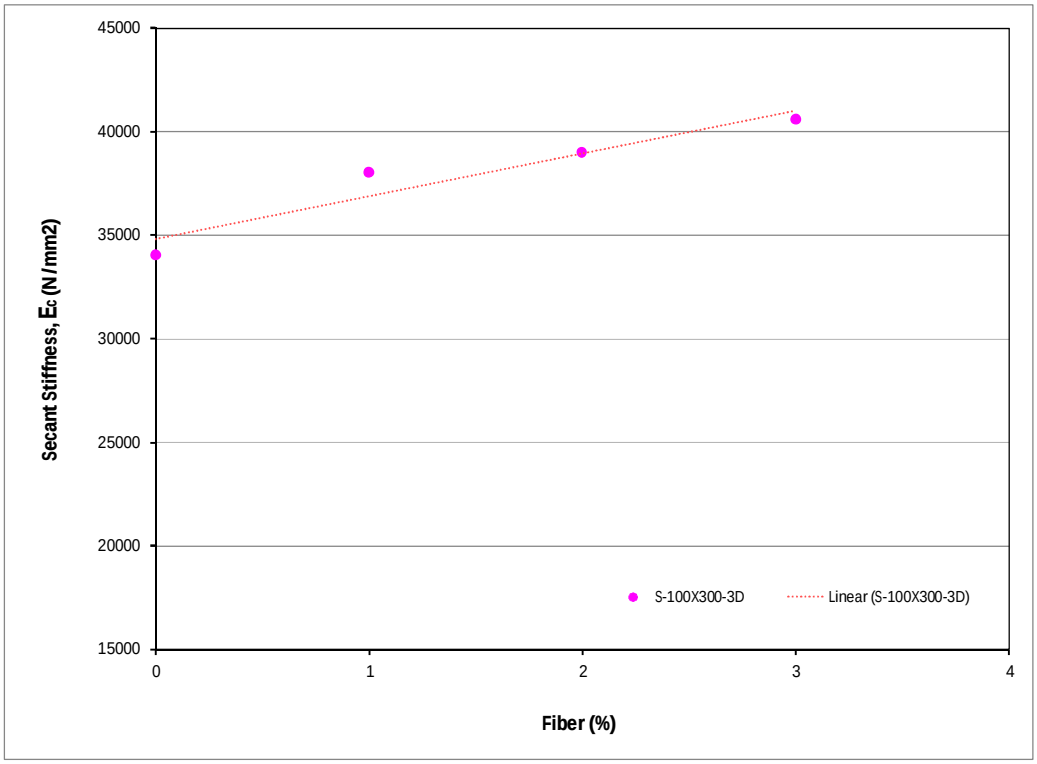

Fig.6.11 Quantification of secant stiffness for test series – 4 specimens

In each test series, the 95% confidence interval of upper and lower values is shown. In Table 6.2 the results of a regression study to identify the variation in secant stiffness with variations in fiber volumeV and type are presented where the variation in secant stiffness E_c is in the general form

$$E_c = AV + B \qquad \text{Equation (6.4)}$$

Where the parameters A and B are summarised in Table 6.2

Table 6.2 Secant stiffness results for regression analysis

Specimen Series	A	B
S-100x200-3D	1209	33014
S-100x200-4D	1260.2	34039
S-100x200-5D	1118.1	32133
S-100x400-3D	1874	35366
S-100x400-5D	-334.29	33462
S-100x400-4D	231.23	34902
S-100x300-4D	2066.3	34795

Comparing the results for all fibres in Table 6.2 it can be seen that there is very little difference in the elastic modulus of UHPFRC with differences in between the same size with different fibre type and volume, however it shows a variation when the size of the specimen makes doubled. This is to be expected as in Stage 1 of Fig.6.4 only micro cracks can be expected to have formed and thus there is little engagement of the fibres such that the modulus is mainly a function of the mortar which in this case is identical for all of test specimens.

Now consider the limit to Stage 1, that is the peak strength f_c. In Figs.6.12 to 6.15 the variation of fc with fibe type and quantity is shown.

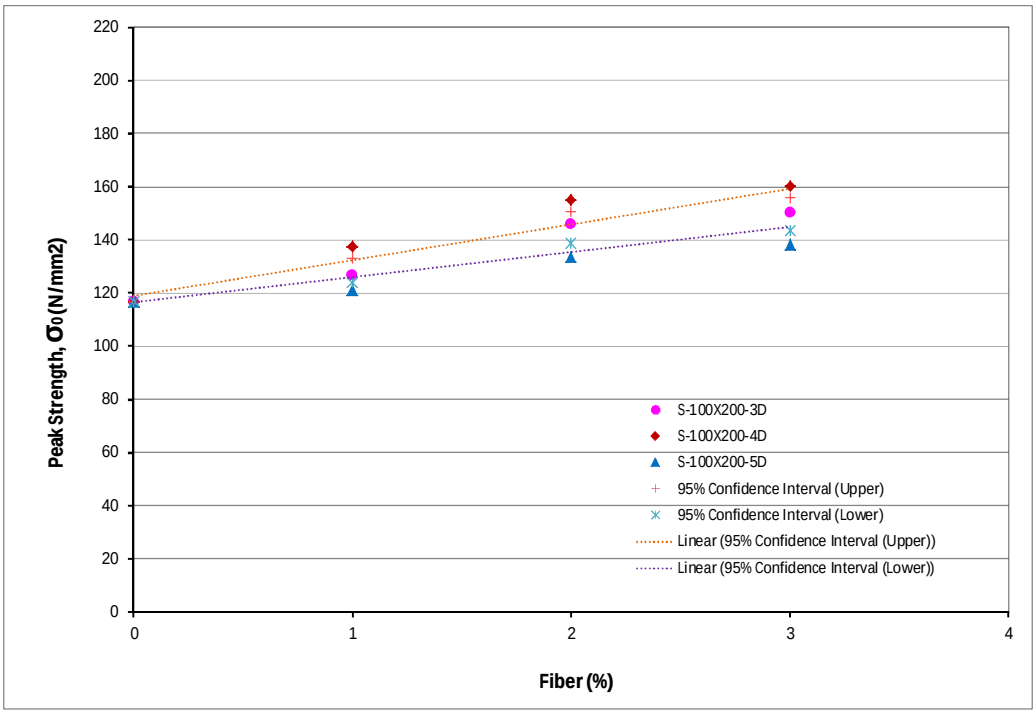

Fig.6.12 Quantification of peak strength for test series – 1 specimens

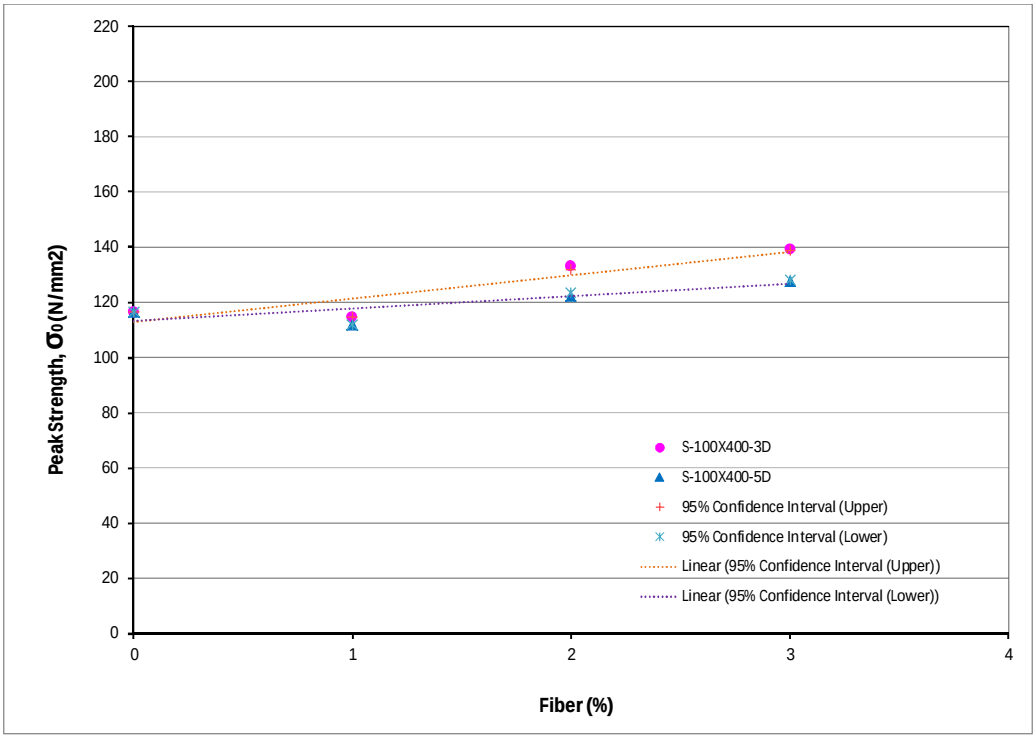

Fig.6.13 Quantification of peak strength for test series – 2 specimens

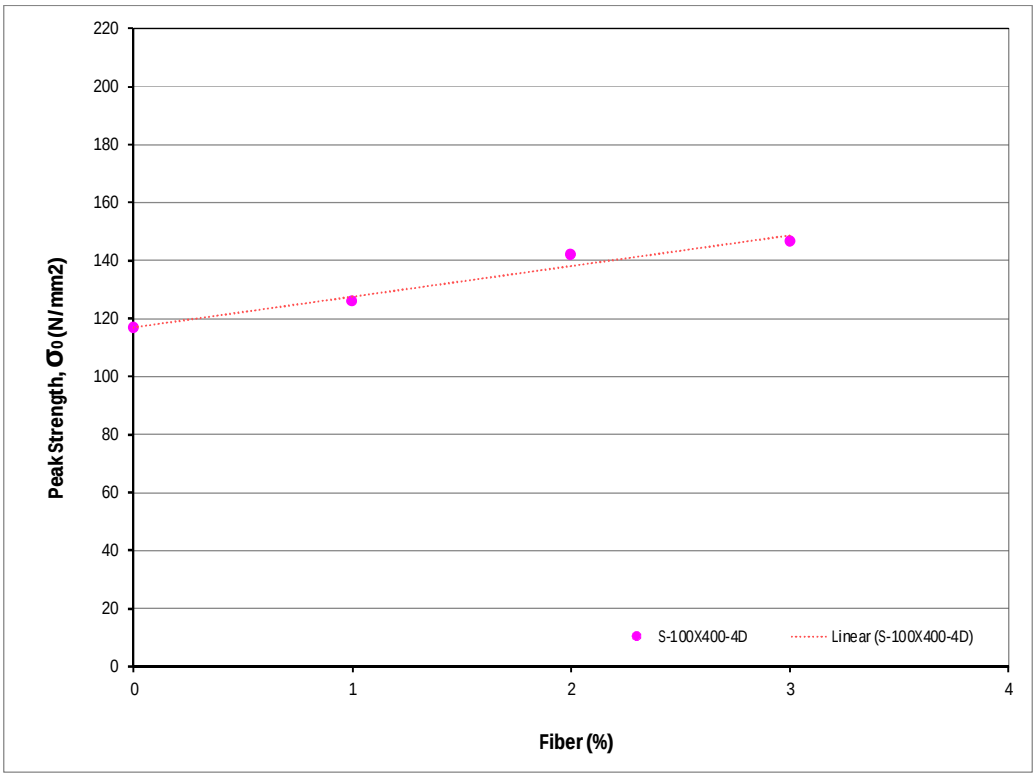

Fig.6.14 Quantification of peak strength for test series - 3

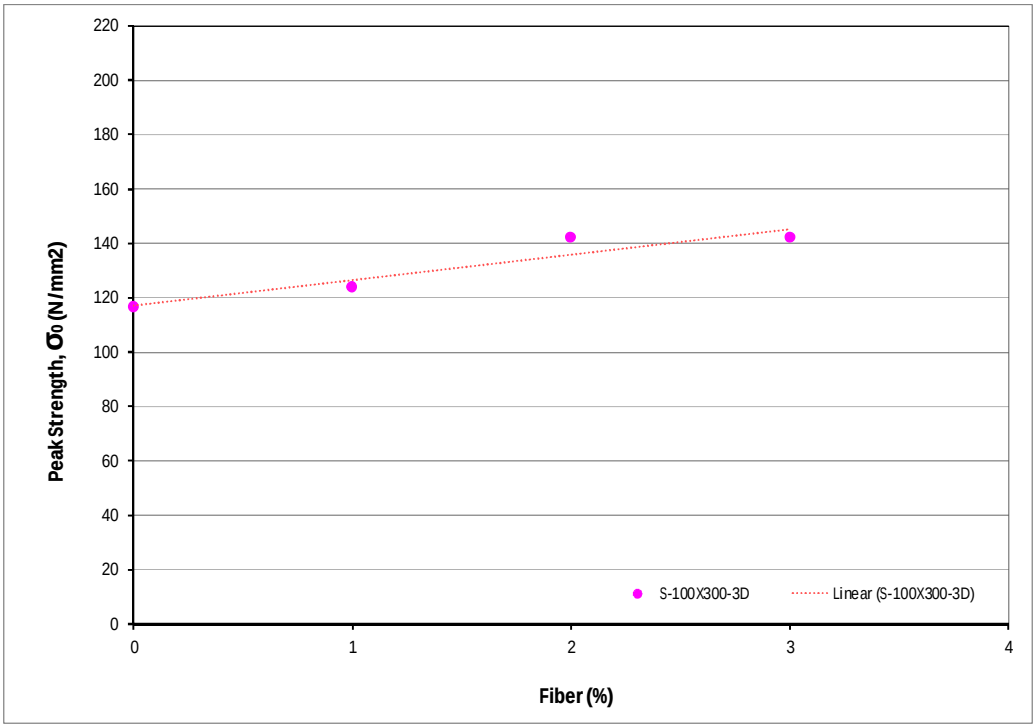

Fig.6.15 Quantification of peak strength for test series - 4

Again the variation in stress is regressed as a function of the fibre volume in the form

$$f_c = CV + D \qquad \text{Equation (6.5)}$$

Where the parameters C and D are summarised in Table 6.3

Table 6.3 Peak strength results for regression analysis

Specimen Series	C	D
S-100x200-3D	11.999	116.87
S-100x200-4D	14.804	120.09
S-100x200-5D	7.6531	115.79
S-100x400-3D	8.3804	112.93
S-100x400-5D	10.538	116.95
S-100x400-4D	4.3664	113.07
S-100x300-4D	9.4347	117.01

From the Table 6.3 it can be observed that there is small variation in the peak strength of UHPFRC with differences in between the same size with different Fibre type and Volume, however it exhibit a variation when the size makes doubled or 1.5 time., particularly at the long specimen of 4D fiber type. This can be happened as in Stage 1 of Fig.6.4 shows linear variation can be expected and thus there is little involvement of the fibres such that the peak is mainly a function of the mortar.

As was done for E_c and f_c the change in the strain at peak stress ε_c with variation in fibre type and volume is summerised in Figs.6.16 to 6.19.

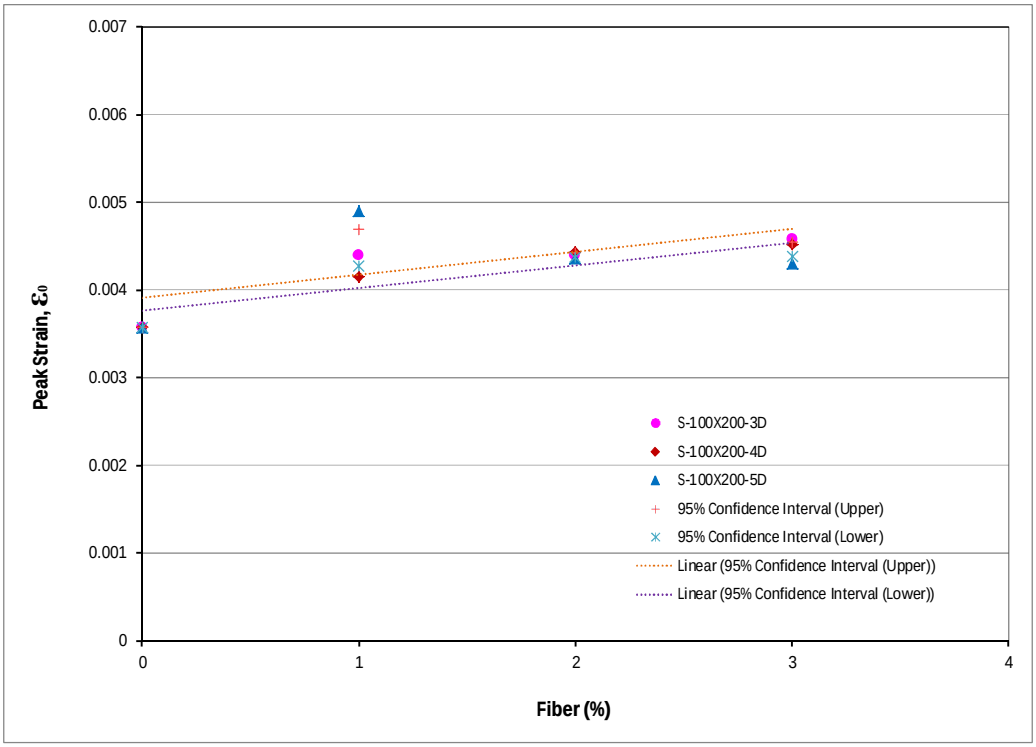

Fig.6.16 Quantification of strain at peak stress test series -1

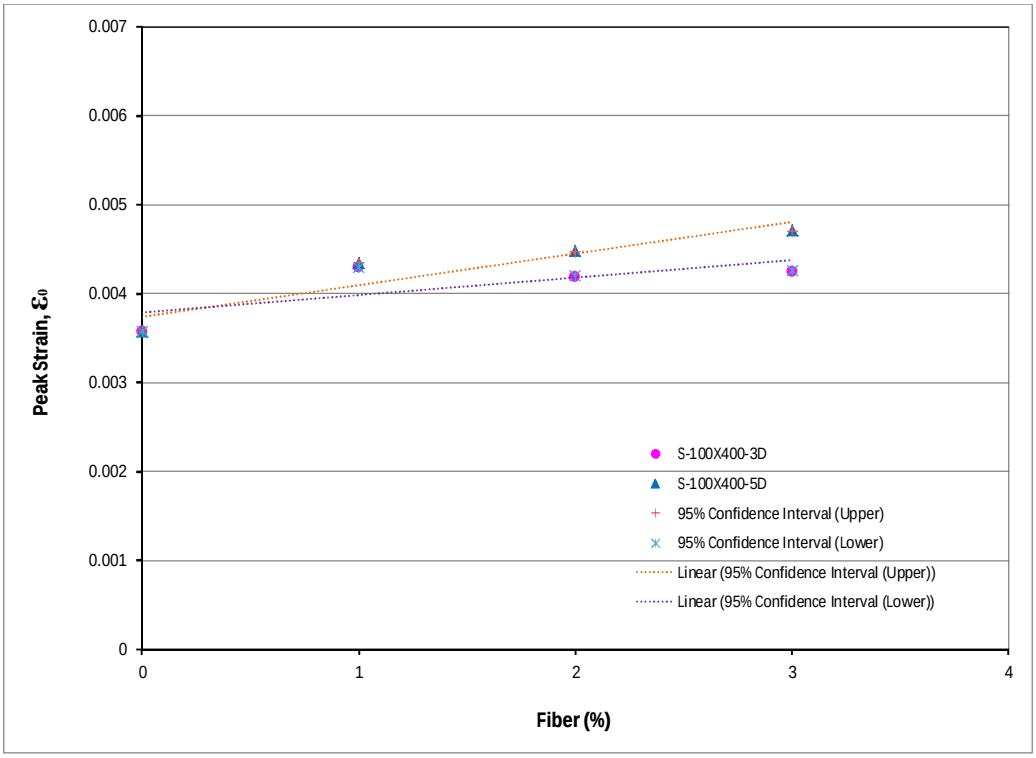

Fig.6.17 Quantification of strain at peak stress test series

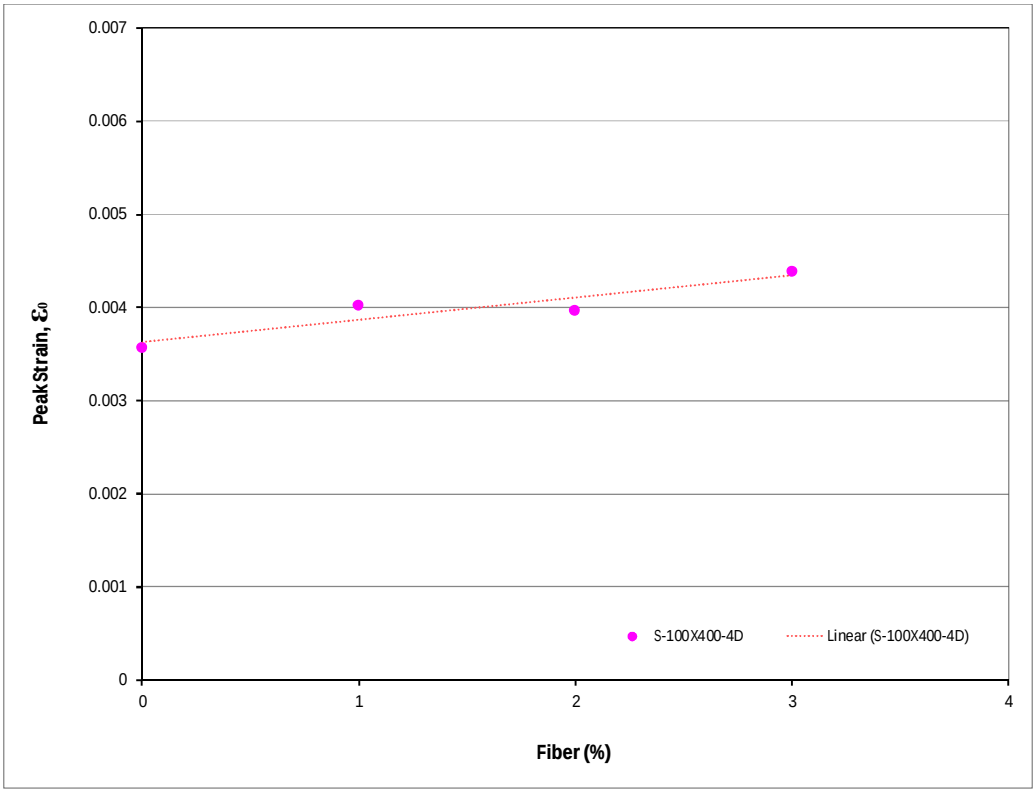

Fig.6.18 Quantification of strain at peak stress test series -3

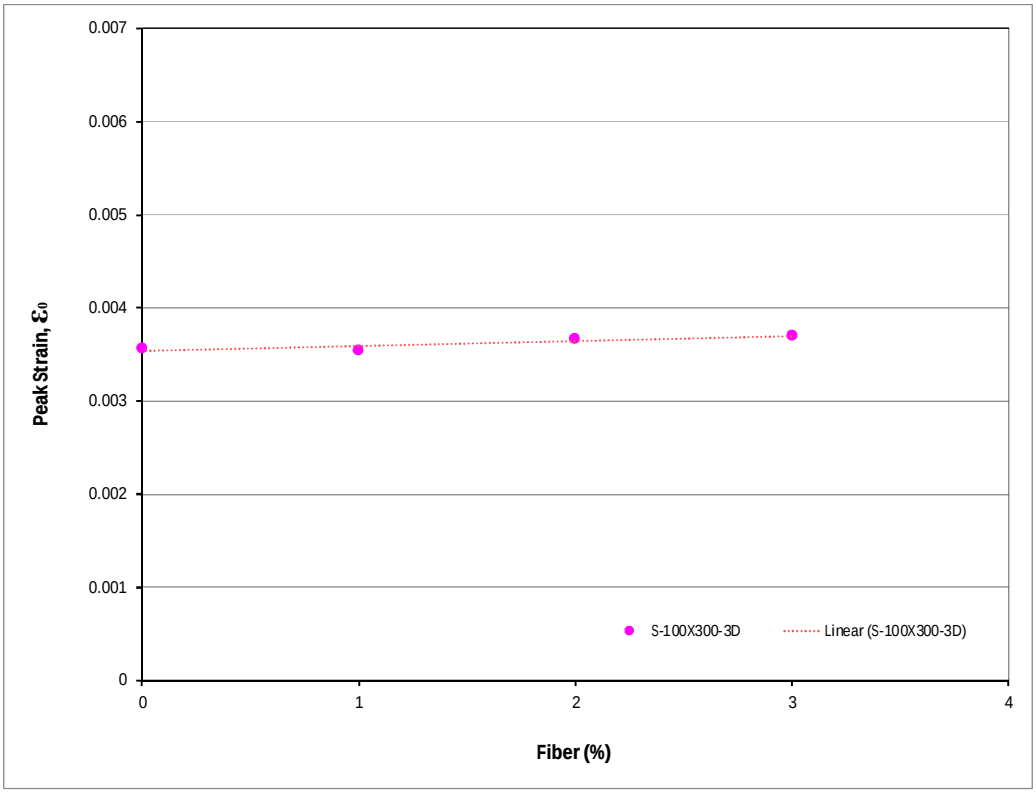

Fig.6.19 Quantification of strain at peak stress test series -4

The results of a regressing study to quantify the variation of the strain at peak stress with fibre type and volume is summerised in Table 6.4

$$\varepsilon = EV + F \qquad \text{Equation (6.6)}$$

Where the parameters E and F are summarised in Table 6.4

Table 6.4 Strain at peak stress results for regression analysis

Specimen Series	E	F
S-100x200-3D	0.0003	0.0038
S-100x200-4D	0.0003	0.0037
S-100x200-5D	0.0003	0.004
S-100x400-3D	0.0002	0.0038
S-100x400-5D	0.0004	0.0037
S-100x400-4D	0.0002	0.0036
S-100x300-4D	0.00005	0.0035

Table 6.4 following the peak strength of UHPFRC shows quiet similar behaviour between the same size but different fibre type and volume, however longer specimen demonstrate a slight difference then the other specimen. This may be attributed as in Stage 1 of Fig.6.4 exhibit linear variation with small hair crack and the peak strain is differentiate the behaviour from elastic to plastic region of specimen.

Having defined the elastic modulus of the concrete as well as the peak stress and the strain at peak stress the ascending region of the stress strain relationship in Figure 6.4 is now defined for a range of fibre type and volume fraction. Hence let us now consider Stage 2 in Figure 6.4 which is considered to be linear such that it can be defined by a single point.

In order that there is a clear delineation between Stages 2 and 3 the point chosen to define Stage 2 has been taken as the stress and strain corresponding to $0.5f_c$. Within Stage 2 the total strain consists of: the material strain $\varepsilon_{mat\text{-}A}$ which is identical to the strain at the corresponding stress on the ascending branch; and the equivalent non

materialshear friction strain $\varepsilon_{SF\text{-}AC}$ which required quantification here. Hence in Figures 6.20 to 6.23 the axial contraction H_{AC} due to sliding is quantified for variations in fibre type, volume and specimen height.

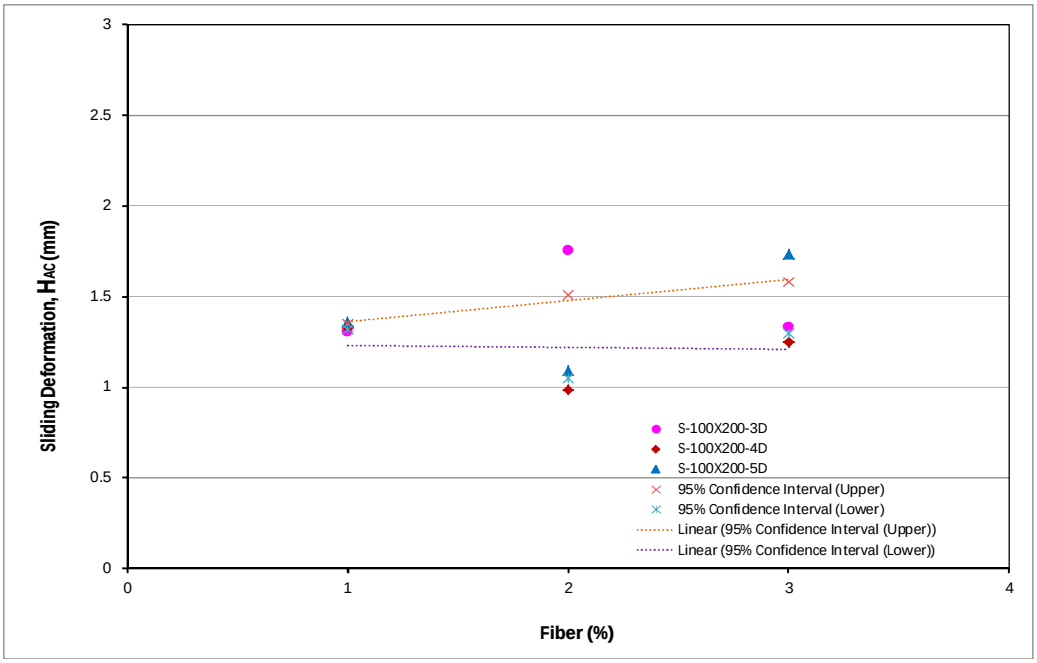

Fig.6.20 Sliding deformation at 0.5fc for test series – 1 specimen

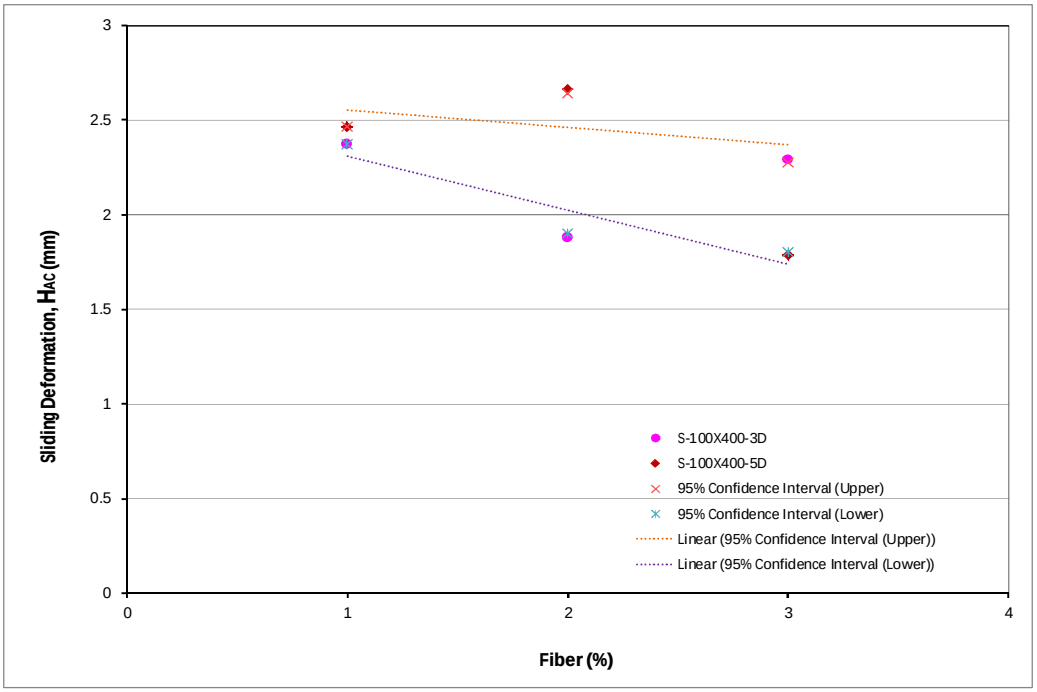

Fig.6.21 Sliding deformation at 0.5fc for test series – 2 specimen

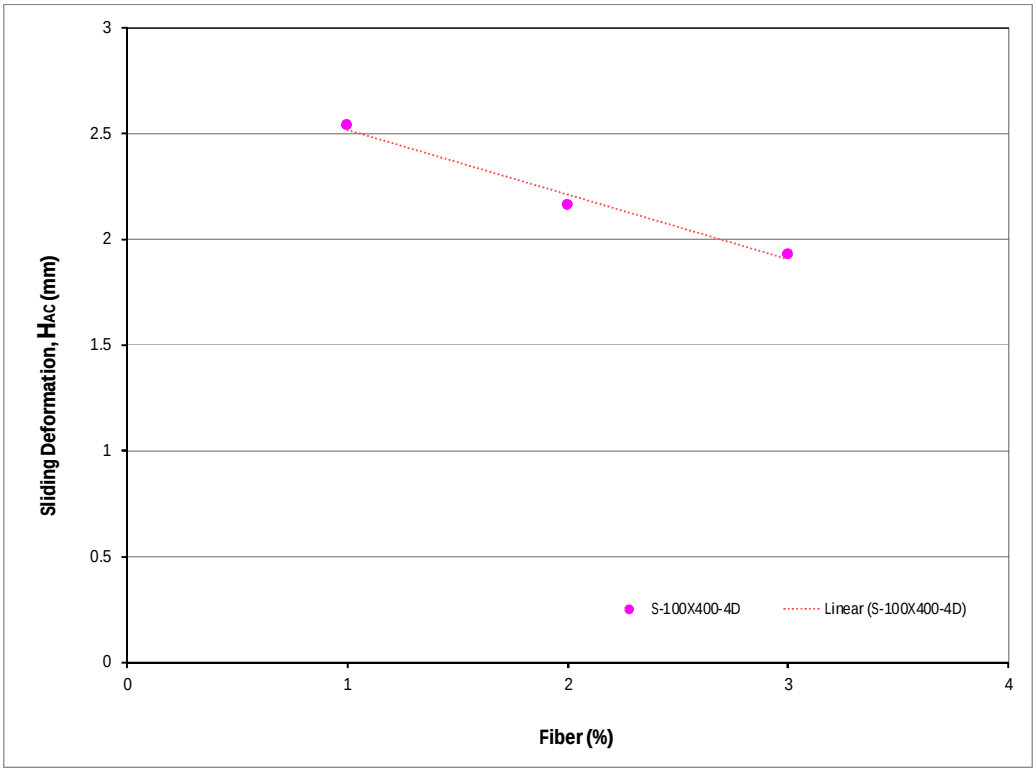

Fig.6.22 Sliding deformation at 0.5fc for test series – 3 specimen

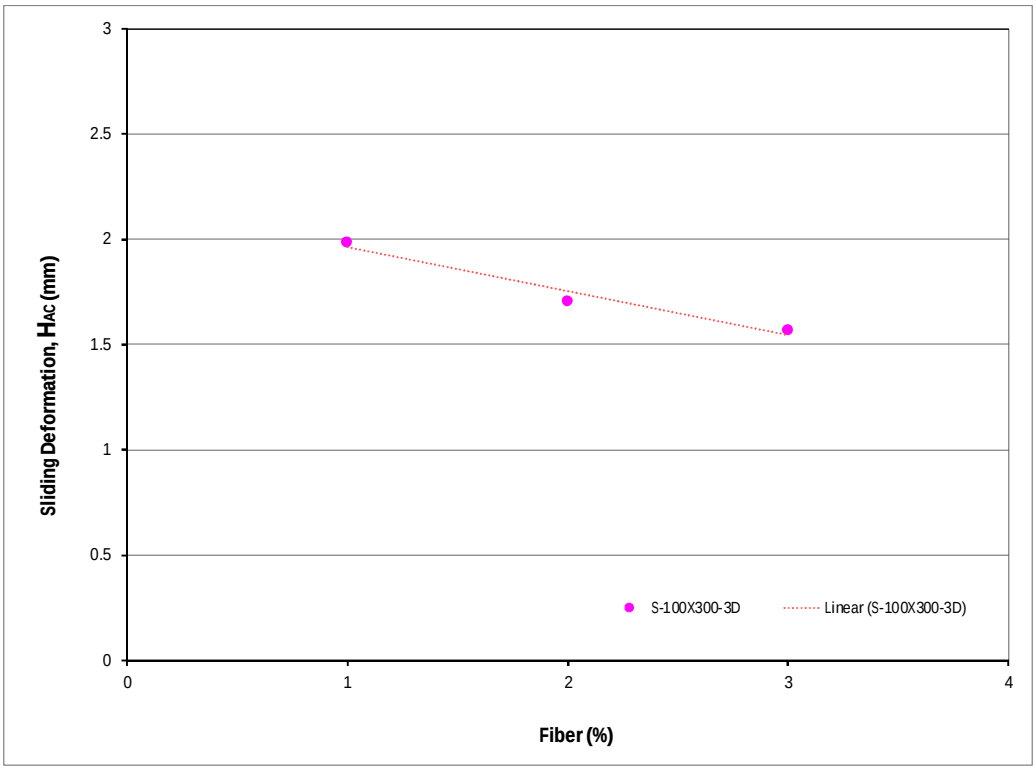

Fig.6.23 Sliding deformation at 0.5fc for test series – 4 specimen

The variation in sliding H was quantified in terms through a regression analysis in the form

$$H = IV + J \qquad \text{Equation (6.7)}$$

Where I and J are defined for each series in Table 6.5

Table 6.5 Sliding deformation results for regression analysis

Specimen Series	I	J
S-100x200-3D	0.0147	1.434
S-100x200-4D	-0.0389	1.264
S-100x200-5D	0.187	1.02
S-100x400-3D	-0.042	2.26
S-100x400-5D	-0.337	2.98
S-100x400-4D	-0.3052	2.82
S-100x300-4D	-0.2101	2.1737

Comparing the results for all fibres in Table 6.5 it is seen that there is a difference in the sliding deformation of UHPFRC with differences in between the same size and different fibre type and volume, however it shows a variation when the size makes doubled. This is to be expected as in Stage 2 of Fig.6.4 major cracks started can be expected to have formed and thus there is little bit variation of the fibres such that the sliding deformation is mainly a function of the mortar and fiber together.

Having now defined the sliding deformation H in Figure 6.1, is now possible to define the size dependent stress strain relationship of Stage 2, for the specific stress $0.5f_c$. That is

$$\frac{H_{AC}}{L_{def}} = \varepsilon_{SF-AC} = \frac{IV + J}{L_{def}} \qquad \text{Equation (6.8)}$$

We can now use the expression for Point B (ε_0/f_c) and the expression for Point C ($\varepsilon_{SF-AC}/0.5f_c$) in Fig.6.4 to quantify the falling branch B-C-D-E as follows. Importantly as the stress strain relationship is a function of H it is size dependent and hence applies to any prism length L_{def} in Figure 6.1.

In Stage 3, itis needed now to quantify Stage 3 in Fig.6.4; not only the slope of the variation but also the experimentally determined limit at Point G. There will be a large scatter where Stage 2 intercepts Stage 3. To omit this scatter when deriving Stage 3, the results are used where the strains in Stage 3 are larger that ε_E shown in Fig.6.4. it is greater than $1.2\varepsilon_E$ and do not appear to be outliers. To perform the analysis properly, as in Stage 2, we should take away ε_{mat} from the total strain ε_{tot} to get ε_{SF} and multiply this by the prism height L_{def} to get H so that it can compare the deformations from all the tests directly to find the variation. However, for all intents and purposes, since ε_{mat} is two orders of magnitude smaller than ε_{SF} we can simply ignore ε_{mat} for this part of the analysis.

In the Fig.6.4 may help quantify this Stage 3 variation for different % fibres and for different fibre types. It is a linear expression for each test for Equation 6.9, which is for a specific fibre type and % fibre. The equation of the line represents deformation limit corresponding to fiber percentage. Figures 6.24 to 6.27 shows the deformation limit for different fiber types and content.

$$\sigma = \sigma_0 - mH_{S3} \qquad \text{Equation (6.9)}$$

$$H_{S3} = \left(\sigma_0 - \sigma \middle/ m\right) \qquad \text{Equation (6.10)}$$

$$\varepsilon_{S3} = \frac{H_{S3}}{L_{def}} = \frac{\sigma_0 - \sigma}{mL_{def}} \qquad \text{Equation (6.11)}$$

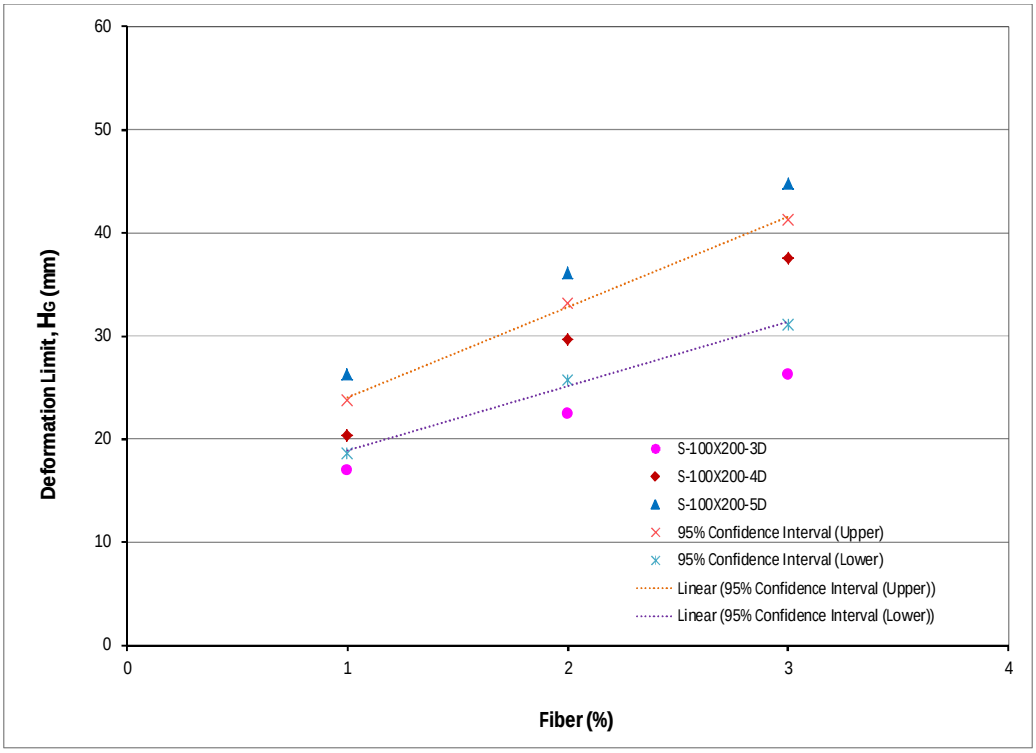

Fig.6.24 Derivation of limiting Stage 3 deformation for test series – 1 specimen

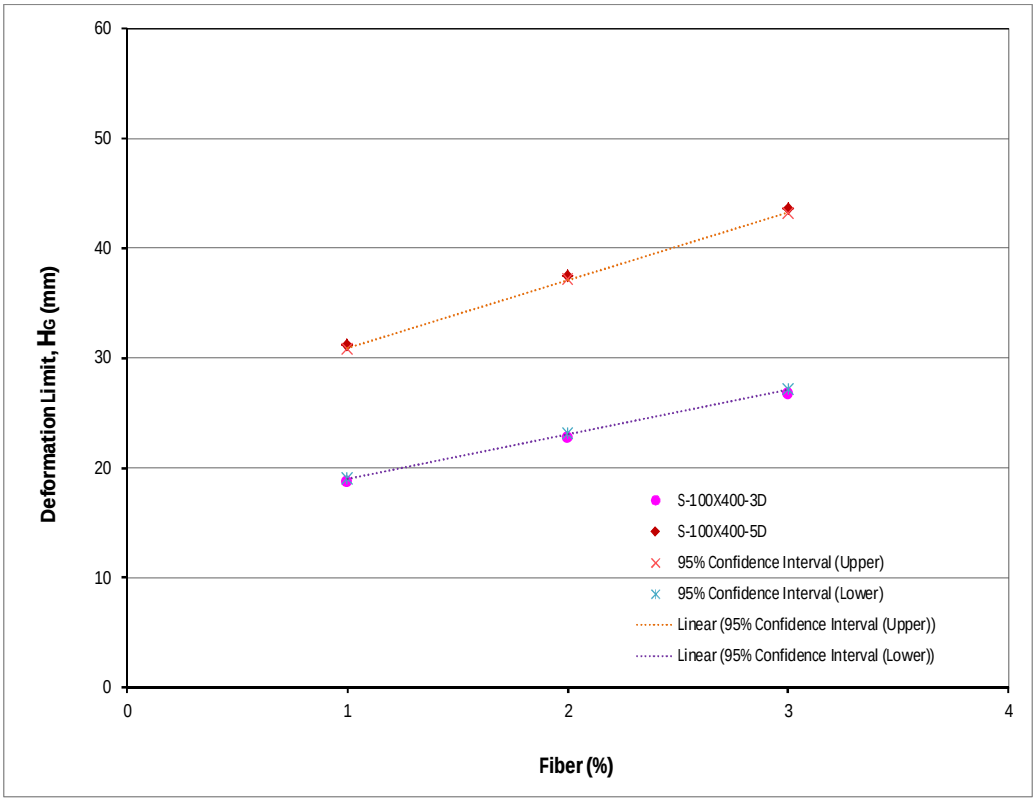

Fig.6.25 Derivation of limiting Stage 3 deformation for test series – 2 specimen

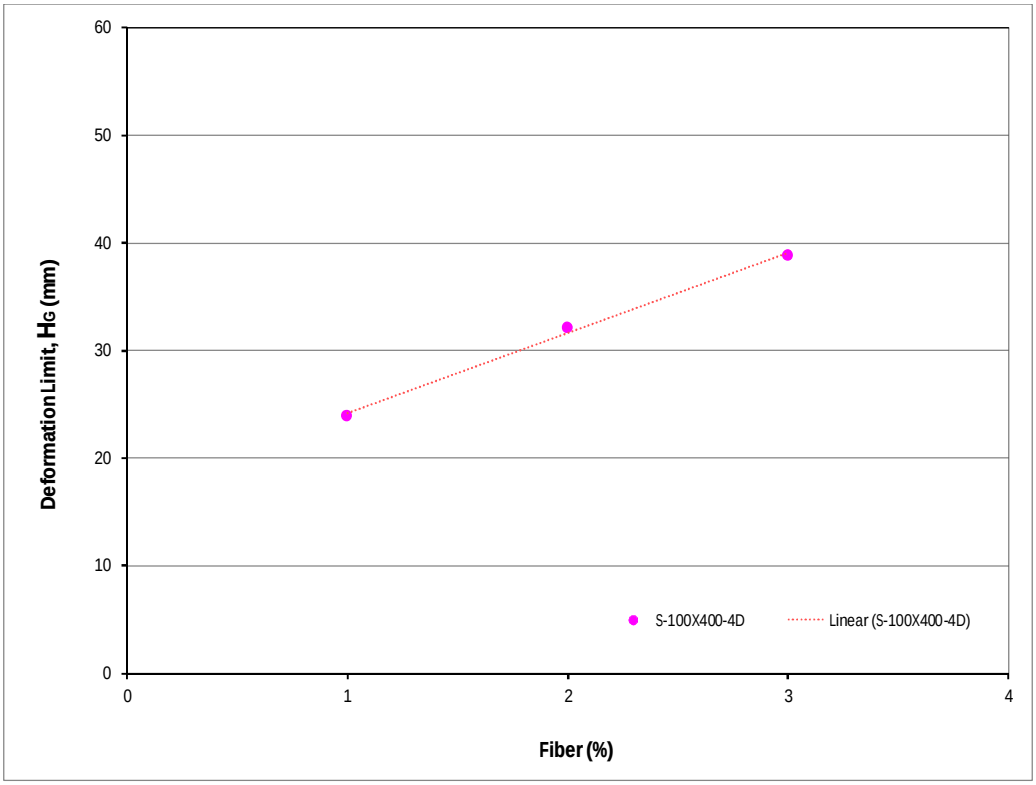

Fig.6.26 Derivation of limiting Stage 3 deformation for test series – 3 specimens

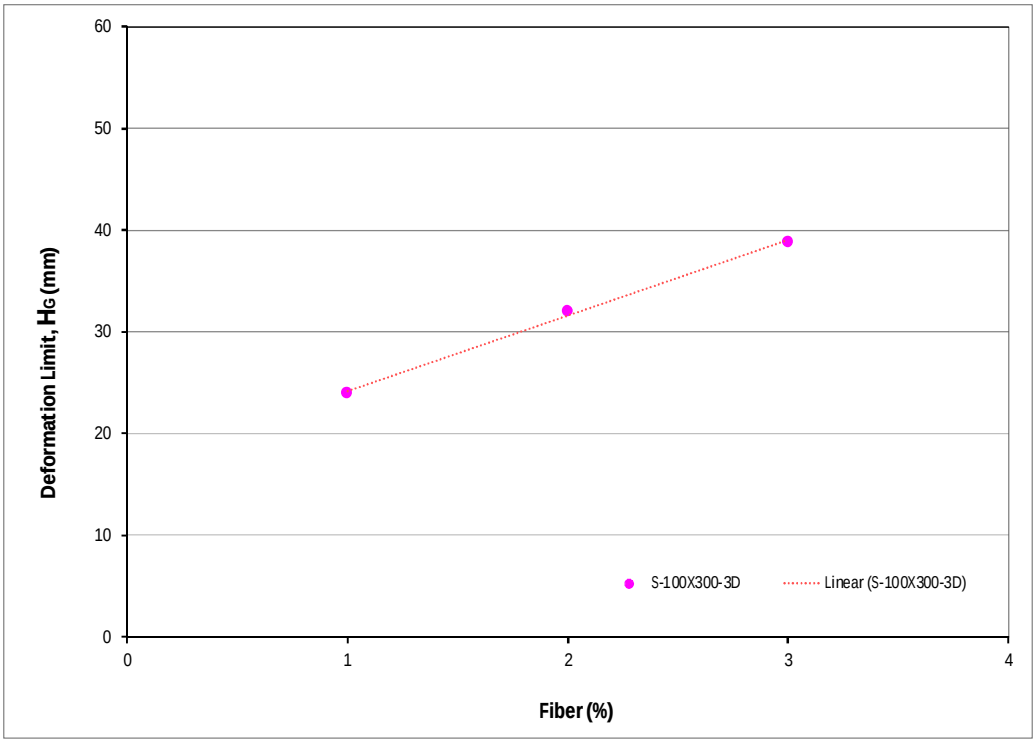

Fig.6.27 Derivation of limiting Stage 3 deformation for test series – 4 specimens

Eq. 6.9 can be rearranged as in Eq. 6.11 to get a Stage 3 stress-strain which you can see is size dependent and which can be used to derive the intercept D in Fig.6.4 and which has the limit at Point G. Point G can be derived from an analysis of the raw data as in Fig.6.24 to 6.27 where H_G is simply the prism deformation D in Fig.6.4. There may be a large scatter but a conservative value should be chosen

$$\sigma_0 - \sigma = \varepsilon_{S3} m L_{def} \qquad \text{Equation (6.12)}$$

$$\sigma = \sigma_0 - \varepsilon_{S3} m L_{def} \qquad \text{Equation (6.13)}$$

The variation in sliding K was quantified in terms through a regression analysis in the form

$$K = LV + M \qquad \text{Equation (6.14)}$$

Where I and J are defined for each series in Table 6.6

Table 6.6 Deformation Limit results for regression analysis

Specimen Series	L	M
S-100x200-3D	4.69	12.53
S-100x200-4D	8.61	11.96
S-100x200-5D	9.23	17.28
S-100x400-3D	4.00	14.73
S-100x400-5D	6.22	25.04
S-100x400-4D	5.16	21.376
S-100x300-4D	5.974	21.495

It can be seen from Table 6.6 that there is very little variation in the deformation limit of UHPFRC with differences in between the same size and different fibre type and volume, however it shows a variation when the size makes doubled. This is because of the ultimate failure stage of the specimen can be expected to have formed and thus there is variation of the fibres such that the deformation limit is mainly a function of the mortar and fiber together at stage 3 which in this case is identical for all test specimen. The ultimate failure or failure strength of the specimens are shown in Figs.6.28 to 6.31. The line represents the equation that corresponds to the fiber percentage and type.

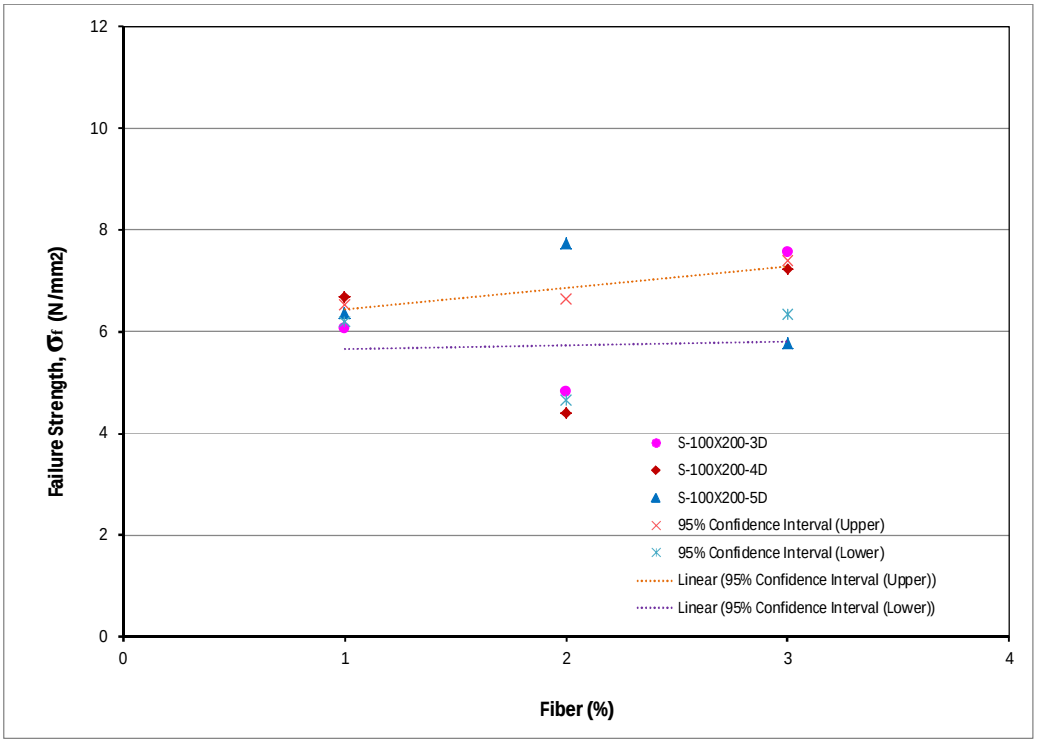

Fig.6.28 Failure strength determination of test series – 1 specimen

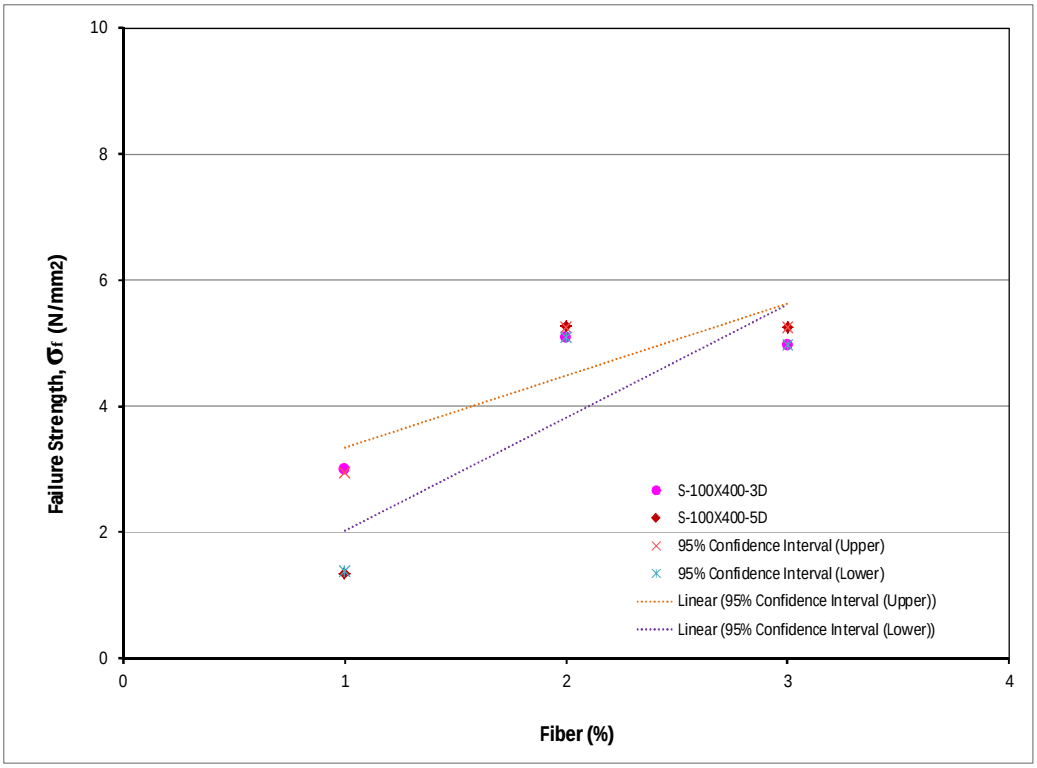

Fig.6.29 Failure strength determination of test series – 2 specimen

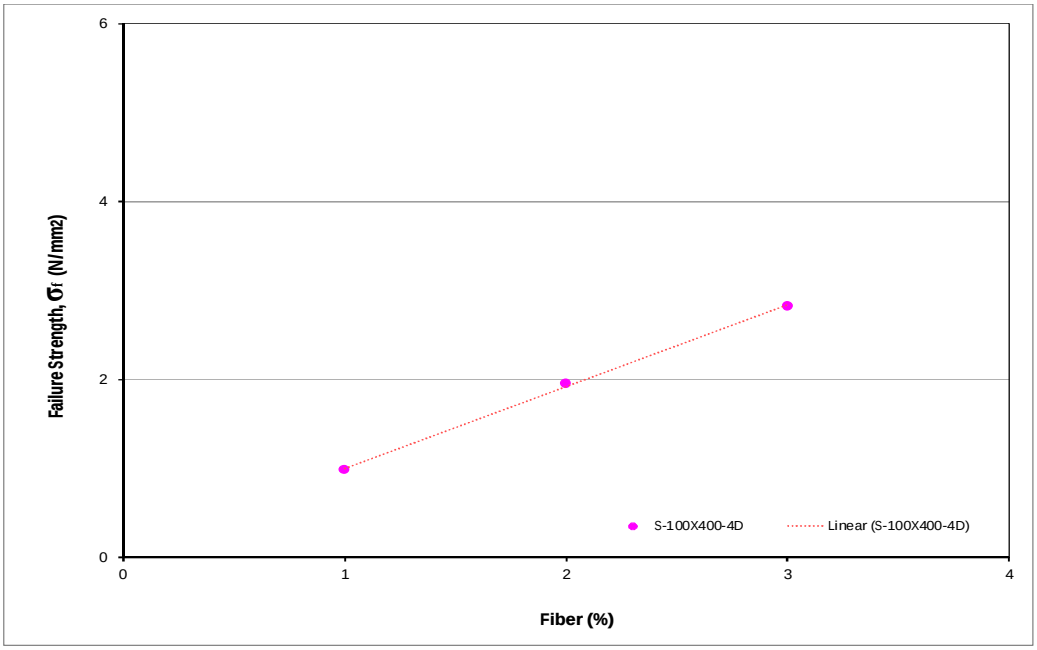

Fig.6.30 Failure strength determination of test series – 3 specimen

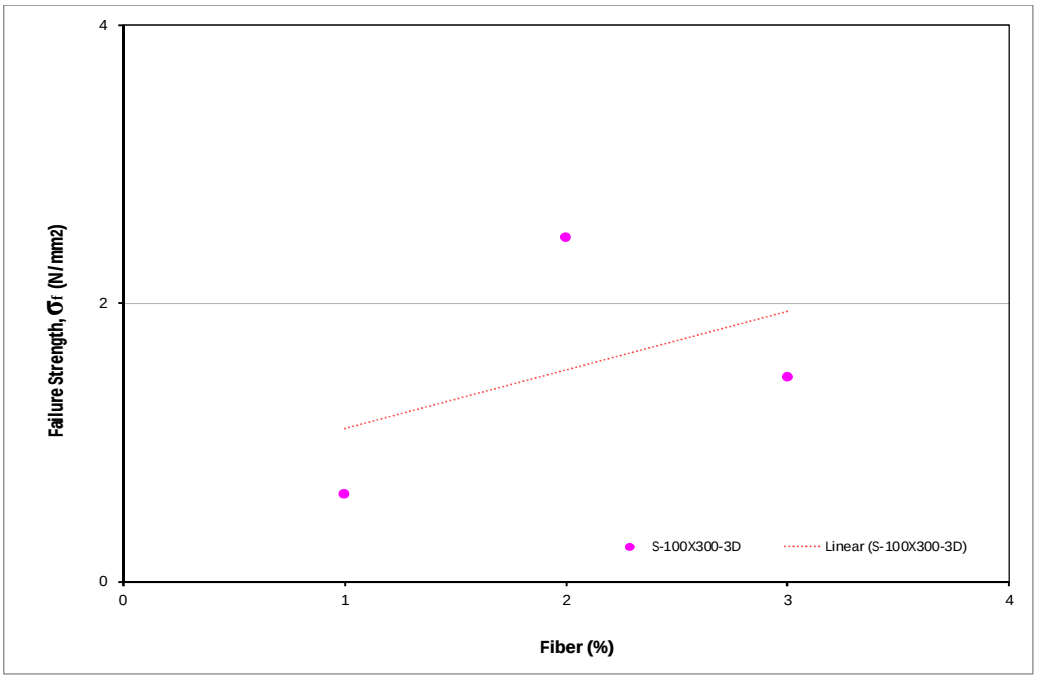

Fig.6.31 Failure strength determination of test series – 4 specimens

The variation in sliding N was quantified in terms through a regression analysis in the form

$$N = OV + P \qquad \text{Equation (6.15)}$$

Where O and P are defined for each series in Table 6.7

Table 6.7 Failure strength results for regression analysis

Specimen Series	O	P
S-100x200-3D	-0.292	4.64
S-100x200-4D	0.275	5.55
S-100x200-5D	0.757	7.20
S-100x400-3D	1.790	2.37
S-100x400-5D	0.986	0.237
S-100x400-4D	0.918	0.078
S-100x300-4D	0.420	0.684

Following the ultimate deformation limit, it can be observedfrom Table 6.7 that there is also very little variation in the failure strength of UHPFRC with differences in between the same size and different fibre type and volume, especially when the size of the specimen makes doubled. The larger the specimen size greater is the snap back observed during testing. This behaviour can be attributed due to the failure of the specimen and cannot bear any load by concrete and thus there is variation of the fibres such that the failure strength is mainly a function of the fiber at stage 3 from Fig. 6.4 which in this case is identical for all test specimens.

Having now determined the key points of the stress strain relationship in Figure 6.4, these can now be used to construct a stress-strain for a specific prism height L_{def}. Let us now consider how the size dependent stress strain relationship can be used in the analysis of the hinge region of a UHPFRC beam. The properties from the stress-strain curve of UHPFRC have been extracted and incorporated these properties into segmental moment-rotation numerical modelling to quantify the behaviours of UHPFRC beam including size effect for different fiber types and amount.

6.3 Segmental Moment-rotation (M/θ) Analysis

Conventional design and analysis techniques for reinforced concrete are strain based. Hence in order to quantify the rotation capacity of a plastic hinge the ultimate strain is multiplied by a hinge length (Oehlers et al., 2008a; Panagiotakos & Fardis, 2001; Visintin et al., 2012b) which is based on test observations.

The fundamental limitation to strain based approaches is that they do not simulate what is seen in practice (Daniell et al., 2008; Debernardi & Taliano, 2001). That is they assume full interaction between the reinforcement and the concrete and hence do not allow for the partial interaction or relative slip between the reinforcement and the concrete which controls: crack formation, crack widening, tension stiffening and additional deformations due to shrinkage. Furthermore the moment curvature approach cannot consider the formation and failure of concrete softening wedges, that is, they do not allow for the shear friction slip H in Figure 6.1.

Instead of directly quantifying the partial interaction (PI) mechanisms seen in practice strain based models rely on empiricisms such as empirical tension stiffening equations such as that of (Bischoff, 2001; Branson, 1977), empirical crack with formulations, and empirical hinge length equations(Corley, 1966; Panagiotakos & Fardis, 2001; Priestley & Park, 1987). Although now well-defined for standard reinforced concrete the development these empirical models are based on decades of testing at a material and member scale. Hence the repetitions of these test for each new material developed represent a large barrier to material development.

To address the shortcomings of strain based approaches a novel rigid body moment-rotation mechanism for reinforced concrete beam has been developed for quantifying hinge rotation (Haskett et al., 2009b). The moment-rotation approach directly quantifiestheslip between the reinforcement and concrete through partial-interaction (PI) structural mechanics and hence directly simulates the formation and widening of cracks and the formation of wedges and automatically allows for tension stiffening.

The approach will now be described in terms of a UHPFRC member. Consider the segment of a reinforced concrete beam of length of $2L_{def}$ in Fig.6.32 in which L_{def} is taken as the minimum of the half the primary crack spacing or the length of the

softening wedge (Visintin et al., 2012b). Let us also define the base line (A, B) and datum (E) for analysis. It is also noted that the prism under consideration is symmetric about the two cracks and hence only half the prism from A to E needs to be considered for analysis.

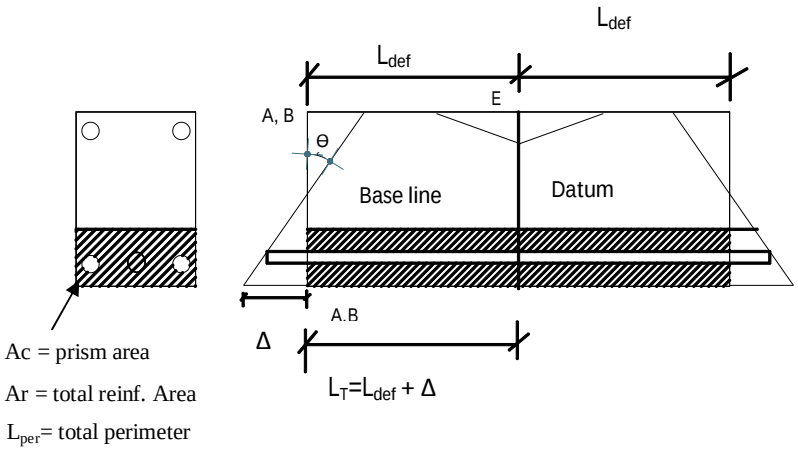

Fig.6.32 Segmental moment-rotation analysis for RC beams

6.3.1 Analysis method of segmental approach

The analysis is carried out to determine the moment (M) for a given imposed end rotation (θ) of a beams in Figure 6.33. For the given rotation the corresponding top fibre deformation (δ_{top}) is guessed thus defining the neutral axis depth (d_n).

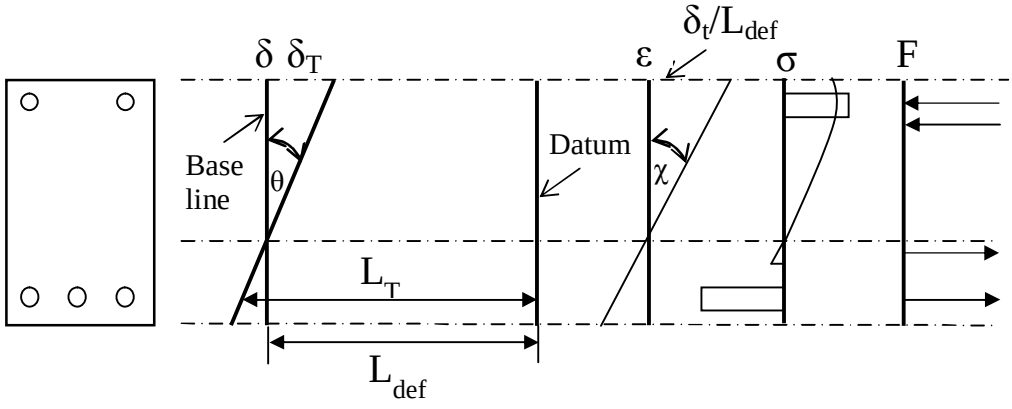

Fig.6.33 Segmental moment-rotation analysis for half section

In the uncracked region the deformation A-A to B-B in Figure 6.33 must be accommodated over the half segment length L_{def}, thus dividing the deformation A-A to B-B by L_{def} yields the effective strain (ε) in the uncracked region. Applying a size dependent stress strain (σ, ε) relationship where L_{def} is taken as the cylinder height the stress in Figure 6.33 and hence force (F) in the concrete in Figure 6.33 can be determined. It should be noted the same approach can be applied in the region where the concrete is in tension. For the tension reinforcement the slip of the reinforcement from the crack face Δ can be determined geometrically. If the analysis is focusing on the serviceability limit state the force in the reinforcement can be determined directly from the slip using well-established partial interaction theory (Oehlers et al., 2011; Seracino et al., 2002; Visintin et al., 2012b; Wu et al., 2002) which is based on the bond between the reinforcement and the concrete (Haskett et al., 2009a; Muhamad et al., 2011). When considering the ultimate hinge rotation in UHPFRC crack widths are typically very wide and hence tension stiffening plays a minor role and hence here tension stiffening is not explicitly allowed for. Thus dividing the reinforcement slip Δ by the deformation length L_{def} gives the strain in the reinforcement. Based on the constitutive stress strain relationship for the reinforcing bars the corresponding stress (σ) and hence force (F) in Figure 6.33 can be determined. Having defined the internal forces (F) in Figure 6.33 they can be summed to confirm if for the given guess δ_{top} equilibrium was achieved. If it was the moment corresponding to the rotation θ can be determined, if not the guess δ_{top} can be adjusted until equilibrium is obtained from the analysis.

A flow chart diagram summarising the application of the segmental moment rotation approach for UHPFRC is shown in Figure 6.34.

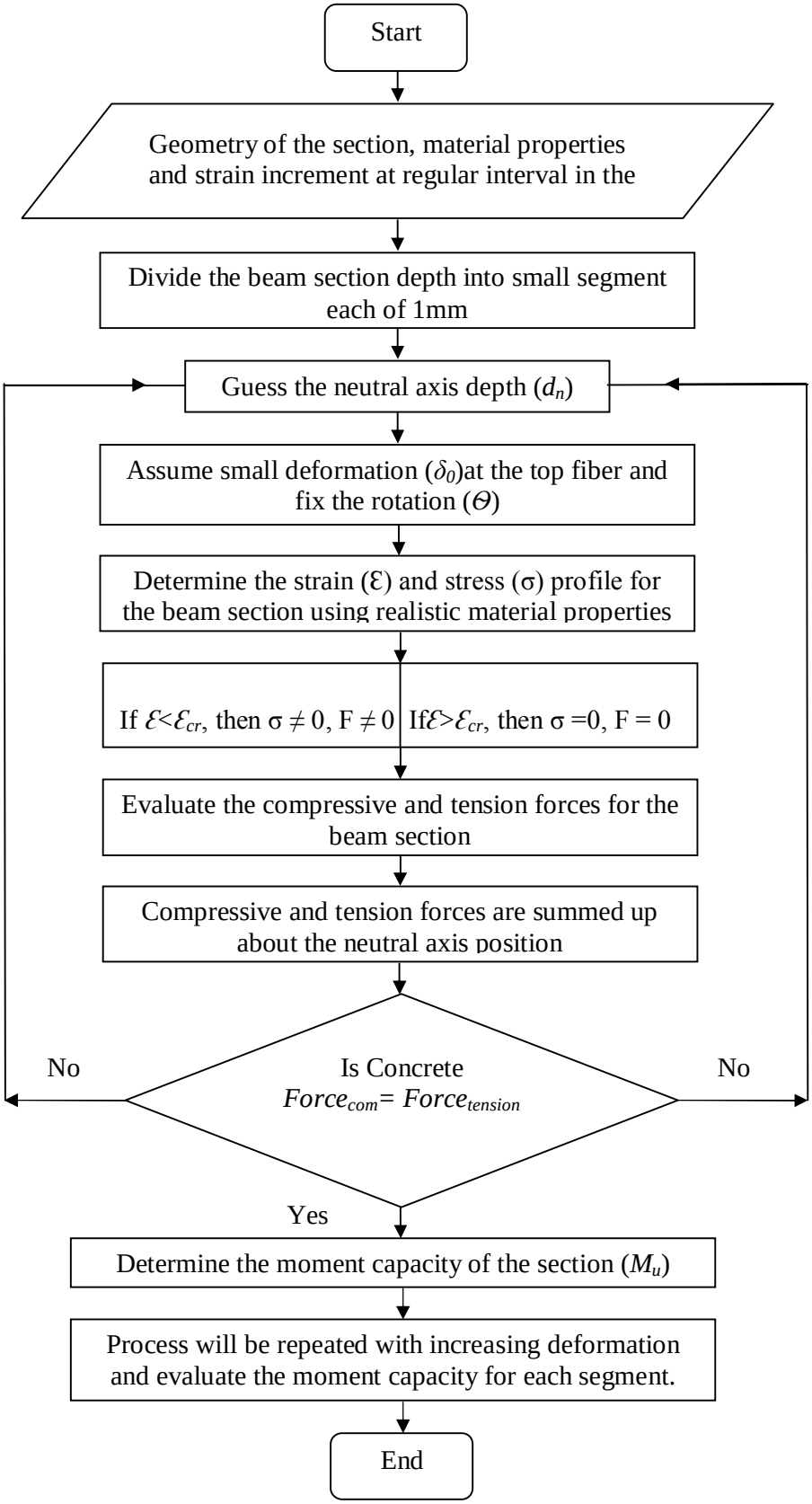

Fig.6.34 Flow chart diagram to perform the segmental analysis

6.3.2 Example of application of the segmental analysis for UHPFRC beams

The segmental moment-rotation approach has been incorporated with full range stress-strain behaviour of UHPFRC in order to quantify the behaviour of UHPFRC beams. As an example considered a UHPFRC beam of cross section 150x350mm with and effective depth of beam is 314mm and which is reinforced with 3-16mm diameter steel reinforcing bars at tension region and 2-10mm diameter bars in the compression region. The steel reinforcement is considered to be elastic-perfectly plastic condition and the yield strength of reinforcing steel is 450MPa for tension and compression region zone. Following the flowchart in Fig.6.34, the segmental analysis has been done incorporating the UHPFRC and steel reinforcement bar material properties into the numerical model to construct a moment-rotation plots. In the following analysis the influence of different fibre type and volume of UHPFRC is considered to quantify the rotation capacity of reinforced UHPFRC beam element.

6.3.2.1 Influence of specimen size on moment-rotation (M/θ) response of UHPFRC beams

The moment-rotation responses of UHPFRC beams incorporating the material properties of 100x200mm, 100x300mm and 100x400mm prisms with fiber volume fractions of 0, 1, 2, and 3% are quantified as shown in Fig.6.35 to Fig.6.38 for different types of fiber. The rotation capacity of UHPFRC beams was obtained by performing segmental analysis along with numerical modelling. It is interesting to mention from all Figures that an increasing the size or increase the slenderness of the specimens, the UHPFRC beams shows a snap back or more brittle nature and the size effect is clearly observed from Fig.6.35 to Fig.6.38. The analysis appears same shape of graph generated over the entire range of behaviours due to the influence of size, volume fraction of fiber and type, especially 3D and 4D fiber specimens when the slenderness ratio make it doubled. The size effects of the beams are observed in

terms of moment, rotation and ductility response. It is also noticed from Fig.6.35 to Fig.6.38 that the rotation decreases as the specimen size or slenderness of the specimen increases. It is obvious that the highest rotation capacity of beams exhibits due to 5D fibers when the slenderness ratio is considered 2; however the quite similar rotation capacity of beam observed for 3D and 4D fiber specimens. This behaviour attributed to the highest deformation capacity of 5D fibers that measured from the compressive stress-strain curves. With fiber volume-fraction 1 and 3%, a 62.5% and 53.7% decrease the rotation capacity was observed when doubling the specimen size for 3D fiber with slenderness ratio (*l/d =2*), 61.7% and 60% decreased rotation for 4D fiber with slenderness ratio (*l/d =2*), 53.7% and 50.7% decreased rotation for 4D fiber with slenderness ratio (*l/d =4*) and 78%, and 72% decreased rotation for 5D fibers (*l/d =4*). It is important to mention that the ultimate moment capacity is quiet similar for all type of fiber content and types of specimen.

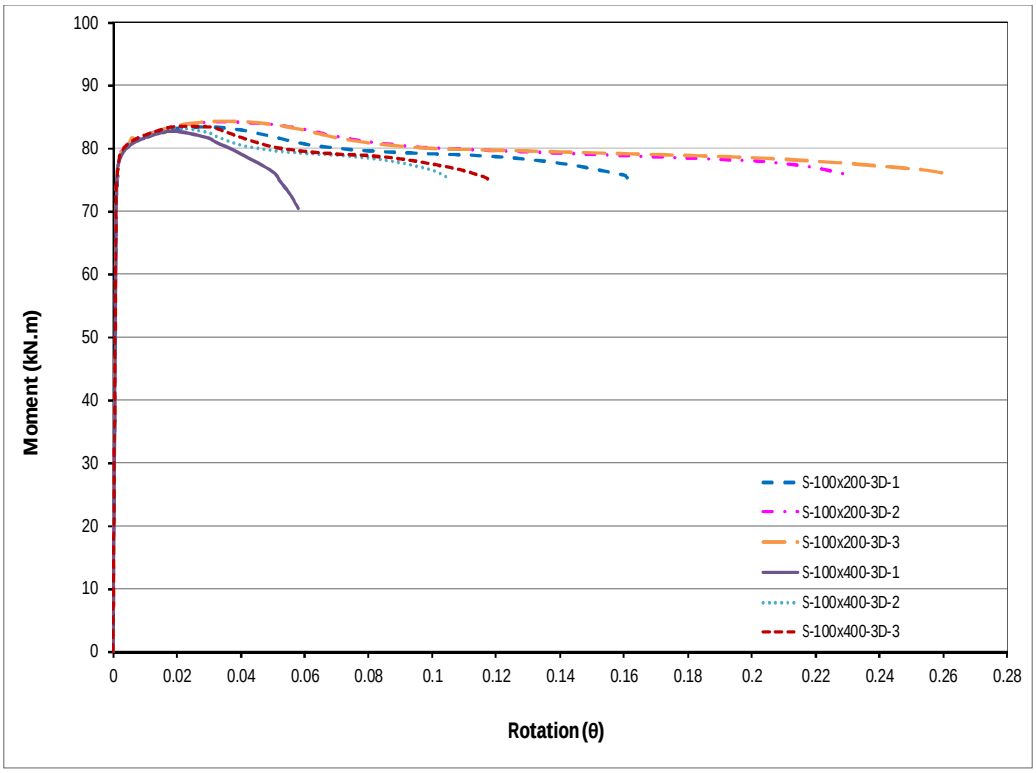

Fig.6.35 Influence of size on M/θ response of UHPFRC beams with 3D fiber

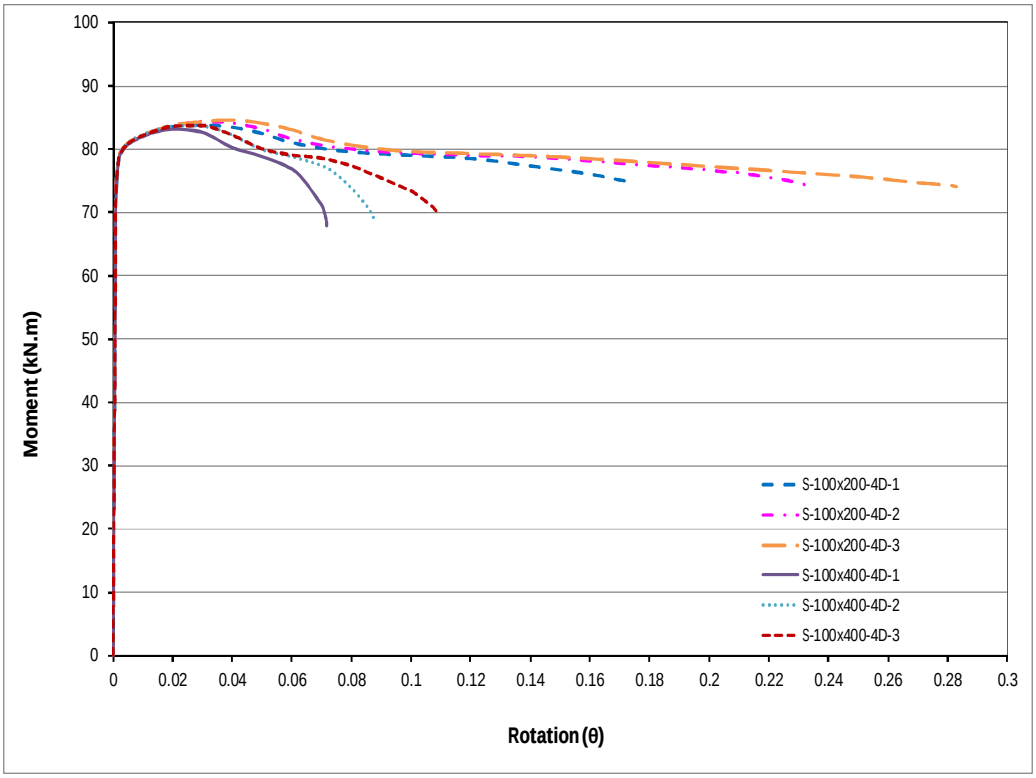

Fig.6.36 Influence of size on M/θ response of UHPFRC beams with 4D fiber

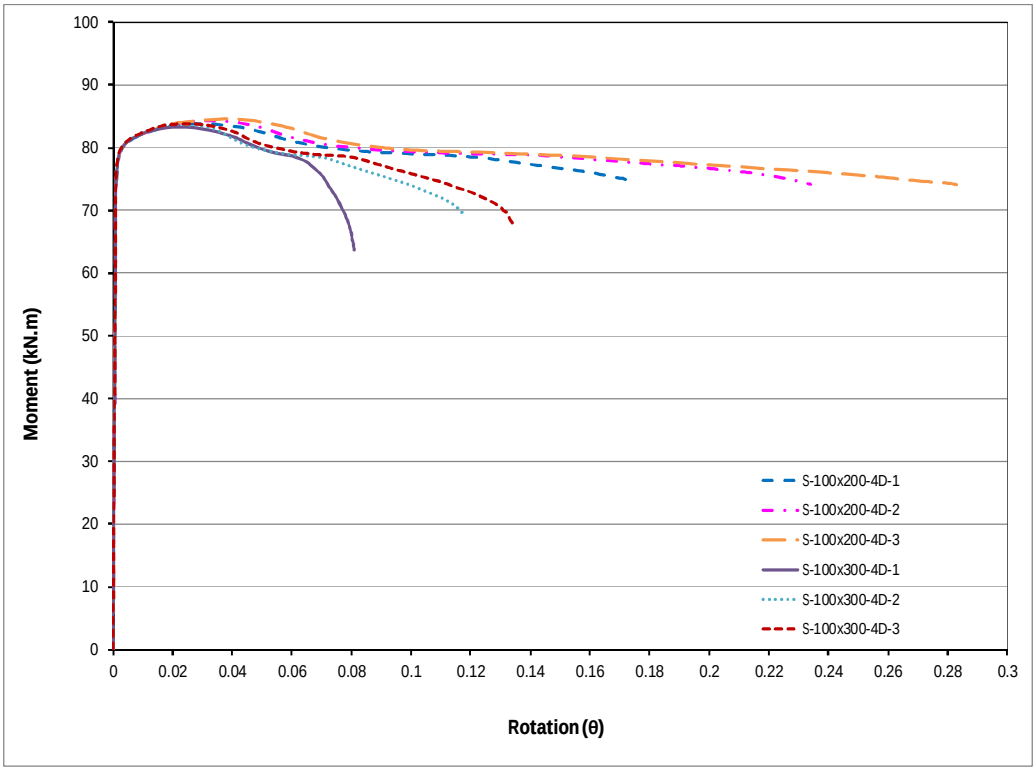

Fig.6.37 Influence of size on M/θ response of UHPFRC beams with 4D fiber

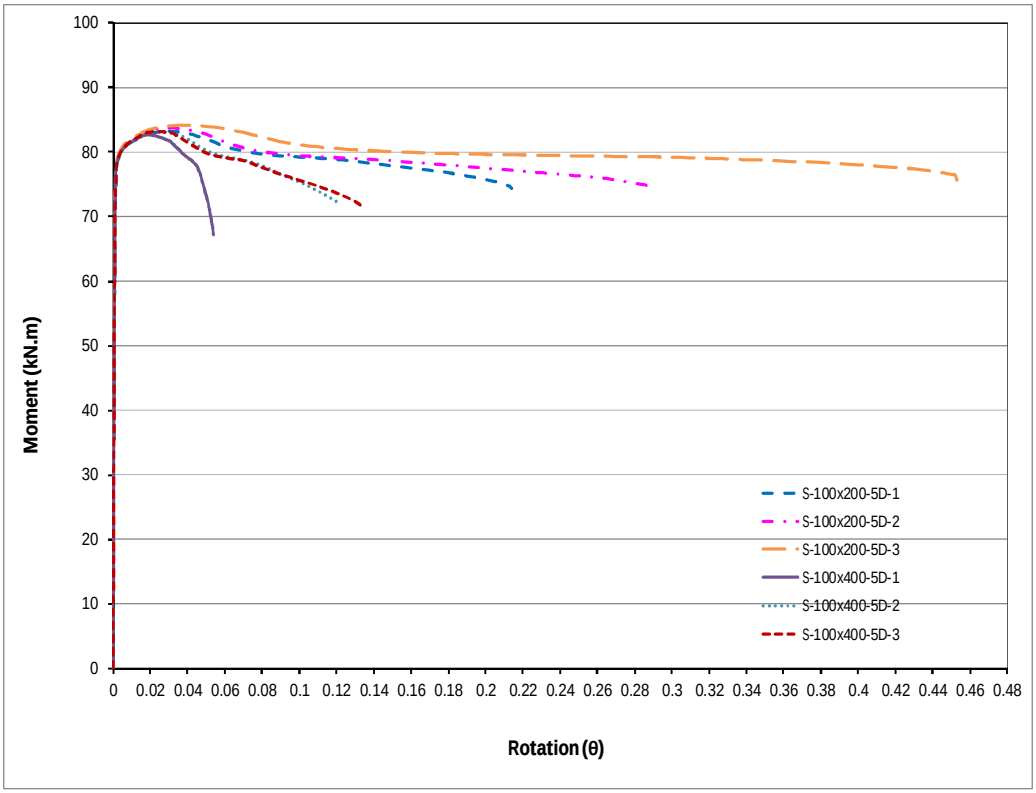

Fig.6.38 Influence of size on M/θ response of UHPFRC beams with 5D fiber

6.3.2.2 Influence of fiber on moment-rotation (M/θ) response of UHPFRC beams

The moment-rotation responses of UHPFRC beams incorporating the stress-strain material properties of 100x200mm, 100x300mm and 100x400mm prisms specimens with fiber volume fractions of 0, 1, 2, and 3% are depicted in Fig.6.39 to Fig.6.44 for 3D, 4D and 5D fibers. It is observed from Figures.6.39 and 6.44 that the amount of fiber content significantly affects the ductility behaviour of UHPFRC beams, especially it is more obvious for 2% and 3% fiber specimens with slenderness 2 and 4 when comparing 3D, 4D and 5D fiber. It is also noticed that lowest fiber content (1%) beams exhibits lowest rotation capacity particularly when the corresponding slenderness ratio is reached at 4. This characteristic is attributed to the smallest deformation obtained from the compressive stress-strain test and the opposite phenomenon is true when higher fiber content considered and these behaviours is

directly correspond the ductility response of beams. It is observed from the Figures that the peak moment capacities of beams are quite similar shape and value for fiber amount and type. It is also demonstrate the accuracy of the segmental analysis.

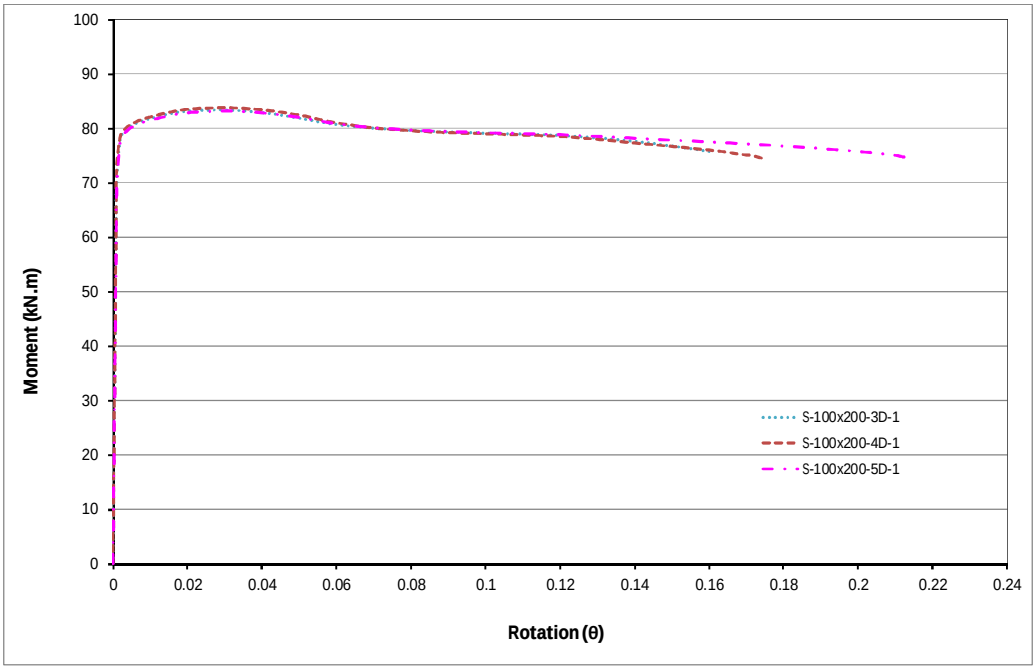

Fig.6.39 Influence of fiber on M/θ response of UHPFRC beams with 1% fiber

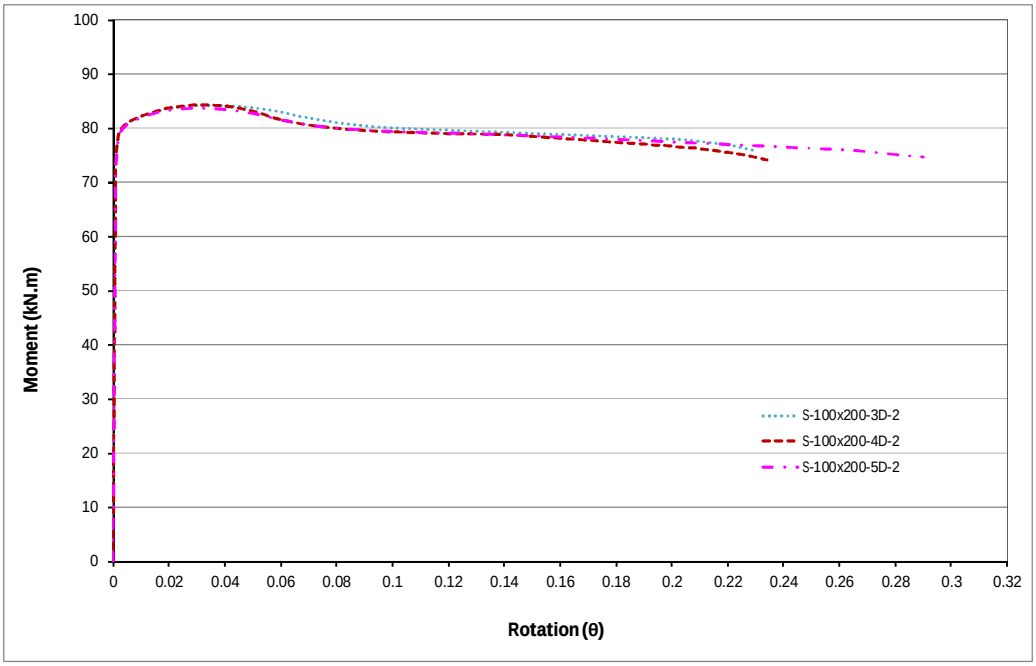

Fig.6.40 Influence of fiber on M/θ response of UHPFRC beams with 2% fiber

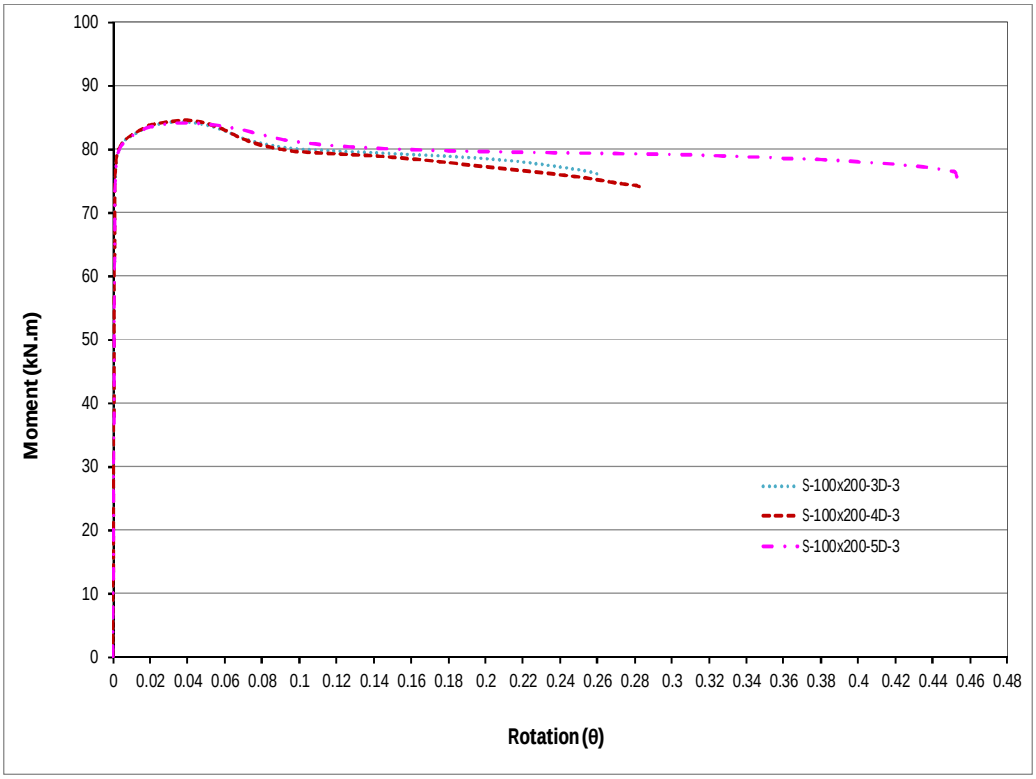

Fig.6.41 Influence of fiber M/θ response of UHPFRC beams with 3% fiber

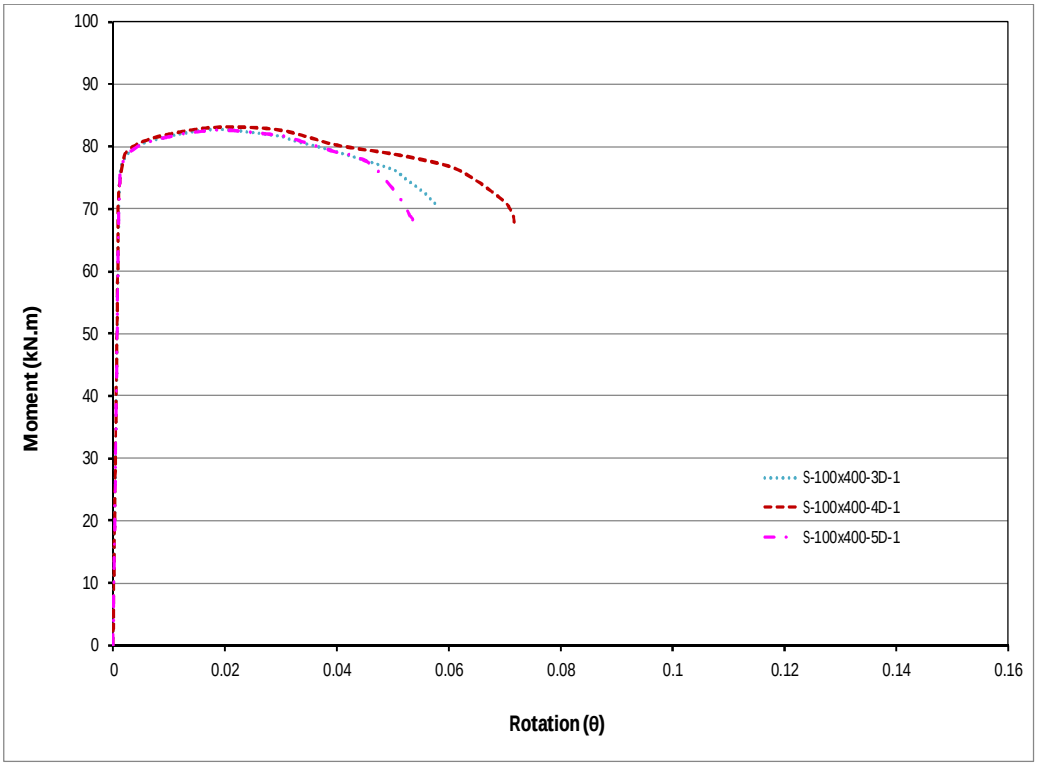

Fig.6.42 Influence of fiber on M/θ response of UHPFRC beams with 1% fiber

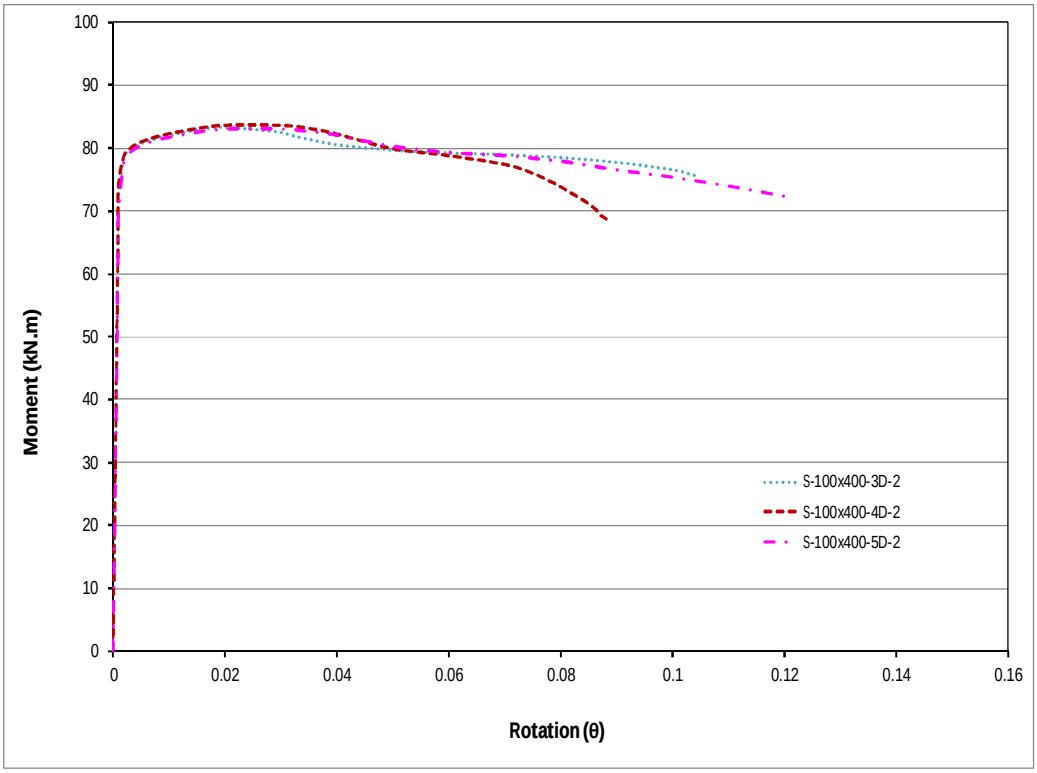

Fig.6.43 Influence of fiber on M/θ response of UHPFRC beams with 2% fiber

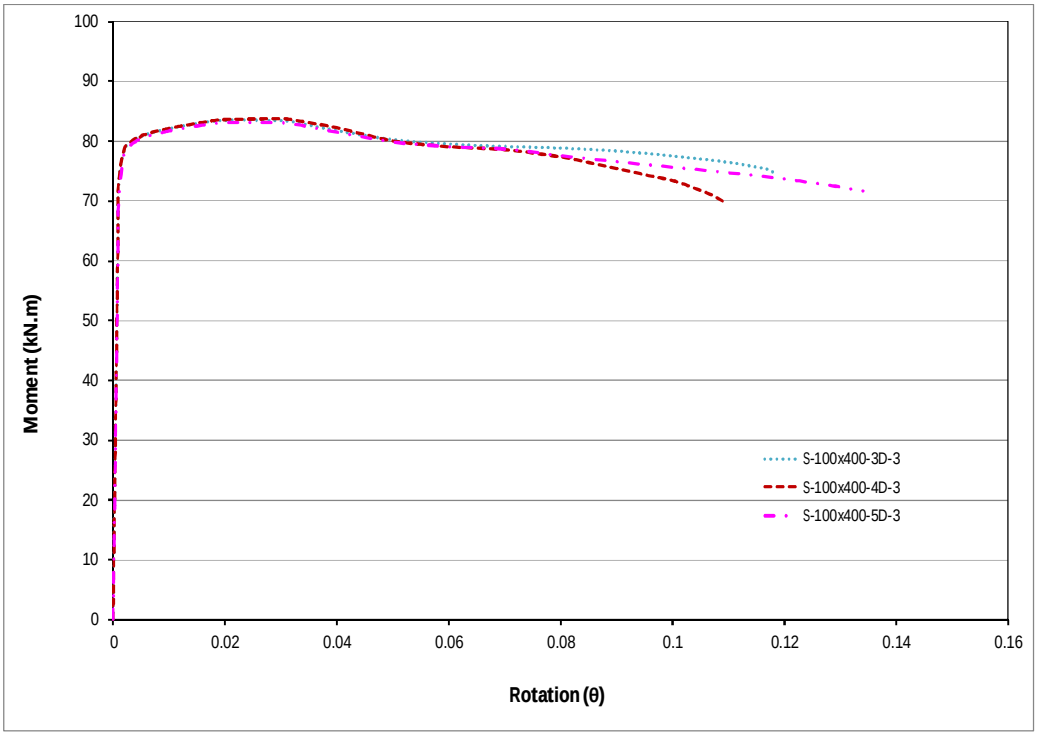

Fig.6.44 Influence of fiber on M/θ response of UHPFRC beams with 3% fiber

6.4 Summary

The major conclusions can be drawn from the segmental moment-rotation (M/θ) analysis of UHPFRC beam with different fiber content and types:

First, an experimental study was carried out to quantify the influence of member size and shape on the ductility of UHPFRC with a wide range of fibre types and volume fractions. After that, quantified the size dependent stress strain relationship for UHPFRC from these experimental results and how this relationship could be incorporated into the segmental moment rotation approach in order to analyse the UHPFRC beam hinges.

From the segmental moment-rotation (M/θ) analysis, it can be seen that quantifying the behaviours of RC beams with different fiber type and content is appropriate. The rotation capacity of RC beams was observed to increase as fiber content increased, however it decreased when the material specimen size doubled. In this study, the tension stiffening did not allow for the analysis because ultimate hinge rotation in UHPFRC crack widths are typically very wide, however it can be good approach to check the behaviour of RC beams with tension stiffening effect.

CHAPTER 7

CONCLUSIONS AND RECOMMENDATIONS

7.1 General Remarks

The research presented in this thesis covers the development and analysis of ultra-high performance fiber reinforced concrete (UHPFRC) from mix design to material and member behaviour at structural level.

The major outcomes of this research are: (i) the development of UHPFRC utilising conventional materials and production methods; (ii) the quantification of a size dependent stress strain relationship for UHPFRC; and (iii) the extension of a numerical segmental moment-rotation approach to allow for the simulation of flexural ductility of reinforced UHPFRC beams incorporating the compressive material properties including size effect responses from (i) and (ii).

7.2 Manufacturing and Production Methods of UHPFRC

Ultra-high performance fiber reinforced concrete has the potential to revolutionise the construction industry because of its superior strength and ductility behaviours. Conventionally UHPFRC is produced with specially graded fine aggregates and utilises specialist technique for mix design and preparation. The use of these specialist materials and sophisticated manufacturing procedures increases the cost of UHPFRC production and therefore limits its use in practice. Therefore, it is of great interest to obtain a UHPFRC of similar strength and workability using conventional materials and methods such that the cost of production is reduced.

In this research it was shown that UHPFRC could be manufactured with conventional materials and preparation techniques and without the need to specialist curing. The test results indicated that adequate compressive strength and workability was achieved such that the materials proposed could be used in practice.

Based on the experimental results and observations of the mix design portion of this research the following specific conclusions can be drawn:

1. UHPFRC with strengths and secant stiffness in the ranges of 130-160MPa and 34000-42000MPa respectively can be produced with conventional mixing and curing regimes by utilising conventional natural and manufactured fine aggregates, including granulated slag. The mix designs developed showed very good workability and the influence of superplasticizer (SP) content on mix rheology was quantified. The slump and j-ring spread were achieved in the ranges of 258-783mm, and 190-770mm and 193-678mm and 183-628 without and with fiber respectively.

2. It has been proven from the experimental results and observations that there exists a strong inverse correlation between the fineness modulus of the fine aggregate and the compressive strength and this relationship is independent of the total water to cement ratio and the SP ratio.

3. It can be observed that the compressive strength can be related to the sp:c/FM which is not sensitive to the w:c ratio. This behaviour is attributed to the reduction in entrained air as the sp:c increases which in turn leads to a reduction of air voids and therefore an increase in concrete density.

4. A strength reduction observed due to the shrinkage micro cracks formed between 56 and 90 days mixes both with and without coarse aggregate. Further study is required to quantify the extent of this strength decrement and it is suggested that for concretes with a high cement ratio such as UHPFRC that the 28 day strength may not be an adequate representation of strength for use in structural design.

5. The addition of a small quantity of coarse aggregate where the ratio of coarse aggregate to fine aggregate (CA:FA) is less than 0.5 does not lead to a reduction in workability or strength suggesting that the economy of the mix can be improved through coarse aggregate addition.

6. The addition of coarse aggregate at ratios of CA:FA in the ratios of between 0.33 and 1.00 leads to a reduction in 90 day strength of between 0 and 7% and a reduction in slump flow of up to 55%. Both the reduction in strength and the reduction in workability have been quantified over a wide range of CA:FA ratio that is from 0 to 3.

7. The compressive strength of UHPFRC was achieved with expensive silica sand in the range of 90MPa to 162MPa to the corresponding test age 7 to 90 days. The results indicate that the UHPFRC with conventional fine aggregate shows quiet similar compressive strength and so it could be a good low cost alternative fine aggregate for the production of UHPFRC.

8. The compressive strength obtained in the range of 140MPa to 151MPa and 144 MPa to 149MPa for expensive silica sand and manufactured sand with heat cured respectively; for test days 7 to 90 days. Heat curing was shown to increase the 7 day strength to on average 94% of ultimate strength. Further it was found that the increase in early age strength was independent of sand type.

9. The axial and lateral stress-strain relationship for 27 mixes using a range of sand types and both with and without coarse aggregate were presented and from these a generic axial and lateral stress-strain relationship is proposed. It was found that the ascending region of the stress strain relationship was similar for all types of aggregate; however there was significant scatter in the post peak behaviour.

10. An investigation of the lateral stress strain behaviour found that the lateral deformation is on average 60-73% smaller than then axial deformation for all of the UHPFRC mixes. In general, theoretical axial and lateral stress-strain curves developed gave a reasonable prediction of the experimental results.

7.3 Size Effect and Ductility Responses of UHPFRC

The stress strain material properties and ductility of any type of concrete are known to depend on both the size and the geometry of the sample tested. Hence in the second part of the research presented an experimental study was undertaken to quantify the influence of member size and shape on the ductility of UHPFRC with a wide range of fibre types and volume fractions. It was then shown how the results could be used to develop a size dependent stress strain relationship for UHPFRC and how this relationship could be incorporated into the segmental moment-rotation approach in order to analyse the UHPFRC beam hinges. The major conclusions drawn from the second phase of this research are:

1. The contribution of different steel fiber type and amount on the strength and ductility responses of UHPFRC is distinctly proven through experimental investigation.

2. The post-peak responses of stress-strain curves with different steel fiber and types are dependent on the size of specimen. It was shown that doubling the height of the specimen tested significantly reduced the ductility of UHPFRC and that this behaviour was dependent on both fibre volume fraction and fibre type. For example, mixes with a fiber volume-fraction of 1 and 3% resulted in a 44.76% and 49.2% decrease of deformation capacity as specimen height was doubled. Similarly a reduction of 35%, 51% and 51.2% was observed when fibre type was changed from 3D to 4D and to 5D respectively.

3. When the specimen sizes doubled (*l/d =2 to l/d =4)* the compressive strength decreased on average 7-8.5% for 3D, 4D and 5D fiber with the addition of 1% to 3% fibres in the mixes. This change is considered to be within sampling variation considering the small sample size of tests and hence the influence of specimen size on the strength of UHPFRC is considered to be negligible.

4. The amount of fiber and types significantly affects the softening behaviours of UHPFRC specimens. For each type of fibers, it has been shown that increasing the fiber content leads to improved ductility. It is also found that the longest fiber (5D) exhibited highest deformation of about 19% and 70% more than 4D and 3D fibers for fiber volume fraction 3%, however it attain lower peak strength then other fibers type.

5. Crack patterns observed during testing were found to be influenced by the shape of the specimens. A single failure plane was initiated on the cylinder surfaces from the mid height; however the rectangular prism single failure plane observed from top to bottom height of the specimen and spalled the concrete on both surfaces of prism. This behaviour is more significant with higher fiber content specimens.

6. The numerical simulation following the segmental moment-rotation (M/θ) approach with incorporating UHPFRC material properties is suitable for predicting behaviours of RC beams with different fiber type and content.

7. The rotation capacity of RC beams was observed to increase as fiber content increased; however it decreased when the material specimen size doubled. When comparing the 100x200mm to100x400mm specimens, a 62.5% and 53.7% decrease the rotation capacity was found for 3D fiber, 61.7% and 60% decreased rotation for 4D fiber, 53.7% and 50.7% decreased rotation for 4D fiber100x300 specimen and 78%, and 72% decreased rotation for 5D fibers for fiber volume-fraction 1 and 3% respectively. It is also noticed that the ultimate moment capacity of RC beams is quiet similar for all types of fiber content and types.

7.4 Recommendations for Future Work

Although lot of research has been conducted on the UHPFRC, is required to obtain a better understanding the material and structural level performance. Based on the experimental results and numerical simulation of this research the following changes in the variables are recommended as a possible future extension of this work:

1. The influence conventional fine aggregate on the workability and strength of UHPFRC with different fineness modulus has been conducted in this research. To reduce the cost of UHPFRC production, alternative coarse or fine aggregate such as recycled glass, and different grading of conventional fine aggregate could be a potential option to prepare environmental friendly UHPFRC.

2. The test results proven that SP and binder content are the most critical components in the UHPFRC mix, these affects the workability and the strength.

The influence of SP dosage for mixes with different proportions of and silica fume and cement is of great interest as this information would allow for the development of a mix design guideline.

3. UHPFRC properties have been carried out with industrial waste material granulated led smelter slag in this research. However, it would be a great concern to produce moderate strength UHPFRC utilising industrial by-product such as rich husk, oil palm shell and other copper slag leading to a reduction in the environmental impact of manufacture.

4. The present study has investigated the workability and compressive properties of UHPFRC with coarse aggregate particle size of 10mm and it decreased the strength between 56 and 90 days test specimen. Further study is required to quantify the extent of this strength decrement with smaller varies particle size to achieve more homogeneity concrete mix and it is suggested that for concretes with a high cement ratio such as UHPFRC that the 28 day strength may not be an adequate representation of strength for use in structural design.

5. A large-volume of experimental work is required in the structural level to understand fully of UHPFRC members including flexural and time-dependent behaviour under various loading conditions (such as sustained loads) and environmental exposures (such as freeze thaw, temperature, heat treatment). Due to high strength of UHPFRC, creep and shrinkage effect can be investigated in the material and structural level.

6. Segmental moment-rotation (M/θ) approach did not allow the tension stiffening to perform the analysis of UHPFRC beams. To allow the tension stiffening with partial-interaction analysis that is slip between the reinforcement and the concrete

will provide better quantifying moment-rotation behaviour that determines the structural response including formation of single and multiple crack and wedge formation. Creep and shrinkage effect could be included into the moment-rotation approach to quantifying the response of UHPFRC members.

REFERENCES

Acker, P., & Behloul, M. (2004). Ductal® technology: A large spectrum of properties, a wide range of applications. *Proc. of the Int. Symp. on UHPC Kassel, Germany*, pp. 11-23.

ACI-211.1. (reapproved in 2002). Standard Practice for Selecting Proportions for Normal, Heavyweight, and Mass Concrete (ACI 211.1–91). *American Concrete Institute.*

AFGC/SETRA. (2002). Ultra High Performance Fibre-Reinforced Concrete–Interim Recommendations. *Report, Association Française de Génie Civil, Paris, France*.

Ahmad, S., Hakeem, I., & Maslehuddin, M. (2014). Development of UHPC Mixtures Utilizing Natural and Industrial Waste Materials as Partial Replacements of Silica Fume and Sand. *The Scientific World Journal 2014*, 8.

Aignesberger, A., & Kern, A. (1981). Use of Melamine-Based Super-plasticizer as a Water Reducer. *ACI Special Publication 68*.

Al-Jubory, N.H. (2013). Mechanical Properties of Reactive Powder Concrete (RPC) with Mineral Admixture. *Al-Rafadain Engineering Journal 21(5)*.

Al-Jabri, K.S., Hisada, M., Al-Saidy, A.H., & Al-Oraimi, S.K. (2009). Performance of high strength concrete made with copper slag as a fine aggregate. *Construction and Building Materials 23(6)*, 2132-2140.

Al Madhoun, A.T. Mechanical Properties of Ultra High Performance Fiber Reinforced Self-Compacting Concrete. In.: The Islamic University of Gaza.

Alford, N.M., & Birchall, J.D. (1985). The Properties and Potential Applications of Macro-Defect-Free Cement. *MRS Online Proceedings Library Archive 42*, null-null.

Allena, S., & Newtson, C.M. (2011). Ultra-high strength concrete mixtures using local materials. *Journal of Civil Engineering and Architecture 5(4)*, 322-330.

Ambily, P., Umarani, C., Ravisankar, K., Prem, P.R., Bharatkumar, B., & Iyer, N.R. (2015). Studies on ultra high performance concrete incorporating copper slag as fine aggregate. *Construction and Building Materials 77*, 233-240.

AS-3972. (2010). General purpose and blended cements. *Australian Standard 3972-2010*.

Askar, L.K., Tayeh, B.A., & Bakar, B.A. (2012). Effect of different curing conditions on the mechanical properties of UHPFC. *Awam International Conference on Civil Engineering (AICCE'12) and Geohazard Information Zonation (GIZ'12)*, pp. 28-30.

Attard, M., & Setunge, S. (1996). Stress-strain relationship of confined and unconfined concrete. *ACI Materials Journal 93(5)*.

AS/NZS-2350.11:06. (2006). Methods for testing Portland, blended and masonry cements-compressive strength. In. Sydney Standards Australia.

AS/NZS-2350.13:06. (2006). Methods for testing Portland, blended and masonry cements – determination of drying shrinkage of cement mortars. In. Sydney Standards Australia.

ASTM-C469-94. (1994). Standard Test Method for Static Modulus of Elasticity and Poisson's Ratio of Concrete in Compression. In. West Conshohocken, PA: ASTM International.

ASTM-C39/C39M-12. (2012). Standard Test Method for Compressive Strength of Cylindrical Concrete Specimens. In. West Conshohocken, PA: ASTM International.

ASTM-C143/C143M-12. (2012). Standard Test Method for Slump of Hydraulic-Cement Concrete. In. West Conshohocken, PA: ASTM International.

ASTM-C1611/C1611M-09b. (2009). Standard Test Method for Slump Flow of Self-Consolidating Concrete. In. West Conshohocken, PA: ASTM International.

ASTM-C1621/C1621M-09a. (2009). Standard Test Method for Passing Ability of Self-Consolidating Concrete by J-Ring. In. West Conshohocken, PA: ASTM International.

Austin, S., Robins, P., & Issaad, A. (1992). Influence of curing methods on the strength and permeability of GGBFS concrete in a simulated arid climate. *Cement and Concrete Composites 14(3)*, 157-167.

ASTM-C1611/C1611M-09b. (2009). Standard Test Method for Slump Flow of Self-Consolidating Concrete. In. West Conshohocken, PA: ASTM International.

ASTM-C1621/C1621M-09a. (2009). Standard Test Method for Passing Ability of Self-Consolidating Concrete by J-Ring. In. West Conshohocken, PA: ASTM International.

ASTM-C31/C31M-12. (2012). Standard Practice for Making and Curing Concrete Test Specimens in the Field. In. West Conshohocken, PA,: ASTM International.

ASTM-C39/C39M-12. (2012). Standard Test Method for Compressive Strength of Cylindrical Concrete Specimens. In. West Conshohocken, PA: ASTM International.

ASTM-C143/C143M-12. (2012). Standard Test Method for Slump of Hydraulic-Cement Concrete. In. West Conshohocken, PA: ASTM International.

Australia, S. (1999). Methods of testing concrete–determination of the compressive strength of concrete specimens. In.: AS.

Batoz, J.-F., & Behloul, M. (2009). UHPFRC development on the last two decades: an overview. *France: Marseille, UHPFRC conference*.

Bache, H.H. (1987). Introduction to compact reinforced composite. *Nordic concrete research (6)*, 19-33.

Basile, F., Biagini, S., Ferrari, G., & Collepardi, M. (1989). Influence of Different Sulfonated Naphthalene Polymers on the Fluidity of Cement Paste. *ACI Special Publication 119*.

Bigaj, A., & Walraven, J. (2002). Size effects in plastic hinges of reinforced concrete members. *Heron, Vol. 47 (2002) No. 2, pp. 79-80*. Delft University of Technology.

Birchall, J., Howard, A., & Kendall, K. (1981). Flexural strength and porosity of cements.

Bischoff, P.H. (2001). Effects of shrinkage on tension stiffening and cracking in reinforced concrete. *Canadian Journal of Civil Engineering 28(3)*, 363-374.

Bonneau, O., Lachemi, M., Dallaire, É., Dugat, J., & Aitcin, P.-C. (1997). Mechanical properties and durability of two industrial reactive powder concretes. *ACI Materials Journal 94(4)*.

Brouwers, H.J.H., & Radix, H.J. (2005). Self-Compacting Concrete: Theoretical and experimental study. *Cement and Concrete Research 35(11)*, 2116-2136.

Branson, D.E. (1977). *Deformation of concrete structures*. McGraw-Hill Companies.

BS-1881-121:1983. (1983). Testing concrete. Method for determination of static modulus of elasticity in compression. In. UK: British Standards Institution.

Bumanis, G., Toropovs, N., Dembovska, L., Bajare, D., & Korjakins, A. (2015). The Effect of Heat Treatment on the Properties of Ultra High Strength Concrete. *Environment. Technology. Resources. Proceedings of the International Scientific and Practical Conference*, Vol. 1, pp. 22-27.

Buitelaar, P. (2004). Heavy reinforced ultra high performance concrete. *Proceedings of the Int. Symp. on UHPC, Kassel, Germany*, pp. 25-35.

Camacho, E., & Serna, P. (2010). Optimización de dosificaciones de hormigón autocompactante de muy alto rendimiento renforzado con fibras híbrido. *2º Congresso Ibérico sobre HAC, Guimaraes, Portugal*, pp. 1-2.

Camacho Torregrosa, E.E. (2014). Dosage optimization and bolted connections for UHPFRC ties. In.

Carreira, D.J., & Chu, K.-H. (1985). Stress-strain relationship for plain concrete in compression. *ACI Journal proceedings*, Vol. 82. ACI.

Cavill, B., & Chirgwin, G. (2004). The world's first RPC road bridge at Shepherds Gully Creek, NSW. *Austroads Bridge Conference, 5th, 2004, Hobart, Tasmania, Australia*.

Chen, Y., Visintin, P., Oehlers, D., & Alengaram, U. (2013). Size-Dependent Stress-Strain Model for Unconfined Concrete. *Journal of Structural Engineering 140(4)*, 04013088.

Chen, Y., Zhang, T., Visintin, P., & Oehlers, D.J. (2015). Concrete Shear-Friction Material Properties: Application to Shear Capacity of RC Beams of all Sizes. *Advances in Structural Engineering 18(8)*, 1187-1198.

Collepardi, S., Coppola, L., Troli, R., & Collepardi, M. (1999). Mechanisms of Actions of Different Superplasticizers For High Performance Concrete. *ACI Special Publication 186*.

Corley, W. (1966). Rotational capacity of reinforced concrete beams. *journal of the Structural Division 92(5)*, 121-146.

Daniell, J., Oehlers, D., Griffith, M., Ali, M.M., & Ozbakkaloglu, T. (2008). The softening rotation of reinforced concrete members. *Engineering Structures 30(11)*, 3159-3166.

Debernardi, P.G., & Taliano, M. (2001). Softening behaviour of concrete prisms under eccentric compressive forces. *Magazine of Concrete Research 53(4)*, 239-249.

de Larrard, F., & Sedran, T. (1994). Optimization of ultra-high-performance concrete by the use of a packing model. *Cement and Concrete Research 24(6)*, 997-1009.

de Andrade Lima, L.R.P., & Bernardez, L.A. (2011). Characterization of the lead smelter slag in Santo Amaro, Bahia, Brazil. *Journal of Hazardous Materials 189(3)*, 692-699.

Del Viso, J., Carmona, J., & Ruiz, G. (2008). Shape and size effects on the compressive strength of high-strength concrete. *Cement and Concrete Research 38(3)*, 386-395.

Desayi, P., & Krishnan, S. (1964). Equation for the stress-strain curve of concrete. *ACI Journal Proceedings*, Vol. 61. ACI.

Dils, J., De Schutter, G., & Boel, V. (2012a). Influence of mixing procedure and mixer type on fresh and hardened properties of concrete: a review. *Materials and Structures 45(11)*, 1673-1683.

Dils, J., De Schutter, G., & Boel, V. (2012). Influence of mixing procedure and mixer type on fresh and hardened properties of concrete: a review. *Materials and Structures 45(11)*, 1673-1683.

Dils, J., De Schutter, G., Boel, V., & Braem, E. (2012b). Influence of vacuum mixing on the mechanical properties of UHPC. *3rd International Symposium on UHPC and Nanotechnology for High Performance Construction Materials: Ultra-High Performance Concrete and Nanotechnology in Construction (HIPERMAT-2012)*, Vol. 19, pp. 241-248. Kassel University Press GmbH.

Dugat, J., Roux, N., & Bernier, G. (1996). Mechanical properties of reactive powder concretes. *Materials and Structures 29(4)*, 233-240.

EFNARC, S. (2002). Guidelines for self-compacting concrete. *London, UK: Association House*, 32-34.

EN-206-1. (2002). 206-1. Concrete-Part-1: Specification, Performance, Production and Conformity. *Turkish Standards Institution, Ankara*.

Fehling, E., Bunje, K., Schmidt, M., Tue, N.V., Schreiber, W., & Humburg, E. (2007). Design of First Hybrid UHPC-Steel Bridge across the River Fulda in Kassel, Germany. *IABSE Symposium Report*, Vol. 93, pp. 1-8. International Association for Bridge and Structural Engineering.

Gagn, R., Boisvert, A., & Pigeon, M. (1996). Effect of superplasticizer dosage on mechanical properties, permeability, and freeze-thaw durability of high-strength concretes with and without silica fume. *ACI Materials Journal 93(2)*.

Gerlicher, T., Heinz, D., & Urbonas, L. (2008). Effect of finely ground blast furnace slag on the properties of fresh and hardened UHPC. *Proceedings of the Second International Symposium on UHPC, Universität Kassel*, pp. 367-374.

Graybeal, B., & Hartmann, J. (2005). Construction of an Optimized UHPC Vechicle Bridge. *ACI Special Publication 228*.

Graybeal, B.A. (2007). Compressive behavior of ultra-high-performance fiber-reinforced concrete. *ACI Materials Journal 104(2)*, 146.

Graybeal, B., & Davis, M. (2008). Cylinder or cube: strength testing of 80 to 200 MPa (11.6 to 29 ksi) ultra-high-performance fiber-reinforced concrete. *ACI Materials Journal 105(6)*, 603-609.

Graybeal, B.A. (2005). Characterization of the Behaviour of Ultra-high Performance Concrete. In *Department of Civil and Environemnt Engineering* Vol. Doctor of Philosophy, p. 377. USA: University of Maryland, College Park

Graybeal, B.A., & Baby, F. (2013). Development of Direct Tension Test Method for Ultra-High-Performance Fiber-Reinforced Concrete. *ACI Materials Journal 110(2)*.

Graybeal, B.A., & Hartmann, J.L. (2003). Strength and durability of ultra-high performance concrete. *Concrete Bridge Conference, Portland Cement Association*.

Habel, K., Viviani, M., Denarié, E., & Brühwiler, E. (2006). Development of the mechanical properties of an Ultra-High Performance Fiber Reinforced Concrete (UHPFRC). *Cement and Concrete Research 36(7)*, 1362-1370.

Habel, K. (2004). Structural behaviour of elements combining ultra-high performance fibre reinforced concretes (UHPFRC) and reinforced concrete. In.: EPFL.

Habel, K., Charron, J.-P., Braike, S., Hooton, R.D., Gauvreau, P., & Massicotte, B. (2008). Ultra-high performance fibre reinforced concrete mix design in central Canada. *Canadian Journal of Civil Engineering 35(2)*, 217-224.

Haque, M. (1990). Some concretes need 7 days initial curing. *Concrete International 12(2)*, 42-46.

Haskett, Ali, M.M., Oehlers, & Wu. (2009a). Influence of bond on the hinge rotation of FRP plated beams. *Advances in Structural Engineering 12(6)*, 833-843.

Haskett, M., Oehlers, D.J., Ali, M.M., & Wu, C. (2009b). Rigid body moment–rotation mechanism for reinforced concrete beam hinges. *Engineering Structures 31(5)*, 1032-1041.

Haskett, M., Oehlers, D.J., Ali, M.S.M., & Wu, C. (2009). Yield Penetration Hinge Rotation in Reinforced Concrete Beams. *ASCE 135(2)*, 130-138.

Hassan, A., Jones, S., & Mahmud, G. (2012). Experimental test methods to determine the uniaxial tensile and compressive behaviour of ultra high performance fibre reinforced concrete (UHPFRC). *Construction and Building Materials 37*, 874-882.

Heinz, D., & Ludwig, H.-M. (2004). Heat treatment and the risk of DEF delayed ettringite formation in UHPC. *Proceedings of the 1st international symposium on ultra high performance concrete, Kassel, Germany*, pp. 717-730.

Heinz, D., Urbonas, L., & Gerlicher, T. (2012). Effect of heat treatment method on the properties of UHPC. *Ultra High Performance Concrete and Nanotechnology in Construction, 3rd Intl. Symp. on Ultra High Performance Concrete and Nanotechnology for High Performance Construction Materials*, pp. 283-290.

Hemmati, A., Kheyroddin, A., & Sharbatdar, M.K. (2013). Plastic hinge rotation capacity of reinforced HPFRCC beams. *Journal of Structural Engineering 141(2)*, 04014111.

Hemalatha, T., Sundar, K.R., Murthy, A.R., & Iyer, N.R. (2015). Influence of mixing protocol on fresh and hardened properties of self-compacting concrete. *Construction and Building Materials 98*, 119-127.

Hirschi, T., & Wombacher, F. (2008). Influence of different superplasticizers on UHPC. *Proceedings of the 2nd International Symposium on Ultra High Performance Concrete, Kassel, Germany*, pp. 77-84.

Hjorth, L., Alford, N.M., Mangabhai, R.J., Hirsch, P., Moir, G.K., Jefferis, S.A., Blundell, R., Kelly, A., Defosse, C., Sing, K.S.W., Massazza, F., & Bensted, J. (1983). Development and Application of High-Density Cement-Based Materials [and Discussion]. *Philosophical Transactions of the Royal Society of London. Series A, Mathematical and Physical Sciences 310(1511)*, 167-173.

Hobbs, D. (1974). Influence of aggregate restraint on the shrinkage of concrete. *ACI Journal Proceedings*, Vol. 71. ACI.

Hognestad, E. (1951). Study of combined bending and axial load in reinforced concrete members. *University of Illinois. Engineering Experiment Station. Bulletin; no. 399*.

Hong, K.N., Kang, S.T., Kim, S.W., Park, J.J., & Han, S.H. (2010). Material properties of air-cured ultra-high-performance steel-fiber-reinforced concrete at early ages. *International Journal of the Physical Sciences 5(17)*, 2622-2634.

Hsu, L.S., & Hsu, C.T. (1994). Stress-strain behavior of steel-fiber high-strength concrete under compression. *ACI structural journal 91(4)*.

Hüsken, G.G. (2010). A multifunctional design approach for sustainable concrete: with application to concrete mass products. In.: Technische Universiteit Eindhoven.

Kampmann, R. (2012). *The influence of the compression interface on the failure behavior and size effect of concrete*.

Ipek, M., Yilmaz, K., Sümer, M., & Saribiyik, M. (2011). Effect of pre-setting pressure applied to mechanical behaviours of reactive powder concrete during setting phase. *Construction and Building Materials 25(1)*, 61-68.

Jansen, D.C., & Shah, S.P. (1997). Effect of length on compressive strain softening of concrete. *Journal of Engineering Mechanics 123(1)*, 25-35.

Jayakumar, K. (2004). Role of silica fume concrete in concrete technology. *Proc., Int. Symp. on UHPC*, pp. 165-174.

Justs, J., Shakhmenko, G., & Bajare, D. (2010). Effect of different mix compositions and curing regimes on ultra high performance concrete compressive strength. *publication. editionName*, 112-116.

Kay Wille, A.E.N., & Gustavo, J.P.-M. (2014). Ultra-High Performance Concrete with Compressive Strength Exceeding 150 MPa (22 ksi): A Simpler Way. *Materials Journal 108(1)*.

Kazemi, S., & Lubell, A.S. (2012). Influence of Specimen Size and Fiber Content on Mechanical Properties of Ultra-High-Performance Fiber-Reinforced Concrete. *ACI Materials Journal 109(6)*.

Khanzadi, M., & Behnood, A. (2009). Mechanical properties of high-strength concrete incorporating copper slag as coarse aggregate. *Construction and Building Materials 23(6)*, 2183-2188.

Kheyroddin, A., & Naderpour, H. (2007). Plastic hinge rotation capacity of reinforced concrete beams. *International Journal of Civil Engineering (IJCE) 5(1)*.

Kim, D.J., Park, S.H., Ryu, G.S., & Koh, K.T. (2011). Comparative flexural behavior of Hybrid Ultra High Performance Fiber Reinforced Concrete with different macro fibers. *Construction and Building Materials 25(11)*, 4144-4155.

Kim, J.-K., & Yi, S.-T. (2002). Application of size effect to compressive strength of concrete members. *Sadhana 27(4)*, 467-484.

Kwan, A., & Mora, C. (2002). Effects of various, shape parameters on packing of aggregate particles. *Magazine of Concrete Research*.

Lange, F., Mörtel, H., & Rudert, V. (1997). Dense packing of cement pastes and resulting consequences on mortar properties. *Cement and Concrete Research 27(10)*, 1481-1488.

Lappa, E.S. (2007). *High strength fibre reinforced concrete: static and fatigue behaviour in bending*. TU Delft, Delft University of Technology.

Lee, K., Lee, H., Lee, S., & Kim, G. (2006). Autogenous shrinkage of concrete containing granulated blast-furnace slag. *Cement and Concrete Research 36(7)*, 1279-1285.

Lei, Y., Nematollahi, B., Mohamed Said, A.B., Gopal, B.A., & Yee, T.S. (2012). Application of ultra high performance fiber reinforced concrete–the malaysia perspective. *International Journal of Sustainable Construction Engineering and Technology 3(1)*, 26-44.

Li, V.C., & Leung, C.K. (1992). Steady-state and multiple cracking of short random fiber composites. *Journal of Engineering Mechanics 118(11)*, 2246-2264.

Lohaus, L., & Ramge, P. (2008). Robustness of UHPC–A new Approach for mixture Proportioning. *Procedings of the 2nd Int. Symposium on Ultra HighPerformance Concrete, Fehling E., Schmidt M. Stürwald S.(Eds), Kassel University Press, Kassel*, pp. 113-120.

Lopes, S., & Bernardo, L. (2003). Plastic rotation capacity of high-strength concrete beams. *Materials and Structures 36(1)*, 22-31.

Lubell, S.K., & A.S. (2011). Size effect on the mechanical properties of UHPFRC. *Proceedings 2nd International Engineering Mechanics and Materials Specialty Conference*. Canadian Society for Civil Engineering.

Ma, J., Orgass, M., Dehn, F., Schmidt, D., & Tue, N. (2004). Comparative investigations on ultra-high performance concrete with and without coarse aggregates. *Proceedings International Symposium on Ultra High Performance Concrete (UHPC), Kassel, Germany*.

Mander, J.B., Priestley, M.J., & Park, R. (1988). Theoretical stress-strain model for confined concrete. *Journal of Structural Engineering 114(8)*, 1804-1826.

Mazanec, O., & Schiessl, P. (2008). Improvement of UHPC properties through an optimized mixing procedure. *8th International symposium on utilization of high-strength and high-performance concrete, Tokyo, Japan*, Vol. 2729.

Muhamad, R., Mohamed Ali, M.S., Oehlers, D., & Hamid Sheikh, A. (2011). Load-slip relationship of tension reinforcement in reinforced concrete members. *Engineering Structures 33(4),* 1098-1106.

Naaman, A.E., & Wille, K. (2012). The path to ultra-high performance fiber reinforced concrete (UHP-FRC): five decades of progress. *Proceedings of Hipermat 2012 3rd international symposium on UHPC and nanotechnology for high performance construction materials, Kassel, Germany*, pp. 3-13.

Neville, A. (1981). Properties of concrete Pitman. In.: London.

Neville, A.M. (1995). *Properties of concrete.*

Obla, K.H., Hill, R.L., Thomas, M.D., Shashiprakash, S.G., & Perebatova, O. (2003). Properties of concrete containing ultra-fine fly ash. *ACI Materials Journal 100(5),* 426-433.

Odler, I., & Becker, T. (1980). Effect of some liquefying agents on properties and hydration of Portland cement and tricalcium silicate pastes. *Cement and Concrete Research 10(3),* 321-331.

Oehlers, D., Ali, M.S.M., & Griffith, M. (2008). Concrete Component of the Rotational Ductility of Reinforced Concrete Flexural Members. *Advances in Structural Engineering 11(3),* 281-291.

Oehlers, D., Ali, M.S.M., & Griffith, M. (2008a). Concrete Component of the Rotational Ductility of Reinforced Concrete Flexural Members. *Advances in Structural Engineering 11(3),* 281-291.

Oehlers, D., Mohamed Ali, M., Haskett, M., Lucas, W., Muhamad, R., & Visintin, P. (2011). FRP-Reinforced Concrete Beams: Unified Approach Based on IC Theory. *Journal of Composites for Construction 15(3),* 293-303.

Oehlers, D.J., Rashid, R., & Seracino, R. (2008b). IC debonding resistance of groups of FRP NSM strips in reinforced concrete beams. *Construction and Building Materials 22(7),* 1574-1582.

Oehlers, D.J., Haskett, M., Ali, M.M., & Griffith, M.C. (2010). Moment redistribution in reinforced concrete beams. *Proceedings of the ICE-Structures and Buildings 163(3)*, 165-176.

Ogundiran, M.B., Nugteren, H.W., & Witkamp, G.J. (2013). Immobilisation of lead smelting slag within spent aluminate—fly ash based geopolymers. *Journal of Hazardous Materials 248–249*, 29-36.

Panagiotakos, T.B., & Fardis, M.N. (2001). Deformations of reinforced concrete members at yielding and ultimate. *ACI structural journal 98(2)*.

Park, J.-S., Kim, Y.J., Cho, J.-R., & Jeon, S.-J. (2015). Early-Age Strength of Ultra-High Performance Concrete in Various Curing Conditions. *Materials 8(8)*, 5537-5553.

Perry, V., & Zakariasen, D. (2004). First use of ultra-high performance concrete for an innovative train station canopy. *Concrete Technology Today 25(2)*, 1-2.

Perry, V.H., & Seibert, P.J. (2008). The use of UHPFRC (Ductal®) for bridges in North America: The technology, applications and challenges facing commercialization. *Proceedings of Second International Symposium on Ultra High Performance Concrete, University of Kassel, Germany*, pp. 815-822.

Piotrowski, S., & Schmidt, M. (2012). Life cycle cost analysis of a UHPC-bridge on example of two bridge refurbishment designs. *Proceedings of the 3rd international symposium on ultra-high performance concrete and nanotechnology for high performance construction materials, Kassel*, pp. 957-964.

Ponikiewski, T., & Gołaszewski, J. (2013). COMPOSITION OF STEEL FIBRE REINFORCED SELF-COMPACTING CONCRETE FOR OPTIMAL RHEOLOGICAL AND MECHANICAL PROPERTIES. *7th International RILEM Conference on Self-Compacting Concrete. The 1st International RILEM Conference on Rheology and Processing of Construction Materials.*

Popovics, S. (1973). A numerical approach to the complete stress-strain curve of concrete. *Cement and Concrete Research 3(5)*, 583-599.

Popovics, S. (1998). *Strength and related properties of concrete: A quantitative approach*. John Wiley & Sons.

Prabha, S.L., Dattatreya, J., Neelamegam, M., & Seshagirirao, M. (2010). Study on Stress-Strain Properties of Reactive Powder Concrete under Uniaxial Compression. *International Journal of Engineering Science and Technology 2(11)*, 6408-6416.

Priestley, M., & Park, R. (1987). Strength and ductility of concrete bridge columns under seismic loading. *ACI structural journal 84(1)*.

Prem, P.R., Bharatkumar, B., & Iyer, N.R. (2013). Influence of curing regimes on compressive strength of ultra high performance concrete. *Sadhana 38(6)*, 1421-1431.

Randl, N., Steiner, T., Ofner, S., Baumgartner, E., & Mészöly, T. (2014). Development of UHPC mixtures from an ecological point of view. *Construction and Building Materials 67, Part C*, 373-378.

Rebentrost, M. (2005). Design and Construction of the First Ductal® Bridge in New Zealand. *22nd Biennial Conference of the Concrete Institute of Australia*.

Richard, P., & Cheyrezy, M. (1995). Composition of reactive powder concretes. *Cement and Concrete Research 25(7)*, 1501-1511.

Rilem, T. (2000). 148-SSC: Strain softening of concrete—test methods for compressive softening. Test method for measurement of the strain-softening behaviour of concrete under uniaxial compression. *Materials and Structures 33(230)*, 347-351.

Rodríguez, E.D., Soriano, L., Payá, J., Borrachero, M.V., & Monzó, J.M. (2012). Increase of the reactivity of densified silica fume by sonication treatment. *Ultrasonics sonochemistry 19(5)*, 1099-1107.

Rossi, P. (1992). Mechanical behaviour of metal-fibre reinforced concretes. *Cement and Concrete Composites 14(1)*, 3-16.

Rossi, P. (2013). Influence of fibre geometry and matrix maturity on the mechanical performance of ultra high-performance cement-based composites. *Cement and Concrete Composites 37*, 246-248.

Rossignolo, J.A. (2007). Effect of silica fume and SBR latex on the pasteaggregate interfacial transition zone. *Materials Research 10(1)*, 83-86.

Rougeau, P., & Borys, B. (2004). Ultra high performance concrete with ultrafine particles other than silica fume. *Proceedings of the international symposium on ultra high performance concrete. Kassel: University of Kassel*, pp. 213-226.

Saenz, L.P. (1964). Discussion of equation for the stress-strain curve of concrete by Desayi and Krishnan. *ACI journal 61(9)*, 1229-1235.

Safiuddin, M., West, J., & Soudki, K. (2008). Durability performance of self-consolidating concrete. *Journal of Applied Sciences Research 4(12)*, 1834-1840.

Sakai, E., Aizawa, K., Nakamura, A., Kato, H., & Daimon, M. (2008). Influence of superplasticizers on the fluidity of cements with different amount of aluminate phase. *Proceedings of the 2nd International Symposium on Ultra High Performance Concrete, Kassel, Germany*, pp. 85-92.

Sbia, L.A., Peyvandi, A., Soroushian, P., Balachandra, A.M., & Smith, I. (2014). Optimization of ultra-high-performance concrete with nano-and micro-scale reinforcement. *Cogent Engineering 1(1)*, 990673.

Schachinger, I., Schubert, J., & Mazanec, O. (2004). Effect of Mixing and Placement Methods on Fresh and Hardened Ultra High Performance Concrete (UHPC). *International Symposium on Ultra High performance Concrete*, pp. 575-586. Kassel, Germany

Scheydt, J., Herold, G., Mueller, H.S., Kuhnt, M., Fehling, E., Schmidt, M., & Stürwald, S. (2008). Development and application of UHPC convenience blends. *Second international symposium on ultra high performance concrete, Kassel*, pp. 69-76.

Schießl, P., Mazanec, O., Lowke, D., Plank, J., & SCHRÖFL, C. (2010). Rheology of UHPC—Effect of Superplasticizer and Silica Fume on Mixing and Workability of UHPC. *3rd*.

Schmidt, M., & Fehling, E. (2005). Ultra-high-performance concrete: research, development and application in Europe. *ACI Special Publication 228*.

Schröfl, C., Gruber, M., & Plank, J. (2008). Structure performance relationship of polycarboxylate superplasticizers based on methacrylic acid esters in ultra high performance concrete. *Ultra High Performance Concrete (UHPC)-Proceedings of the 2nd International Symposium on Ultra High Performance Concrete, Kassel, Germany: Kassel University*, pp. 383-390.

Seracino, R., Oehlers, D.J., & Yeo, M.F. (2002). Partial-interaction fatigue assessment of stud shear connectors in composite bridge beams. *Structural Engineering and Mechanics 13(4)*, 455-464.

Šerelis, E., Deligia, M., Vaitkevičius, V., & Kerševičius, V. (2015). Influence of Water to Cement Ratio with Different Amount of Binder on Properties of Ultra-High Performance Concrete. *Journal of Sustainable Architecture and Civil Engineering 10(1)*, 78-86.

Shihada, S., & Arafa, M. (2010). Effects of silica fume, ultrafine and mixing sequences on properties of ultra high performance concrete. *Asian Journal of Materials Science 2(3)*, 137-146.

Skazlić, M., Serdar, M., & Bjegović, D. (2008). Influence of test specimen geometry on compressive strength of ultra high performance concrete. *Second International Symposium on Ultra High Performance Concrete*.

Stähli, P. (2008). *Ultra-fluid, oriented hybrid-fibre-concrete*. Diss., Eidgenössische Technische Hochschule ETH Zürich, Nr. 17996, 2008.

Stark, U., & Mueller, A. (2008). Optimization of packing density of aggregates. *Second International Symposium on Ultra High Performance Concrete. Kassel*, pp. 121-127.

Stiel, T., Karihaloo, B., & Fehling, E. (2004). Effect of casting direction on the mechanical properties of CARDIFRC. *Proceedings of the International Symposium on Ultra High Performance Concrete*, pp. 481-493.

Safi, B., Aboutair, A., Saidi, M., Ghernouti, Y., & Oubraham, C. (2014). Effect of the heat curing on strength development of ultra-high performance fiber reinforced concrete (UHPFRC) containing dune sand and ground brick waste. *Journal of Building Materials and Structures 1(2)*, 40-46.

Semioli, W.J. (2001). The new concrete technology. *Concrete International 23(11)*, 75-79.

Stark, U., & Mueller, A. (2008). Optimization of packing density of aggregates. *Second International Symposium on Ultra High Performance Concrete. Kassel*, pp. 121-127.

Steinberg, E. (2009). Structural reliability of prestressed UHPC flexure models for bridge girders. *Journal of Bridge Engineering 15(1)*, 65-72.

Tafraoui, A., Escadeillas, G., Lebaili, S., & Vidal, T. (2009). Metakaolin in the formulation of UHPC. *Construction and Building Materials 23(2)*, 669-674.

Teichmann, T., & Schmidt, M. (2004). Influence of the packing density of fine particles on structure, strength and durability of UHPC. *Proceedings of the 1st International Symposium on Ultra High Performance Concrete, Kassel, Germany*, pp. 313-323.

Talebinejad, I., Bassam, S.A., Iranmanesh, A., & Shekarchizadeh, M. (2004). Optimizing mix proportions of normal weight reactive powder concrete with strengths of 200–350 MPa. *Proceedings of the first ultra high performance concrete. Kassel (Germany): Die Deutsche Bibliothek*, 133-141.

Terzijski, I. (2004). Compatibility of Components of High and Ultra High Performance Concrete. *Proceedings of the 1st International Symposium on Ultra High Performance Concrete, Kassel, Germany*, pp. 175-186.

Toropovs, N., Bajare, D., Shakhmenko, G., Korjakins, A., & Justs, J. (2013). Effect of Thermal Treatment on Properties of High Strength Concrete. *CIVIL ENGINEERING'13*, 129.

Tsai, W.T. (1988). Uniaxial compressional stress-strain relation of concrete. *Journal of Structural Engineering 114(9)*, 2133-2136.

Tue, N.V., Ma, J., & Orgass, M. (2008). Influence of addition method of superplasticizer on the properties of fresh UHPC. *Proceedings of Second International Symposium on Ultra High Performance Concrete, University of Kassel, Germany*, pp. 93-100.

Urbonas, L., Heinz, D., & Gerlicher, T. (2013). Ultra-High Performance Concrete Mixes with Reduced Portland Cement Content. *Journal of Sustainable Architecture and Civil Engineering 3(4)*, 47-51.

Van Tuan, N., Ye, G., Van Breugel, K., Fraaij, A.L., & Dai Bui, D. (2011). The study of using rice husk ash to produce ultra high performance concrete. *Construction and Building Materials 25(4)*, 2030-2035.

Van, V.-T.-A. (2013). Characteristics of Rice Husk Ash and Application in Ultra-High Performance Concrete Charakterisierung von Reisschalenasche und deren Verwendung im Ultrahochfesten Beton. In. Weimar-Germany: Bauhaus-Universität Weimar, Professur Werkstoffe des Bauens.

Vicenzino, E., PERRY, V.H., CHOW, T.S., CULHAM, G., & ZAKARIASEN, D. (2005). First use of UHPFRC in thin precast concrete roof shell for Canadian LRT station. *PCI journal 50(5)*, 50-67.

Visintin, P., Chen, Y., & Oehlers, D. (2015). Simulating the Behavior of FRP-Confined Cylinders Using the Shear-Friction Mechanism. *Journal of Composites for Construction*, 04015014.

Visintin, P., & Oehlers, D. (2012). A mechanics based simulation of an RC hinge with FRP reinforcement. *International Conference on FRP Composites in Civil Engineering (6th: 2012: Rome, Italy)*.

Visintin, P., Oehlers, D., Haskett, M., & Wu, C. (2012a). Mechanics-based hinge analysis for reinforced concrete columns. *Journal of Structural Engineering 139(11)*, 1973-1980.

Visintin, P., Oehlers, D., Wu, C., & Haskett, M. (2012b). A mechanics solution for hinges in RC beams with multiple cracks. *Engineering Structures 36*, 61-69.

Voo, Y.L., & Foster, S.J. (2010). Characteristics of ultra-high performance 'ductile'concrete and its impact on sustainable construction. *The IES Journal Part A: Civil & Structural Engineering 3(3)*, 168-187.

Wang, C., Yang, C., Liu, F., Wan, C., & Pu, X. (2012). Preparation of Ultra-High Performance Concrete with common technology and materials. *Cement and Concrete Composites 34(4)*, 538-544.

Wee, T., Chin, M., & Mansur, M. (1996). Stress-strain relationship of high-strength concrete in compression. *Journal of Materials in Civil Engineering 8(2)*, 70-76.

Wight, G., Rebentrost, M., & Cavill, B. (2007). Designing Bridges with Ductal® Reactive Powder Concrete. *23 rd Biennial Conference*, pp. 249-258.

Wille, K., El-Tawil, S., & Naaman, A.E. (2014). Properties of strain hardening ultra high performance fiber reinforced concrete (UHP-FRC) under direct tensile loading. *Cement and Concrete Composites 48*, 53-66.

Wille, K., El-Tawil, S., & Naaman, A.E. (2014a). Properties of strain hardening ultra high performance fiber reinforced concrete (UHP-FRC) under direct tensile loading. *Cement and Concrete Composites 48*, 53-66.

Wille, K., Naaman, A.E., & Parra-Montesinos, G.J. (2011). Ultra-high performance concrete with compressive strength exceeding 150 MPa (22 ksi): A simpler way. *ACI Materials Journal 108(1)*.

Wille, K., Naaman, A., El-Tawil, S., & Parra-Montesinos, G. (2012). Ultra-high performance concrete and fiber reinforced concrete: achieving strength and ductility without heat curing. *Materials and Structures 45(3)*, 309-324.

Wille, K., Tue, N., & Parra-Montesinos, G. (2014b). Fiber distribution and orientation in UHP-FRC beams and their effect on backward analysis. *Materials and Structures 47(11)*, 1825-1838.

Wille, K., & Boisvert-Cotulio, C. (2015). Material efficiency in the design of ultra-high performance concrete. *Construction and Building Materials 86*, 33-43.

Wille, K., Naaman, A.E., & El-Tawil, S. (2011a). Optimizing ultra-high-performance fiber-reinforced concrete. *Concrete International 33(9)*, 35-41.

Wu, C., Oehlers, D., Rebentrost, M., Leach, J., & Whittaker, A. (2009). Blast testing of ultra-high performance fibre and FRP-retrofitted concrete slabs. *Engineering Structures 31(9)*, 2060-2069.

Wu, Y., Oehlers, D., & Griffith, M. (2002). PARTIAL-INTERACTION ANALYSIS OF COMPOSITE BEAM/COLUMN MEMBERS*. *Mechanics of Structures and Machines 30(3)*, 309-332.

Wu, W., Zhang, W., & Ma, G. (2010). Optimum content of copper slag as a fine aggregate in high strength concrete. *Materials & Design 31(6)*, 2878-2883.

Yaman, I.O., Hearn, N., & Aktan, H.M. (2002). Active and non-active porosity in concrete Part I: Experimental evidence. *Materials and Structures 35(2)*, 102-109.

Yang, J., Peng, G.-F., & Gao, Y.-X. (2012a). Characteristics of mechanical properties and durability of ultra-high per-formance concrete incorporating coarse aggregate. *Proceedings of HiPerMat*, 257-264.

YANG, J., PENG, G., GAO, Y., & WANG, B. (2012b). Influences on Compressive Strength of Ultra-High Performance Concrete Incorporating Coarse Aggregate [OL].[2012-09-05 14:21:14].

Yang, I.H., Joh, C., & Kim, B.-S. (2010). Structural behavior of ultra high performance concrete beams subjected to bending. *Engineering Structures 32(11)*, 3478-3487.

Yan, H., Sun, W., & Chen, H. (1999). The effect of silica fume and steel fiber on the dynamic mechanical performance of high-strength concrete. *Cement and Concrete Research 29(3)*, 423-426.

Yang, S.L., Millard, S.G., Soutsos, M.N., Barnett, S.J., & Le, T.T. (2009). Influence of aggregate and curing regime on the mechanical properties of ultra-high performance fibre reinforced concrete (UHPFRC). *Construction and Building Materials 23(6)*, 2291-2298.

Yazici, H. (2007). The effect of curing conditions on compressive strength of ultra high strength concrete with high volume mineral admixtures. *Building and environment 42(5)*, 2083-2089.

Yazıcı, H., Yardımcı, M.Y., Yiğiter, H., Aydın, S., & Türkel, S. (2010). Mechanical properties of reactive powder concrete containing high volumes of ground granulated blast furnace slag. *Cement and Concrete Composites 32(8)*, 639-648.

Yazıcı, H., Yiğiter, H., Karabulut, A.Ş., & Baradan, B. (2008). Utilization of fly ash and ground granulated blast furnace slag as an alternative silica source in reactive powder concrete. *Fuel 87(12)*, 2401-2407.

Yi, N.-H., Kim, J.-H.J., Han, T.-S., Cho, Y.-G., & Lee, J.H. (2012). Blast-resistant characteristics of ultra-high strength concrete and reactive powder concrete. *Construction and Building Materials 28(1)*, 694-707.

Yip, W. (1998). Generic form of stress-strain equations for concrete. *Cement and Concrete Research 28(4)*, 499-508.

Yoo, D.-Y., Kang, S.-T., & Yoon, Y.-S. (2014). Effect of fiber length and placement method on flexural behavior, tension-softening curve, and fiber distribution characteristics of UHPFRC. *Construction and Building Materials 64*, 67-81.

Yoo, D.-Y., Zi, G., Kang, S.-T., & Yoon, Y.-S. (2015). Biaxial flexural behavior of ultra-high-performance fiber-reinforced concrete with different fiber lengths and placement methods. *Cement and Concrete Composites 63*, 51-66.

Yoo, D.-Y., & Yoon, Y.-S. (2015). Structural performance of ultra-high-performance concrete beams with different steel fibers. *Engineering Structures 102*, 409-423.

Yu, R., Spiesz, P., & Brouwers, H. (2014). Mix design and properties assessment of Ultra-High Performance Fibre Reinforced Concrete (UHPFRC). *Cement and Concrete Research 56*, 29-39.

Yu, R., Spiesz, P., & Brouwers, H.J.H. (2015). Development of an eco-friendly Ultra-High Performance Concrete (UHPC) with efficient cement and mineral admixtures uses. *Cement and Concrete Composites 55*, 383-394.

Yudenfreund, M., Odler, I., & Brunauer, S. (1972a). Hardened portland cement pastes of low porosity I. Materials and experimental methods. *Cement and Concrete Research 2(3)*, 313-330.

Yudenfreund, M., Skalny, J., Mikhail, R.S., & Brunauer, S. (1972b). Hardened portland cement pastes of low porosity II. Exploratory studies. Dimensional changes. *Cement and Concrete Research 2(3)*, 331-348.

Zhifu Yang, Karol J. Kowalski, Jan Olek, & Tommy, N. (2014). Effects of Sand Characteristics and Fly Ash Contents on Properties of Flowable Fill. *Materials Journal 111(5)*.